UNIVERSITAT POLITÈCNICA DE VALÈNCIA

Departament d'Enginyeria Electrònica

"Non-invasive identification of atrial fibrillation drivers"

Tesi Doctoral

Autor
Miguel Rodrigo Bort

Dirigida per:
Dra. María de la Salud Guillem Sánchez
Dr. Batiste Andreu Martínez Climent
Dr. Felipe Atienza Fernández

València, 11 de Novembre de 2016

Agraïments

La realització d'una tesi doctoral es per una part el treball científic més important en la carrera d'un jove investigador, però d'altra part també representa el proces vital que completa l'etapa d'aprenentage i dona pas a l'etapa adulta. Aquesta tesi ha suposat doncs no sols un proces de desenvolupament científic, sino també un desenvolupament personal modelat per les relacions humanes en aquest període involucrades. Per això, em cal agrair a totes aquelles persones que han fet posible el transcórrer d'aquest treball la seua participació.

En primer lloc, he tingut el plaer de treballar amb persones de les que he aprés molt més del que els podré agrair: Edu, Conrad, Xavi, Santi, Jaume, Adolfo, Cristina, Ramón, Ismael, Toni, Álvaro, Paco, Javier, Lluis, Laia, Irene i molts més. També he d'agraïr a Pepe la seua aposta per un jove teleco que poc més que ganes de treballar podía oferir. Gràcies especials a Alejandro i a Jorge, el vostre treball ha sigut indispensable per a aquesta tesi, i heu sigut uns excelents companys tant en el treball com en l'oci. Espere que totes aquestes relacions pervisquen per molts anys.

María i Andreu, rebeu el meu sincer agraïment, vostra ajuda i direcció ha sigut indispensable, i el vostre treball incansable. Sou responsables de que hui en dia el grup de investigació siga el que és, i a més heu conseguit convertir-lo en una gran família. També m'és indispensable agrair a Omer Berenfeld la ajuda que desde l'altra part del Atlantic m'ha proporcionat, així com a l'acolliment amb els braços oberts durant l'estada en el seu grup d'Ann Arbor. També he d'agrair de manera especial la ajuda del doctor Felipe Atienza en aquesta tesi.

Per altra banda, i de manera infinitament més ampla, tinc que donar gràcies als meus pares, sense els quals no haguera pogut recorrer ni una fracció del camí que m'ha dut fins ací. A ma mare, de la que he heretat la que espere serà la meua professió en els pròxims passos d'aquest camí, la docència. I per extensió, a tots els mestres que m'han conduït fins ací i m'han permés vore el món des dels muscles d'un gegant.

Per últim, a la persona més important de la meua vida, en la que compartisc aquest camí i fa que sols tinga sentit poder recorrer-lo amb ella. Aquest treball ha sigut gràcies a tu.

Contents

Acronyms

AF	Atrial fibrillation
AFL	Atrial flutter
AP	Action potential
AT	Atrial tachycardia
BB	Bachman's bundle
BSPM	Body surface potential mapping
CAT	Computerized axial tomography
CFAE	Complex fractionated atrial electrogram
CS	Coronary sinus
CT	Crista terminalis
dB	Decibel
DF	Dominant Frequency
ECG	Electrocardiogram
ECGI	Electrocradiographic imaging
EGM	Electrogram
FIRM	Focal impulse and rotor modulation
HDF	Highest dominant frequency
icEGM	Inverse-computed electrogram
IVC	Inferior vena cava
LA	Left atrium
LAA	Left atrial appendage
LA-HDF	Left atrial highest dominant frequency
LIPV	Left inferior pulmonary vein
LSPV	Left superior pulmonary vein
MRI	Magnetic Resonance Imaging
MV	Mitral valve
PLAW	Posterior left atrial wall

PSD	Power spectral density
PVI	Pulmonary vein isolation
RA	Right atrium
RAA	Right atrial appendage
RA-HDF	Right atrial highest dominant frequency
RIPV	Right inferior pulmonary vein
RSPV	Right superior pulmonary vein
SN	Sinus node
SNR	Signal-to-noise ratio
SP	Singularity point
SVC	Superior vena cava
TV	Tricuspid valve
WCT	Wilson central terminal

Abstract

Atrial fibrillation (AF) is nowadays one of the most common cardiac arrhythmias in clinical practice, whose electrophysiological mechanisms of initiation and maintenance are not fully understood. The characterization of the fibrillatory electrical activity performed by the development of high-resolution cardiac mapping techniques led to the emergence of theories mantaining that the fibrillatory process is caused by certain atrial regions whose reentrant high-frequency activity propagates the fibrillatory activity to the rest of the atrial tissue. These theories have been positively proven in clinical practice since the electrical isolation of these key regions from the rest of the atrium can terminate the fibrillatory process and prevent the appearance of new episodes.

The location of the dominant atrial regions in patients with AF represents a major challenge in the diagnosis and treatment of this arrhythmia. The most widely used techniques in clinical practice are based on the analysis of cardiac electrical activity obtained by intracardiac catheters. However, the characterization of this arrhythmia by invasive methods is only available for those patients already selected for the ablation therapy. With the aim to detect and locate the fibrillatory sources prior to surgical procedure, non-invasive methods for studying the atrial electrical maps have been developed. Body surface electrical mapping (BSPM) allows to study with high spatial resolution the electrical activity on the torso surface, while electrocardiographic imaging (ECGI) allows to non-invasively reconstruct the cardiac electrical activity in the atrial surface. Given the relative novelty of both noninvasive diagnostic systems and theories on the maintenance of AF, both technologies suffer from a lack of scientific knowledge about the physical and technical mechanisms that support their operation. Therefore, the aim of this thesis is to increase that scientific and technical knowledge, as well as studying the effectiveness of these technologies for the identification and localization of dominant regions in patients with AF, making use of both patient recordings and mathematical models of atrial electrical activity.

First, it has been shown that BSPM systems are able to noninvasively identify atrial rotors by recognizing reentrant patterns in the surface phase signal after

band-pass filtering at the highest dominant frequency band. Furthermore, the position of such surface rotors is related to the atrial rotor location, allowing the distinction between left or right atrial rotors. Moreover, it has been found that the surface electrical maps in AF suffer a spatial smoothing effect by the torso conductor volume, so the surface electrical activity can be studied with a relatively small number of electrodes. Specifically, it has been seen that 12 uniformly distributed electrodes are sufficient for the correct identification of atrial dominant frequencies, while at least 32 leads are needed for non-invasive identification of atrial rotors.

Secondly, the effect of narrowband filtering on the effectiveness of the location of reentrant patterns was studied. It has been found that this procedure allows isolating the reentrant electrical activity caused by the rotor, increasing the detection rate for both invasive and surface maps. However, the spatial smoothing caused by the regularization of the ECGI added to the temporal filtering causes a large increase in the spurious reentrant activity, making it difficult to detect real reentrant patterns. However, it has been found that maps provided by the ECGI without temporal filtering allow the correct detection of reentrant activity, so narrowband filtering should be applied for intracavitary or surface signal only.

Finally, we studied the stability of the markers used to detect dominant regions in ECGI, such as frequency maps or the rotor presence. It has been found that in the presence of alterations in the conditions of the inverse problem, such as electrical or geometrical noise, these markers are significantly more stable than the ECGI signal morphology from which they are extracted. In addition, a new methodology for error reduction in the atrial spatial location based on the curvature of the curve L has been proposed.

The results presented in this thesis showed that BSPM and ECGI systems allows to non-invasively detect and locate the presence of high-frequency rotors, responsible for the maintenance of AF. This detection has been proven to be unambiguous and robust, and the physical and technical mechanisms that support this behavior have been studied. These results indicate that both non-invasive systems provide information of great clinical value in the treatment of AF, so their use can be helpful for selecting and planning atrial ablation procedures.

Resum

La fibril·lació auricular (FA) és a dia d'avui una de les arítmies cardíaques més freqüents a la pràctica clínica, els mecanismes electrofisiològics d'inici i manteniments de la qual no són completament entesos. La caracterització de l'activitat elèctrica fibril·latoria duta a terme gràcies al desenvolupament de tècniques de mapeig cardíac d'alta resolució ha propiciat l'aparició de teories que defensen que el procés fibrilatori està provocat per certes regions auriculars l'activitat reentrant d'alta freqüència de les quals manté l'activitat fibril·latoria a la resta del teixit auricular. Aquestes teories han estat afirmativament contrastades en la pràctica clínica, veient que l'aïllament elèctric d'aquestes regions dominants de la resta de l'auricula permet aturar el procés fibrilatori i prevenir l'aparició de nous episodis.

La localització de les regions auriculars dominants en pacients amb FA suposa a dia d'avui un gran repte en el diagnòstic i tractament d'aquesta arítmia. Els mètodes més utilitzats en la pràctica clínica estan basats en l'anàlisi de l'activitat elèctrica cardíaca obtinguda mitjançant catèters intracavitaris. No obstant això, la caracterització d'aquesta arítmia mitjançant mètodes invasius només està a l'abast per a aquells pacients ja seleccionats per a una teràpia d'ablació. Amb l'objectiu de poder detectar i localitzar fonts fibril·latories amb anterioritat al procediment quirúrgic s'han desenvolupat mètodes no invasius per a l'estudi dels mapes elèctrics auriculars. La cartografia elèctrica de superfície (CES) permet estudiar amb gran resolució espacial l'activitat elèctrica en la superfície del tors, mentre que l'electrocardiografia per imatge (ECGI) permet obtenir de manera no invasiva l'activitat elèctrica cardíaca en la superfície auricular. Donada la relativa novetat tant dels sistemes no invasius de diagnosi com de les teories sobre el manteniment de la FA, ambdues tecnologies pateixen d'una manca de coneixement científic sobre els mecanismes físics i tècnics que sustenten el seu funcionament. Per tant, l'objectiu d'aquesta tesi és augmentar aquest coneixement cientificotècnic, així com estudiar l'eficàcia d'aquestes tecnologies per a la identificació i localització de regions dominants en pacients amb FA, fent ús tant de registres de pacients com de models matemàtics de l'activitat elèctrica auricular.

En primer lloc, s'ha vist que els sistemes CES permeten identificar rotors auriculars de manera no invasiva mitjançant el reconeixement de patrons reentrants en el senyal de fase superficial després del filtrat en banda estreta a la freqüència dominant més alta. A més, la posició dels rotors superficials està relacionada amb la localització auricular d'aquests rotors, permetent la distinció entre rotors de aurícula dreta o esquerra. També s'ha vist que els mapes elèctrics superficials durant FA pateixen una gran suavitzat espacial per l'efecte del volum conductor del tors, el que permet que l'activitat elèctrica superficial pugui ser estudiada amb un nombre relativament reduït d'elèctrodes. Concretament, s'ha vist que 12 elèctrodes uniformement distribuïts són suficients per a una correcta identificació de freqüències dominants auriculars, mentre que són necessaris almenys 32 per a una correcta identificació de rotors auriculars.

D'altra banda, també s'ha estudiat l'efecte del filtrat en banda estreta sobre l'eficàcia de la localització de patrons reentrants. Així, s'ha vist que aquest procediment permet aïllar l'activitat elèctrica reentrant provocada pel rotor, augmentant la taxa de detecció tant pel senyal obtingut de manera invasiva com per als mapes superficials. No obstant això, el suavitzat espacial provocat per la regularització de la ECGI unit al filtrat temporal provoca un gran augment de l'activitat reentrant espúria que dificulta la detecció de patrons reentrants reals. A més, s'ha vist que els mapes proporcionats per la ECGI sense filtrat temporal permeten la detecció correcta de l'activitat reentrant, per la qual cosa el filtrat en banda estreta hauria de ser aplicat únicament per a senyal intracavitària o superficial.

Per últim, s'ha estudiat l'estabilitat dels marcadors utilitzats en ECGI per a detectar regions auriculars dominants, com són els mapes de freqüència o la presència de rotors. S'ha vist que en presència d'alteracions en les condicions del problema invers, com soroll elèctric o geomètric, aquests marcadors són significativament més estables que la morfologia del mateix senyal ECGI de la qual són extrets. A més, s'ha proposat una nova metodologia per a la reducció de l'error en la localització espacial de l'aurícula basat en la curvatura de la corba L.

Els resultats presentats en aquesta tesi revelen que els sistemes de CES i ECGI permeten detectar i localitzar de manera no invasiva la presència de rotors d'alta freqüència, responsables del manteniment de la FA. S'ha vist que aquesta detecció és unívoca i robusta, i s'han estudiat els mecanismes físics i tècnics que sustenten aquest comportament. Aquests resultats indiquen que els dos sistemes no invasius proporcionen informació de gran valor clínic en el tractament de la FA, pel que el seu ús pot ser de gran ajuda per a la selecció i planificació de procediments d'ablació auricular.

Resumen

La fibrilación auricular (FA) es a día de hoy una de las arritmias cardiacas más frecuentes en la práctica clínica, cuyos mecanismos electrofisiológicos de inicio y mantenimiento no son completamente entendidos. La caracterización de la actividad eléctrica fibrilatoria llevada a cabo gracias al desarrollo de técnicas de mapeo cardiaco de alta resolución ha propiciado la aparición de teorías que defienden que el proceso fibrilatorio está provocado por ciertas regiones auriculares cuya actividad reentrante de alta frecuencia mantiene la actividad fibrilatoria en el resto del tejido auricular. Estas teorías han sido afirmativamente contrastadas en la práctica clínica, viéndose que el aislamiento eléctrico de estas regiones dominantes del resto de la auricula permite detener el proceso fibrilatorio y prevenir la aparición de nuevos episodios.

La localización de las regiones auriculares dominantes en pacientes con FA supone a día de hoy un gran reto en el diagnóstico y tratamiento de esta arritmia. Los métodos más utilizados en la práctica clínica están basados en el análisis de la actividad eléctrica cardiaca obtenida mediante catéteres intracavitarios. No obstante, la caracterización de esta arritmia mediante métodos invasivos solo está al alcance para aquellos pacientes ya seleccionados para una terapia de ablación. Con el objetivo de poder detectar y localizar fuentes fibrilatorias con anterioridad al procedimiento quirúrgico, se han desarrollado métodos no invasivos para el estudio de los mapas eléctricos auriculares. Mientras que la cartografía eléctrica de superficie (CES) permite estudiar con gran resolución espacial la actividad eléctrica en la superficie del torso, la electrocardiografía por imagen (ECGI) permite obtener de manera no invasiva la actividad eléctrica cardiaca en la superficie auricular. Dada la relativa novedad tanto de los sistemas no invasivos de diagnosis como de las teorías sobre el mantenimiento de la FA, ambas tecnologías adolecen de una falta de conocimiento científico sobre los mecanismos físicos y técnicos que sustentan su funcionamiento. Por lo tanto, el objetivo de esta tesis es aumentar dicho conocimiento cientificotécnico, así como estudiar la eficacia de estas tecnologías para la identificación y localización de regiones dominantes en

pacientes con FA. Para ello se ha hecho uso tanto de registros de pacientes como de modelos matemáticos de la actividad eléctrica auricular.

En primer lugar, ha visto que los sistemas CES permiten identificar rotores auriculares de manera no invasiva mediante el reconocimiento de patrones reentrantes en la señal de fase superficial tras el filtrado en banda estrecha a la frecuencia dominante más alta. Además, la posición de los rotores superficiales está relacionada con la localización auricular de dichos rotores, permitiendo la distinción entre rotores de aurícula derecha o izquierda. Por otra parte, se ha visto que los mapas eléctricos superficiales durante FA sufren una gran suavizado espacial por el efecto del volumen conductor del torso, lo que permite que la actividad eléctrica superficial pueda ser estudiada con un número relativamente reducido de electrodos. Concretamente, se ha visto que 12 electrodos uniformemente distribuidos son suficientes para una correcta identificación de frecuencias dominantes, mientras que son necesarios al menos 32 para una correcta identificación de rotores auriculares.

Por otra parte, también se ha estudiado el efecto del filtrado en banda estrecha sobre la eficacia de la localización de patrones reentrantes. Así, se ha visto que este procedimiento permite aislar la actividad eléctrica reentrante provocada por el rotor, aumentando la tasa de detección tanto para señal obtenida de manera invasiva como para los mapas superficiales. No obstante, el suavizado espacial provocado por la regularización de la ECGI unido a dicho filtrado temporal provoca un gran aumento de la actividad reentrante espúrea que dificulta la detección de patrones reentrantes reales. Sin embargo, se ha visto que los mapas proporcionados por la ECGI sin filtrado temporal permiten la detección correcta de la actividad reentrante, por lo que el filtrado en banda estrecha debería ser aplicado únicamente para señal intracavitaria o superficial.

Por último, se ha estudiado la estabilidad de los marcadores utilizados en ECGI para detectar regiones dominantes, como son los mapas de frecuencia o la presencia de rotores. Se ha visto que en presencia de alteraciones en las condiciones del problema inverso, como ruido eléctrico o geométrico, estos marcadores son significativamente más estables que la morfología de la propia señal ECGI de la que son extraídos. Además, se ha propuesto una nueva metodología para la reducción del error en la localización espacial de la aurícula basado en la curvatura de la curva L.

Los resultados presentados en esta tesis revelan que los sistemas de CES y ECGI permiten detectar y localizar de manera no invasiva la presencia de rotores de alta frecuencia, responsables del mantenimiento de la FA. Se ha visto que esta detección es univoca y robusta, y se han estudiado los mecanismos físicos y técnicos que sustentan dicho comportamiento. Estos resultados indican que ambos sistemas no invasivos proporcionan información de gran valor clínico en el tratamiento de la FA, por lo que su uso puede ser de gran ayuda para la selección y planificación de procedimientos de ablación auricular.

Chapter 1

Introduction

One of the most important advances in the history of mankind has been the development of modern medicine. For millennia we have studied and controlled the behavior of the human body, allowing milestones such as doubling our life expectancy or eradicate diseases, and has given a health condition inconceivable a couple of centuries ago. The development of modern medicine has been nourished by technical advances from other scientific areas and has always promoted a remarkable two-way relationship between medicine and engineering.

Due to the breakthrough of science and technology in the last two centuries, modern medicine has incorporated more and more instruments and techniques arising from both the medical and the engineering development. In the last half century, the complexity of the techniques and instruments used in medicine makes both branches of knowledge so closely linked that a new branch of engineering has arose, called biomedical engineering, exclusively dedicated to the study of engineering in the medical scope. The PhD program in which this thesis is framed, health and welness technologies, shows the need for this intimate link between medicine and engineering which allows to propose and study new tools for diagnosis and treatment.

Cardiology has been one of the medical fields where technological advances have played a crucial role. The discovery by Einthoven of the electrocardiography was perhaps one of the great steps in this regard ***[Einthoven 1906]***, since it allowed cardiologists to study in a simple and accessible way the electrical activity which modulates the cardiac muscle contraction. Since then, the bond between cardiac electrical activity and cardiac diseases has been deeply evaluated, and has provoked the appearance of a medical specialty dedicated to the study of the heart electric behaviour: cardiac electrophysiology.

One area of cardiology in which the study of electrical activity is more important, and therefore the connection between medical practice and engineering is essential, is the area of cardiac arrhythmias. Many cardiac arrhythmias are originated by disturbances on the heart's electrical system, and an electrophysiological study can provide their adequate treatment. In this thesis new diagnostic techniques for one of the most common arrhythmia in clinical practice, atrial fibrillation (AF), will be tackled. AF is a non mortal arrhythmia which has a large prevalence in the eldelry, affecting more than 10% in the population older than 70 years ***[Krahn 1995]***, and the general prevalence will increase due to the the population aging. In addition, currently there is no broad consensus on the nature of the mechanisms that initiate and sustain this cardiac arrhythmia, so the pharmacological treatments do not have the expected success taking into account the magnitude of this heart disease.

1.1. Motivations

During the last three decades the growth of new maping techniques to record the atrial electrical activity in both experimental and clinical practice has promoted the appearance of new theories regarding the nature of the mechanisms sustaining AF ***[Haissaguerre 1998, Jalife 2002, Sanders 2005]***. These new theories maintain that AF can be sustained by certain atrial regions whose electrical activity in form of high frequency rotors promotes the fibrillatory behaviour on the rest of the tissue ***[Narayan 2012, Haissaguerre 2015, Atienza 2014]***, opposing to previous theories which defended the absence of dominant atrial regions in AF ***[Allessie 2014]***. The focal theory has promoted the development of novel therapies based on the electrical isolation of such dominant regions in order to detain the AF. Although there is still certain controversy about this novel theory and its therapies ***[Jarman 2012, Benharash 2015]***, the evidences about its usefulness in clinical practice are becoming a great advance in the AF therapies ***[Narayan 2014, Haissaguerre 2014, Atienza 2014]***.

The development of these new therapies has been emcompassed with novel methods to characterize the electrical activity of AF, in order to map the position of such dominant regions and to guide the isolation procedures. The most extended mapping systems are based on the recording of the atrial electrical activity through catheters inserted into the atrial cavity through blood vessels. The great advantage of this mapping technique is its accuracy, as it allows obtaining the atrial electrical activity locally and reliably, and allows identifying the dominant regions either by using monopolar catheters to measure the frequency of the atrial signal ***[Sanders 2005, Atienza 2009]*** or by using multipolar catheters to find focal or reentrant sources ***[Narayan 2012]***.

Although these systems have proven their validity, their use in clinical practice is quite limited, since invasive mapping can be only carried out once the

patient has already been selected for the ablation procedure. In addition, the spatial resolution of the catheters is quite limited, so although they provide precise electrical recordings, the percentage of atrial area recorded and the relatively high spacing between electrodes may not be enough to clearly identify the underlying electrical pattern ***[Benharash 2015]***.

In order to provide the cardiologist information regarding the AF maintenance mechanisms prior to the ablation procedure, non-invasive techniques for atrial mapping have been developed. The basis of these techniques is the use of Body Surface Potential Mapping (BSPM) systems in order to record the atrial electrocardiographic activity on the torso with the greatest accuracy ***[Guillem 2009]***. BSPM recordings are being used to non-invasively characterize the atrial activity during AF episodes, since the surface signal contains relevant charateristics regarding the underlying AF process ***[Guillem 2013]***. Furthermore, the electrocardiographic imaging (ECGI) technique allows using the BSPM recordings to reconstruct the former electrical activity in the atrial surface ***[Messinger-Raport 1990]***. This atrial activity non-invasively obtained allows characterizing the AF patterns with greater spatial resolution than other invasive techniques, and both BSPM and ECGI can be used to identify atrial drivers sustaining AF in form of high frequency rotors.

BSPM and ECGI present promising results for helping in selecting and guiding AF ablations, and can potentially constitute a major a breakthrough in the diagnosis and treatment of AF. However, the intrinsic chaotic nature of the AF electrical patterns supposes a great challenge for using non-invasive techniques, whose accuracy raises some skepticism in the scientific community. Moreover, the use of various methods of signal processing to extract the relevant electrophysiological information feeds the controversy over the reproducibility and suitability of these analytical methods. Finally, this controversy adds to the lack of a scientific consensus on the nature of the maintenance mechanisms of AF, which may imply that certain methods may be useful in certain cases, but may not cover the full range of AF patients.

Thus, given the novelty of BSPM and ECGI systems as well as the theories in whose basis these systems are supported it is mandatory to validate them before they can be recommended to the clinical community as a first-line alternative.

1.2. Objectives

The aim of the present thesis is to characterize both BSPM and ECGI systems as non-invasive diagnostic tools of AF patients. Concretely, whether the information regarding the AF drivers in form of high frequency rotors provided by both systems is univocal and useful for clinical practice will be addressed, and also how their diagnostic capacity can be improved. To do so, we will make use of electrophysiological signals from both AF patients as well as from mathematical

models of the atrial electrical activity. The main objective of this thesis can be broken down into the following points:

- To study the ability of the BSPM systems to identify surface reentrant fibrillatory patterns in patients with AF, and whether this identification and location is useful for AF diagnosis.
- To evaluate the effect of the electrocardiographic projection of the atrial signal on the patient's torso and the consequences of this electrical projection on BSPM and ECGI maps, specifically for AF electrical patterns.
- To assess the spatial resolution of BSPM systems, both regarding the number of electrodes and their distribution, so that the non-invasive identification and location of AF drivers be clinically useful in simplified BSPM systems.
- To evaluate the effect of the signal processing involved in the noninvasive detection of atrial drivers both by BSPM and ECGI, namely the phase transform and the narrow-band filtering, and how this processing affects the atrial driver detection.
- To assess the reliability of ECGI systems in non-invasively detecting AF drivers against uncertainties in the system conditions, such as electrical noise or spatial errors.
- To propose new methods to reduce the spatial uncertainties in ECGI systems and increase their diagnostic power.

1.3. Structure of the thesis

This thesis is structured in the following chapters:

Chapter 2: State of the art. This chapter broadly describes the main concepts addressed in this thesis. Atrial electrophysiology will be introduced including a deep description of atrial fibrillation and its sustaining mechanism theories and therapies. Non-invasive diagnostic techniques for AF diagnosis will be introduced concretelly electrocardiography, body surface potential mapping and electrocardiographic imaging. Moreover, a modest review of the mathematical formalisms involved in these techniques and used in cardiac mapping will be addressed. Finally, the varying kinds of mathematical models used for AF investigation will be introduced, from the cell to the whole body models.

Chapter 3: General materials and methods. The aim of this chapter is to describe the common database and methods used during the thesis. The mathematical simulation of atrial fibrillation will be described, as well as the recording protocol for AF patients. Dominant frequency and rotor detection methods will be also addressed.

Chapter 4: Body surface localization of left and right atrial high frequency rotors in atrial fibrillation patients. This chapter describes how the narrow-band pass filtering allows BSPM systems to non-invasively identify and locate reentrant AF drivers. Furthermore, simplistic mathematical models are used to describe the projection of the atrial electrical activity during AF episodes on the torso and its implication on the surface electrical maps.

Chapter 5: Minimal configuration of body surface potential mapping for discrimination of left and right atrial drivers during atrial fibrillation. The number and configuration of the BSPM electrodes are assessed in this chapter in order to investigate the optimal BSPM configuration for non-invasive AF driver identification.

Chapter 6: Understanding phase mapping and temporal filtering for reentrant activity identification in atrial arrhythmias. This chapter describes how the phase transform and the narrow-band pass filtering affect the ability of EGM, BSPM and ECGI systems to detect reentrant patterns, and how both techniques may be applied in order to obtain the best performance.

Chapter 7: Highest dominant frequency and rotor positions are stable markers for atrial driver location in non-invasive mapping of atrial fibrillation. In this chapter, the stability of the dominant frequency and rotor position measurements in ECGI systems will be tested against uncertainties in the system conditions, such as electrical or spatial noise.

Chapter 8: Solving inaccuracies in anatomical models for electrocardiographic inverse problem resolution by using electrical information. This chapter describes how the curvature of the L-curve can be used to reduce the spatial uncertainities on the atrial anatomy location for ECGI systems.

Chapter 9: Discussion and conclusion. The results and main findings introduced in this thesis are discussed and compared with previous works. The conclusions are listed and a guideline for future works is proposed.

Chapter 10: Contributions. The scientific contributions associated to this thesis and derived from the present dissertation are listed in this chapter. The scientific framework in which this thesis has been involved is also described including the research stays and collaborations.

Chapter 2

State of the art

This chapter reviews the fundamentals on the different research fields that are discussed in this thesis. This is a multidisciplinary work that comprises different fields, as cardiology, electrophysiology, electrocardiographic interpretation or computing simulation, so a broad introduction for each topic is presented in this chapter.

2.1. Introduction to atrial fibrillation

2.1.1. The cardiac electrical activity

The heart is the muscular viscera located in the centre of the thoracic cavity whose main function is to pump blood throughout the body supplying the nutrients and oxygen for the cellular homeostasis. This pumping is provoked by rhythmic contractions of the cardiac muscle which ejects the blood out of the cardiac cavities and is mediated by the cardiac valves that avoids the blood retraction.

The contractions of the heart occur as a consequence of the electrical activation of individual myocardial cells, which experience an increase in their intracellular potentials. This change of the transmembrane electric potential, called Action Potential (AP) is generated by a sequence of ion fluxes though specific ion channels located in the membrane of myocardial cells (see Figure 2.1), and is the responsible of the myocardial mechanical contraction.

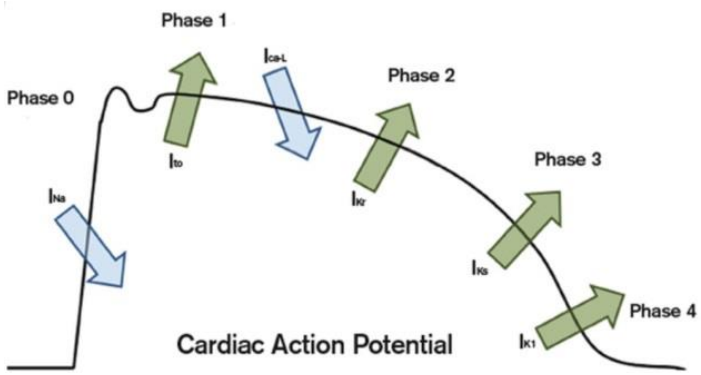

Figure 2.1 – Cardiac action potential. From [Lancet 2008].
The sodium current provides the depolarization of the cardiac cell (Phase 0), calcium current maintains the potential in high values to promote cell contraction (Phase 1 and 2) and potassium current returns the cardiac cell to the resting potential (Phase 3 and 4).

In a healthy heart, electrical activation is initiated by an autonomous stimulus generated at the sinoatrial node. This small mass of cells with pacemaker properties is located in the wall of the right atrium and has the ability to self generate an action potential. Electrical impulses are then propagated through the atrial wall allowing the atria to contract and arrive at the atrioventricular node, delaying the electrical propagation before activating the ventricular muscle promoting its coordinate contraction (see Figure 2.2). This sequence of electrical activations provokes the appearance of the electrocardiographyc signal on the torso.

When the electrical activation of the heart does not follow a natural spontaneous activation of the sinus node at 60 to 100 beats per minute (the so-called sinus rhythm), the heart rhythm is referred as a cardiac arrhythmia. Cardiac arrhythmias can be classified as supraventricular arrhythmias, when they involve heart structures above the atrio-ventricular node or as ventricular arrhythmias, when they mainly involve the ventricles.

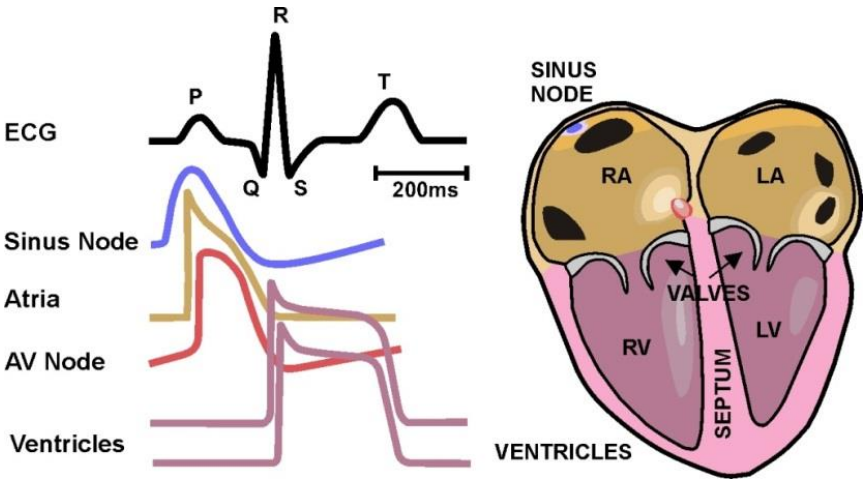

Figure 2.2 – Normal ECG tracing synthesis. From [Rodrigo 2014b].
ECG tracing in black and the APs responsible of each wave are depicted. Colors in APs correspond to those presented in the scheme of the heart. It can be observed how depolarization of atrial cells corresponds with the P wave, QRS complex and T wave correspond with depolarization and repolarization in the ventricles respectively.

2.1.2. Atrial fibrillation

Atrial fibrillation (AF) is a supraventricular arrhythmia characterized by a disorganized atrial activation. During the episodes of this arrhythmia, the atrial electrical activity is characterized by a set of rapid and disorganized wavefronts with variable amplitude, duration, extension and shape. This disorganized activity inhibits the synchronized atrial contraction and thus provoke inefficiency fn the atrial pump function. Furthermore, this kind of atrial propagation promotes an irregular and abnormally rapid ventricular function, since the conduction at the atrio-ventricular node remains intact.

Although AF is not fatal, this is not a benign arrhythmia, and influences negatively the quality of life of patients by altering the hemodynamic system and increasing the thromboembolic risk. This is due to the lack of mechanical function of the atrium, where the blood remains creating blood clots that can move to other regions of the body. In addition, AF is associated with increased morbidity and mortality ***[Krahn 1995]***, especially in cases of congestive heart failure ***[Fuster 2006]***.

The incidence of AF in the same patient can vary over time and this recurrence is used by the clinician to establish a diagnosis. Although there are different classifications of AF according to the clinical guidelines used, the classification according to incidence most used by clinicians is as follows ***[Fuster 2006]***:

• First detected. The clinician can distinguish a first episode of AF, although the episode can be or not symptomatic or self-limited. This classification is subject to uncertainty about the duration of the episode and about previous undetected episodes.

• Recurrent. When the patient has had two or more episodes of AF is considered recurrent.

- Paroxysmal. When AF starts and terminates spontaneously.
- Persistent. When AF is maintained for 7 days and requires pharmacologic therapy or cardioversion for termination. This category also includes cases of long-term FA (over a year), usually leading to permanent AF, in which case cardioversion has failed or has not been attempted.

The first detected AF may be either paroxysmal or persistent.

• Permanent. It occurs when the patient has a state of continuous AF that cannot be stopped, or when after cardioversion the patient takes a new episode of AF after a short period of time.

A set of processes collectively referred as atrial remodeling add complexity to the physiology of AF ***[Allessie 2002]***. Atrial remodeling is a set of changes on atrial tissue properties as a result of AF episodes, which favours the onset and maintenance of the arrhythmia. This remodeling can be divided into three types:

• Electrical remodeling. Alteration of the electrophysiological properties resulting in a shortening of the atrial refractory period. It develops during the first few episodes and helps to increase the stability of AF.

• Contractile remodeling. Loss of myocardial contractility muscle that persists after restoration of sinus rhythm.

• Structural remodeling. It is associated with the appearance of atrial fibrosis that occurs when the AF is maintained for long periods of time.

While the first two types of remodeling are reversible, structural remodeling persists for very long periods of time even after interruption of fibrillation ***[Wyse 2004]***.

2.1.3. Mechanisms of initiation and maintenance of atrial fibrillation

The mechanisms underlying the initiation and maintenance of AF are not yet fully known. During the twentieth century the theories currently still debating were forged, and these have been defended with greater or lesser force depending on the diagnosis and treatment techniques that have been developed over the last 100 years. Early theories which attempted to explain the mechanisms of AF were based

on the existence of multiple random sources distributed around the atrium ***[Winterberg 1907]*** or the existence of propagation in a closed circuit ***[Mines 1913]***. These theories were the basis of the explanation of the mechanisms of AF during the entire first half of the twentieth century, and that by themselves, or with minor variations, were dominant throughout this period of time ***[Rosenblueth 1947, Scherf 1958]***. However, the modern age of research about AF began with the hypothesis published by Moe and Abildskov ***[Moe 1959],*** which contradicted the previous two theories. This novel approach proposed the possibility that fibrillatory conduction could occur as a result of a random propagation of multiple wavefronts on the atrial tissue independently of any arrhythmic initiator event.

Moe et al. demonstrated, using a computational model, that fibrillatory conduction as observed during AF episodes could be caused by the presence of random wave propagation in inhomogeneous tissue ***[Moe 1964]***. Thus, AF was defined as a self-sustaining process independent from either a promoter event, such as an ectopic focus, or the atrial structure needed to maintain a circular propagation. However, refutation or confirmation of this hypothesis had to wait 20 years until the development of recording techniques that allowed capturing the electrical activity in a sufficiently large number of electrodes simultaneously.

In 1985, Allesie et al. ***[Allessie 1995]*** were able to record the electrical activity of dog hearts during AF, induced by high frequency stimulation. These recordings were the first demonstration in vivo that multiple wave propagation could be responsible for the maintenance of AF. However, this study also concluded that the minimum number of different wavefronts which would allow the maintenance of AF was between 4 and 6, since with a smaller number of wavefronts they joined with each other restoring sinus rhythm. Moreover, this theory defended a maintenance mechanism of the arrhythmia, but did not throw light on its initiation.

However, the multiple wave's theory was not the unique attempt to explain the maintenance of AF. Dr. Haisagguerre demonstrated that AF episodes could be initiated by focal triggers located mainly at the pulmonary veins and characterized by their rapid activation rate ***[Haissaguerre 1998]***. At the same time, Jalife et al. demonstrated both theoretically and experimentally ***[Jalife 1998, Jalife 2002, Jalife 2004, Berenfeld 2001]*** that maintenance of AF could be explained by a rotatory pattern, where a single electrical wave turns over a refractary region in a high activation rate, provoking fibrillatory conduction in their surroundings. Rotor theory maintains that there is a primary generator, in this case a functional reentry, responsible of the maintenance of the fibrillatory activity which appears when the atrial tissue presents a set of abnormal electrophysiological characteristics, as reduction of refractory period or decrease of conduction velocity ***[Jalife 2002, Akar 2000].***

Therefore, the different theories that attempt to explain the mechanisms of initiation and maintenance of atrial fibrillation can be classified into two groups:

• Focal theory, which suggests that AF is caused by the irregularity present on the interactions between the high frequency wavefronts produced by a primary generator (ectopic focus or functional microoreentry) and the variable refractoriness properties present in the atrial tissue (see Figure 2.3A-B). Several studies indicate that the pulmonary veins are the most common areas that act as primary generators ***[Chen 1999]***, although these have also been found in the superior vena cava, ligament of Marshall, left posterior wall, crista terminalis and coronary sinus ***[Tsai 2000, Lin 2003]***.

• Multiple waves hypothesis, which proposes that the irregular atrial activity is a consequence of a primary arrhythmogenic mechanism ***[Moe 1959]***, wherein the fractionation of the wave fronts propagating through the right atrium results in the self-maintenance of the chaotic activity (see Figure 2.3C). Tissue heterogeneity is vital in the explanation of this hypothesis, as it is responsible for the fractionation and perpetuation of the wavefronts. According to this theory, an atrial tissue with wide variability in their refractory period (being quite short) as well as delayed conduction properties has an increased probability of developing sustained AF. This theory is nowadays defended by the existence of transmural conduction that explains the endocardial and epicardial electrical breakthroughs that otherwise are attributed to focal activity ***[Eckstein 2013]***.

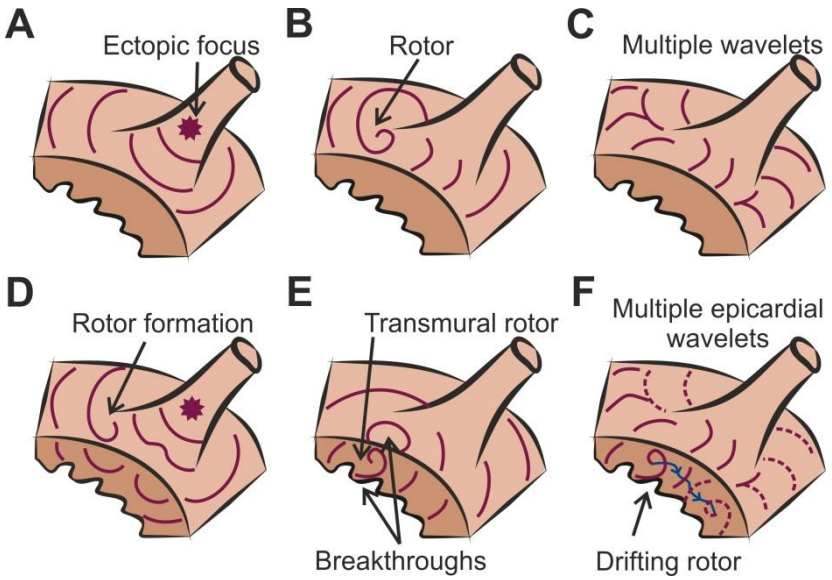

Figure 2.3 – AF mechanisms. From [Guillem 2016].
(A) Ectopic focus on the pulmonary veins. (B) Rotor in the piosterior wall of the left atria. (C) Multiple wavelets. (D) Rotor formation by an ectopic focus in the pulmonary veins. (E) Transmural rotor. (F) Mutiple epicardial wavelets provoked by transmural drifting rotors.

Although the two main theories about the maintenance of AF seem to be mutually exclusive, they are closely linked and must be interpreted togheter. At the case of focal theories, atrial rotors can be initiated by a focal discharge due to a wavefront break (Figure 2.3D), so the focal triggered activity could be acting as an AF initiation mechanism. Moreover, the existence of intramural rotors can be reflected as breakthroughs in the atrial wall and they can be interpret as endo or epicardially focal sources (Figure 2.3E), thus focal and rotor hyphothesis are not mutually exclusive. Finally, the existence of transmural and drifting rotors can create also multiple epicardial wavelets (Figure 2.3F), so focal and multiple wavelets theories could be compatible.

2.1.4. Clinical treatment of atrial fibrillation

Due to the ambiguity about the initiation and maintenance mechanisms of AF its therapies do not have the success rate expected for such an extended arrhythmia. In order to eliminate or reduce the effects of this arrhythmia, pharmacological and surgical treatments are commonly used. Surgical treatments can be differentiatied between as heuristic approaches or mechanistically based. Moreover, electrical cardioversion is commonly used to arrest AF episodes, but does not prevent for the apparition of new AF episodes.

Pharmacological therapies

Antiarrhythmic drugs are the most common treatment option for reducing AF episodes or its symptoms. The main objectives of these drugs are preventing arrhythmia episodes, controlling cardiac frequency –sinus and atrioventricular nodes–, anticoagulating blood or performing chemical cardioversion. In patients with paroxysmal AF and whose atrial tissue has not developed remodelling, arrhythmia usually ends after cardioversion. After restoration of sinus rhythm, the administration of antiarrhythmic drugs has been shown to improve recurrence ratios ***[De Simone 1999]***. For patients with permanent AF and a remodelled atrial tissue, therapies that seek to restore normal rhythm are not recommended, and patients are treated with drugs in order to control the ventricular rate.

Antiarrhythmic drugs are classified depending on the receptor or ionic mechanisms affected, and they can have an effect in many ionic currents at the same time despite having a prevalent effect in some ion channels. However, since antiarrhythmic drugs do not affect only the atria, they have important side effects which increase mortality rates ***[Nattel 1998, Nattel 2002]***.

Heuristic surgical therapies

Due to the knowledge of the chaotic nature of AF propagation patterns, the first attempt to surgically intervene in AF patients was the MAZE procedure. This highly aggressive treatment compartmentalizes the atrial tissue by radiofrequency

ablation or by tissue dissection (see Figure 2.4). The overall aim is that the area of each separate region is insufficient for maintenance of the arrhythmia, as there is not enough space to accommodate the required number of multiple wavefronts to propagate the fibrillatory activity, or in case there is a fibrillatory source its activity is not propagated to the rest of the atrium.

Although MAZE ablation technique has been demonstrated to be effective in disrupting AF, this clinical practice is very aggressive and limits the normal atrial function ***[Calkins 2007]***. Therefore, modified MAZE strategies have been proposed with less ablation lines in order to maintain the mechanical function of the atria ***[Lee 2015]***.

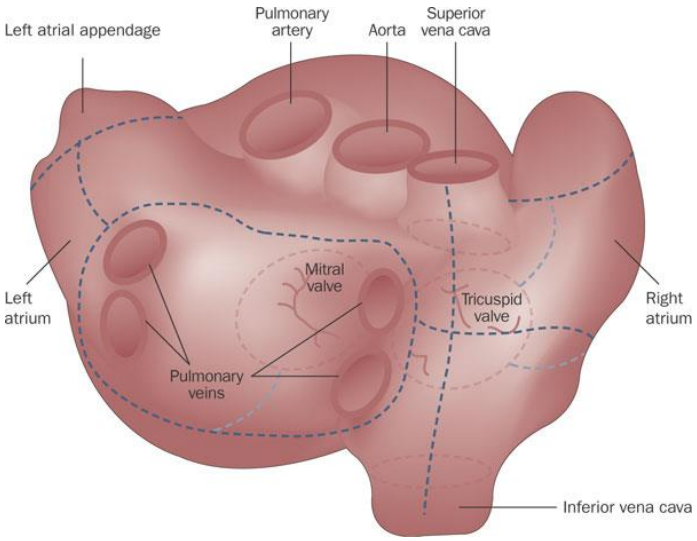

Figure 2.4 – MAZE ablation scheme. From [Lee 2009].
Atrial tissue is segmented into small sections in order to prevent the apparition of fibrillatory processes.

Due to the high aggressiveness of the MAZE approach and the empirical evidences supporting that in most patients AF can be caused by spontaneous triggered activity at the pulmonary veins ***[Haïssaguerre 1998]***, one of the most extended surgical therapies for AF patients is the pulmonary vein isolation (PVI). This technique consists in the electrical isolation of the pulmonary veins from the posterior atrial wall tissue, commonly by using radiofrequency ablation (see Figure 2.5A). This procedure can be applied with some additional linear ablations, in order to isolate other atrial regions which have been proved to provoke AF episodes, like the atrial appendages or the cava veins (see Figure 2.5B-C).

Pulmonary vein isolation has become the most used surgical treatment for patients in whom the pharmacological treatment has not the expected effect. However, the success rate of this technique is highly dependent on the AF state,

showing up to 85% AF episodes in paroxysmal AF patients down to 28% in persistent AF patients ***[Chao 2012]***. This wide range of success rate can be related with the mechanisms that govern the AF episodes and the pathophysiological state of the atrial myocardium. Paroxysmal AF patients are presumed to be at the first stages of the fibrillation process, and its electrical pattern is mainly governed by focal triggered activity or simple stable rotors, which can be easily isolated by PVI. However, in persistent AF patients the atrial tissue has been higly electrically and structurally remodeled, so the electrical pattern can be maintained by fibrillatory sources everywhere or by multiple wavelets, so PVI does not prevent the fibrillatory process.

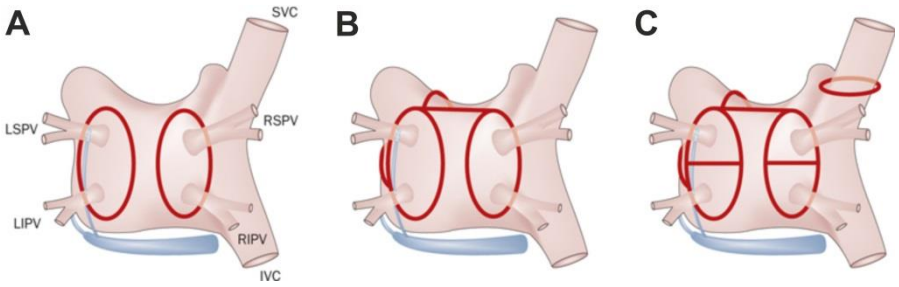

Figure 2.5 – Pulmonary vein isolation. From [Dewire 2010].
(A) Circumferential ablation lesions around the pulmonary veins. (B)PV circumferential lesions with "roof" line and a "mitral isthus" line connecting mitral valve and PV circle. (C) Similar to panel B, but with additional linear ablation lesions between superior and inferior PVs and an encircling lesions in the superior vena cava.

Mechanistic based surgical therapies

Experimental and theoretical studies demonstrated that AF could be maintained by a hierarchical process governed by a focal source, as trigger activity or reentrant patterns ***[Jalife 1998, Haissaguerre 1998]***. Thus, new therapheutic approaches emerged which tried to individually characterize the AF process for each patient by identifying the AF sources, with the aim to electrically isolate only such atrial regions. However, triggered activity and rotors are easily identified in experimental procedures but their translation to the clinical practice was not immediate. Thus, several analysis techniques to identify atrial drivers and to guide the ablation procedures have been defended.

The first attempt to a guided ablation procedure was based on the EGM signal fractionation ***[Nademanee 2004]***. The basis of this technique was to locate the atrial regions with complex fractionated atrial electrograms (CFAEs), since these regions were assumed to harbor AF drivers. The fractionation of the EGM signal was defended to be provoked by focal microreentries, slow conduction areas, pivot or anchor points or for common collision points of the multiple wavelets ***[Allessie***

1996]. However, it has been demonstrated that some of the mechanisms causing CFAEs are not dominant sources, like the fractionation of the signal at the borderzone of the mother rotors and areas of higher dominant frequencies ***[Kalifa 2006]***. Furthermore, clinical application of this technique did not increase the success ratio of the ablation procedures ***[Providência 2015]***, so nowadays its use has decreased.

Since trigger drivers and rotors are characterized by a higher activation rate than the rest of the tissue, next EGM analysis technique to locate AF drivers was based on the Dominant Frequency (DF) identification. This technique measures the activation rate of an atrial region from the spectral content of its EGM signal, since the greater spectral contribution of the EGM signal reveals its activation rate in Hz or beats per second. DF technique has been used first in experimental procedures in which the atrial electrical activity is recorded optically, and revealed the DF gradient from the driver region to the rest of the atria (see Figure 2.6) ***[Mansour 2001]***.

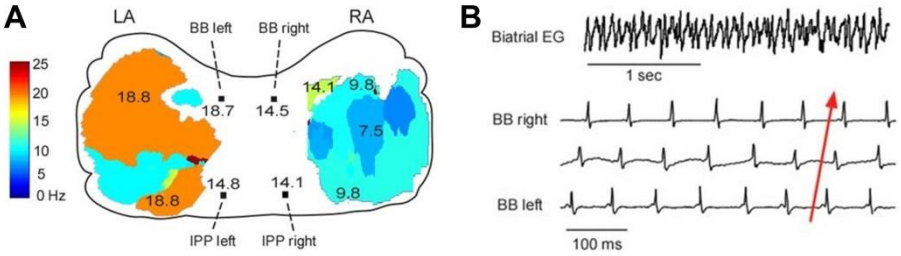

Figure 2.6 – Dominant Frequency in Optical Mapping. From [Mansour 2001].
(A) DF maps of epicardial surfaces of LA and RA, with values of DFs along Bachmann's bundle (BB) and infero-posterior pathway (IPP), showing a DF decrement from LA to RA. (B) Recordings from 3 electrodes along BB, bottom tracing being most leftward, showing directionality of activation from LA (fast DF) to RA (slow DF).

The use of DF methodology in clinical practice was introduced by the analysis of the activation rate of EGM signals throughout the atrium by using intracavitary catheters ***[Atienza 2009]***. Atrial navigation systems allow sequentially obtaining the local DF values along the whole atrium and then applying the electrical isolation in regions where higher activation rates are detected (see Figure 2.7). Clinical studies over large patient populations have proven the effectiveness of this technique, whose success ratio is at least comparable to the PVI technique alone ***[Atienza 2015]***. However, the DF mapping is nowadays sequentially performed in AF patients by placing the catheter on different atrial regions and measuring their activation rate. This latter has provoked controversy over whether the detected pattern is stable over time ***[Jarman 2012]***.

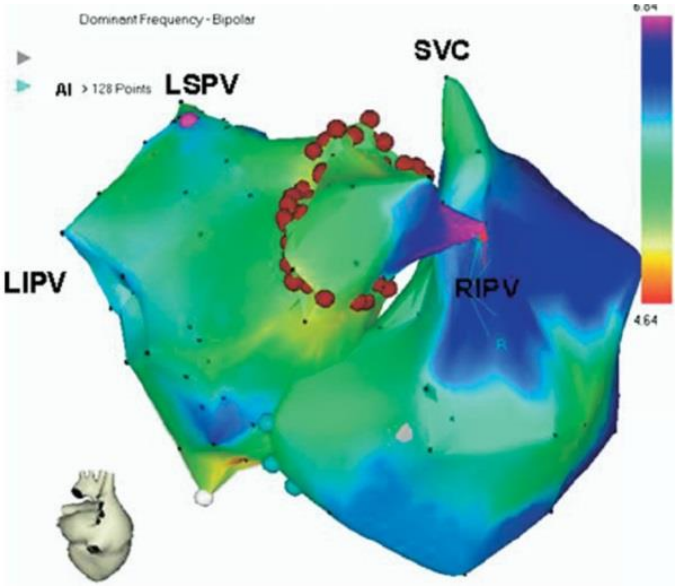

Figure 2.7 – Dominant Frequency in patients. From [Atienza 2009].
Real-time atrial DF map (posterior view; CARTO system) in a paroxysmal AF patient. Purple, primary DFmax site on right intermediate PV (RIPV). Red dots, circumferential ablation line. AF terminated after RIPV isolation.

Last AF driver identification technique is based on mapping the atrial surface by using multipolar basket catheters in order to obtain a simultaneous and panoramic view of the atrial electrical activity (see Figure 2.8). Then the multiple EGM recordings are analyzed with the focal impulse and rotor modulation (FIRM) technique that allows localizing the AF drivers in the atrium ***[Narayan 2014]***. This technique has been also clinically tested in large populations and its success ratio is greater than PVI technique alone ***[Narayan 2014]***, although both the electrophysiologcal mapping system and the signal analysis have generated controversy ***[Benharash 2015]***.

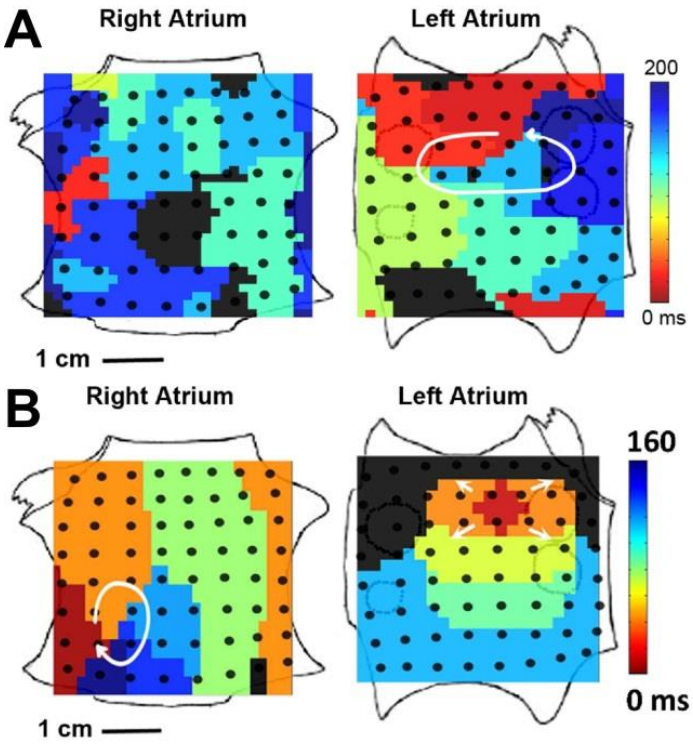

Figure 2.8 – FIRM mapping. From [Narayan 2012].
(A) LA rotor with counterclockwise activation and disorganized RA during AF in a 60-year-old man. Ablation at LA rotor terminated AF to sinus rhythm in <1 min. The patient was AF-free on implanted cardiac monitor at >1 year. B) RA rotor (clockwise) and simultaneous left atrial focal impulse (arrowed) during persistent AF in a 47-year-old man. Ablation at RA rotor terminated AF to sinus rhythm in 5.5 min.

2.2. Electrocardiography

Electrocardiographic signals (ECG) recorded on the human torso has become one of the most powerfull diagnosis techniques in cardiology since Einthoven invented its recording technique. ECG signals have been broadly studied for all cardiac diseases, and more specifically in cardiac arrhythmias, due to the importance of the cadiac electrical activity in such cardiac diseases. Atrial fibrillation is not an exception, and ECG signals have been broadly used to diagnose and classify AF patients.

The standard ECG leads are recorded by placing 3 electrodes on the right arm, left arm and left foot respectively, defining a triangle around the heart ***[Einthoven 1906]***. The electric potential is studied then as the potential difference between each pair of vertices of the triangle (Lead I, II and III). Three additional

leads are calculated as the difference between a one vertex of the triangle and the average potential of the two other vertexes, called augmented derivations (aVR, aVL and aVF). Finally, six more electrodes are placed on the anterior and left side of the chest, defining the precordial leads (V1-V6). Potential signals on precordial leads are measured with respect to the Wilson Central Terminal (WCT), which is the average of the limb signals (right and left arms and left leg).

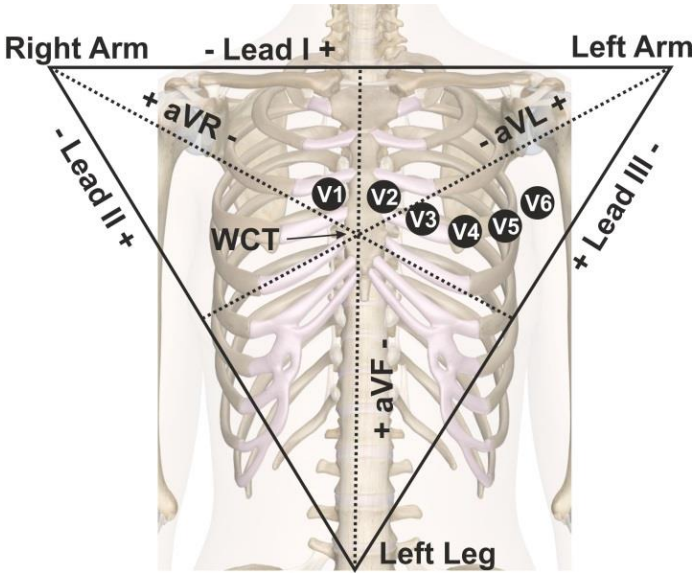

Figure 2.9 – 12-leads ECG.
Einthoven triangle for ECG recording (right arm, left arm and left leg). Leads I, II and III at the three edges of the triangle, and augmented leads (aVR, aVL and aVF) between vertex and midle point of each side. The precordial leads (V1-V6) are calculated as the potential between each precordial recording site and the Wilson Central Terminal (WCT), the average potential of the Enthoven triangle vertex.

2.2.1. Electrocardiography in AF

The study of the ECG is essential for diagnosis of AF, since its syntoms can be easily attributed to other diseases. Although some AF patients can suffer severe syntoms like breathlessness, intense chest pain or unconsciousness, in most cases AF provokes mild symtoms like palpitations or dizziness, so the diagnosis by its syntoms suffers from high uncertainty. Therefore, the ECG is broadly used to diagnose AF, since the ECG trace is unequivocal (see Figure 2.10). Whereas a healthy ECG shows the atrial activation as a P wave and a regular ventricular rate (RR), an AF trace lacks P waves and shows irregular AF waves between ventricular activations, whose RR interval is irregular too. Due to the importance of the AF episode length and its incidence, in patients suspected of having AF

Holter systems are used to record the ECG signal for long periods of time (from hours to weeks) in order to establish the impact of the disease in each patient ***[Su 2013]***.

Besides the use for diagnosis and incidence classification, analysis of classic 12-lead ECG signals can provide additional information about AF mechanisms and prognosis. The complexity of the atrial ECG waves, measured as fibrillatory wave rate ***[Slocum 1992, Holm 1998, Bollmann 2008]***, amplitude ***[Cheng 2013]*** or sample entropy ***[Alcaraz 2011]*** has presented a signifficant correlation with the degree of complexity of the atrial substrate or with the AF recurrence ratio. Moreover, the standard lead distribution has been used to study the activation rate of the atria during AF by measuring the DF of the ECG trace, reporting a good correlation between measurements from RA with lead V1 and from LA with V6 ***[Dibs 2008, Petrutiu 2009]***. However, the use of classic 12-lead ECG signal for AF characterization has severe limitations, due to the intrinsic complex nature of AF and to the location of the electrodes which do not allow adequate signal recording of both atria ***[Lankveld 2014]***. For this reason, electrophysiological measures over the 12-lead ECG only provide global measures of the fibrillatory process and do not allow the local characterization of the arrhythmia ***[Guillem 2013]***.

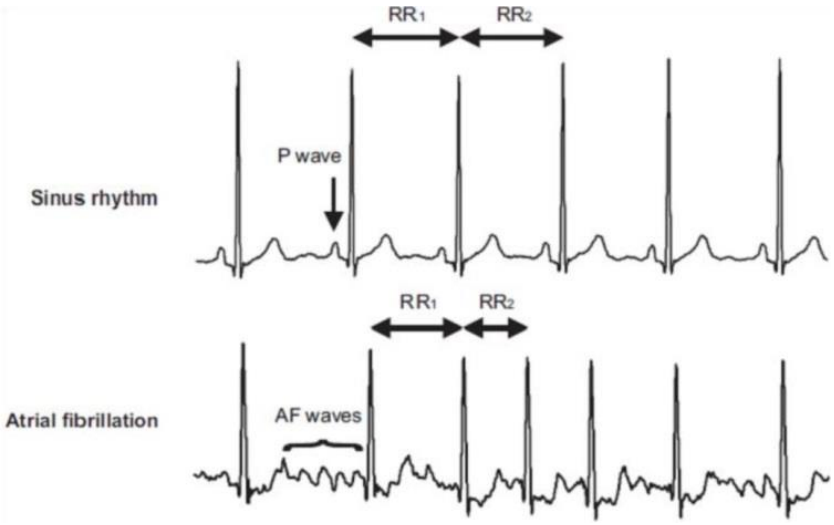

Figure 2.10 – AF trace at ECG. Extracted from [Guillem 2008].
ECGs during sinus rhythm (up) and during atrial fibrillation (down). Notice that during AF the ventricular activation rate (RR) is variable.

2.3. Body surface potential mapping

For most heart diseases the 12-lead ECG is accurate enough for the study of the electrical cardiac activity. This is because the simple pathologies with relatively uniform electrical patterns can be summarized as the activity of a single electrical dipole, so even the recording with 12 leads is redundant ***[Frank 1954]***. However, there are cardiac diseases in which the cardiac activity presents different wavefronts and the electric potential on the torso shows multiple maxima and minima, so the description by a single electric dipole is not correct in these cases, and the use of the classic ECG system cannot display accurately the whole electrical activity on the torso ***[Taccardi 1963]***. In order to accurately record the electrical activity on the torso in these more complicated heart diseases the registration with high spatial resolution of this electrical activity has been proposed.

The mapping system to record the surface electrical activity with high spatial resolution is called Body Surface Potential Mapping (BSPM). It consists of the electrical recording of the ECG signal with 32 to 256 electrodes on the patient's torso (see Figure 2.11). There is no standard for the number of electrodes used and for their position, although most systems tend to use more electrodes on the front due that the potential variation of the ECG signal is significantly larger in this region.

Figure 2.11 – Body surface potential mapping systems.
Two examples of electrode distribution for BSPM recording.

BSPM recordings allow the detection of electrical phenomena that the 12–lead ECG is unable to detect ***[Taccardi 1998, Carley 2003, Finlay 2005]***. For Brugada's syndrome, analysis of BSPM recordings have revealed that the QRS integral and the gradient of the ST segment are markers for this syndrome ***[Bruns 2002]*** and the presence of late potentials and ST segment elevation are markers of ventricular tachyarrhythmias inducibility ***[Eckart 2002]*** or that the BSPMs at the end of the QRS complex is a more robust indication of the Brugada's syndrome than the ST morphology ***[Guillem 2016]***. In Wolf–Parkinson–White patients

BSPM recordings can be used for the localization of accessory pathways and thus for guiding the ablation procedures ***[Dubuc 1993]***. At the case of atrial arrhythmias, it has been proven that BSPM recordings allow to detect the origin of focal tachyarrhythmias ***[SippensGroenewegen 1998]*** or to elucidate the reentrant circuit during atrial flutter ***[SippensGroenewegen 2000]***.

2.3.1. Body surface potential mapping in AF

The inherent spatial complexity of the atrial activity during episodes of AF makes the 12-lead ECG insufficient for the spatial characterization of atrial electrical activity, and BSPM systems solve these pifalls since allow recording the surface electrical activity in all its extension. Although registration by BSPM is a relatively mature technique, at present there are not many studies that use it for the study of AF. Guillem et al. showed that atrial propagation patterns could be identified in the surface potential maps ***[Guillem 2009]*** and such maps allowed assessing the organization degree during fibrillatory episodes. In a latter study, Guillem et al. also demonstrated that the electrical activity from the left and right atria are projected on different torso regions, and the measurement of the DF in such regions agreed with the intracardiac DF measures (see Figure 2.12). This work demonstrated that non-invasive measures of DF with BSPM would allow to discriminate between RA and LA dominant patients and therefore to planning ablation procedures.

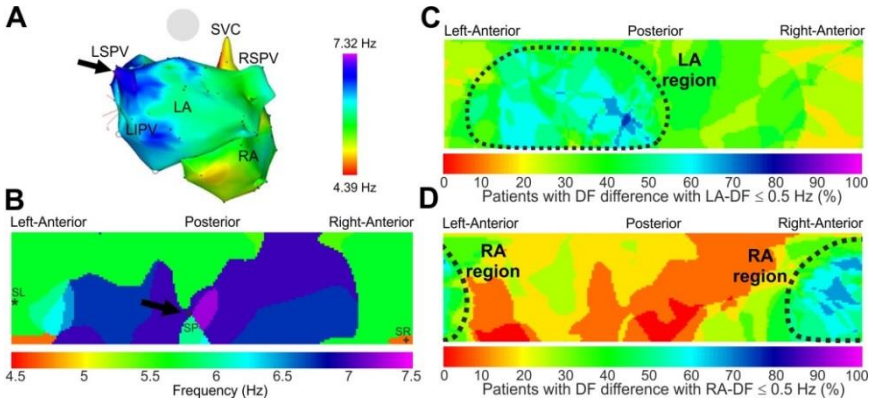

Figure 2.12 – Correlation between intra-cardiac and BSPM DF maps. Extracted from [Guillem 2013].

(A) DF map of the atrium. (B) DF map of the torso by BSPM. Black arrows point to the matching HDFs at the left superior PV (LSPV) and at the the center of the posterior body surface DF. (C) and (D) Summary maps showing the percent patients with the surface DFs <0.5 Hz different than the maximal left (C) and maximal right (D) intracardiac DFs. Areas outlined by the dashed curves represent the portion of the torso with a best correspondence with left and right EGMs

2.4. Electrocardiographic imaging

Electrocardiographic imaging (ECGI) is a medical tool for non-invasively obtaining the electrical activity on the cardiac surface. This technique uses three-dimensional models of the patient's torso and heart together with the surface electrical activity recorded with a BSPM system in order to reconstruct the electrical activity on the heart surface (see Figure 2.13). The reconstruction of the intracardiac activity requires a mathematical algorithm that solves the so-called inverse problem of electrocardiography, i.e. the calculation of epicardial potentials from BSPM recordings. Oppositely, the forward problem of electrocardiology provides the electricaly activity on the torso (ECG) from the cardiac electrical activity (EGM). Since the forward problem has a closed mathematical formulation defined by the biophysical equations and the torso conductor volume, such formulation can be inverted in order to obtain the epicardial electrical activity from the rest of the known variables ***[Horacek 1997]***. This methodology has been experimentally validated under pathological conditions in animal models and human studies ***[Oster 1997, Ghanem 2005]***.

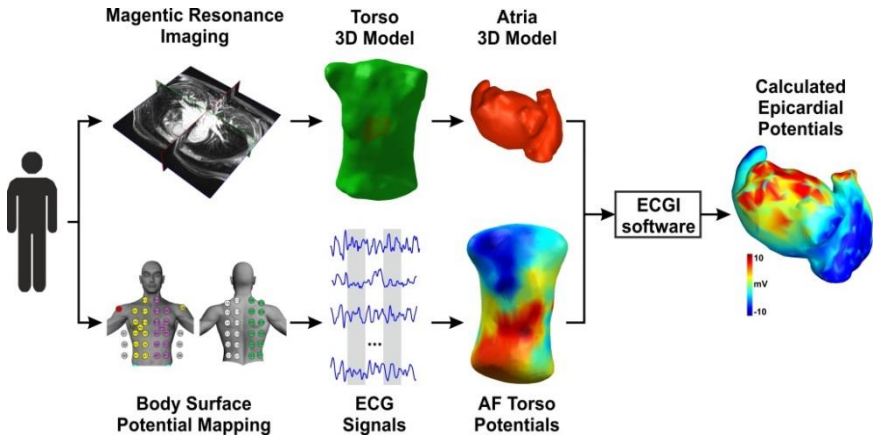

Figure 2.13 – Scheme of electrocardiographic imaging process.
Patient 3D models of the torso and atria are segmented from MRI images and toghether with the BSPM recordings allows calculating the epicardial potentials.

ECGI has been widely used to study cardiac diseases ***[MacLeod 1995, Oster 1997]***, since it provides non-invasively and prior to surgical procedures the intracardiac activity in a similar way than invasive methods based on catheters but with much greater spatial resolution. It has been used to assess the electrical circuit in Wolf-Parkinson-White patients ***[Berger 2011]*** and thus for guiding the ablation procedure. In patients with congestive heart failure, ECGI allowed to reconstruct the activation sequences for identifying suitable candidates for cardiac resynchronization therapy and for guiding lead placement ***[Dimaano 2010, Jia***

2006, Silva 2009]. ECGI has been also used to delimit the scar region in patients with myocardial infarction ***[Cuculich 2011]*** and for identifying the slow conduction regions that could provide the formation of reentrant arrhythmias. Due to the high spatial resolution and the simultaneity of the reconstructed electrograms, ECGI is highly adequate for the study of ventricular arrhythmias, such as ventricular tachycardia (VT), since it allows showing the VT formation and continuation ***[Wang 2011]*** with an acceptable risk to the patient.

2.4.1. Electrocardiographic imaging in AF

Electrical patterns from atrial arrhythmias are more complicated to reconstruct using ECGI because the atrial signal is masked by the QRS complex, that reflects the ventricular electrical activity. In the atria, ECGI has been used for characterizing atrial flutter scars ***[Wang 2007]*** or for identifying the origin of atrial tachycardias ***[Hocini 2015, Shah 2013, Roten 2012]***. However, AF is the atrial arrhythmia for which the ECGI presents more promising results, due to its temporal complexity which prevents from performing activation mapping based on sequential intracavitary recordings and the opportunity of noninvasively detecting potential fibrillatory drivers. Nevertheless, the complexity of fibrillatory patterns provokes some skepticism in the scientific community about the possibility that the inverse problem provides reliable results. In this sense, the existence of more than one wavefront precludes the use of physiology-guided techniques for the solution of the inverse problem, limiting its use to obtain epicardial potentials. In addition, the complexity of the fibrillatory patterns necessitates the use of signal processing techniques, which in turn introduces further uncertainty about the results.

For AF patients, Cuculich et al. demonstrated that fibrillatory patterns could be non-invasively reconstructed with ECGI ***[Cuculich 2010]***, and showed that the AF pattern presented an increasing complexity with the AF duration. In a more recent study, Haissaguerre et al. used the ECGI in a large cohort of patients for AF driver location prior to the ablation procedure, and the non-invasively detected atrial drivers were used to guide the ablation ***[Haissaguerre 2014]***. They found that the number of atrial regions containing drivers which had to be targeted to detain the AF process increased with the duration of continuous AF (see Figure 2.14). However, the findings of Haissaguerre's work regarding the mechanisms of AF maintenance detected by the inverse solution greatly differed from those from Cuculich's work. While Cuculich et al. rarely detected rotor activity (15%) in the inverse-computed epicardial maps and the most common detected pattern was multiple wavelets (92%), Haissaguerre et al. detected reentrant activity during 62% of the recorded time across the patient population. Differences between the findings of these two works could be explained by the signal treatment applied to the inverse solution, since the inverse-computed EGM trace greatly differ from a current EGM trace endocardially recorded.

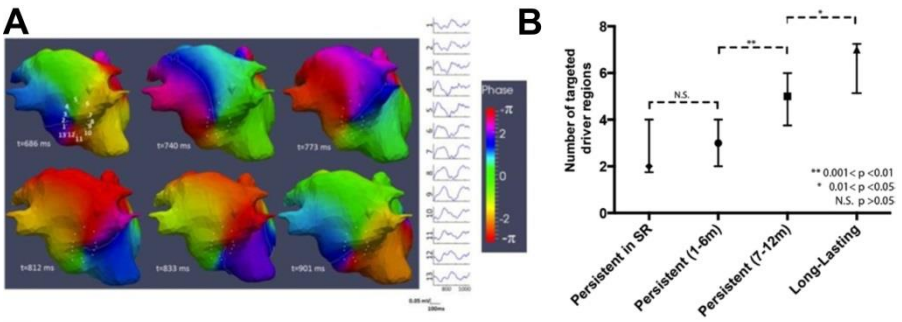

Figure 2.14 – Identification of ablation targets by ECGI. Extracted from [Haissaguerre 2014].

(A) Phase maps of the inverse-computed EGM showing a clockwise rotor in the posterior left atrial wall. Thirteen icEGMs around the rotor are depicted on the right. (B) The median (first and third quartiles) number of driver regions ablated to terminate AF increases with the duration of persistent AF.

Recently, our group published the first work in which AF patients were simultaneously recorded with ECGI and intracavitary multipolar catheteres and the accuracy of noninvasive estimation was tested against intracavitary measurements ***[Pedrón-Torrecilla 2016]***. Comparison between invasive and inverse-computed EGMs in voltage and phase domains revealed that inverse solution provides noninvasive estimations with a considerable amount of uncertainty, since the relative errors between invasive and non-invasive measurements were 32% for the voltage domain and 65% for the phase domain (see Figure 2.15). However, this work demonstrated that inverse-computed DFs correlated well with the invasive DF measures, and noninvasive measures in the frequency domain presented lower relative errors (9%) compared with voltage or phase measurements.

The ECGI technique is postulated then as a useful technique for AF characterization and for planning and guiding ablation procedures, since the *a priori* knowledge of the driver distribution can shorten the ablation procedure time. However, although some source identification methods, such as the idenfication of highest DF sites have been invasively validated ***[Pedrón-Torrecilla 2016]***, some other techniques such as rotor detection have not been validated against an independent technique yet, and reveal great differences among studies ***[Haissaguerre 2014, Cuculich 2010]***. Thus, nowadays one of the main challenges associated to ECGI mapping in AF patients is the validation of the signal processing applied to the inverse solutions, because there are still some questions to be solved. The signal processing applied to inverse-computed EGMs must be then profusely studied, with the aim of choosing those methodologies which provide the most accurate solutions and can help in planning and guiding ablation procedures.

.

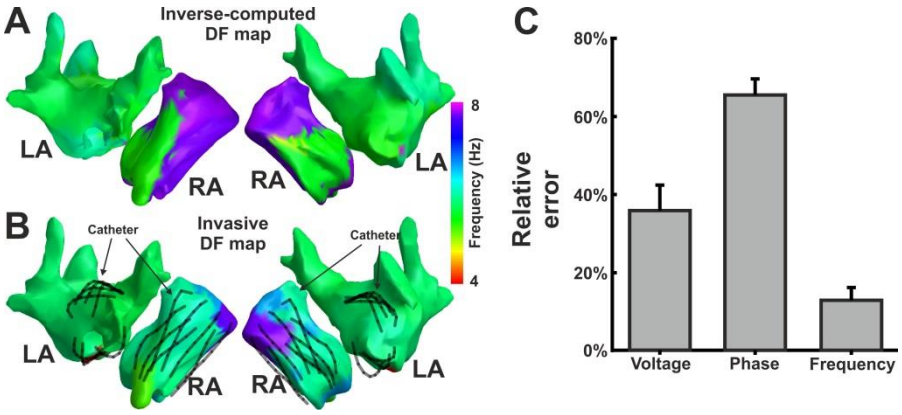

Figure 2.15 – Non-invasive DF map by ECGI. Extracted from [Pedrón-Torrecilla 2016].

(A) Inverse computed and (B) simultaneously inctracardially recorded DF maps for a patient a multipolar catheter was sequentially placed in the right and left atria. (C) Numerical analysis of the relative error in the voltage, phase and frequency reconstruction in 2 patients for a total of 287 EGMs recorded.

2.5. Atrial fibrillation modelling

The breakthrough in computing power during the last decades has allowed cardiac modeling to become an essential tool in the investigation of cardiac arrhythmias. Mathematical modeling allows a much wider vision on pathological cardiac physiology as it allows the access to a range of variables not available in the experimental field and at the same time reduces costs and avoids technical and ethical problems. Moreover, mathematical models allow a multiscale overview, covering the ionic channels, cell, tissue, atrial anatomy and computation of electrocardiograms. This section offers a broad overview of the different types of mathematical models that are used in the study of AF.

2.5.1. Action potential modelling

The first attempt to mathematically simulate the electrical activity of a cell was carried out by Hodgkin and Huxley in the 50s ***[Hodgkin and Huxley 1952]***. They used experimental data from patch clamp measurements in giant squid axons and constructed a mathematical model to describe such results. Hodgkin and Huxley's formulation paves the way for the cellular electrical modelling and has constituted the basis of the majority of electrophysiological cell models developed from that time. Their model was based on the equivalent circuit of the cell membrane separating the intra and extracellular mediums and the ionic channels present therein (see Figure 2.16). Internal and external mediums were characterized as ideal conductors, the cell membrane was characterized as a capacitance C_m and

the currents through the ionic channels were represented by a variable resitance and a resting potential. Once all these elements are particularized, electrical laws can be applied in order to calculate the membrane potential values along time.

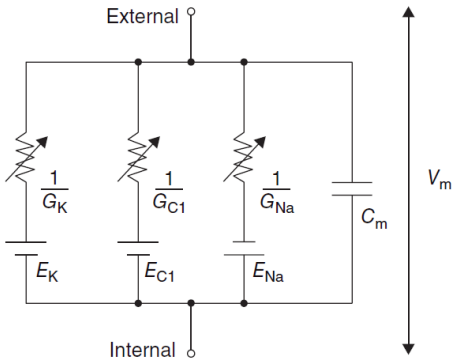

Figure 2.16 – Hudgkin and Huxley's cell model. Extracted from [Jalife 2009]. *Membrane voltage Vm depends on the charge of the membrane capacitor C_m which is modulated by the ionic channels (modelled as variable resistors or conductances) representing the different ionic currents.*

Although the basis of mathematical modeling is relatively simple, for an electrophysiologically accurate model it is necessary that all ionic currents be exhaustively characterized. Countless patch clamp experiments have been carried out in this sense, allowing the individual measurement of all these ionic currents in isolated cells, and these measures have been used to extract the electrical parameters which define the main ionic currents. First mathematical model of cardiac myocytes was done by Denis Noble by modifiying the Hodgkin and Huxley's model ***[Noble 1962]***, and the posterior experimental data allowed to improve its cardiac myocyte model with the description of ionic pumps and differentiation of ionic currents ***[McAllister 1975, Difrancesco 1985]***. This model was modified by Luo and Rudy to construct the first mammalian ventricular myocyte model ***[Luo and Rudy 1991]***, who was also improved by Iyer and ten Tusscher ***[Iyer 2004, ten Tusscher 2004]***.

Human atrial myocyte modelling began with two different models published at the same time in the late 90's: Courtemanche's model ***[Courtemanche 1998]*** and Nygren's model ***[Nygren 1998]***. They presented some differences in the action potential shape, as it can be observed in Figure 2.17, although both were based in the same experimental data. Posteriorly, Maleckar et al. improved the formulation of some repolarizing currents ***[Maleckar 2008]***, Koivumäki et al. included a detailed formulation for the sarcoplasmic reticulum and Ca^{2+} dynamics ***[Koivumäki 2011]*** and Grandi et al. also improved the Ca^{2+} management ***[Grandi 2011]***.

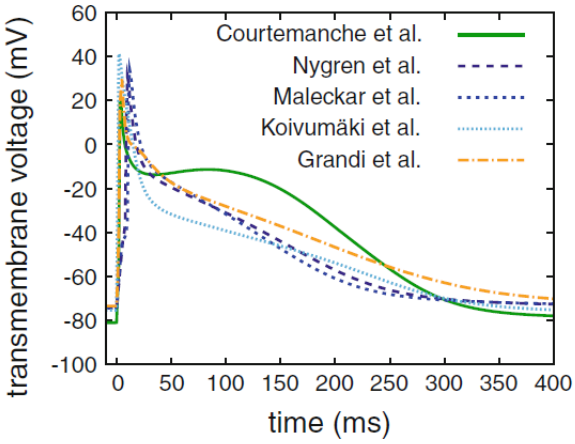

Figure 2.17 – Action potentials from different human atrial models. Extracted from [Doessel 2012].
Membrane potentials during an action potential for electrphysiological models of Courtemanche, Nygren, Maleckar, Koivumäki and Grandi.

Atrial myocyte mathematical models have been mainly used to evaluate the effect of the electrical and structural remodelation provoked by AF and their relation with the arrhythmia inducibility. Electrical remodelling has been observed to provoke a reduction in the AP duration, which has been reported to be caused by changes in some specific ionic conductances ***[Doessel 2012, Skasa 2001, Workman 2001, Brundel 2001]***. Besides, it has been shown that a reduced Ca^{2+} handling, which corresponds with lower intracellular Ca^{2+} transients, resulted in a reduction of cell contractility, another characteristic property of remodeled cells ***[Schotten 2001]***. Finally, the electrophysiological effect of the structural remodelling has been mathematically modelled as atrial myocytes electrically linked to cardiac fibroblasts ***[Maleckar 2009]***, and by the dilation of atrial cells which results in an increase in the membrane capacitance ***[Schotten 2002, Corradi 2012, Koivumaki 2014]***. All these mathematical simulations of single atrial myocytes have allowed investigating the relationships between the different ionic currents and their effect on the electrophysiological behavior of atrial cells as well as the effect of AF progression such as electrical and structural remodeling.

2.5.2. Tissue modelling

Although cell mathematical models provide very useful information for the study of cardiac arrhythmias they only reproduce the behavior of isolated cells. In order to study the behavior of the whole atrial tissue, mathematical models to simulate the electrical activity propagation on the myocardial muscle have been developed. Electrical propagation is provoked by differences in electrical potential

between neighboring cardiomyocytes, which cause an ionic current through the proteins linking cardiac cells, called gap junctions, and such ionic currents promote the depolarization of the neighboring cells. The behavior of this excitable medium can be modeled by a reaction-diffusion model, which allows computing the currents supplied or received by each atrial myocyte from each of its neighbors. These currents are also modulated by the cardiac media anisotropy, since there is much more electrical connectivity in the direction in which the cells are aligned (see Figure 2.18).

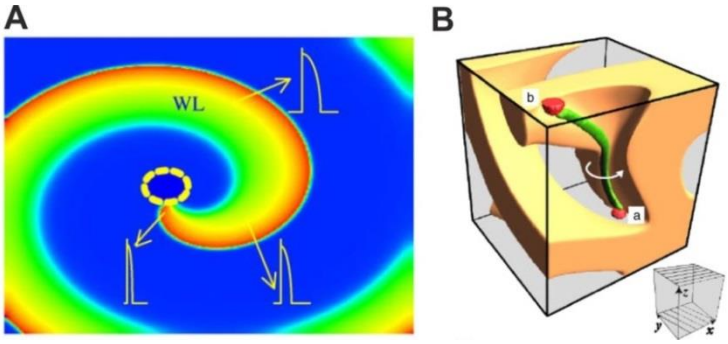

Figure 2.18 – Tissue models. Extracted from [Jalife 2004].
(A) Transmembrane potential map with a propagation pattern manintained by a rotor. Cardiac anisotropy can be observed in the ovoid shape of the rotor front. (B) Three-dimensional tissue model with a rotor. Green filament marks the position of the reentrant axis.

Cardiac propagation can be then described as a reaction-diffusion model with anisotropy, and usually is mathematically constructed using a monodomain model, which involves applying the reaction-diffusion equations only to the potential membrane ***[Dossel 2012, Clayton and Panfilov 2008]***. However, cardiac propagation can be more exhaustively described by a bidomain model, in which the variations in ionic concentrations and electric potentials are described separately for intra and extracellular media ***[Trayanova 2006]***, significantly increasing the size of the equations system and the computational costs. Monodomain models can reproduce the most of the phenomena related with electrical propagation and, therefore, are widely used because of their simplicity ***[Doessel 2012]***. Nevertheless, other phenomena like current injections provoked by electrical cardioversion have to be addressed by bidomain models ***[Trayanova 2006]***.

Like cellular models, tissue simulations have been used to evaluate the mechanisms involved in AF initiation and maintenance as well as to study their relation with the remodeling. In this sense, some studies have used tissue simulations to study the effect of the electrical remodeling on cardiac propagation ***[Kharche 2008]***, and the effect of fibrotic ***[Ashihara 2012]*** or stretched ***[Yamazaki***

2009] tissue. Propagation models have been also used to reproduce the rotor formation ***[Berenfeld 2001, Jalife 2004, Clayton 2006, Wellner 2002]*** and its behavior in the presence of electrophysiological variations ***[Calvo 2014, Atienza 2006]***, and tissue simulations have a relevant role in the rotor theory foundation ***[Jalife 2011]***. Finally, propagation models have also helped in the development of mapping and treatment techniques for AF, as for rotor mapping ***[Rappel 2013, Iyer 2001]*** or ablation ***[Rappel 2015]***.

2.5.3. Atria modelling

The inclusion of the propagation model previously described in an atrial anatomical geometry allows the simulations of electrical patterns in the whole organ. These complete simulations allow to realistically reproduce atrial propagation patterns in a physical environment with the characteristics of the atria. To this end, different geometric models that follow atrial anatomy have been developed. Since the atrial wall tends to be slim, these models can be represented as a single surface and be based on triangular meshes ***[Jacquemet 2006, van Dam 2003]***. However there are models including the thickness of the atrial wall and whose elements are defined by tetrahedrons or cubes ***[Krueger 2011, Aslanidi 2011, Tobon 2013, Krueger 2013]***. They are commonly extracted from medical image techniques, as computer axial tomography ***[Burdumy 2012]*** or magnetic resonance ***[Virag 2002]***, and they can implement also anisotropic conduction properties ***[Doessel 2012]***. Moreover, they can include several atrial regions in which the cellular model takes different electrophysiological properties ***[Tobon 2013]***.

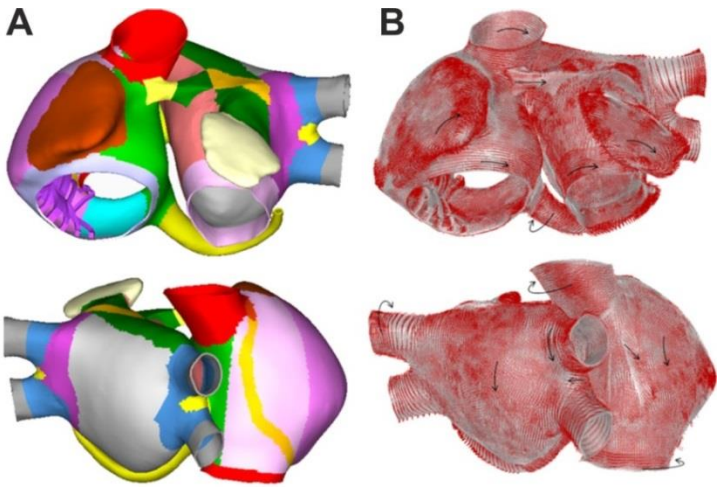

Figure 2.19 – Atrial model. Extracted from [Tobon 2013].
(Left) Atrial model color-coded accorded to the division in 42 areas depending on the atrial structure. (Right) Fiber orientation.

Similar to tissue models, atrial models have been used to study the mechanisms that promote and maintain AF episodes. Virag et al. studied the distribution of rotors in presence of anatomical obstacles ***[Virag 2002]***, and Blanc et al. studied how the depolarization alternans could be the mechanism responsible for rotor initiation in presence of anatomical obstacles ***[Blanc 2001]***. Electrical and structural remodeling has been studied also in anatomical models and their susceptibility to generate functional reentries ***[Colman 2013, Kharche 2008, McDowell 2012]***. Finally, detailed anatomical AF models have been used to develop therapies based on catheter ablation ***[Blanc 2001, Reumann 2008, Tobon 2010]*** or to evaluate the effect of gaps in ablation lines ***[Dang 2005, Hwang 2016]***.

2.5.4. Torso modelling

Once the electrical activity in the atrial muscle is known, it is possible to obtain the electric potential on the torso surface generated by such atrial activity. This process requires the three-dimensional model of the human torso on which the bioelectric propagation equations are solved to calculate the electric potential on the torso (see Figure 2.20). As discussed above, this process is called the forward problem of electrocardiography and on itself does not have direct application in cardiology, as torso potentials are directly recorded in patients. However, the forward problem is a powerful tool to study how the atrial activity during AF is electrically projected on the torso potential distribution, mainly in mathematical models. Moreover, the formulation of the forward problem is essential for the ECGI technique, since is the basis for the inverse problem resolution.

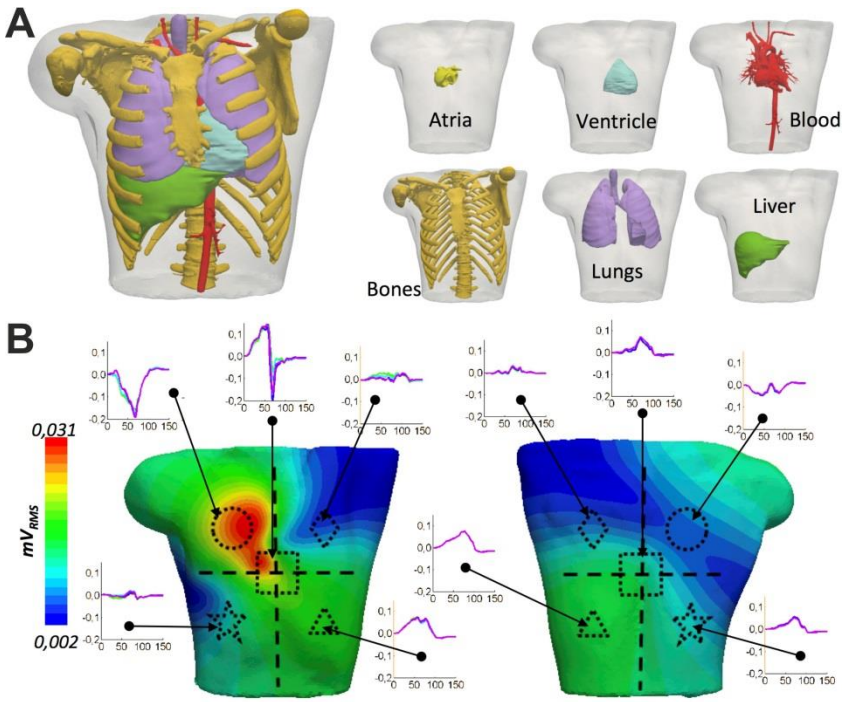

Figure 2.20 – Torso model. Extracted from [Ferrer 2015].
(A) Torso model included atria, ventricle, blood vessels, bones, lungs and liver. (B) Calculated BSPM signals on the torso surface.

The forward problem is mathematically defined as a linear equations system as follows:

$$U_T = M \cdot U_H \tag{1}$$

where U_T and U_H represents the torso and heart potentials respectively (EGMs and ECGs) and M is the transfer matrix that allows to calculate the torso potentials from the cardiac potentials. Please note that M is independent of the heart and torso potentials, so its calculation depends just on the anatomical environment. Calculation of the transfer matrix is based on the 3D model of the human torso, including the atrial model in which the potentials are defined, and the electric conductivities of the tissue.

The differential equations that are the basis of the forward problem can be solved with different numerical approachs, depending on how the tissue is particularized. The finite difference method (FDM) discretizes the torso volume in a three-dimensional grid of nodes. This method is based on the solution of the Kirchoff's law in each individual node, in which the conductivies with the neighboring nodes are stablished by the tissue conductivity and the anisotropy

[Walker 1987]. This approach allows obtaining the electric potential not only at the torso surface, but also at the complete grid of the torso volume, and allows introducing anisotropy in the torso tissue.

The finite element method (FEM) is similar to FDM, but in this case the torso volume is discretized into contiguous volume elements, commonly tetrahedrons, in which the electric field equations are solved using continuous functions inside each element. FEM solutions require more computational costs, since the differential equations systems are more complicated than FDM, but produces results with high accuracy because the system of equations ensures that the electric field equations are explicitly met ***[Fischer 2000]***.

The finite volume method (FVM) is similar to the previous approaches, since the torso volume is discretized into volumetric contiguous elements, but the electric field equations are solved only for an individual point at the center of each volumetric element. This method needs a fine discretization to obtain results comparable to FEM ***[Abboud 1994]***.

Finally, the boundary elements method (BEM) uses a fundamental solution approach, that is, it only requires the discretization of the boundary surfaces of the different conductor volumes, which are assumed to be homogeneous and isotropic. The BEM solution uses the Green's theorem for converting the potential volume problem in a surface problem, so avoids the discretization of the whole volume conductor. In some cases, this method has a much lower computational cost than finite elements aproaches but has the limitation that only allows solving the forward problem for homogeneous and isotropic volumes. The finite element method (FEM) and the boundary element method (BEM) are the most commonly used ***[Seger 2005, Fischer 2000]***.

2.6. Numerical methods for inverse problem solution

As has been discussed in the previous section, the electric potentials on the torso are mathematically related with the cardiac potentials through the transfer matrix (Eq. (1)). Therefore, obtaining the cardiac potentials from the torso potentials, knowing the transfer matrix, implies the solution of the following equation:

$$U_H = M^{-1} \cdot U_T \tag{2}$$

However, this linear system is ill-posed and, therefore, little changes in its conditions, such as electrical noise or geometrical errors involve important changes in the solution. Moreover, numerical errors when inverting the matrix M avoid the direct application of Eq. 2, so the least squares method provides inadequate results.

Two main numerical approaches have been used in the literature to reconstruct the cardiac potentials. The first approach is the reconstruction of the electric potential distribution which generates the torso activity by using numeric regularization methods. By this approach, electric cardiac activity is reconstructed in form of surface or volumetric sources ***[Wang 2010, Ramanathan 2004, Ghosh 2011, Cuculich 2010]*** and assumes that any potential distribution can be possible. This assumption involves a significant uncertainity, since it may result in potential distributions without electrophysiological sense.

The second approach aims at solving the problem of the solutions with no electrophysiological sense by restricting the solution to some constraints previously chosen. In this sense, constraints with different basis have been used to limit the possible solutions of the cardiac activity. Cuppen and van Oosterom proposed the replacement of the electric potential distribution by a spatial function marking the depolarization time for each cardiac region ***[Cuppen 1984, Huiskamp 1997]***. This approach allows reducing the time and space variables of the potential distribution to a single spatial function marking the depolarization time instant, and then the inverse problem provides isochronal maps instead of potential distributions. In a similar way, Liu et al. proposed to solve the inverse problem by obtaining volumetric current densities instead of potential distributions, since it is known that current density is considerabily higher in depolarization regions and, therefore, the wavefront can be easily identified ***[Liu 2006]***. Finally, there are approaches in which cardiac potential distributions are *a priori* calculated and then their forward problem is calculated and compared with the measured BSPM potentials ***[He 2003, Liu 2006]***. Recently, Rahimi et al. published a work which studies the effect of these physiological restrictions when trying to reconstruct electrical patterns not contemplated in a priori predictions, concluding that fixed models best suited in situations where the prior assumption fits the actual case, but adaptive models may have the ability to better address model-data mismatch ***[Rahimi 2016]***.

Physiologically-based approaches for the inverse problem solution have achieved a major advance in the study of ventricular arrhythmias, since in most cases the assumption that there is a unique wavefront is correct and such assumption considerably enhances the system accuracy ***[Rahimi 2016]***. However, in atrial arrhythmias, and in special AF, these electrophysiological constraints become invalid and thus the first approach in which the reconstructed electric potential may adopt any possible distribution is widely used ***[Cuculich 2010, Haissaguerre 2014, Pedron-Torrecilla 2016, Wang 2010]***.

Non-constrained approaches are based on the modification of the transfer matrix M from Eq. (2) in order to obtain an invertible matrix. Since the mathematical problem of the inverse solution is reduced to the non-reversibility of the transfer matrix, regularization methods are used to modify the M matrix in order to obtain a new invertible matrix altough incurring in some errors in its

solution provoked by the regularization. The regularization is usually made dependent on a λ parameter that allows the regularization to be less or more aggressive. Then, this λ parameter is used to choose the degree of regularization that balances the numerical errors introduced by the non-invertibility of the M matrix and the numerical errors introduced by the regularization itself. Several mathematical methods have been used both for the regularization and for choosing the best regularization parameter.

A first attempt to solve the inverse problem by a regularization method was proposed by Tikhonov ***[Tikhonov 1963]***. His regularization method modifies Eq. (2) to:

$$U_H = (M^t \cdot M + \lambda \cdot I^t \cdot I)^{-1} \cdot M^t \cdot U_T \quad (3)$$

where λ is the regularization parameter, I is a spatial regularization matrix and suffix t denotes the transpose operator. Then, non-invertible M^{-1} matrix is replaced by $M(\lambda) = (M^t \cdot M + \lambda \cdot I^t \cdot I)^{-1}$ matrix, which for high values of λ is invertible. The regularization problem is solved by minimization of the following equation:

$$min\{\|M(\lambda) \cdot U_H(\lambda) - U_T\|^2 + \lambda\|I \cdot U_H(\lambda)\|^2\} \quad (4)$$

where the first part $\|M(\lambda) \cdot U_H(\lambda) - U_T\|^2$ quantifies the numerical error produced by the non-invertibility of the M matrix and the second part $\lambda\|I \cdot U_H(\lambda)\|^2$ quantifies the numerical error introduced by the regularization.

Diverse regularization methods have been proposed inspired by Tikhonov's regularization method. Twomey et al. introduced a priori estimation of the epicardial potential U_H which increased the accuracy of the inverse solutions ***[Twomey 1963]***. This method has been used to introduce temporal consistency on the solution, since solutions on prior instants is used to estimate the next potential distribution ***[Oster 1992]***. Nevertheless, this technique is very sensitive to the previous solution and thus to the initial estimation, so is not suitable for complex propagation patterns. Other regularization approaches like truncated single value decomposition ***[Hansen 1990]*** or generalized eigensystem ***[Throne 1994]*** have used matrix decompositions to ignore small singular values of the M matrix in order to improve the regularization performance. In a similar way, truncated total least squares method individually measures geometrical and noise errors in order to perform the regularization according to these errors ***[Shou 2008]***.

All regularization approachs previously presented need a mathematical method to choose the regularization parameter λ allowing the best balance between the two types of errors involved in the inverse problem. For small values of λ the M matrix is under regulated and then the solution is very sensitive to perturbations, provoking oscillations in the obtained potentials in form of abnormal high

potentials. On the other hand, large values of λ lead to overregulated solutions where the effect of the regularization matrix I dominates in the obtained potentials, obtaining over smoothed epicardial potentials.

Several mathematical formulations have been proposed to quantitatively choose the regularization parameter λ. Some of these formulations are based on the a priori knowledge of the BSPM noise variance, such as the discrepancy technique ***[Morozov 1984]***, and others like generalized cross-validation and the maximum likelihood estimator do not need a priori estimations ***[Golub 1979, Wahha 1977]***. However, the most used techniques in bioengineering for the regularization parameter estimation are the composite residual and smoothing operator (CRESO) ***[Colli-Franzone 1985]*** and the L-curve method ***[Hansen 1993, Miller 1970, Horácek 1997]***, this last closely linked to zero-crossing and minimum product methods ***[Johnston 1997, Vazouras 2004]***. Whereas CRESO methodology uses a closed mathematical formulation for the parameter estimation, the L-curve is based on a graphical approach which allows visualizing the regularization problem.

The L-curve is a log-log representation of the norm of the regularized solution versus the corresponding residual norm for the different regularization parameters λ (see Figure 2.21). At the horizontal axis the residual error norm $\|M(\lambda) \cdot U_H(\lambda) - U_T\|^2$ measures the solution error provoked by the regularization, which is higher for larger regularization values. At the vertical axis, the solution error norm $\|I \cdot U_H(\lambda)\|^2$ measures error provoked the non-invertibility of the original M matrix, which is higher for lower values of the regularization parameter. This graph allows identifying the optimal regularization parameter placed on the curve "corner", which best balances both errors. This identification is commonly carried out by measuring the curvature of each L-curve position ***[Horácek 1997]***.

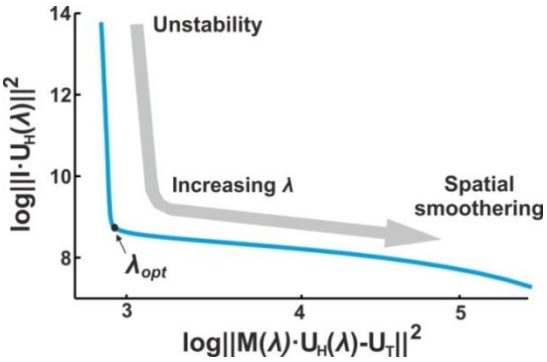

Figure 2.21 – L-curve representation.
The logaritmic values of the measured errors from the regularization perturbation (horizontal) and from the non-inversibility of the M matrix (vertical) are represented for the different regularization parameters λ. The optimal value of the regularization parameter is on the "corner" of the L-curve.

Chapter 3

General materials and methods

Common materials and methods used in different chapters of this thesis are presented in this section. In particular, the database of mathematical models and patient recordings are described, and also the methodology used for the forward and inverse solution and for driver identification. Specific materials and method will be described at each chapter.

3.1. Mathematical models of atrial fibrillation

Several sections of this thesis make use of mathematical simulations of the atrial electrical activity in order to model and characterize the AF electrical patterns and their manifestation at electrophysiological recording techniques. These mathematical models embrace from the simulation of the electrical activity of a single atrial cardiomyocyte to the electrical signal generated on the torso.

3.1.1. Atrial myocyte model

Most of the electrophysiological mathematical simulations carried out during this thesis were based on the atrial cell model developed by Koivumaki et al. ***[Kiovumaki 2011, Koivumaki 2014]*** based on the model of Nygren et al. ***[Nygren 1998]***. Similar to other Hodgkin-Huxley like models, the electrical activity of a single atrial myocyte is described in terms of its transmembrane potential and its transmembrane ionic currents as follows:

$$\frac{\partial V}{\partial t} = -\frac{I_{ion}}{C_m} \tag{5}$$

where V represents the transmebrane potential, I_{ion} the transmembrane ionic currents and C_m the cell membrane capacitance. Koivumaki's cell model includes all the transmembrane ionic currents from Nygren's models ($I_{ion} = I_{Na}, I_{Nab},$

I_{to} , I_f, I_{Kr}, I_{Ks}. I_{Kur}, I_{K1}, I_{CaL}, I_{Cab}, I_{NaK}, I_{PMCA}, I_{NCX}) but included minor changes in I_f and I_{CaL} and remodelled the compartmentalization of intracellular and sarcoplasmic reticulum media. Formulation is described in detail in the original reports by Koivumaki ***[Koivumaki 2011, Koivumaki 2014]*** and a schematic view of the transmembrane currents and intracellular compartimentalization is depicted in Figure 3.1.

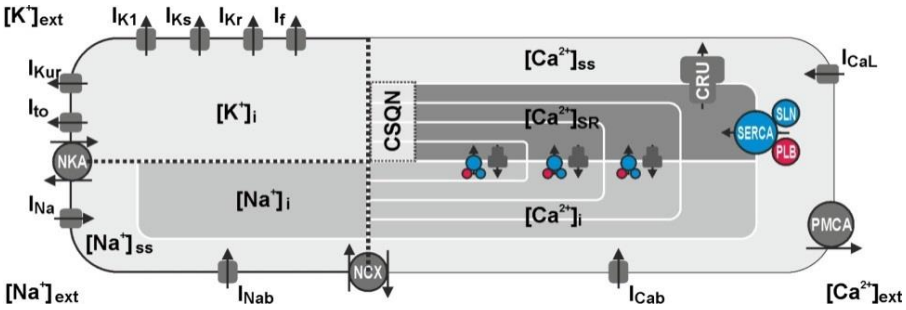

Figure 3.1 – Koivumaki cell model scheme. Based on [Koivumaki 2014].
Transmembrane currents and intracellular compartimentalization are depicted.

Electrophysiological remodelling observed in atrial cells from long-standing AF patients was also included in the atrial cell model by introducing changes in the transmembrane ionic current conductances according to measurements in AF remodeled atrial cells ***[Koivumaki 2014]***. In particular, completely remodeled atrial cells were simulated by a 59% decrease in I_{CaL}, a 62% decrease in I_{to} , a 62% increase in I_{K1} and a 38% decrease in I_{Kur}. Remodelling was proportionally applied to atrial cells as a function of the remodeling degree, being a 0% of remodelling the departing ionic conductances and 100% of remodeling the above commented changes.

3.1.2. Atrial model

The atrial cell model was used to simulate the electrical activity of the whole atria during AF episodes. The geometrical model used in his thesis was developed by Krueger et al. ***[Krueger 2013, Dössel 2012]*** from magnetic resonance images. This atrial geometrical model was composed by 284,578 nodes and 1,353,783 tetrahedrons (673.4±130.3 μm between nodes), and the cellular mathematical model was simulated for each of node. Krueger's geometrical model included atrial tissue segmentation and fiber orientation, as can be observed in Figure 3.2:

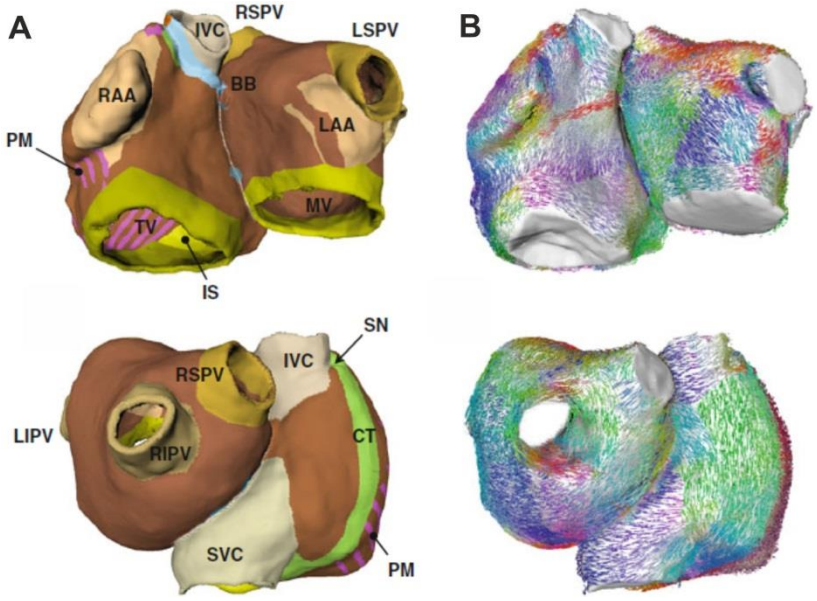

Figure 3.2 – Atrial geometrical model scheme. Extracted from [Dossel 2012].
(A) Tissue segmentation for the different atrial structures. (B) Cardiac fiber orientation. BB: Bachamn's Bundle. CT: Crista Terminalis. IVC: Inferior Vena Cava. IS:Cavotricuspid Isthmus. LAA: Left Atrial Appendage. LIPV: Left Inferior Pulmonary Vein. LSPV: Left Superior Pulmonary Vein. MV: Mitral Valve. PM: Pectinate Muscles. RAA: Right Atrial Appendage. RIPV: Right Inferior Pulmonary Vein. RSPV: Right Superior Pulmonary Vein. SN: Sinus Node. SVC: Superior Vena Cava. TV: Tricuspid Valve.

Electrical propagation of the cellular activity was mathematically simulated by including in the cell formulation (Eq. (5)) the transmembrane currents provoked by the inter-cellular gap junction current provoked by the transmembrane potential gradient between adjancent miocytes:

$$\frac{\partial V_k}{\partial t} = -\frac{I_{ion}}{C_m} - \sum_{i=1}^{N} D_{k,i} \frac{V_k - V_i}{d_{k,i}^2} \quad (6)$$

where V_k represents the transmebrane potential at node k and V_i the transmembrane potential at the reighbour node i. $D_{k,i}$ and $d_{k,i}$ are the diffusion coefficient and the distance between the node k and its neighbor node I, respectively. The conductance $D_{k,i}$ modulates the intercelular ionic current that provides the electrical propagation of the action potential, and allows including the effect of fiber orientation in the electrical propagation. In an anisotropic propagation like the atrial electrical activity the conduction velocity is larger in the longitudinal fiber orientation than at the transverse fiber orientation, and this performance was included in the diffusion coefficient determination as follows:

$$D_{k,i} = D_{long} \cdot cos^2\alpha + D_{trans} \cdot sin^2\alpha \quad (7)$$

being α the angle between the longitudinal fiber orientation and the vector linking nodes k and i, and D_{long} and D_{trans} the longitudinal and transverse diffusion coefficient respectively. Values for longitudinal and transverse diffusion coefficients varied at different atrial tissue regions and were adjusted as described in the literature ***[Krueger 2011]***:

Table 3.1– Diffusion values for the different areas of the atria.

Atria region	D_{trans} **µm²/ms**	D_{long}/D_{trans}
Atrial myocardium	0.12	3.75
Appendages	0.12	3.75
Rings and valves	0.12	3.63
Cavotricuspid isthmus	0.12	1
Crista terminalis	0.12	6.56
Bachmann's Bundle	0.12	3.88
Pectinate muscles	0.05	23.25
Sinus node	0.44	1

The structural remodelling produced in long-standing AF patients was also included in the atrial model by gradually reducing both diffusion coefficients up to -75% for a 100% remodeling degree ***[Koivumaki 2014, Dössel 2012]***. Aditionally, fibrotic and scar regions were simulated as non connective tissue by setting to 0 the diffusion values of the involved nodes. Fibrotic tissue was simulated as a percentage from 20% to 60% of randomly distributed disconnected nodes, whereas scar tissue was modelled as 100% of disconnected nodes.

The S1-S2 stimulation protocol was used to initiate simulations of the AF electrical pattern maintained by functional reentries (see Figure 3.3). A set of 31 simulations of AF episodes maintained by a single rotor were carried out, varying the rotor location and the tissue properties, as can be observed in Table 3.2. The system of differential equations in the atrial cell model was solved by using Runge-Kutta integration based on a graphic processors unit (NVIDIA Tesla C2075 6G) ***[Garcia 2014]***.

Table 3.2– AF simulations.

#	Rotor position	Rotor remodelling	No rotor remodelling	Fibrosis	Rotor DF	No rotor DF
1	PLAW	100%	100%	-	6,6	4,5
2	PLAW	100%	0%	-	4,8	3
3	PLAW	100%	0-100%	47%	5,6	3,4
4	PLAW	100%	0%	47%	5,7	3,6
5	PLAW	100%	50%	47%	5,7	3
6	PLAW	100%	0%	60%	5,7	2,3
7	RAFW	100%	0-100%	-	7,3	4,7
8	RAFW	100%	0%	-	7,65	3,3
9	RAFW	100%	50%	-	7,6	6,3
10	RAFW	100%	25%	-	7,6	3,8
11	RAFW	100%	50%	35%	7,6	5,8
12	RAFW	100%	25%	-	5,4	4,1
13	RAFW	100%	25%	35%	5,4	3,8
14	RAFW	100%	25%	47%	5,4	3,4
15	RAFW	100%	25%	55%	5,4	3,1
16	RAFW	100%	75%	55%	5,3	1,8
17	RAA	100%	0%	-	5	3,1
18	RAA	100%	0%	-	5,8	3
19	RAA	100%	35%	-	6,2	3,9
20	RAA	100%	35%	-	6,2	4
21	RAA	100%	35%	60%	5	3
22	RAA	100%	35%	40%	6.2	4
23	RAA	100%	35%	20%	6	3,9
24	LSPV	100%	50%	50%	7,8	6,5
25	RSPV	100%	50%	50%	8,3	6,1
26	RSPV	100%	0%	25%	6,8	5,4
27	LIPV	100%	0%	50%	5,8	3,1
28	LIPV	100%	10%	50%	5,5	4,3
29	RIPV	100%	0%	50%	5,5	3,3
30	RIPV	100%	10%	55%	5,4	4,4
31	LSPV	100%	0%	50%	7,8	6,2

PLAW: Posterior Left Atrial Wall. LIPV: Left Inferior Pulmonary Vein. LSPV: Left Superior Pulmonary Vein. RAA: Right Atrial Appendage. RAFW: Right Atrial Free Wall. RIPV: Right Inferior Pulmonary Vein. RSPV: Right Superior Pulmonary Vein.

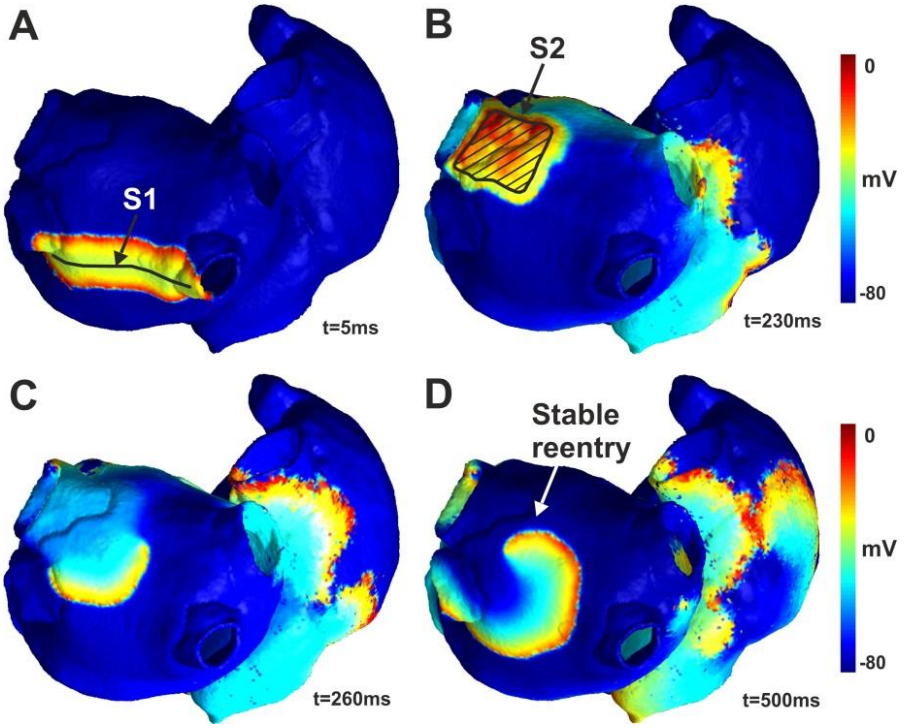

Figure 3.3 – Initiation of AF rotor by S1-S2 stimulation protocol.
Rear view of the transmembrane potential map. (A) S1 stimulus, a line between the inferior pulmonary veins. (B)S2 stimulus, a square adjacent to LSPV. (C) Reentry initiation at the S2 square border due to the refractoriness of part of the adjacent tissue. (D) Stabilization of the reentry in the posterior left atrial wall.

3.1.3. Torso model

The atrial electrical activity provoked by the AF simulated episodes was also studied on the torso surface. A geometrical model of the human torso composed by 771 nodes and 1538 faces ***[MacLeod 1991]*** was used and the atrial geometry was located according to the anatomy.

Figure 3.4 – Torso geometrical model.
Front (left) and rear view (right) of the geometrical model of the human torso (green) and the atrial geometrical model (red).

3.2. Patient recording

The methodology and procedures proposed in this thesis were evaluated in a cohort of AF patients. Although the database used in each chapter slightly varies, the data acquisition protocol was similar for all patients.

All patients included in this thesis were admitted for ablation of drug-refractory paroxysmal and persistent AF in the cardiology service of the Hospital General Universitario Gregorio Marañón in Madrid, Spain. All patients gave informed consent and the protocol was approved by the Institutional Ethics Committee.

3.2.1. Intracardiac mapping

The electrophysiological study was performed under general anesthesia and periodic heparin bolus administration. Intracardiac electrograms (EGM) were obtained from both atria during the procedure by using a combination of the following catheters introduced via the right femoral vein: (1) a standard tetrapolar catheter in the right atrial (RA) appendage; (2) a deflectable 4-mm mapping catheter (Marinr; Medtronic Inc., Minneapolis, MN) in the distal coronary sinus; (3) a decapolar circular mapping Lasso catheter (Biosense-Webster, Diamond Bar, CA) used to map the pulmonary vein – left atrial (LA) junctions; (4) a standard tetrapolar catheter placed in the coronary sinus (CS); (5) a 64-pole basket catheter

(Constellation, Boston Scientific, Natick, MA) located sequentially on the right and left atria; and (6) a 20-poles catheter in the opposite atrium to the basket catheter. Atrial anatomy was reconstructed using the software for the 3D navigation of the EGM catheters used in the AF ablation (Boston Scientific, Natick, MA).

In patients arriving in sinus rhythm, AF was induced by burst pacing. AF episode durations longer than 5 minutes were required for inclusion in the study. During stable AF episodes, ventricular activation was stopped by administration of a central venous bolus of adenosine (12-18 mg) which blocked the atrioventricular node for 5 to 10 seconds.

3.2.2. Body surface potential mapping

Surface electrocardiograms (ECGs) were recorded simultaneously with the intracardiac EGMs using a grid of electrodes covering the torso. At chapters 4 and 5 the BSPM system was based in a vest with 67 electrodes distributed as follows: 28 electrodes on the anterior, 34 on the posterior, 2 on each lateral side of the torso and 3 extra electrodes to obtain a Wilson Central Terminal (see Figure 3.5A-B). For recordings of chapter 5, the BSPM system had to be compatible with the catheter navigation patches, and therefore BSPM signals were recorded using adhesive stripes with 57 standard ECG leads covering the entire torso and distributed as follows: 24 electrodes on the anterior, 24 on the posterior, 3 on each lateral side and 3 extra electrodes to obtain a Wilson Central Terminal (see Figure 3.5C-D).

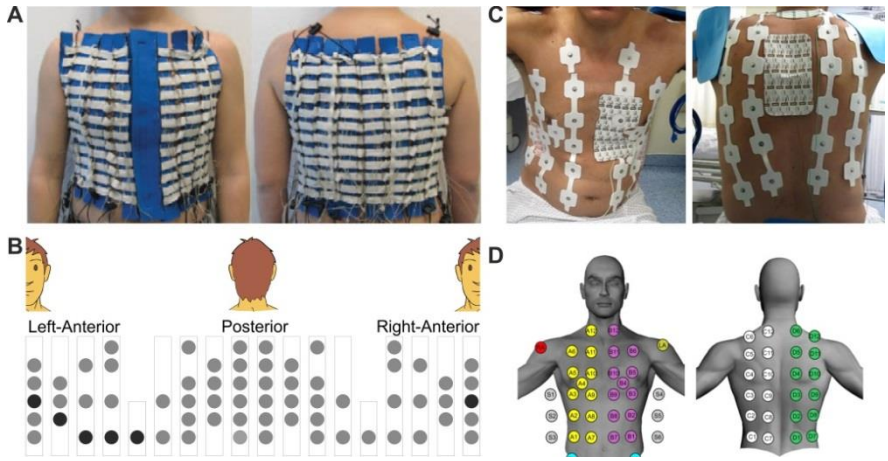

Figure 3.5 – Body surface potential mapping.
(A) Anterior and posterior view of the BSPM vest. (B) Surface distribution of the BSPM leads. Dark dots represent standard V1-V6 derivations. (C) Anterior and posterior view of the BSPM electrodes. (D) Surface distribution of the BSPM electrodes.

3.3. Calculation of electrophysiological signals

This thesis studies the atrial electrophysiological signals produced by AF patterns from the transmembrane potential to the ECG. In the mathematical simulations, the transmembrane potential signals were used to obtain the EGM signals, and then these EGM signals were used to obtain the ECG signals through the solution of the forward problem of electrocardioogy. Then, both ECG signals from mathematical models and patients were used to obtain the inverse-computed EGM (icEGM) signals through the inverse problem of electrocardiology. In this section, the mathematical formulation for the obtention of the EGM, ECG and inverse-computed EGM are explained.

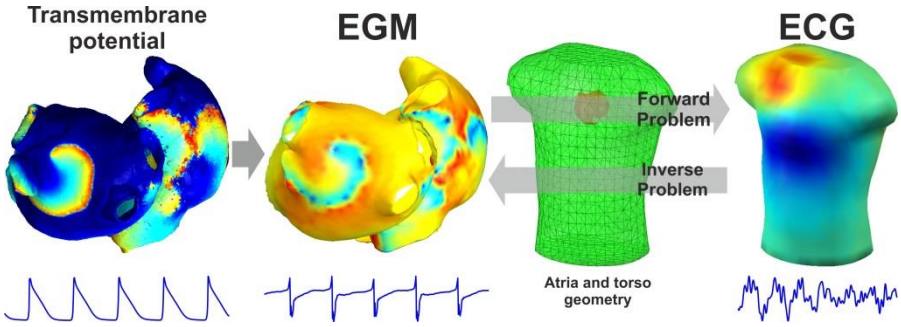

Figure 3.6 – Scheme of signal calculation.
Transmembrane potential signal is used to obtain the EGM signals and then by solving the forward problem the ECG signals. Inverse problem allows to obtain the icEGM signals.

3.3.1. Electrogram calculation

For each simulation, a uniform mesh of 2048 unipolar EGMs was calculated surrounding the epicardial surface (1 mm distance) under the assumption of a homogenous, unbounded and quasi-static conducting medium by summing up all effective dipole contributions over the entire model as:

$$V_{\vec{r}} = \sum_{\vec{r}} \left(\frac{\vec{r}}{r^3}\right) \cdot \vec{\nabla} V_m \tag{8}$$

where $V_{\vec{r}}$ is the EGM signal at the measuring point, V_m is the transmembrane potential distribution along the whole atria, $\vec{r}$ is the distance vector between the measuring point and a point in the tissue domain (r is the distance scalar), and $\vec{\nabla}$ denotes the gradient operator. The summation involves all nodes in the atrial mesh for every EGM signal obtenition. Since the transmembrane potentials were defined in a scattered tridimensional mesh, its gradient was calculated by interpolating a quadratic function in the sourrounding of each point ***[Lawson 1984]*** as follows:

$$V_{m,i} - V_{m,j} = c_1 x + c_2 y + c_3 z + c_4 x^2 + c_5 y^2 + c_6 z^2 + c_7 xy + c_8 yz + c_9 xz \quad (9)$$

where $V_{m,i}$ and $V_{m,j}$ are the transmembrane potentials at points *i* and *j* and x, y and z are the incrementary cartesian coordinates from point *j* respect to point *i*. Coefficients c_1 to c_3 were calculated by least square method using Eq. (9) in at least 9 neighboring points of each location, and the gradient $\vec{\nabla} V_m$ at point *i* was defined as:

$$\vec{\nabla} V_m = c_1 \hat{x} + c_2 \hat{y} + c_3 \hat{z} \quad (10)$$

Since the above described formulas had to be solved for each of the 2048 nodes and for each time interval, this algorithm was executed in a cluster (5 blades, DELL) with parallel Matlab architecture (The Mathworks Inc, Natick, MA).

3.3.2. Forward problem

The forward problem of electrocardiography allows calculating the ECG signals from the EGM potentials and the atrial and torso geometry. These two magnitudes are related by a linear algebraic system as follows:

$$ECG = M \cdot EGM \quad (11)$$

where *M* is the field transfer matrix that governs the projection of the EGM potentials on the surface ECG signals. The *M* matrix is just anatomical dependent, and can be obtained with the Boundary Elements Method ***[Horácek 1997]*** with the information of the atria and torso shell and their electrical conductivities:

$$M = [D_{TT} - G_{TA} G_{AA}^{-1} D_{AT}]^{-1} \cdot [G_{TA} G_{AA}^{-1} D_{AA} - D_{TA}] \quad (12)$$

where D_{XY} is the potential contribution matrix of a bounding surface *Y* to a surface *X* and G_{XY} is the matrix representing the contribution of the voltage gradient of a bounding surface *Y* to a surface *X*. In Eq. (12) subindexs *A* and *T* represent the external atrial boundary surface and torso boundary surface respectively.

The voltage gradient between points in *X* and *Y* boundary surface are represented in matrix G_{XY} and only geometrical aspects are involved on its calculation [ref]. The D_{XY} matrix has a different description for the potential contribution of two different surfaces (Eq. (13)) or for one surface over itself (Eq. (14)):

$$D_{XY} = \frac{1}{4\pi} [(\sigma_Y' - \sigma_Y'') \Omega_{XY}] \quad (13)$$

$$D_{XX} = \frac{1}{4\pi} [(\sigma_X' - \sigma_X'') \Omega_{XX}] + \left(\frac{\sigma_X' - \sigma_X''}{2} \right) I_{N_X} \quad (14)$$

where σ'_X and $\sigma'_X{}'$ are the inner and outer electrical conductivities of the boundary surface *X*, I_{N_X} is an identity matrix whose size is the number of nodes in *X* surface and Ω_{XY} is the matrix of solid angles between points in surface *X* and *Y*.

3.3.3. Inverse problem

We estimated the inverse-computed EGM (icEGM) from both patient recordings and mathematical models by computing the inverse of the field transfer atrial-torso matrix:

$$icEGM = M^{-1} \cdot ECG \tag{15}$$

where *M* is the field transfer matrix between the atria and the torso obtained from the forward problem ***[Horácek 1997]***. Since *M* is ill-conditioned its inverse matrix cannot be computed in terms of classical linear algebra. We solved the system by using zero-order Tikhonov's method in which the potentials on the surface of the atria were estimated from the potentials on the torso according to Eq. (16) ***[Pedrón-Torrecilla 2016, Tikhonov 1963]***.

$$icEGM(\lambda) = (M^t \cdot M + \lambda \cdot I^t \cdot I)^{-1} \cdot M^t \cdot ECG \tag{16}$$

where *I* is the identity matrix and λ is the regularization parameter. The optimal regularization parameter was chosen according to the L-curve method, which calculates the maximum curvature of the graph provided by the error norm ($\|M \cdot icEGM(\lambda) - ECG\|^2$) in the abscissa axis and the solution norm ($\|icEGM(\lambda)\|^2$) in the ordinate axis for the different regularization parameters. The regularization parameter obtained at the point that minimizes:

$$F(\lambda) = \|M \cdot icEGM(\lambda) - ECG\|^2 + \lambda^2 \|I \cdot icEGM(\lambda)\|^2 \tag{17}$$

is the point of maximal curvature (the "corner") at the L-curve, and provides the icEGM solution that best satisfies Eq. (15) and minimizes the extreme values on the solution caused by the numerical errors involved in the transfer matrix inversion ***[Horácek 1997]***. The curvature of the L-curve was quantified by using the following equation:

$$curvature(\lambda) = \frac{\frac{dx}{d\lambda}\frac{d^2y}{d\lambda^2} - \frac{dy}{d\lambda}\frac{d^2x}{d\lambda^2}}{\left[\left(\frac{d^2x}{d\lambda^2}\right) + \left(\frac{d^2y}{d\lambda^2}\right)\right]^{3/2}} \tag{18}$$

where *x* is the logarithm of the error norm ($log\|M \cdot icEGM(\lambda) - ECG\|^2$) and y is the logarithm of the solution norm ($log\|I \cdot icEGM(\lambda)\|^2$). The optimal regularization parameter was chosen at the first local maximum curvature value .

3.3.4. Electrical reference

Please note that Eq. (7) is defined for unipolar potentials which implies that electric potentials are referenced to ground. However, ECG recordings in patients are commonly referenced to the WCT, due to the electrical noise of the ground, and thus the transfer matrix *M* in Eq. (15) must be corrected in order to include the effect of the WCT reference on the ECG signals. ECG recordings referenced to WCT can be described as follows:

$$ECG_b = ECG - ECG_{WCT} \tag{19}$$

and WCT signal (ECG_{CTW}) as the average of the N_{WCT} ECG signals at the WCT points:

$$ECG_{WCT} = \frac{1}{N_{WCT}} \sum_{N=WCT} ECG = \frac{1}{N_{WCT}} \sum_{N=WCT} M \cdot EGM \tag{20}$$

The last part of Eq. (20) can be expressed also as:

$$\frac{1}{N_{WCT}} \sum_{N=WCT} M \cdot EGM = \frac{1}{N_{WCT}} M_{WCT} \cdot EGM \tag{21}$$

where M_{WCT} is a matrix of zeros except for the rows that correspond to the WCT leads, that are set to the same values of the M matrix. Then, applying Eq. (21) in Eq. (19):

$$ECG_b = M \cdot EGM - \frac{1}{N_{WCT}} M_{WCT} \cdot EGM =$$

$$= \left(M - \frac{1}{N_{WCT}} M_{WCT}\right) \cdot EGM = M_b \cdot ECG \tag{22}$$

a new transfer matrix $M_b = M - \frac{1}{N_{WCT}} M_{WCT}$ was defined which defines the relation between EGM signals and WCT referenced ECG signals, and thus can solve the inverse problem for ECG recordings referenced to WCT.

In order to use the same methodology for both patients and mathematical models, synthetic ECG signals from mathematical models were referenced to WCT too, and the corrected matrix M_b was used in both scenarios.

3.4. Identification of atrial fibrillation drivers

As has been previously described, AF drivers can be identified in electrophysiological signals by their pattern analysis. In this work DF and rotor identification tehniques have been used according to the most used techniques in the clinical practice.

3.4.1. Dominant frequency

For DF analysis, electrophysiological signals were first baseline-removed in order to remove the low-frequency variations in the signal baseline provoked by electrical artifacts without altering the electrophysiological signal shape. Baseline of electrophysiological signals was estimated by decimation to 12.5 Hz and filtering with a Butterworth 10th-order low-pass filter with a cut-off frequency of 2 Hz. This signal was interpolated to the original sampling frequency and subtracted from the original signal. Signals were then low-pass filtered with a 10th-order Butterworth filter with a cut-off frequency of 15 Hz ***[Guillem 2013]***, since values for DF greater than 15 Hz were considered as non- physiologically reliable. Power spectral density of all signals was computed using Welch's periodogram (65536 point Fast Fourier transform and 80% overlap) to determine the local DFs with a spectral resolution of 0.01Hz ***[Guillem 2013]***.

3.4.2. Phase mapping and rotor identification

Rotor location was carried out by identification of singularity points (SP) in the phase map obtained with the Hilbert Transform ***[Zlochiver 2008]***. Phase values were obtained along 3 different circles surrounding each evaluated point, and six to twelve points per circle were used for the phase analysis in which the signal was interpolated by a weighted average of the neighboring nodes, being d^{-2} the weight for each node and d the distance between nodes (see Figure 3.7).

An evaluated point was defined as a SP only when the phases of at least two of these three circles was monotonically increasing or decreasing for a total of 2π. A rotor was defined as the connection between SPs across time. The distance between SPs at consecutive time instants should be less than 1 cm (EGM and icEGM) or 5 cm (ECG) to be related and maintain a continuity of rotation. Finally, only long lasting rotors, defined as those that complete at least one rotation were considered as rotors and other SPs were discarded.

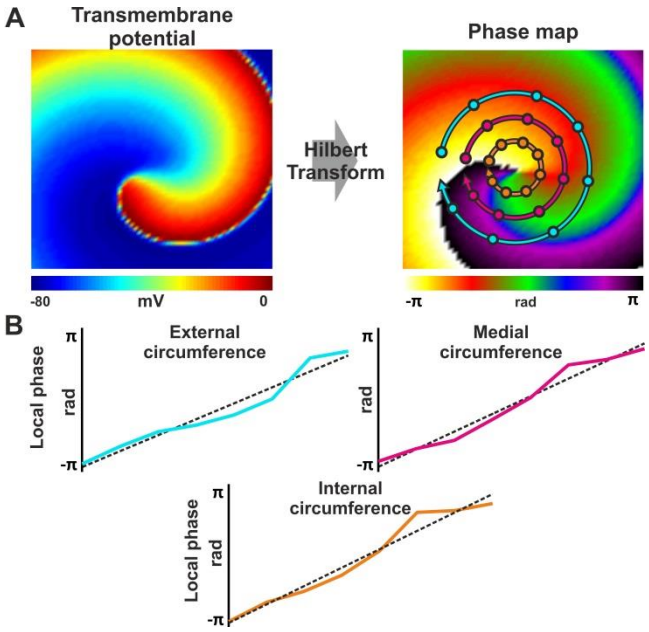

Figure 3.7 – Phase transform and singularity point detection.
Panel A shows a transmembrane potential map with a stable rotor and the Hilbert transform of this map. Panel B depicts the phase values at three concentric circles surrounding the rotor tip in panel A, were the monotonically increasing phase values from –π to π can be observed.

Chapter 4

Body surface localization of left and right atrial high frequency rotors in atrial fibrillation patients

4.1. Introduction

Recent invasive ***[Atienza 2009, Narayan 2012]*** and noninvasive ***[Guillem 2009, Cuculich 2010, Guillem 2013, Haissaguerre 2013]*** mapping studies of human AF have demonstrated a variety of spatiotemporal patterns of activation, including high frequency sites, rotors and focal discharges during human AF. Arguably, the identification of the AF mechanism in each patient may help selecting the best therapy or ablation strategy to deliver to that individual patient. However, how to map effectively and determine the specific mechanisms of AF maintenance in individual patients is still elusive ***[Berenfeld 2012]***.

It has recently been shown that non-invasive mapping allows the identification of high dominant frequency (DF) atrial sources during human AF ***[Guillem 2013]***. However, the ability of surface mapping data to determine the specific activation patterns underlying the fast activation that characterize AF (i.e. focal vs. re-entrant activity) has not been studied before. The aim of this chapter is to investigate the potential use of surface mapping recordings for the estimation of propagation patterns during AF on an individual patient basis

4.2. Methods

4.2.1. Patients and body surface potential recording

The 14 patients included in this study were admitted for ablation of drug-refractory paroxysmal and persistent AF (see Table 4.1). All patients gave informed consent. The protocol was approved by the Institutional Ethics Committee. In patients arriving in sinus rhythm, AF was induced by electrical burst pacing. Intracardiac electrograms (EGMs) were sequentially obtained from both atria during the procedure ***[Guillem 2013]*** and power spectral density of EGMs was computed to determine the local DFs in each atrium.

Table 4.1– Patient's characteristics.

N	14
Age Range	56 ± 8 years 47 – 68 years
Gender - male	13 (93%)
Year since AF diagnosis Range	5 ± 4 years 1 - 17 years
AF type - paroxysmal	10 (71%)
# of previous ablations Range	1 ± 1 0 - 3
DF gradient in EGMs	12 (86%)

Surface electrocardiograms (ECGs) were recorded simultaneously with intracardiac electrograms (EGMs) using a grid of 67 electrodes on a vest covering the torso distributed as follows: 28 electrodes on the anterior, 34 on the posterior and 2 on each lateral side of the torso (Figure 4.1) ***[Guillem 2013]***. Three limb leads were also recorded to obtain a Wilson Central Terminal. The signals were recorded using a commercial system (Active Two, Biosemi, The Netherlands) at a sampling frequency of 2048 Hz and were stored for off-line analysis. A central venous bolus of adenosine (12-18 mg) was administered in order to produce a significant atrio-ventricular block and to remove the ventricular activation ***[Atienza 2006]***. At peak adenosine effect, the 67 surface ECGs were recorded and a 4-seconds segments surrounding the longest RR interval was used for the analysis. In cases with ventricular activation pauses shorter than 4 seconds, the QRST were cancelled ***[Castells 2005]***.

Surface potentials were processed using Matlab 7.10.0 (The Mathworks Inc, Natick, MA). Recorded ECG signals properly arranged in space were used to estimate ECG signals at non-recorded positions using cubic spline interpolation ***[Guillem 2009]***. Baseline was estimated by decimation to 51.2 Hz and filtering with a Butterworth 10th-order low-pass filter with a cut-off frequency of 2 Hz. This signal was interpolated to 2048 Hz and subtracted from the original signal

[Guillem 2006]. Leads presenting >0.5% of their spectral content at 50Hz were filtered with a second-order infinite impulse response notch filter centered at 50 Hz. Potential signals were low-pass filtered with a 10th-order Butterworth filter with a cut-off frequency of 30 Hz. All leads were visually inspected after filtering and leads with noticeable noise were excluded from further analysis. Power spectral density of all signals free of ventricular activity was computed using Welch periodogram (2-second Hamming window with an 8192 point Fast Fourier transform per window and 50% overlap) to determine the local DFs and their distribution on the body surface.

Surface ECGs were then filtered at the highest DF (HDF) found on the torso surface or at the highest DF found at either left atrium EGMs (LA-HDF) or right atrium EGMs (RA-HDF) by using a cascade of a high-pass Chebyshev 10th order filter with cut-off frequency equal to HDF - 1 Hz and a low-pass 10th order Chebyshev filter with a cut-off frequency equal to HDF + 1 Hz after decimation of ECG signals down to a sampling frequency of 128 Hz.

4.2.2. Computational models of the atria and torso

To guide processing and interpretation of the recorded body surface potentials we simulated the electric potentials behavior on a computerized model of the atria within the torso during different impulse propagation patterns. This approach will enable investigating for the first time the manifestation of atrial reentrant activity on both the internal volume and the torso surface. We constructed a generic atria-torso model consisting of a spherical shell of active tissue, representing the atria, within a passive torso modeled as a uniform volume conductor bounded by a spherical surface with no-flux conditions. This non-realistic modeling of the electrical activity allows the study of the electric activity propagation between the atrium and the torso without being affected by the complex geometry of real atrium.

The active tissue of the atria consisted of a 2.5 cm radius sphere incorporating 163,842 nodes (average inter-nodal distance of 236,07 ± 15.35 μm) on which the transmembrane potential kinetics ionic formalism ***[Courtemanche 1998, Kneller 2002]*** was used. The system of differential equations was solved by using Runge-Kutta integration with an adaptive temporal step based on a graphic processors unit (NVIDIA Tesla C2075 6G) ***[García 2013]***. All signals were re-sampled at sampling frequency of 1 kHz.

Three atrial tissue types were used to construct different propagation patterns: Right atrium (RA) tissue, left atrium (LA) tissue and fibrotic tissue. The LA and RA tissues were modeled by setting the $I_{K,ACh}$ and I_{Kr} conductances to 2 and 1.6 fold, respectively in the LA relative to the RA ***[Atienza 2006]***. Fibrotic tissue was modeled by simply disconnecting 57% of nodes in the RA tissue in order to simulate highly disorganized electrical propagation. Three propagation patterns

were simulated on the atrial sphere: (1) a sphere was divided into a LA hemisphere that harbored a stable functional rotor and a RA hemisphere with fibrillatory activity driven by the LA rotor (Figures 4.3, 4.4 and 4.5); (2) a sphere divided into a LA hemisphere that harbored a stable rotor and another hemisphere with fibrotic conduction (Figures 4.6 and 4.10) and (3) a sphere in which only 5% to 30% of the surface had LA properties and harbored a stable rotor and the remaining surface of the sphere presented fibrotic properties (Figure 4.7).

The electric potential resulting from the wave propagation simulated on the atrial sphere was studied everywhere on 20 concentric spheres of 2562 nodes with increasing radii from 2.5 cm to 12.5 cm. In order to obtain the electric potential, the forward problem formalism was solved by using the Boundary Element Method ***[Horácek 1997]***. The potentials on the external sphere, defined as the torso surface, and in the internal layers were analyzed to characterize the time-course of the potential distribution everywhere; in particular, the patterns and time-course of the filaments resulting from atrial rotors were characterized.

4.2.3. Phase singularity and filaments

Phase maps on the torso surface of patients and in each concentric layer in the computer models were obtained from the potential phase signal of each node by the Hilbert transform ***[Zlochiver 2008]***. To increase reliability, the phase values were obtained along 3 different circles surrounding each evaluated point; an evaluated point was defined as a SP only when the phases of at least two of these three circles was gradually and monotonically increasing or decreasing for a total of 2π.

In patients, the radii of the circles used for evaluating SPs were 1.66%, 3.31% and 5.53% respectively of the individual patient's torso circumference (see Figure 3.7). SPs in consecutive time instants were considered to be related, i.e., belong to the same rotor, if they maintained a continuity of rotation and were separated by <5.53% of the patient's torso circumference. Functional rotors were defined as related SPs that complete at least one turn. In the computational models, the radii of the circles used for detecting SPs were of $0.08 \cdot R$, $0.15 \cdot R$ and $0.2 \cdot R$, where R was the radius of the layer (1, 1.8 and 2.5 cm at the outermost layer).

A filament was defined as the connection between SPs across spherical layers at a given time. Specifically, two SPs in different layers were connected to construct a filament when the distance between these SPs was less than $0.4 \cdot R$. Additionally, the distance between SPs at any layer in consecutive time instants should be less than $0.4 \cdot R$ to be related and maintain a continuity of rotation. Finally, only long lasting filaments, defined as those that completed at least one rotation on the outermost surface, were considered as rotors and all other filaments were discarded.

4.2.4. Statistical analysis

The t-test was used to evaluate the statistical significance between continuous paired or unpaired variables after considering the normal distribution of the data with the Lilliefots test, and statistical significance was considered for $p<0.05$. All data are reported in mean±SD.

4.3. Results

4.3.1. Surface mapping of atrial activity during AF

As an initial step in our study we studied sample surface phase maps recorded from a patient during a typical atrial flutter (Figure 4.1). The surface activation during atrial flutter should represent organized patterns which have a direct correlation with the propagation sequence in the atria and should serve as a reference for further, more complex patterns of atrial activation during AF. Three sequential phase maps during the sample atrial flutter recorded with our surface electrodes grid show a rotational activity with a stable pattern (Figure 4.1). Two SPs appear on the surface phase maps most likely corresponding to a single anatomical reentry.

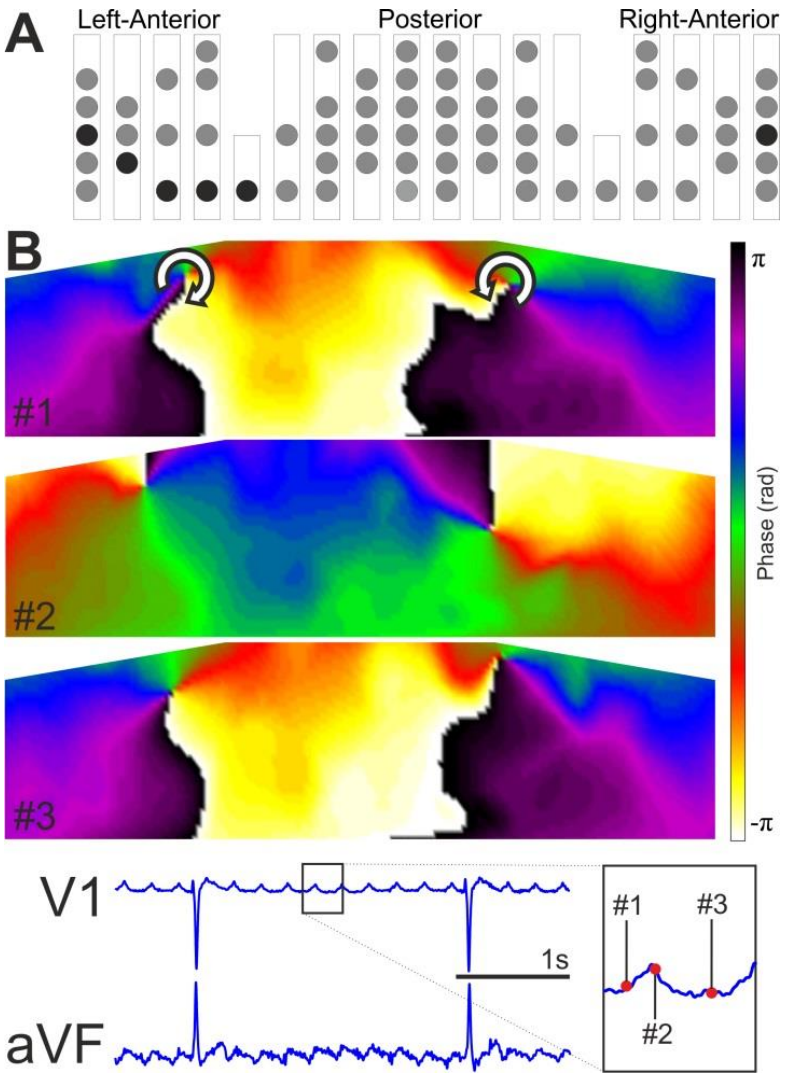

Figure 4.1 – Surface phase maps during organized atrial rhythms.
(A) Schematic geometrical configuration of the surface electrodes relative to the torso. Circles represent the location of recording electrodes. Electrodes at locations corresponding to the standard ECG precordial leads are denoted as black circles. (B) Surface phase maps during typical atrial flutter at three selected time instants. Red dots superimposed on V1 tracings indicate the time instants selected for phase maps representation.

Surface phase maps of the unipolar voltage time-series recorded during AF show unstable patterns, as can be appreciated by the transient SPs seen in the maps from a sample patient presented in Figure 4.2A, as opposed to stable rotational patterns observed during atrial flutter (Figure 4.1). Long-lasting SPs were rarely observed during AF without band-pass filtering and those observed tended to drift erratically large distances in short time. However, after band-pass filtering of the potential signal around the HDF (6.8 Hz), surface phase maps showed more stable SPs for the same AF episode (Figure 4.2A). In Panel B the arrows connecting sequential activations in ECGs recorded around the SP in Figure 4.2A show a clear reentrant pattern which following HDF-filtering transformed into long-lasting rotational patterns with stable SPs.

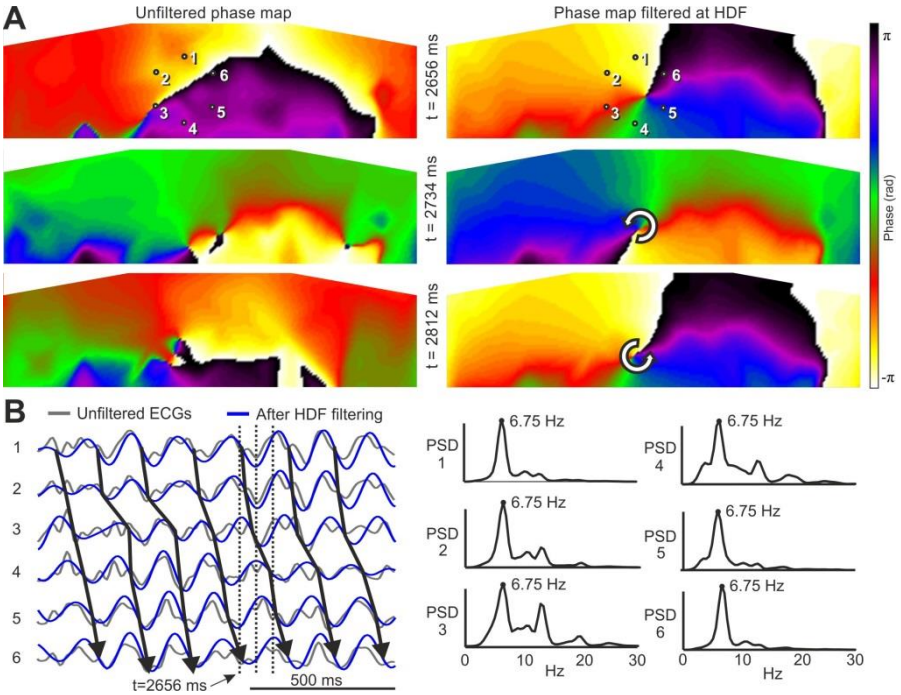

Figure 4.2 – Surface phase maps during AF.
(A) Surface phase maps at three selected times for unfiltered (left) and for HDF-filtered (right) surface potentials. (B) ECGs at positions 1-6 marked in (A) before and after HDF-filtering and Power Spectral Density (PSD) for unfiltered ECGs. Time marker at 2656 ms corresponds to the top map in the HDF-filtered data in (A).

Considering data from all patients, stable SPs were found in unfiltered AF signals during 8.3±5.7% of the time vs. 73.1±16.8% following HDF-filtered signals ($p<0.01$). The average SPs duration concomitantly increased following the HDF-filtering (160±43 vs. 342±138 ms, $p<0.01$). At an average HDF of 9.2±2.3 (BSPM) or 9.3±2.0 (EGM) Hz, the latter corresponds to an average of 2.9±0.7 continuous rotations per SP observed in our cohort of patients.

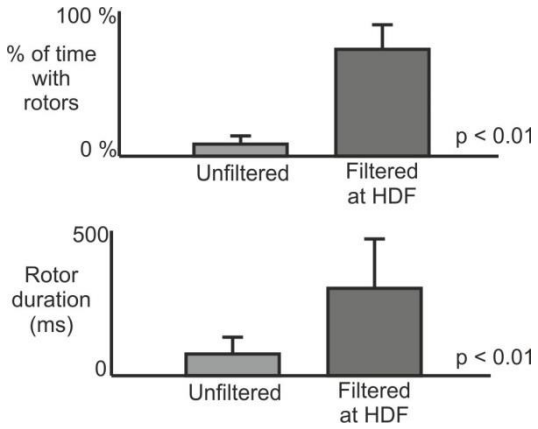

Figure 4.3 – Surface rotor presence during AF.
Percentage of time with rotors (up) and rotor duration (down) in surface phase maps from unfiltered and HDF-filtered surface potentials over the entire cohort.

Many observed SPs drift and appear or disappear on the borders of the surface mapped area, or in the beginning and end of the periods analyzed, thus this average number of rotations represents a lower limit for their life span. Indeed, Figure 4.4A show a rotor in the middle of the mapped area at the beginning of the period analyzed that after about 1400 ms disappears at the lower boundary of the area. After a period of fuzzy SP behavior in the posterior torso for about 330 ms an SP appears and remains in the mapped area for the rest of the analyzed period. This case shows that the actual life span of rotors could be longer than the conservative average life-span we calculate. Further evidence of atrial rotor drifting is provided by the simultaneous EGM recorded at the highest DF site (Figure 4.4B), which is unstable in intervals 1-4 and monomorphic at interval 4-5, which is consistent with the observed drifting on the torso surface.

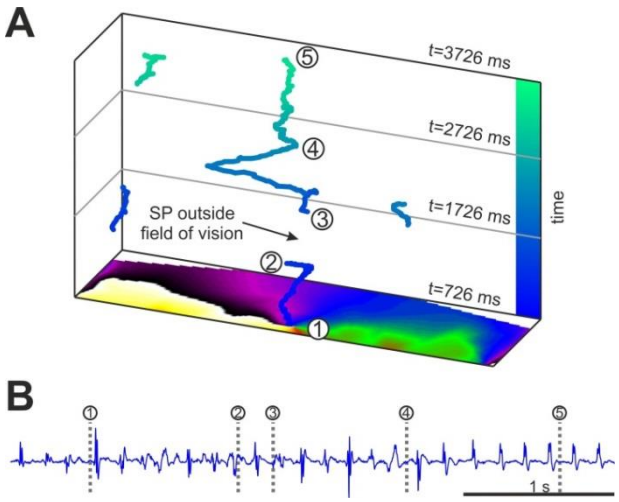

Figure 4.4 – PS surface trajectory and EGM signal.
(A) PSs trajectories on the torso surface during a 3-sec long AF. (B) Electrogram recorded at the highest DF site in the atria (RSPV) simultaneously to the surface recordings.

4.3.2. Simulations to understand HDF band-pass filtering of AF patterns

The finding that the dynamics of the body surface SPs dramatically depends on the HDF-filtering raises questions regarding the phase maps interpretation. Unfortunately, the ability to collect simultaneously electrical data in the atria and inside the torso volume and surface to make inferences between atrial activity and its manifestation on the body surface is limited, leading us to rely on computer simulations for guidance.

In Figure 4.5 a simulation with a LA–RA atrial model and the multi-spheres torso model is depicted. In this model there is a single functional rotor in the LA hemisphere turning at 7.2 Hz while the RA hemisphere is passively activated at lower a frequency (3.9 Hz). Figure 4.5A shows the phase maps of three concentric layers between the epicardium (left) and the torso surface (right) at various times. The phase maps become smoother toward the torso surface, reflecting the low-pass filter effect of the passive torso volume on the extracellular potentials. In the epicardial layer there is one stable SP at the location of the functional rotor (LA) that appears at similar positions in the outer layers, and another SP at the less stable wavebreak location at the interface between the faster LA and the slower RA. Azimuth and elevation of SPs detected on the surface are not preserved across layers, so the filament arising from the LA rotor exhibits a deflection in its trajectory to the torso. The deflection angle of the filaments before HDF-filtering is not stationary over time and, instead, the filament trajectory describes a cone.

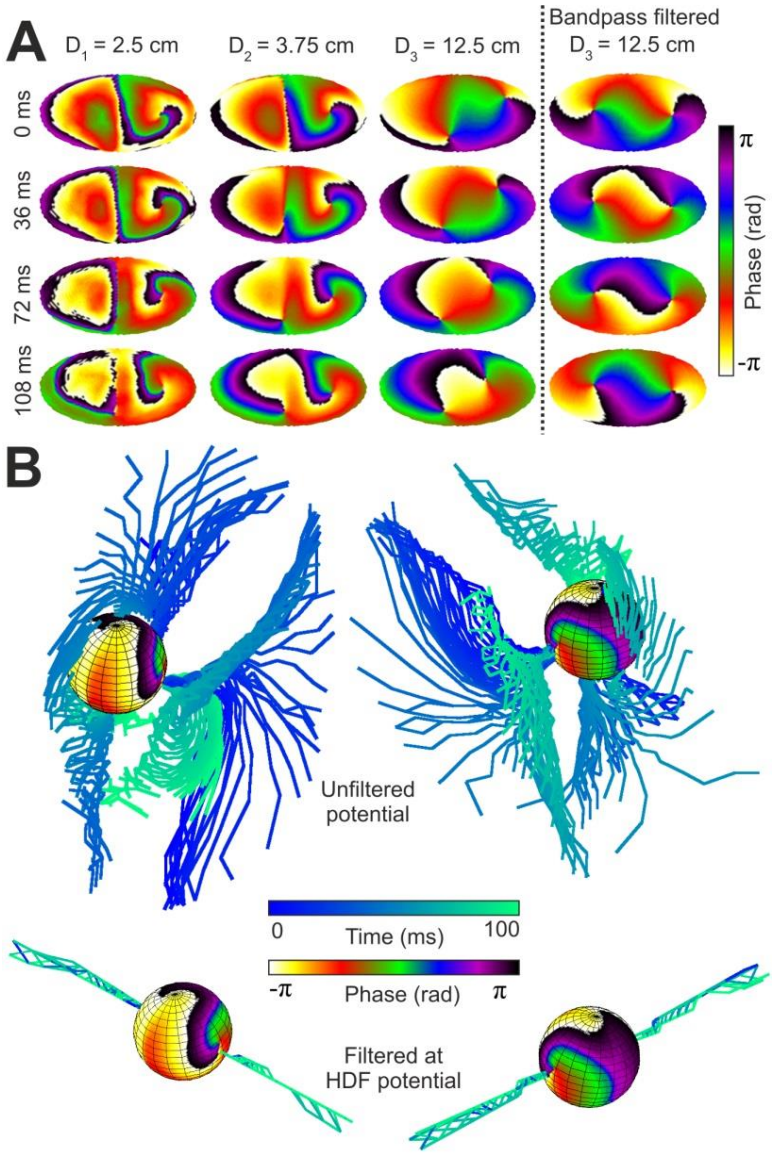

Figure 4.5 – Epicardial and transition to surface phase maps during AF in a 50% LA - 50% RA atrial model.

(A) Phase maps at 4 time instants (top to down) in 3 concentric layers at increasing distances from the epicardium (left to right) and after HDF-filtering of surface potentials. (B) Phase map of epicardial sphere and temporal distribution of filaments for unfiltered potentials and for HDF-filtered potentials.

However, Figure 4.5B shows that HDF-filtering significantly reduces the filaments' deflection and stabilizes them to follow a straight path from the epicardium to the surface. We hypothesize that the HDF-filtering minimized the influence of the atrial activity that is not activated at the HDF and thus stabilized the filament. To corroborate such hypothesis we sum all the RA dipoles into a single equivalent dipole and plot its vector projection on the RA-LA interface (Y,Z) plane (Figure 4.6A). In addition we plot the trajectory of the external SP originated by the LA rotor projection on the same (Y,Z) plane. In Figure 4.6B we notice the match in the time course and rotation frequency between the RA equivalent dipole rotation and the SP trajectory. Accordingly, we conclude that SPs arising at the interface between LA and RA as a consequence of abrupt changes in propagation direction that reached the outermost layer disappear after HDF-filtering since their activation frequencies did not match with the HDF. In addition, we notice that a mirror filament appears with opposite direction and chirality as compared to the true rotor originating at the SP on the LA epicardium. Indeed, following the attenuation of RA activation frequencies, potentials on the RA hemisphere are caused by the rotating electrical activity on the LA and observed from a contralateral point of view (see Figure 4.7).

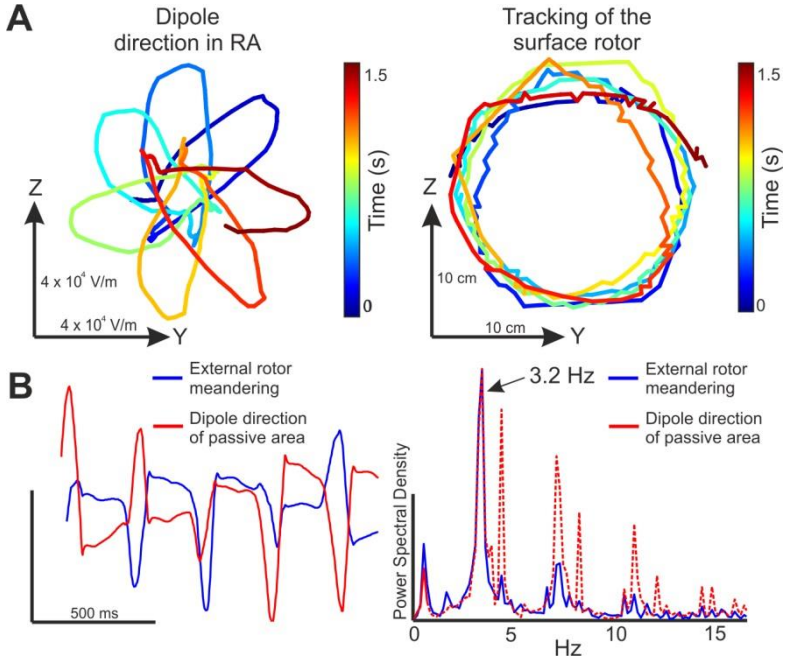

Figure 4.6 – Epicardial and transition to surface phase maps during AF in a 50% LA - 50% RA atrial model.

(A) Tracking of the dipole direction on the RA on the YZ plane (virtual septum plane) and tracking of the surface rotor than arises from the LA without HDF-filtering. (B) Temporal evolution and spectral distribution of Y coordinate for (B).

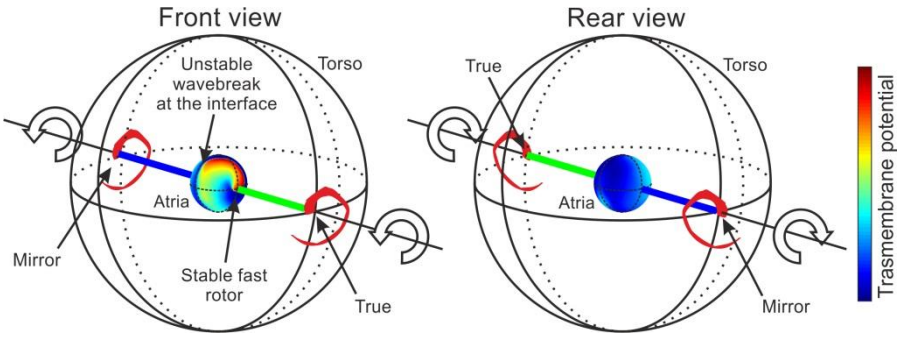

Figure 4.7 – Illustration of the concept of true and mirror rotor filaments.
The figure shows two opposing viewpoints of a simulated activity in a model that includes atrial tissue, torso volume and torso surface. Atrial voltage maps are represented according to a color scale from blue to red (color bar scale). The atrial activity consists of a stable and fast LA rotor with a fixed SP and an unstable wavebreak with unstable SP at the interface of the LA hemisphere with the slower activity at the RA hemisphere (see also Figure 2). Upon band-pass filtering of the surface data at the frequency of the stable LA rotor, two stable reentries (red wavefont patterns on the surface of the torso are the pivoting rotors with the chirality indicated by the circular arrows) with two fixed SPs become visible on the torso surface; one is termed the true SP and the other the mirror SP, based on the trajectory of the filament connecting them with the source atrial rotor. The true SP is connected to the source rotor directly (green filament) and the mirror SP is connected to the source rotor intersecting the contralateral atrial wall (blue filament), where no stable rotor at the frequency of the LA rotor is present (see rear view panel on the right side).

We further explore the behavior of filaments under more complex wave patterns; in Figure 4.8 we analyze simulation results from a 50% LA area and 50% fibrotic area model. In this case epicardial activity consists of a LA rotor with a stable SP and a very disorganized activity with several unstable SPs in the fibrotic area (Figure 4.8A). In Figure 4.8B most of the filaments originate at SPs involving a small piece of fibrotic tissue but do not originate at the driving rotor. As can be seen, the spatial smoothing stabilizes filaments and eliminates all but a single filaments' pair reaching the surface. To understand how the filaments originating at the epicardium disappear inside the torso, we color coded them according to the chirality of the SPs. Figure 4.8C clearly shows that filaments are continuous and do not vanish inside the passive volume conductor, rather a filament does not reach the surface once it joins its counter-rotating neighbor. Overall, that mutual cancelation of filament pairs reduces the average number of SPs at increasing distances from the epicardium (Figure 4.8D). At the outermost layer, only two SPs can be observed: one which is the "true" SP and another that we term the "mirror" SP and appears following the extinction of SPs at the fibrotic area and extension of the stable LA rotor filament to the contralateral aspect of the torso.

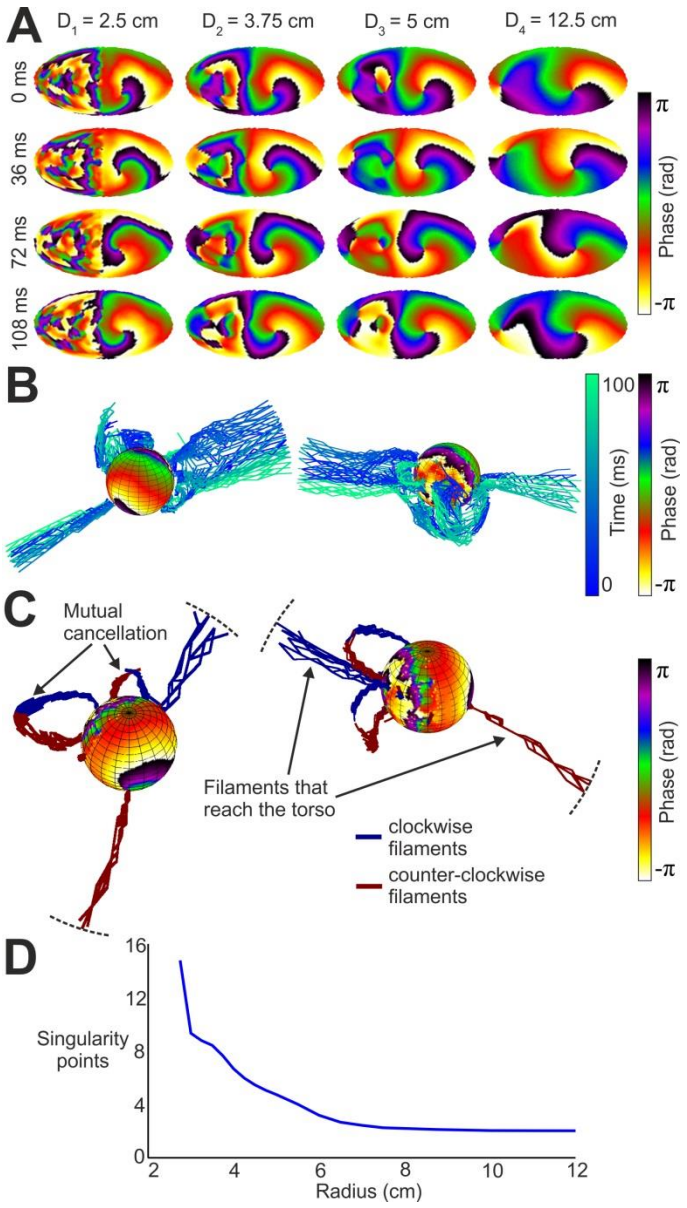

Figure 4.8 – Epicardial and transition to surface phase maps during AF in a 50% LA – 50% fibrosis atrial model.

(A) Phase maps at 4 time instants (top to down) in 4 concentric layers at increasing distances from the epicardium (left to right). (B) Phase map of epicardial sphere and temporal evolution of filaments for unfiltered potentials. (C) Phase map of epicardial sphere and distribution of filaments (clockwise rotations in blue, counterclockwise rotations in red) inside the torso during 10 ms. (D) Average number of rotors per frame.

Mutual cancellation of filaments can indeed result in a failure to detect “true” SPs originating at small atrial areas (Figure 4.9); an effect that may be counteracted by the HDF-filtering. Figure 4.9 demonstrates that the ability of surface potentials to detect SPs may depend on the amount of tissue activated around the SP. In Figure 4.9 we analyze a model with a reduced driving rotor area; the spherical atria is divided into a 10% LA area and 90% fibrotic area and the filament originating at the simulated stable LA rotor is not stable at the surface (Figure 4.9A-B). Following HDF filtering the filament originating at that driving rotor reaches the surface at the nearest point from the epicardial SP and remains stable over time together with its mirror rotor, as can be observed in Figure 4.9B-C. In our simulations, HDF filtering was required in order to detect the “true” SP in simulations for fibrotic tissue covering more than 80% of the atrial surface. Without HDF filtering, detected SPs where unstable: they were not present all of the time and had short-lasting durations (Figure 4.9D).

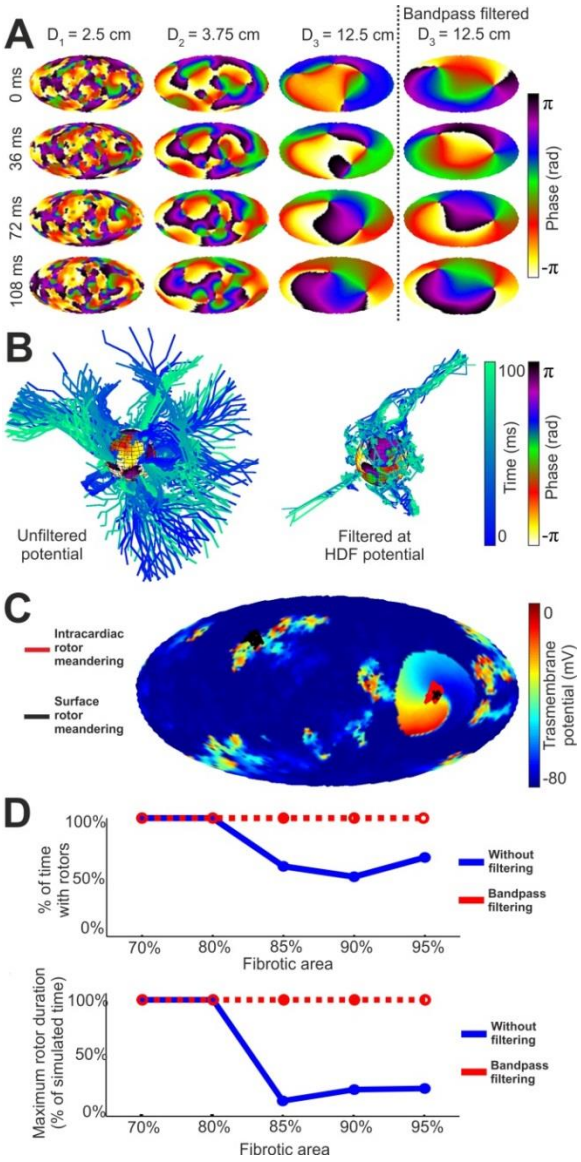

Figure 4.9 – Epicardial and transition to surface phase maps during AF in a 10 % LA – 90 % fibrosis atrial model.

(A) Phase maps at 4 time instants (top to down) in 3 concentric layers at increasing distances from the epicardium (left to right) and after HDF filtering of surface potentials. (B) Phase map of epicardial sphere and temporal evolution of filaments for unfiltered potentials and for HDF-filtered potentials. (C) Transmembrane potential at the epicardial sphere with tracking of intracardiac (red) and surface (black) rotors after HDF filtering. (D) Percentage of time with rotors and maximum rotor duration in surface phase maps from unfiltered and HDF-filtered potentials for increasing sizes of the fibrotic tissue.

The discrimination between true and mirror rotors can be performed based on the spectral properties of surface recordings at the HDF. In Figure 4.10A we show a surface phase map with 2 SPs that resulted from HDF-filtering of a simulation with only one stable rotor. The SP labeled T is the end point of the filament that connects directly to the epicardial SP (hence the label "true" SP); the SP labeled M is the surface end point of a filament originating at the epicardial wall contralateral to the stable rotor (hence the term "mirror" SP; see Figure 4.7). On the phase map these SPs seem undistinguishable; however the spectral power at the rotor frequency band is maximal at the "true" SP. Panel B of Figure 4.10 shows a similar analysis in a patient. The patient's surface phase map shows 2 SPs and the traces below the map show that while in one SP location the maximal power is at the HDF, in the other SP the power at that frequency is much less, indicating that the former is the true SP and the latter is the mirror SP.

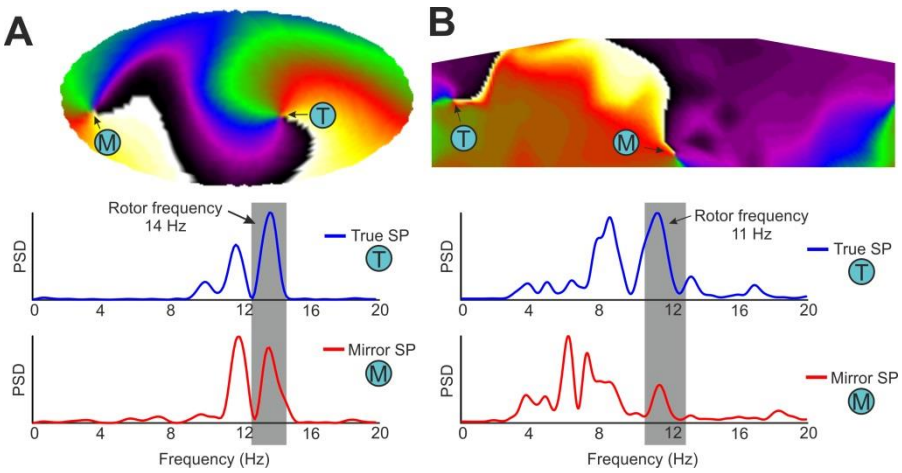

Figure 4.10 – Discrimination of true and mirror SPs at surface phase maps in a simulated and human AF.
(A) Surface phase map in 50% LA – 50% fibrosis atrial model and power spectra of surface potentials at the true rotor location (blue, T) and at the mirror rotor location (red, M). (B) Surface phase map after HDF-filtering from patient #11 during AF and power spectra of surface potentials prior to the filtering at the true rotor location (blue, T) and at the mirror rotor location (red, M).

4.3.3. Centers of rotational activity in human AF

True SPs detected, defined as those with at least 60% of their spectral content at the HDF band (Figure 4.10), tended to concentrate at certain torso areas related with the DF distribution in the atria ***[Guillem 2013]***. In Figure 4.11A, the trajectory of a surface SP that drifted during 2 seconds on the posterior torso of a patient following LA-HDF filtering (band-pass filtering at the HDF found in simultaneous

left intracardiac EGMs recordings) is depicted. In Figure 4.11B the trajectory of a SP that drifted during 500 ms on the right anterior torso in another patient after RA-HDF filtering is shown. In Figure 4.11C, the 2-dimensional histogram of "true" SP locations after LA-HDF filtering in patients with an inter-atrial DF gradient > 1 Hz (n=10) shows a predominant location of SPs on the posterior torso. The 2-dimensional histogram of "true" SP locations after RA-HDF filtering in patients with inter-atrial DF gradient shows a predominant localization on the right anterior torso, Figure 4.11D. The locations of the maximal numbers of true LA or RA SPs (dark red regions) are shown in Panels C and D to reside well within the areas demarcated by the HDFs originating either at the LA or RA, respectively, based on our previous surface-atrial DF distribution correlation study ***[Guillem 2013]***.

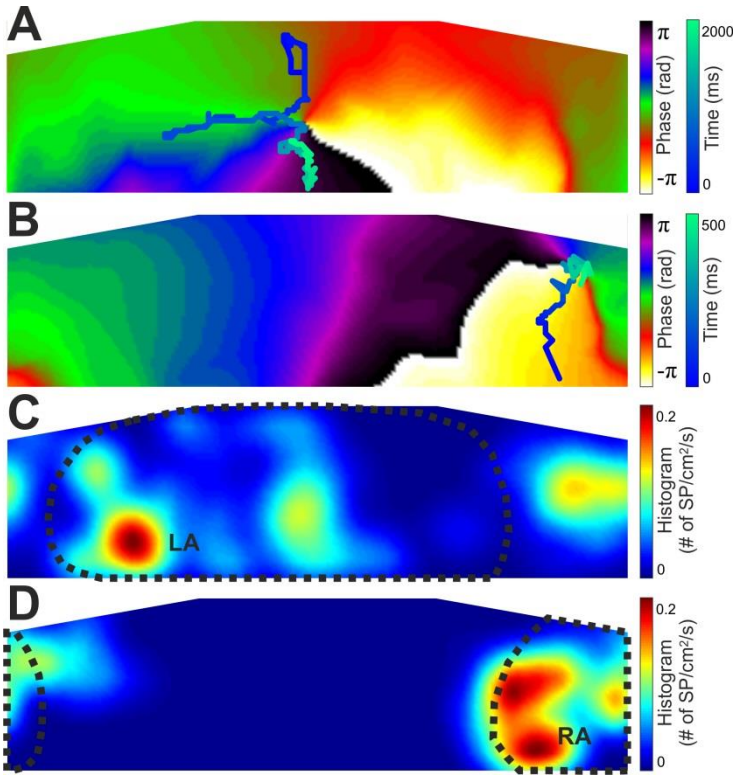

Figure 4.11 – Spatial distribution of surface rotors in human AF.
(A) Phase map and rotor tracking (blue scale) after LA-HDF filtering in an LA-fastest patient. (B) Phase map and rotor tracking (blue scale) after RA-HDF filtering in an RA-fastest patient. (C) Histogram of the rotor position for all rotors detected in patients with an inter-atrial DF gradient after LA-HDF filtering. LA-detected region is outlined with a dotted line. (D) Histogram of the rotor position for all rotors detected in patients with an inter-atrial DF gradient after RA-HDF filtering. RA-detected region is outlined with a dotted line.

4.3.4. Effect of torso volume inhomogeneity in surface phase maps

Our multi-spherical model assumes certain simplifications of the electrical propagation problem between atria and torso, as considering atria and torso as spheres or the homogeneity of the electrical properties of the torso volume. In order to study the effect of the inhomogeneity of the torso volume, we simulated the electrical propagation of the atrial activity also under inhomogeneous volume conductor properties. In particular, we evaluated the effect of subvolumes with a 2.2 fold reduction of electrical conductivity, simulating the lungs, on the surface potentials (Figure 4.12). In Panels B and C, we can notice that insertion of lungs altered the phase map on the torso surface, although the deflection of phase singularities was subtle.

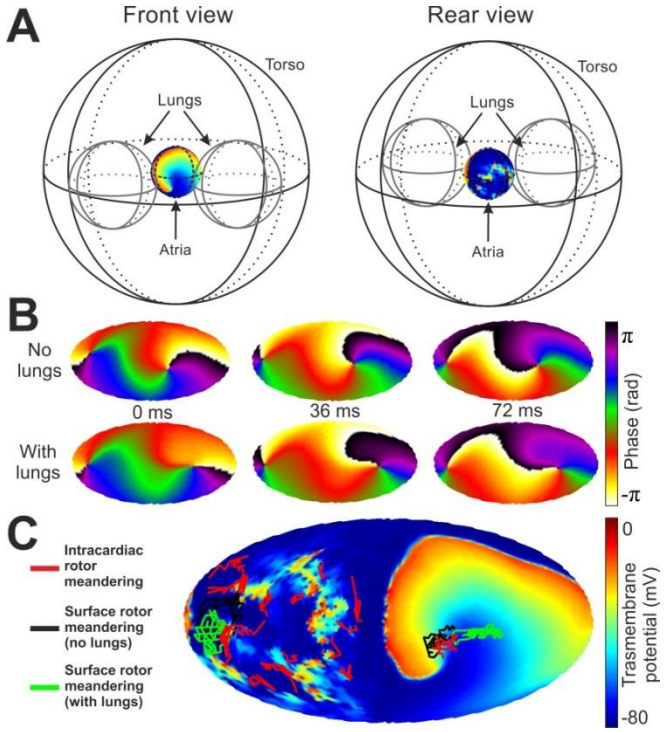

Figure 4.12 – Surface phase maps during AF in a 50 % LA – 50 % fibrosis atrial model with an inhomogeneous torso model including lungs.
(A) Location of lungs inside the torso volume. Lungs were simulated as two spheres with 7.5 cm of diameter placed between atria and torso. (B) Phase maps at 3 time instants (left to right) at the torso sphere in homogeneous torso model (no lungs) and in the inhomogeneous torso model (with lungs). (C) Transmembrane potential at the epicardial sphere with tracking of intracardiac (red) and surface rotors from the homogeneous torso model (black) and at the inhomogeneous torso model (green).

4.4. Discussion

In this study we show that phase maps of surface potentials during AF after HDF-filtering allow observing reentrant patterns with spatiotemporal stability. In contrast, the unfiltered surface phase maps display unstable reentrant patterns. The short-lived and unstable surface reentrant activity in the non-filtered data is suggested by computer simulations to result from superposition of irregular electrical activity at frequencies other than the HDF which may mask the presence of the more stable reentrant activation.

4.4.1. Rotors and AF maintenance in humans

Circus propagation was proposed as a possible mechanism for perpetuation of AF as early as in the 1920 ***[Lewis 1921]*** and gained relevance after experimental demonstration of functional rotors maintaining AF by optical mapping in isolated sheep heart preparations ***[Jalife 2002]***. However some studies continue advocating for the alternative mechanism of multiple wavelets as the predominant mechanism underlying AF maintenance ***[Lee 2013]***. In humans, evidence for stable rotors as a mechanism of AF maintenance was until recently sporadic and indirect ***[Atienza 2006]*** and also questionable ***[de Groot 2010]***. Narayan et al. reported recently that rotor activity is detectable by panoramic intracardiac mapping in about 70% of 98 out of 101 AF patients and brief ablation at the centers of those rotors was effective in terminating or slowing the arrhythmia ***[Narayan 2012]***. Although the interpretation of the mapping and ablation results obtained with the basket catheter are still somewhat controversial ***[Berenfeld 2012]*** they constitute strong evidence for the major role of rotors in maintaining AF. The results presented in this study are consistent with that latter evidence: BSPM detected rotor activity also in about 70% of the time during AF. Our study further demonstrates however, that the rotor activity is the fastest activity in the patients we studied.

4.4.2. Non-invasive identification of rotors in human AF

Previous high-density surface mapping of atrial propagation patterns showed that the presence of surface reentries was infrequent and accounted for few consecutive rotations ***[Guillem 2009, Cuculich 2010]***. Results from our mathematical simulations suggest that the ability of raw surface potentials to detect existing rotors is compromised by (i) the organization degree of areas activated at lower rates than the rotor and (ii) the amount of myocardial tissue activated at the same rate as the rotor. Interestingly, computer simulations demonstrate that the far field influence of areas with low organization could produce less distortion on SPs torso projection than areas with higher organization. However, activity of rotors covering a small atrial portion may be masked by the electrical activity of the rest

of the atria, even if it is a highly disorganized activity (see Figure 4.7). Band-pass filtering of ECG signals at the activation frequency of rotors with a driving role (i.e., a mother rotor) would accentuate the electrical activity taking place at the passing frequency band by attenuating the influence of electrical activity occurring at other rates and therefore, allows the detection of atrial SPs at the nearest projected location on the surface. Altogether, we propose that band-pass filtering may allow observing rotational patterns in cases of rotor involvement of large tissue areas and/or a disorganized activity of areas not involved in the rotation maintenance.

Previous studies in which epicardial potentials were reconstructed through the inverse solution formalism reported that rotor activity was rarely seen and accounted for only 15% of patterns observed ***[Cuculich 2012]***, although consistently observed in some selected patients ***[Haissaguerre 2013]***. These results are consistent with our observations in raw ECG signals from patients, with 8% of processed maps presenting stable rotors with more than one consecutive rotation. Our simulations results show that surface activation patterns do not preserve either the global activation pattern nor the shape of activation wavefronts. In fact, patterns observed on the torso surface represent a spatially smoothened version of epicardial propagation. A novel observation in our simulations analysis is that the filaments of epicardial rotors with opposing chiralities, particularly nearby rotors, may join inside the torso and thus those rotors are not detectable on its surface at all, further smoothing complex patterns and importantly suggesting that their epicardial reconstruction through the inverse solution is not attainable. Thus, the ability of surface ECG data to accurately retrieve complex epicardial propagation AF patterns from the patterns on the torso needs to be further explored.

4.4.3. Phase map analysis in surface ECG signals

Phase map analysis applied to surface signals has been proven useful for displaying the propagation pattern projected on the torso. Atrial rotor patterns with transmural filament, as simulated in our models here, would always produce two contralateral axes of extracellular potential rotation, that is, filaments, in the volume conductor (i.e. one pointing into the atrial cavity and the other out of the cavity). The intersections of those filaments with the torso surface thus produce two SPs: one SP at the nearest point on the surface from the epicardial SP (or "true" SP) and another "mirror" SP at the opposite side. Surface phase maps in patient data do not always reflect two simultaneous SPs because of an incomplete (not geometrically closed) mapping area. Since phase maps are insensitive to the signal power at different locations, both "true" and "mirror" SPs look similar. However, spectral analysis at the location of SPs may allow to discriminate between "true" and "mirror" SPs based on the power content at the HDF.

4.4.4. Rotors and dominant frequencies in human AF

Optical mapping both in Langendorff-perfused animal hearts during fibrillation ***[Mansour 2001]*** and monolayers of neonatal rat ventricular myocytes ***[Campbell 2012]*** has consistently shown that there is a hierarchical distribution of DF in fibrillating cardiac tissue whereby the fastest regions act as sources driving the slower ones. These high-frequency sources sustain in most cases the AF activity of both atria and may harbor functional rotors. These findings are consistent with electrogram analysis of human AF in which this hierarchical DF pattern has been linked to the existence of drivers at high-frequency sites ***[Atienza 2009, Atienza 2006]*** as well as drifting rotors at sites with transient electrogram fractionation ***[Atienza 2011]***. Besides, it has been found that adenosine infusion during AF, increases local DFs, particularly at fastest activating sites at baseline, highlighting the hierarchical organization in the DF and rate of activation of different regions in the atria ***[Atienza 2006]***.

The hierarchical DF patterns can also be detected from surface recordings so that HDF regions can be identified and related to intracardiac DFs and DF gradients ***[Guillem 2013]***. Our results suggest that human AF is driven by rotors most of the time (73%) as they could be detected after HDF-filtering. The possible reasons for the absence of rotors during the other 27% of the time are: (i) a rotational pattern was present outside the mapped area, (ii) the atrial rotor generates an un-detectable signal on the surface, or that (iii) AF was driven by ectopic foci.

4.4.5. Study limitations

We cannot conclusively confirm that rotational patterns observed in patients correspond to actual atrial rotors since we do not have simultaneous epicardial and/or endocardial panoramic data. However, we have made use of mathematical models to demonstrate that in case rotors are present during AF on the body surface, as we demonstrate in the patients, they are generated by atrial rotors. Although the models of the atria-torso system were simple spherical models, these simple models contain the active and passive volume conductor components needed to gain insight into the mechanisms of visual rotor stabilization by HDF-filtering. Insertion of inhomogeneities in the torso model such as lungs did not alter the main conclusions reached here, since they produce a reduction on the surface voltages but not in their morphology (see Figure 4.10). In the human torso as well as in a more realistic anatomical model, the projection of epicardial potentials on the surface of the torso will certainly be altered in comparison to those in the spherical models used here and, in particular, certain atrial areas could be masked, but the effects of the volume conductor and band-pass filtering shown here on the torso filaments and the surface SPs should hold. Finally, to reduce ventricular

activity from the surface recordings and highlight HDF values our AF mapping study was performed in the presence of adenosine which may alter fibrillatory activity and the spatial domain of the rotors in the atria, and potentially alter the sensitivity for their detection of the surface.

4.4.6. Conclusion

Our clinical-computational study suggests that the body surface data on wavebreaks during AF is incomplete, but it contains features that can be linked to reentrant drivers of AF. Narrow band-pass filtering allows selecting the electrical activity projected on the torso at the HDF, which stabilizes the projection of rotors that potentially drive AF on the surface. Phase maps of HDF-filtered surface ECG recordings may allow the noninvasive localization of atrial re-entries during AF, enabling further physiologically-based rationale for considering the constraints of the inverse solutions. This approach may, therefore, help in planning and performing ablation procedures, decreasing the amount of time required for the search of AF drivers.

Chapter 5

Minimal configuration of body surface potential mapping for discrimination of left and right atrial drivers during atrial fibrillation

5.1. Introduction

Several studies have demonstrated the maintenance of atrial fibrillation (AF) by discrete atrial drivers whose ablation is associated with a favourable outcome ***[Atienza 2014, Narayan 2013, Haïssaguerre 2014]*** making the identification and localization of these drivers the goal for AF mapping and ablation ***[Narayam 2013, Atienza 2009]***. Emerging technologies have used Body Surface Potential Mapping (BSPM) systems to non-invasively identify those atrial drivers, either by locating reentrant patterns ***[Haïssaguerre 2014, Lim 2015]*** or Dominant Frequencies (DF) ***[Guillem 2013]***. Although these preliminary results seem promising, the main disadvantage to extend the use of BSPM systems is the complexity of the recording approach with multiple electrodes.

The aim of this study is to determine the minimal configuration of body surface leads necessary to non-invasively identify the atrial drivers during AF and to facilitate the incorporation of the non-invasive mapping to the clinical practice. Previous studies have already investigated how the selection of different leads' sets affects the ECG waveform ***[Lux 1978, Finlay 2008, Guillem 2008]*** and have concluded that for AF signals, systems with more than 32 electrodes do not increase the signal reconstruction accuracy ***[Guillem 2009]***. However, the ability of these lead sets to characterize the nature and position of AF drivers in forms of

rotors has not been studied. The present study demonstrates that BSPM with an approximate uniform distribution of 32 or more electrodes over the torso surface is capable of rotor identification and localization in the left and right atria.

5.2. Methods

5.2.1. Patients

We included 16 patients admitted for ablation of drug-refractory paroxysmal and persistent AF and various numbers of ablation procedures (0-2, see chapter 4.2.1). All patients gave informed consent and the protocol was approved by the Institutional Ethics Committee.

5.2.2. Electrophysiological study and EGM recordings

The electrophysiological study was performed under general anesthesia and periodic heparin bolus administration. Intracardiac electrograms (EGM) were obtained from both atria during the procedure by using the following catheters introduced via the right femoral vein: (1) a standard tetrapolar catheter in the right atrial (RA) appendage; (2) a deflectable 4-mm mapping catheter (Marinr; Medtronic Inc., Minneapolis, MN) in the distal coronary sinus; (3) a decapolar circular mapping Lasso catheter (Biosense-Webster, Diamond Bar, CA) used to map the PV-left atrial (LA) junctions; and an ablation catheter (Navistar cooled-tip catheter, Biosense Webster, Inc, Diamond Bar, CA) in the LA. In two additional patients, body surface recordings were obtained simultaneously with a 64-pole basket catheter (Constellation, Boston Scientific, Natick, MA) located sequentially on the right and left atria. In patients arriving in sinus rhythm, AF was induced by burst pacing. AF episode durations longer than 5 minutes were required for inclusion in the study.

5.2.3. Body surface potential recordings

Surface electrocardiograms (ECGs) were simultaneously recorded with the EGM recordings by using a vest grid of 66 electrodes distributed as follows: 30 electrodes on the anterior, 34 on the posterior and 2 on each lateral side of the torso (Figure 5.1A). An additional left leg electrode was used in order to obtain a Wilson Central Terminal. The signals were recorded using a commercial system (Active Two, Biosemi, The Netherlands) at a sampling frequency of 2048 Hz and were stored for off-line analysis. Ventricular activation was removed by administration of a central venous bolus of adenosine (12-18 mg) and 4-seconds segments of surface ECGs surrounding the longest RR interval were used for the analysis. In

cases with ventricular activation pauses shorter than 4 seconds, the QRSTs were cancelled.

5.2.4. Lead distribution on torso and 3D model

To analyze the effect of lead configuration on AF mapping, different combinations sets of the BSPM electrodes were defined. Those sets included uniform distributions of 8, 12, 18, 24, 32, 42 and 54 electrodes as well as a non-uniform distribution of 8 leads matching the standard ECG derivation distribution (see Figure 5.1A). The surface electrical activity was then projected on the surface of a typical adult human 3D torso model with 771 nodes and 1538 faces (see Figure 5.1B), in which the surface potentials were reconstructed using the ECG signals provided by the different lead sets. The electrical potentials in areas between the nodes selected as electrodes for a particular lead configuration were interpolated as previously described.

Two areas on the surface of the 3D torso model were defined as being dominantly influenced by either left or right atrial electrical activity (Figure 5.1B): an LA area (red) covering the left, upper back and top side; and an RA area (green) covering the right, lower back and front side ***[Guillem 2013]***. Seven smaller surface areas were also defined at the front, upper back, lower back, left, right, top and floor regions for quantification of the rotor distribution (Figure 5.1C).

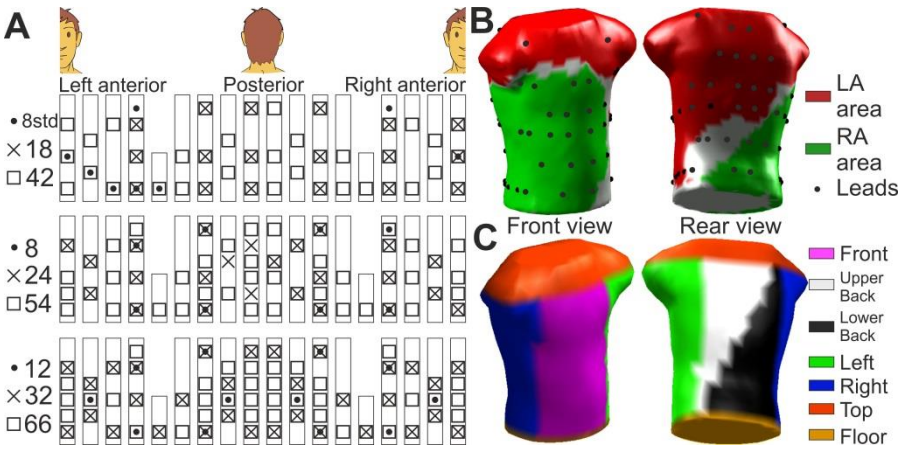

Figure 5.1 – Lead and area distribution on the torso.
(A) Distribution of the lead sets. (B) 3D torso with the 66 leads (black dots) and the LA and RA dominant influence areas (red and green, respectively). (C) Locations and names of the 7 torso areas used to assess the stability of the surface rotors.

5.2.5. Signal analysis and pattern recognition

Baseline of ECG signals was estimated by decimation to 51.2 Hz and filtering with a Butterworth 10th-order low-pass filter with a cut-off frequency of 2 Hz. This signal was interpolated to 2048 Hz and subtracted from the original signal. Leads presenting >0.5 % of their spectral content at 50 Hz were filtered with a second-order infinite impulse response notch filter centered at 50 Hz. Potential signals were then low-pass filtered with a 10th-order Butterworth filter with a cut-off frequency of 30 Hz ***[Guillem 2009]***.

Power Spectral Density (PSD) of EGMs and ECGs was computed by using Welch periodogram (2-second Hamming window with an 8192 point Fast Fourier transform per window and 50% overlap) to determine the DFs. For the reentrant pattern identification, reconstructed surface potentials were resampled at 128 Hz and then filtered at the highest DF (HDF) found on the EGM by using a cascade of a high-pass elliptic filter with cut-off frequency equal to HDF-1 Hz and a low-pass elliptic filter with a cut-off frequency equal to HDF+1 Hz. Phase maps on the torso surface were obtained from the potential phase signal of each node by the Hilbert transform. A Singularity Point (SP) was defined as any point in a phase map which is surrounded by phases monotonically increasing from 0 to 2π. Only those SPs that were present for the duration of at least two full rotations were considered as rotors.

5.2.6. Statistical analysis

The Student t-test was used to evaluate the statistical significance between continuous paired or unpaired variables, and statistical significance was considered for $p<0.05$. All data are reported in mean ± SD.

5.3. Results

5.3.1. Correspondence of full resolution invasive and surface DF measurements

Figure 5.2 shows an example of the surface DF distribution and its relationship with the panoramic intracardiac DF map of two representative cases of AF with right-to-left gradient (i.e. RA-fastest patient). The invasive DF map of patient #1 (Fig. 5.2A) shows a Highest DF (HDF) region located in the right atrial appendage where the HDF was 8.13Hz, while the rest of the atrium maintained DF values lower than 7 Hz and being 6.5 Hz the most representative measurement (6.77 Hz in the left atrial appendage).

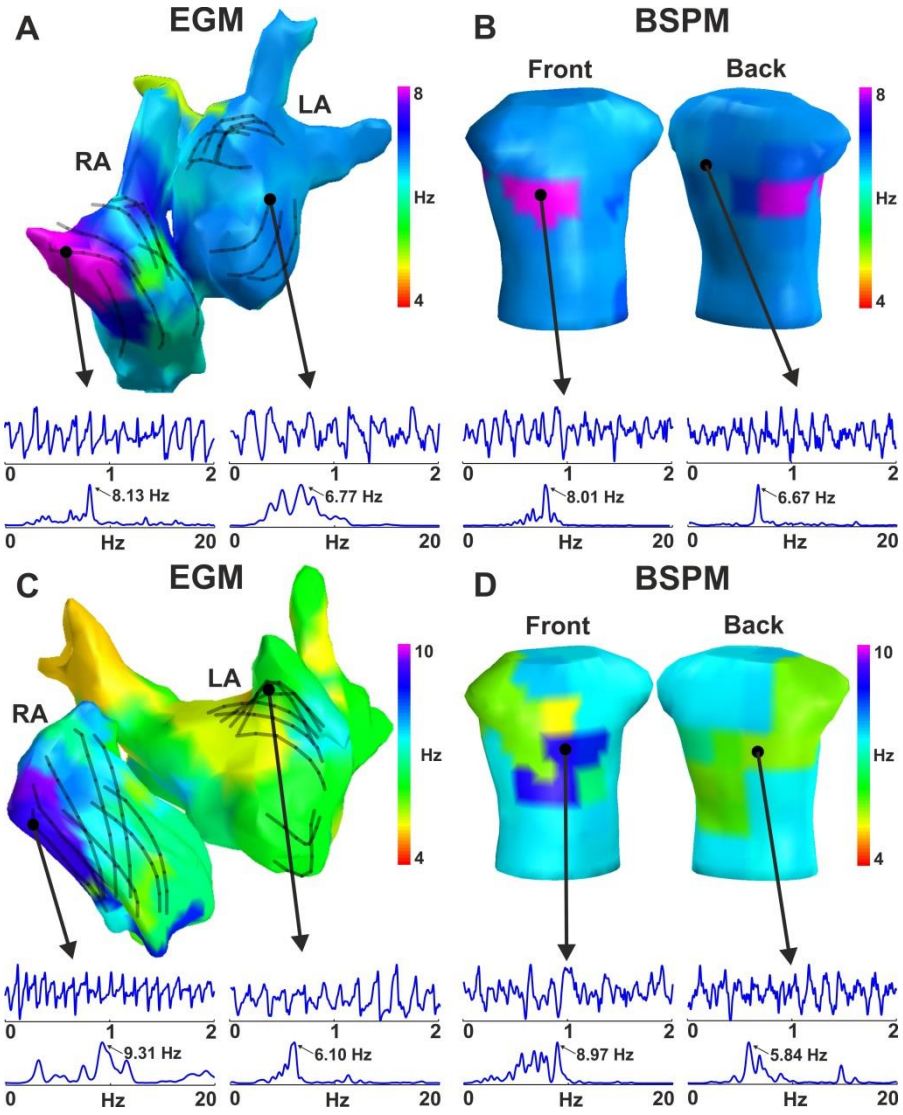

Figure 5.2 – Example of DF distribution in patient #1.
Example of DF distribution in panoramic recordings from 2 patients. Invasive DF distribution from multipolar basket catheters recordings (A,C) and simultaneous non-invasive DFs from BSPM (B,D) and the corresponding voltage signals and their Power Spectral Density (PSD).

The surface DF map obtained with the full leads set (66 electrodes, Fig, 5.2B) is shown to display two well demarcated domains: almost all the torso surface presents a DF value around 6.5 Hz (6.67 Hz in the ECG from the posterior left torso), whereas a reduced region of the right side of the torso (corresponding to the RA influenced region in Figure 5.1B) depicts a higher DF value of 8.01 Hz, similar

to the HDF invasively measured. The panoramic invasive DF map from patient #2 (Fig. 5.2C) shows a similar frequency distribution with the HDF region located in the right atrial appendage (9.31 Hz) while the rest of the atrium was activated between 5 and 7 Hz (6.10Hz at the posterior LA wall). In this case the surface DF map (Fig. 5.2D) depicts a region in the right front side of the torso with a DF of 8.97Hz, whereas the rest of the surface presented lower values, being 5.84Hz the DF in the back.

5.3.2. Surface dominant frequencies for the full BSPM configuration

The distribution and match of the atrial and surface DFs was studied for the the subset of 14 patients with discrete invasive EGM recordings. Average frequency differences between the intracardiac DF from the LA and RA and the surface DFs are depicted in Figure 5.3A. For each atrium, there is a torso area in which the difference between the intracavitary and non-invasive DF is minimal at <0.5 Hz (blue): the left surface side, including the left axillae, for the LA frequency; and the right front surface side of the torso for the RA frequency. The same surface regions can be identified in Figure 5.3B as having the highest correlation coefficient (red) between the intracavitary DFs measurements from the LA and RA and the surface DF values from the BSPM. Overall, this analysis establishes the surface areas that are predominantly influenced by LA and RA activity and were used to define the LA and RA torso areas in Figure 5.1B.

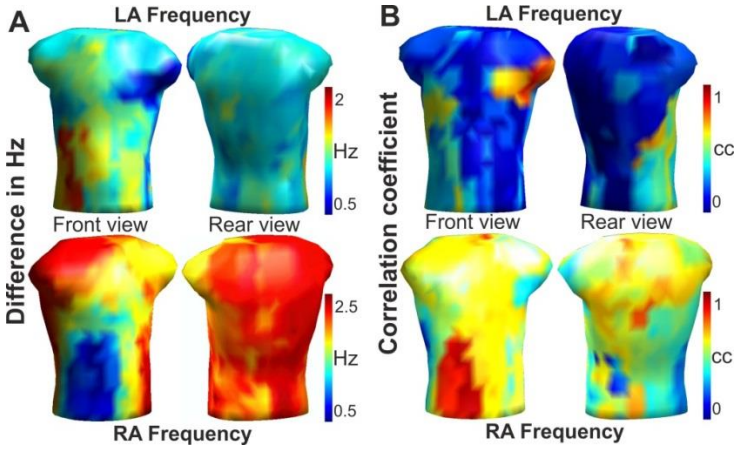

Figure 5.3 – Relationship between invasive and non-invasive DF measurements. *(A) Surface distribution of the error average in Hz between the LA (Top) and RA (Bottom) DFs and the BSPM DF for the 14 patients. (B) Surface distribution of the correlation between the LA (Top) and RA (Bottom) DFs and the BSPM DF for the 14 patients. The areas with lowest errors in (A) (blue) are the areas with the highest cross-correlations in (B) (red).*

5.3.3. Surface distribution of dominant frequencies for reduced-leads BSPM

The errors in the DFs identification from the BSPM relative to the intracavitary recordings were measured for the different lead sets. As shown in Figure 5.4A the Highest DF (HDF) presented its maximal error for the standard 8-leads BSPM configuration (1.3±1.8 Hz), and this error decreased for arrangements with more leads with uniform distribution and stabilized at around 0.35 Hz for 12 or more electrodes. The coincidence between DFs obtained from intracavitary and surface recordings was also evaluated by the correlation coefficient for the highest, LA, RA and LA-RA (gradient) DFs (Figure 5.4B). It is shown that the correlation between invasive and non-invasive DF measurements had low values for low-resolution lead configuration. However, for 12 or more leads, the correlation coefficient reached higher and uniform values for all the lead sets: 0.75 for LA DF, 0.85 for the DF gradient, 0.94 for RA DF and 0.95 for the HDF.

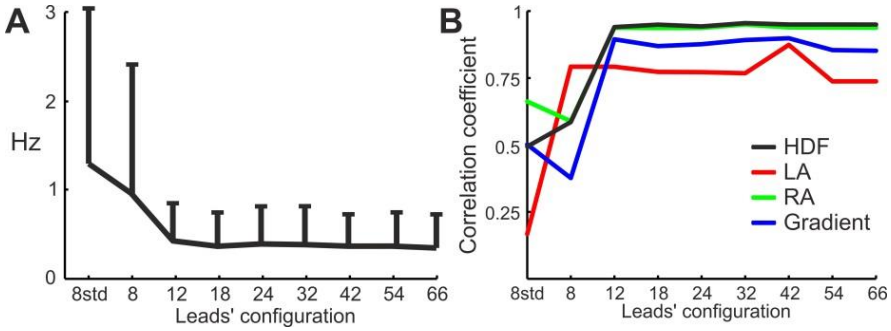

Figure 5.4 –Comparison between invasive and surface DF measurements.
(A) Difference (in Hz) between the Highest DF (HDF) obtained from invasively (EGM) and non-invasively (BSPM) recordings as a function of the leads' configuration. (B) Correlation of the DFs values between the EGM and BSPM signals as a function of the leads' configuration.

5.3.4. Surface distribution of AF drivers for reduced-leads BSPM

With the aim of analyzing the number of leads required to detect AF maintenance mechanisms, we studied the reproducibility of the surface distribution of reentrant patterns for different lead arrangements. Figure 5.5 shows a qualitative example of the phase maps and the rotor distribution obtained for one of the patients using different BSPM lead's distribution. The singularity point that can be observed at the back of that patient is at the same place for 66, 32 and 8 leads distribution, although the lower resolution of the latter also shows a SP in the front

that is not seen at higher resolutions (in the higher resolution of 66 and 32 leads a SP is at the floor of the torso and is not seen in the panels). As shown by the cumulative SP presence maps in the right side panels, the rotor distribution is relatively similar for the 66 and 32 leads, but it considerably altered for the 8 leads configuration.

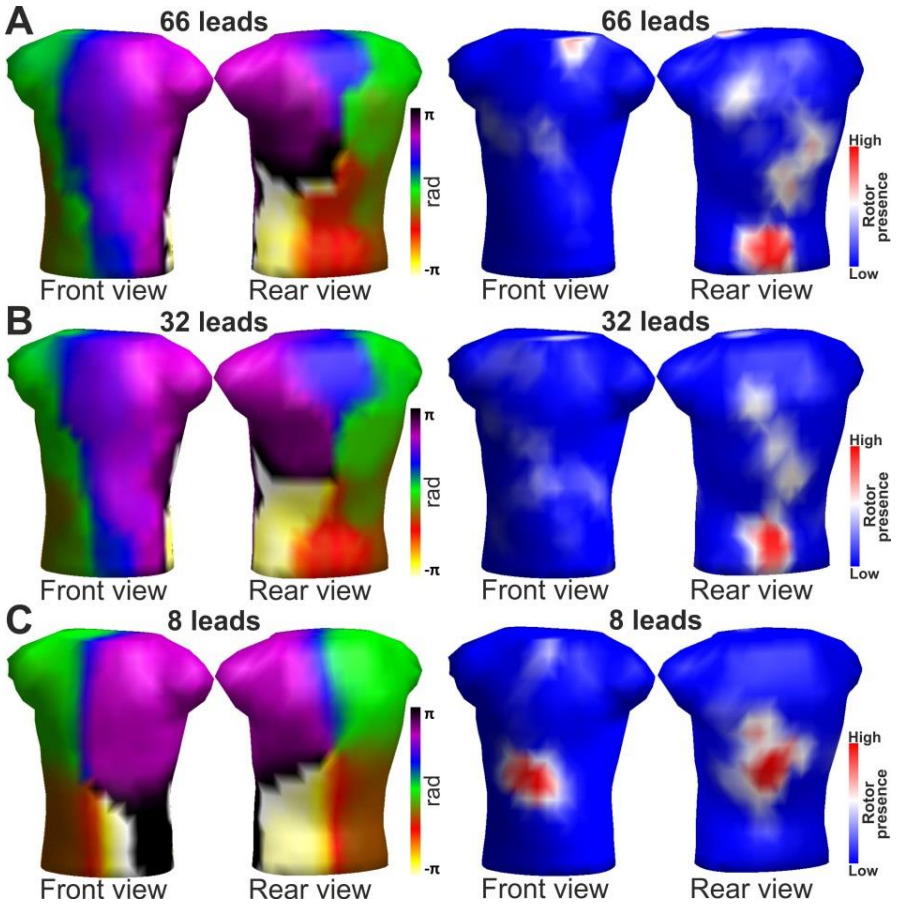

Figure 5.5 – Sample surface phase maps (left) and surface rotor number distributions (right) for different leads BSPM configuration.
(A) 66 leads. (B) 32 leads. (C) 8 leads uniformly distributed.

To quantify such effect of the leads configuration on rotor localization on the surface, the number of SPs and rotors (i.e., SPs lasting more than a full rotation) at 7 distinct torso surface areas, as defined in Figure 5.1C and following HDF band-pass filtering, for the different lead distribution was counted. The number of SPs and rotors at each region for each lead configuration was correlated with the distribution obtained with highest resolution configuration of 66 leads. In Figure 5.6 it is shown that, as expected, the low-resolution leads' configuration showed

low correlation with the full resolution distribution, both for SPs (0.05±0.23) and rotors (-0.23±0.22). The correlation with the full resolution distribution increased with the number of leads, reaching a constant maximum value for 32 or more leads. The SPs distribution reached a maximum correlation of 0.95, while the rotor distribution reached a correlation coefficient around 0.8 for 32 leads configuration or more.

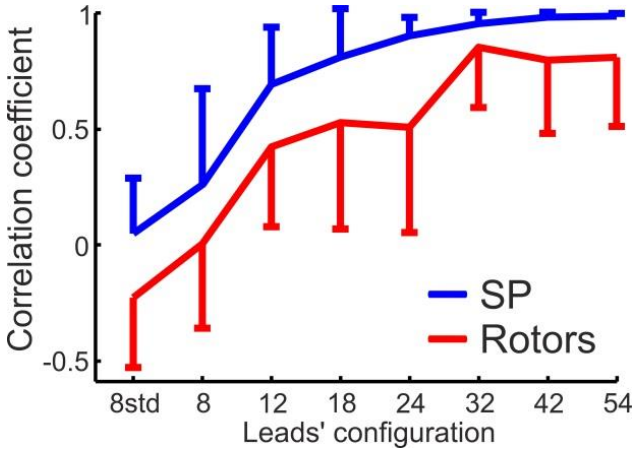

Figure 5.6 – Cross correlation between the amount of SPs and rotors localized to each of the 7 surface regions (defined in Figure 1), as a function of the leads' configuration, for the 14 patients.

5.3.5. Diagnostic value of the non-invasive atrial activity

Once the accuracy of noninvasive measures was evaluated for different leads configurations, we assessed the statistical ability of these configurations to provide localization of drivers in AF patients. We measured the percentage of time in which surface rotors after HDF band-pass filtering were present in the LA and RA surface areas (Figure 5.1B) for the different lead configurations. In Figure 5.7 the patients were separated into LA-fastest patients (bottom bars) and RA-fastest patients (top bars) groups based on whether the DFs at the EGM recordings when the LA-DF was higher than the RA-DF or vice versa, respectively. Here we predict that the surface area corresponding to the atrium with the fastest activation rate would show the highest number of rotors. Indeed, as expected, cumulative data in Figure 5.7 shows the RA-fastest patients present more rotors in the RA surface area than in the LA area, and conversely, the LA-fastest patients present more time with rotors in LA surface area than in RA area. However, this trend is only observable for mid- to high-resolution leads configurations; statistical significance of $p<0.05$ of the distinct rotor presence was obtained only with 18 or more surface electrodes. Specifically, there were significant differences between the number of LA and RA area rotors for 18, 24, 32, 42, 54 and 66 leads for RA-fastest patients, and for 32

leads between LA and RA area rotors for the LA-fastest patients. Comparing the rotor presence in the same area between patients' groups, there was significant difference of rotor presence in the LA area between RA-fastest and LA-fastest patients for 24, 32, 42, 54 and 66 leads; and in the RA area for 32 leads. These results show that BSPM with an approximate uniform distribution of 32 or more electrodes is capable of the rotor localization between the LA and RA similar to differentiation with 66 leads configurations.

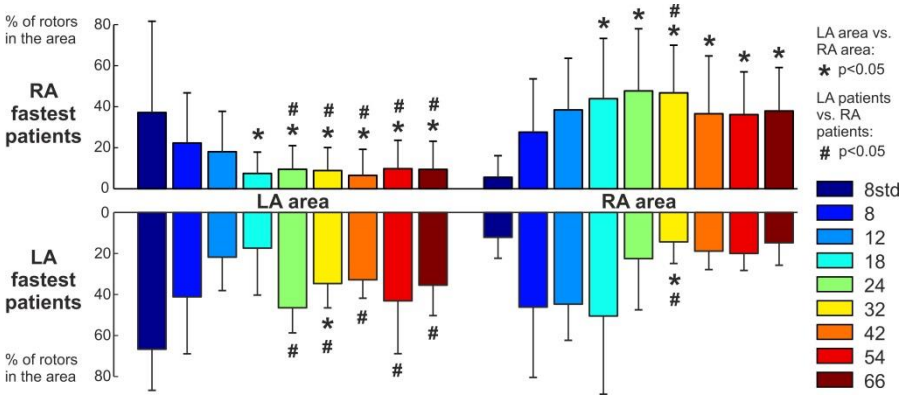

Figure 5.7 – Summary of surface distribution of rotors for the 14 patients.
Bars represent the number of rotors localized to the LA area (left) and RA area (right) for RA-fastest patients (Top, N=10) and LA-fastest patients (Bottom, N=4). Each color represents a different leads' configuration. Statistical comparisons for the 14 patients were made between rotors presence in LA vs RA areas (left and right) for each leads' configuration (*), and between RA-fastest and LA-fastest patients (top and bottom) for each leads' configuration (#).

5.4. Discussion

The present study demonstrates that surface rotor localization based on highest DF distribution assessment with 12 or more electrodes presents a high correlation with the full-resolution BSPM system of 66 leads. Similarly, surface rotor localization based on surface reentrant activity identification at the torso areas enables accurate differentiation between LA and RA fastest patients for lead sets with 32 or more leads. Thus, the increase of the number of uniformly distributed leads above 14 does not increase the BSPM diagnosis value for LA versus RA drivers in AF patients. Therefore, reduced-leads BSPM systems enable non-invasive discrimination between LA or RA atrial drivers with similar results as higher-resolution 66-leads systems.

5.4.1. Mechanisms of AF maintenance and their non-invasive characterization

The mechanisms underlying AF in patients are not always clear. Recent studies utilizing new mapping methods have supported the existence of a hierarchical AF organization of activity whereby identifiable sources of fast activity ***[Atienza 2014, Atienza 2009]*** or in the form of ectopic or rotor activation patterns maintain the arrhythmia ***[Narayan 2013, Haïssaguerre 2014]***, but controversies still exist ***[Narayan 2014, Allessie 2014]***. Arguably, better and easier identification of localized AF sources would render better targets for ablation thus efforts to improve technologies for localization of AF drivers are ongoing ***[Lim 2015, Guillem 2013]***. Although intra-cardiac recordings are considered the most reliable method for AF characterization ***[Narayan 2013]***, they are not free of difficulties ***[Berenfeld 2012]*** and the need for panoramic mapping led to the development of noninvasive AF mapping methods. Noninvasive mapping methods not only would allow for relatively simpler deployment than the usage of multiple intra-cardiac electrodes, but will also enable studying patients outside of the clinical EP laboratory and pre-planning individual ablation procedures. Some of the limitations of non-invasive technologies are their reduced sensitivity to the atrial activity during fibrillation. We have recently studied the effect of the body torso on body surface mapping and found that a significant amount of atrial information is retained on the body surface recordings ***[Guillem 2013, Pedrón-Torrecilla 2016]***. These studies showed that utilizing the appropriate frequency and phase domain processing, with a band-pass filtering at the highest DF and SP detection allows localization of the surface reentrant activity originating at either the LE or the RA. Thus, non-invasive analysis of the AF reentrant activity on the torso surface enables rotor drivers localization at a dominant atrium to facilitate ablation procedures ***[Atienza 2014, Atienza 2009]***.

5.4.2. Lead distribution in body surface electrocardiography

The number of body surface leads and their position have been broadly acknowledged as affecting arrhythmia diagnostic accuracy, but in clinical practice the standard ECG leads configuration largely prevails. Indeed, the standard ECG lead set does not accurately respond to all diagnostic cardiology needs, and for this reason body surface potential mapping (BSPM) systems with a higher number of leads and spatial resolution were developed. However, today there is no standard evaluation or recommendation for the surface electrode configuration for the different cardiac diseases and AF in particular.

The number of electrodes necessary for BSPM utilization has been mostly evaluated for ventricular activity based on the quality of signals ***[Lux 1978, Finlay***

2008, Guillem 2008, Guillem 2009]. Although some studies argue that in the ECG signal there are about 10 statistically independent components ***[Hoekema 1999]***, Lux et al. observed that for the study of healthy ECG, 30 leads allowed to reconstruct the set of torso signals with a correlation of 98% and an error less than 3% with the original signals ***[Lux 1978]***. The position of these 30 electrodes was not uniform across the torso surface, being the front side of the torso the densest area. More recently, a study by Finlay et al in a population of healthy and myocardial infarction patients observed that 32 electrodes were enough to provide an acceptable level of reconstruction, but in this case different configuration of the electrodes yielded little differences in the ECG signals ***[Finlay 2008]***. In agreement to this, we conducted a study in patients with myocardial infarction, bundle-branch block, and ventricular hypertrophy patients and found that increasing the lead number above 30 electrodes had little effect on the ECG signal and the leads configuration had little importance on the signal reconstruction, which was more dependent on the population under study ***[Guillem 2009]***.

Only few studies investigated the role of the number and distribution of BSPM leads in studying atrial electrophysiology. Although the morphology and variability of the standard ECG signal in AF has been widely studied, only few authors have considered that the standard ECG system is sensing mostly the ventricles and have proposed the use of a different arrangement of the 9 standard leads in order to increase the effectiveness in AF characterization ***[Ihara 2007]***. The broader electrode settings of BSPM has been used to study atrial arrhythmias ***[Lim 2015, Gerstenfeld 2000, Lian 2002, Sippensgroenewegen 1998]***, but without an evaluation of accuracy for AF mechanisms characterization. In a recent study, Guillem et al studied the number of leads necessary to properly reconstruct the torso potentials in AF signals ***[Guillem 2009]***. This study showed that during atrial fibrillatory rhythms a set of 34 electrodes was able to reconstruct the surface potential with the same accuracy as systems with more leads, since the reconstruction error reaches the noise level at the recording electrodes. The latter is consistent with our results here: we propose that mapping with 32 or more uniformly distributed surface leads does not increase the diagnostic information of inter-atrial rotor localization. For the DF inter-atrial distribution, even less leads could be enough. In spite of the disorganized AF signal nature, the BSPM systems for the study of the AF seem to need the same amount of electrodes (about 32) as the BSPM systems for the study of ventricular non-fibrillation arrhythmias ***[Lux 1978, Finlay 2008, Guillem 2008, Guillem 2009]***. This observation is also consistent with the natural smoothening filtering effect of the torso volume conductor that projects on the torso surface only the strongest characteristics of the atrial waves, with reduced sensitivity for the small electrical waves, no matter how many leads are used for mapping.

5.4.3. Limitations

The present study was conducted on a small number of 14 patients, however its results are broadly consistent with previous findings ***[Lim 2015, Gerstenfeld 2000, Lian 2002, Sippensgroenewegen 1998]***. Moreover, as the optimal lead configuration on the torso depends on the population under study, we submit that the use of our heterogeneous AF patients cohort, with paroxysmal, persistent and different number of ablation procedures ***[Guillem 2013, Pedrón-Torrecilla 2016]*** justifiably enhances our conclusions on AF inter-atrial characterization. However, the limited number of patients requires us to use uniform lead distributions, since the study of the best lead placement would show results highly dependent from the patients in our dataset.

This study analyses AF under the effect of the adenosine. Although previous studies have reported that Adenosine infusions accelerate the activation rate during AF, they also reported that the DF distribution in the atria remained stable over time ***[Atienza 2006, Atienza 2009]***. Thus, although Adenosine could have affected the local DF values, their distribution across the atria and on the body surface should have been preserved. For outpatient application, however, our BSPM based DF mapping should be performed with software removal of the ventricular electrical activity.

5.4.4. Conclusions

For coarse AF analysis, BSPM systems with 32 or more uniformly distributed leads can achieve the same results as systems with larger number of leads. Consistent with the literature, those leads would be sufficient to properly reconstruct the surface electrical potentials for inter-atrial localization of AF drivers in the form of highest DF or rotors. Medium-resolution BSPM systems retain the relevant clinical information that enables discrimination between RA- or LA-fastest patients, highly relevant for increased ablation effectiveness. The results of this work can be the basis for the BSPM system simplification and wider clinical adoption for better non-invasive AF pre-ablation screening and planning as well as real-time EP mapping auxiliary guidance.

Chapter 6

Understanding phase mapping and temporal filtering for reentrant activity identification in atrial arrhythmias

6.1. Introduction

Reentrant propagation of atrial electrical activity plays a decisive role in the perpetuation of atrial arrhythmias. It is widely accepted that Atrial Flutter (AFL) is caused by a reentrant electrical activity around an anatomical obstacle like valves or veins and that the interruption of such reentrant circuits is crucial to extinguish the arrhythmia ***[García-Cosio 2012]***. The nature of the mechanisms that maintains atrial fibrillation (AF) is still controversial ***[Allessie 2014]***. However, the scientific evidence that atrial fibrillatory process is maintained by functional reentries and that the ablation of the atrial regions harboring such rotors can terminate the AF episodes is increasing both in experimental ***[Berenfeld 2014, Guillem 2016]*** and in clinical practice ***[Narayan 2013]***.

Progress in ablative therapies for AF has been paired with the development of mapping systems able to characterize the atrial electrical activity. These mapping systems are diverse in nature, such as optical systems based on the use of potentiometric dyes ***[Berenfeld 2011]***, endocardial electrical recording systems using catheters with multiple poles ***[Narayan 2013]*** or noninvasive systems such as Body Surface Potential Mapping (BSPM) ***[Guillem 2013]*** or electrocardiographic imaging (ECGI) ***[Haissaguerre 2014]***. Phase analysis of these signals has become the most used method to identify reentrant patterns, since

pivoting activity provokes singularities in the phase maps that can be easily identified ***[Gray 1998]***.

Because of both the novelty of the AF maintenance hypotheses and the mapping techniques themselves, there is no evidence regarding the actual true and false detection rates of phase analysis for detecting AF rotors since other types of non-reentrant electrical activity may also cause the appearance of singularity points. Additionally, some techniques make use of temporal signal filtering for improving the reentrant pattern identification, adding further uncertainty. In this work we made use of mathematical models of different atrial arrhythmias to explain the localization process of reentrant patterns by phase mapping as well as to study the effect of temporal filtering in detecting reentrant patterns.

6.2. Methods

6.2.1. Atrial mathematical models

A realistic 3D model of the atrial anatomy was used to simulate the atrial electrical activity (see chapter 3.1). An ensemble of 17 different arrhythmic electrical patterns was simulated, divided in 4 groups according to the nature of the electrical pattern. Group I was composed by one AF pattern driven by multiple rotatory sources and 4 AF patterns driven by a single rotor at varying locations of the LA: at Pulmonary Veins (PV), at the Posterior Wall of the Left Atrium (PLAW) and at the Right Atrial Appendage (RAA). Group II was composed by 4 Atrial Flutter (AFL) patterns: a typical AFL, a clockwise atypical AFL, an Inferior Vena Cava (IVC) atypical AFL and an atypical AFL turning around the Pulmonary Veins (PV) due to the existence of inactive tissue in the PLAW. Group III was composed by 4 Atrial Tachycardia (AT) models electrically stimulated at different locations of the atria (IVC, LSPV, RIPV and RAA). Group IV was composed by the same AT simulations as Group III in which scar regions were added in order to create more complex propagation patterns.

6.2.2. Signal acquisition

For each simulation, a uniform mesh of 2048 unipolar EGMs was calculated surrounding the epicardial surface and the ECG potentials on the torso model were calculated in a mesh formed by 771 nodes (see chapter 3.3). White Gaussian noise was added to the ECG signals with a signal-to-noise ratio of 60dB and all signals were then referenced to the Wilson Central Terminal. Inverse-computed EGMs (icEGM) were obtained by solving the inverse problem with the zero-order Tikhonov's regularization method and the L-curve method for choosing the best regularization parameter (see chapter 3.3).

For evaluating the performance of the rotor identification technique in scenarios with real reentrant activity versus noisy or highly disorganized scenarios, the rotor detection algorithm was tested for spatially randomized EGM recordings. In such scenarios, the same EGM signals were used but only after replacing them randomly to a different position and thus creating maps that were completely unorganized. These random EGM signals were also used as previously described to obtain the ECG and then the icEGM signals for the rotor analysis.

6.2.3. Signal filtering

Baseline of EGM, ECG and icEGM signals was estimated by decimation to 12.5 Hz and filtering with a Butterworth 10th-order low-pass filter with a cut-off frequency of 2 Hz. This signal was interpolated to 500 Hz and subtracted from the original signal. EGM, ECG and icEGM signals were then low-pass filtered with a 10th-order Butterworth filter with a cut-off frequency of 30 Hz ***[Guillem 2013]***.

For the DF analysis, EGM, ECG and icEGM signals were baseline-removed as previously reported and were then low-pass filtered with a 10th-order Butterworth filter with a cut-off frequency of 10 Hz [Guillem 2013]. Power spectral density of all signals was computed using Welch periodogram (65536 point Fast Fourier transform and 80% overlap) to determine the local DFs with a spectral resolution of 0.01Hz ***[Guillem 2013]***.

Narrow band-pass filtering was carried out in EGM, ECG and icEGM by applying a temporal filter centered at the highest DF (HDF) found on the atrial or torso surface by using a cascade of a high-pass elliptic filter with cut-off frequency equal to HDF - 1 Hz and a low-pass elliptic filter with a cut-off frequency equal to HDF + 1 Hz.

6.2.4. Reentrant activity identification

Rotor location was carried out by identification of singularity points (SP) in the phase signal map obtained with the Hilbert Transform (see chapter 3.4). As it can be observed in Figure 6.1, the phase transformation assigns a phase value between $-\pi$ and π for each sample of the signal, and thus each phase corresponds to a given state of the action potential (i.e. π for resting, $\pi/2$ for depolarization, 0 for plateau and $-\pi$ for repolarization). A phase map, therefore, allows inferring the propagation pattern and the center of rotors appear as points surrounded by phases ranging from $-\pi$ to π.

In order to identify SPs, phase values were obtained along 3 different circles surrounding each evaluated point. Six to twelve points per circle were used for the phase analysis in which the EGM, ECG and icEGM signal was interpolated by a weighted average of the neighboring nodes, being d^{-2} the weight for each node and d the distance between nodes. An evaluated point was defined as a SP only when

the phases of at least two of these three circles was gradually increasing or decreasing for a total of 2π, and if the mean phase error respect to a straight line was lower than a threshold: 0.4 radians for EGM, 0.2 radians for ECG and no threshold for icEGM.

A rotor was defined as the connection between SPs across time. The distance between SPs at consecutive time instants should be less than 1 cm (EGM and icEGM) or 5 cm (ECG) to be related and maintain a continuity of rotation. Finally, only long lasting rotors, defined as those that complete at least half rotation were considered as rotors and other SPs were discarded.

6.3. Results

6.3.1. Restrictions in rotor identification

Figure 6.1A depicts the transmembrane potential map of an electrical pattern driven by a stable rotor placed in the posterior wall of the left atria (PLAW). In order to illustrate the ability of the different mapping techniques to identify singularity points, and thus the position of the rotor, phase mapping was evaluated for transmembrane potential signals. Firstly, Figure 6.1B depicts an illustrative example of the Hilbert Transform in a transmembrane potential signal for two consecutive atrial action potentials. The phase transformation assigns a phase value between $-\pi$ and π for each sample of the signal, and phases are consecutively assigned for each action potential state. By this way, each action potential state corresponds to a different phase value (π for resting, $\pi/2$ for depolarization, 0 for plateau and $-\pi$ for repolarization) and by displaying a map with all the instantaneous phase values all signal states in a time instant can be observed simultaneously. Figure 6.1C depicts the phase mapping process for rotor location in the transmembrane potential signal of the example in Fig. 6.1A. Six transmembrane potential signals around the rotor position are depicted and down their phase transformation. Since the electrical pattern is activated surrounding the rotor tip, cell depolarization is consecutive at the six positions (dashed arrows), and the same consecutive pattern can be observed at the phase transform. In an arbitrary time instant the six marked points showed consecutive phase values, since they were activated consecutively. When all phases for the same time interval are depicted (Figure 6.1C down) they expose a singularity point between the six recording points, where all the phases from $-\pi$ to π converge.

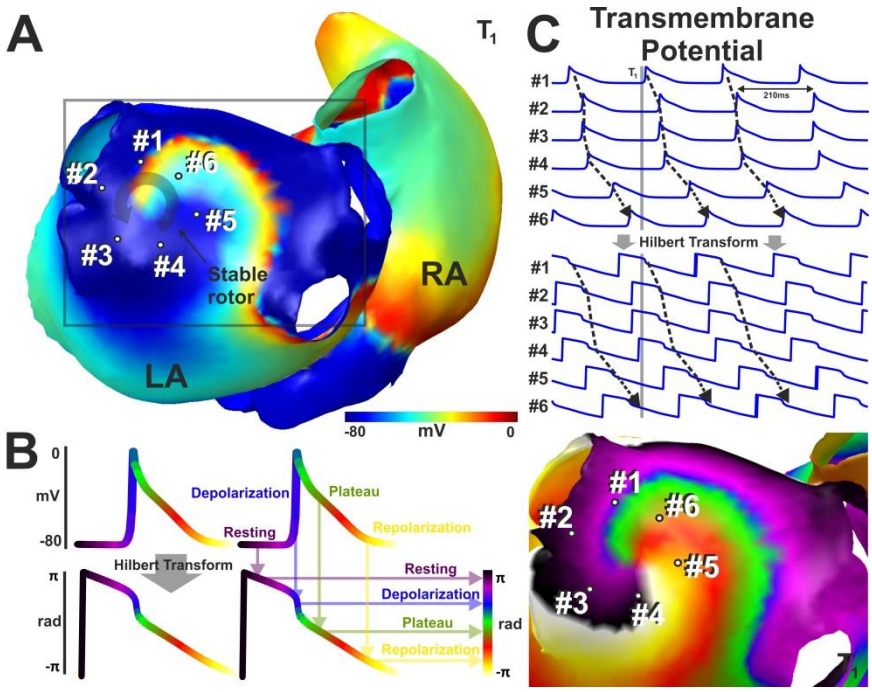

Figure 6.1 – Example of phase mapping in different electrophysiological recordings.

(A) Transmembrane potential map for an AF model maintained by a stable rotor in the posterior wall of the left atria. (B) Transmembrane potential signal (up) and its Hilbert Transform (down). (C) Transmembrane potential at 6 positions marked in (A) (up), its phase transforms (middle) and the correspondent phase map (down).

We found that we were able to identify more SPs in random EGM activity than in rotor-driven AF models, see Figure 6.2D. We found that phase transitions around SPs that arise from non-rotating activity were less gradual than those arising from rotational activity. In Figure 6.2A the phase transitions in three concentrical circles around detected SPs are shown for a rotational and a random pattern. In this example, deviation from a linearly gradual change transition was largest in the outermost circle (1.5 cm radius) for the random pattern since phase was not monotonically increasing. Overall, this deviation was larger in the random patterns than in rotor-driven AF (1.00±0.04 vs 0.47±0.20 rad, $p<0.01$), see Figure 6.2C. In order to reject spurious SP detections a linearity threshold (0.4 rad) was applied to SP detections, resulting in a reduction in the amount of detected SPs, as it can be observed in Figure 6.2D.

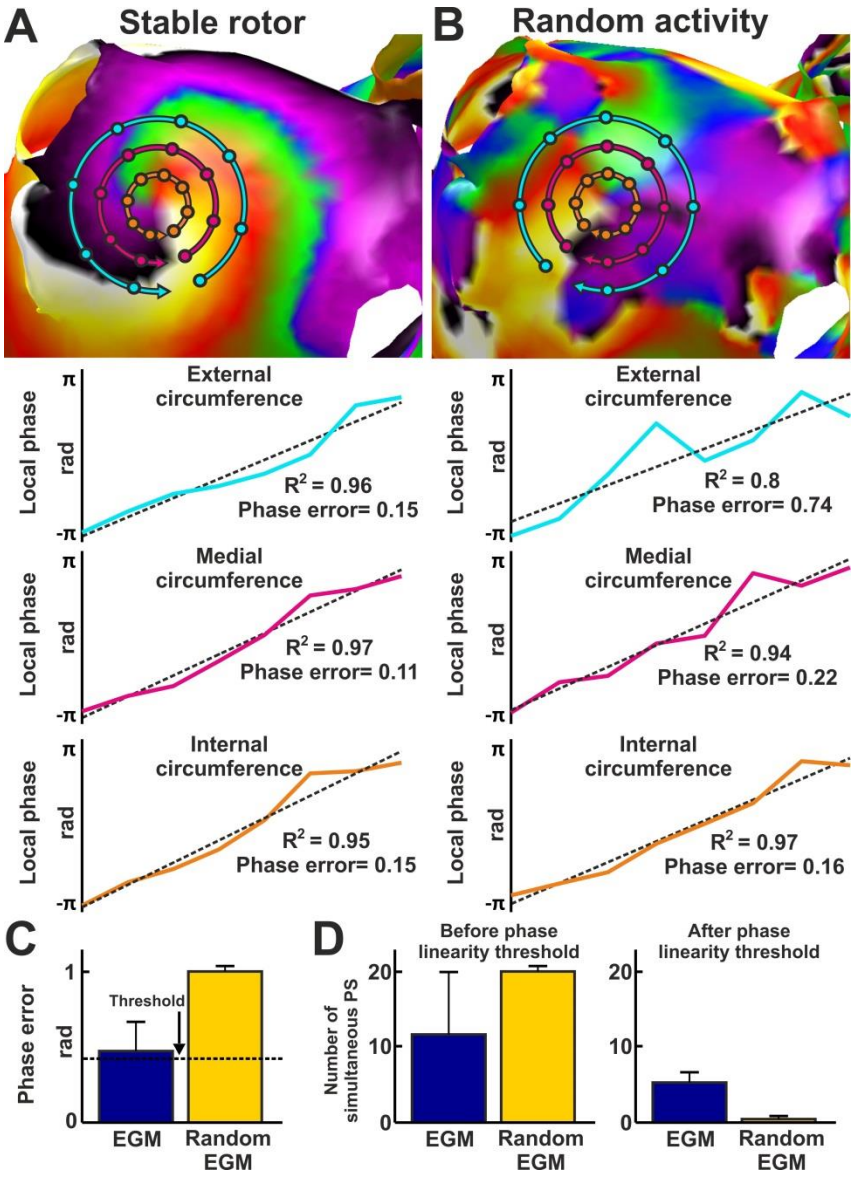

Figure 6.2 – Phase evaluation at three concentric circles.
(A) Phase map of transmembrane potential from a stable rotor in the PLAW (up) and the phase values at the three concentric circles (down). (B) Phase map of transmembrane potential from random activity (up) and the phase values at the three concentric circles (down). (C) Phase linearity error for 5 AF models. (D) Number or simultaneous PS in the AF models before (left) and after (right) applying the linearity threshold.

Transient SPs can also be found in our phase maps that arise from U turns around scars instead of from actual functional rotations. In Figure 6.3 one of such examples is depicted. Overall, if duration of 0.5 turns is required to SPs to be considered as rotors, all false detections in random propagation patterns are rejected, as represented in Figure 6.3D, while most true rotation patterns are detected (66.5±47.2% of time for AF models). However several false positives are detected (6.54±14.1% of time for AF patterns, 32.9±24.5% for AFL patterns or 57.9±43.6% for AT models with scars). Since SPs that do not arise from an actual rotation transiently disappear from the phase maps without completing a rotating cycle (see Figure 6.1C), imposition of a duration threshold of 2 turns reduces considerably the amount of false detections (0% for AF, 0% for AFL and 15.9±28.8% for AT+scar) while keeping almost unaltered the detection of true rotors (60.0±54.7%).

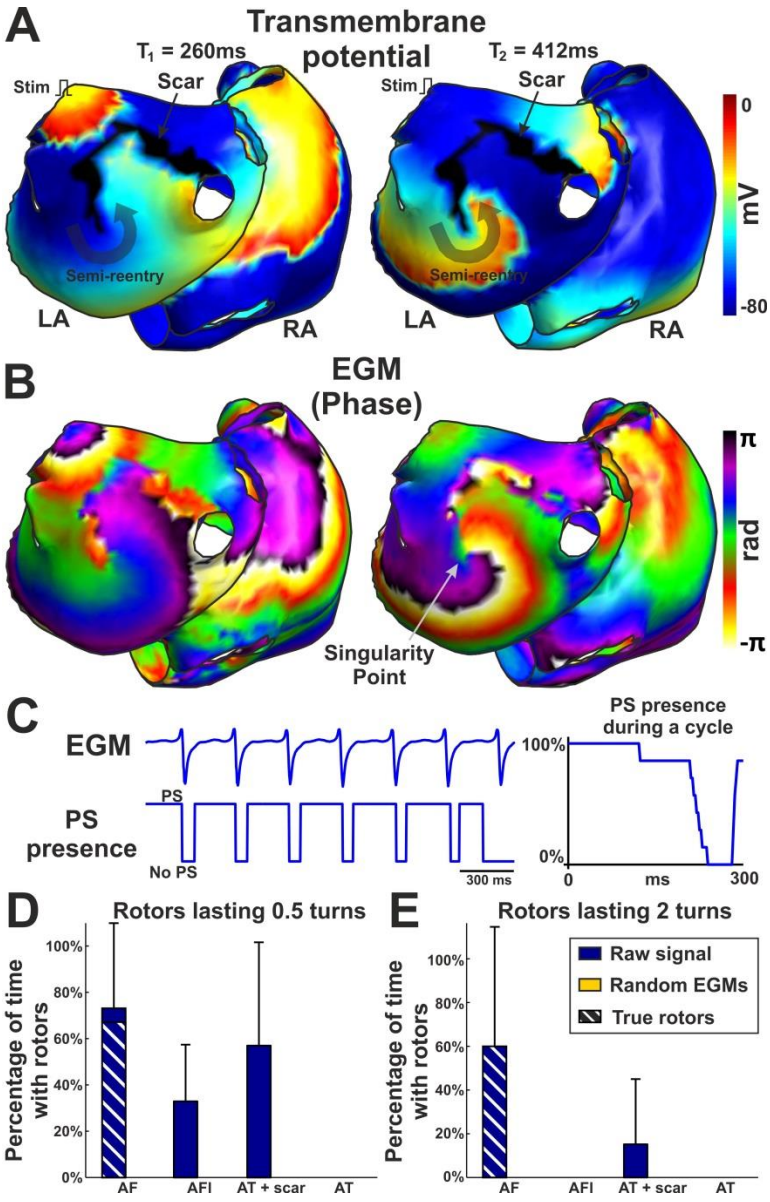

Figure 6.3 – Temporal stability of phase singularities.
(A) Transmembrane potential map of an AT simulation with scar in the PLAW. (B) Phase map of EGM signals. (C) EGM signal at the point marked with an arrow in (B), and the temporal presence of a PS in that point. At right such PS presence has been averaged for a single cycle. (D) Percentage of time with rotors lasting 0.5 turns for the complete cohort of atrial models. (E) Percentage of time with rotors lasting 2 turns for the complete cohort of atrial models.

The reported detection ratio for AF models can be increased by preprocessing the EGMs before performing the phase transformation. Hilbert's transform is particularly well suited for smooth or sinusoidal signals and therefore, a band-pass filter, centred at the activation rate allows increasing the detection ratio (from 60.0±54.7% to 70.9±39.9%) for AF models while the false positive rate detection in AF models is only 2.6±5.1%. This band-pass filtering was found to be required for detecting rotors by using EGMs with multiple deflections, as found in bipolar EGMs. In bipolar EGMs rotors were detected with the same detection rate than in unipolar EGMs but only after band-pass filtering (see Figure 6.4C-D and Figure 6.4F).

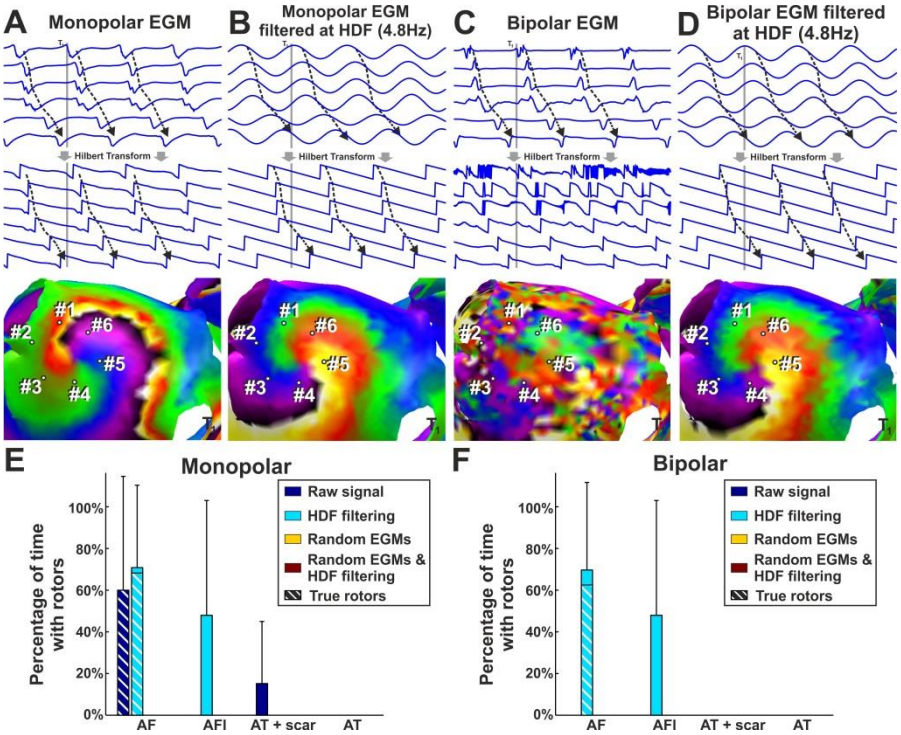

Figure 6.4 – Phase singularity and rotor presence in EGM mapping.
(A) Monopolar EGMs at 6 positions (up), its phase transform (middle) and the correspondent phase map (down). (B) Monopolar EGMs filtered at the HDF (up), its phase transforms (middle) and the correspondent phase map (down). (C) Bipolar EGMs at 6 positions (up), its phase transform (middle) and the correspondent phase map (down). (D) Bipolar EGMs filtered at the HDF (up), its phase transforms (middle) and the correspondent phase map (down). (E) Percentage of time with rotors lasting 2 turns using monopolar signals. (F) Percentage of time with rotors lasting 2 turns using bipolar signals.

However, this increased sensitivity of AF rotors by band-pass filtering takes place at the expense of increasing the detection ratio in AFL models, with up to 47.9±55.3% of time with detected rotors. Figure 6.5 shows an example of a stable macro-reentry around the inferior vena cava. Here, the upward propagation in the RA is followed by propagation through the Bachman's Bundle and subsequent downward depolarization of the posterior wall of the LA. This pattern was not reflected into a stable SP in the EGMs, but got smoothened and stabilized after HDF filtering and an SP appeared. Therefore, HDF filtering may increase the false positive detections that arise from actual rotating patterns -but not rotors- in the tail of the propagating wavefront.

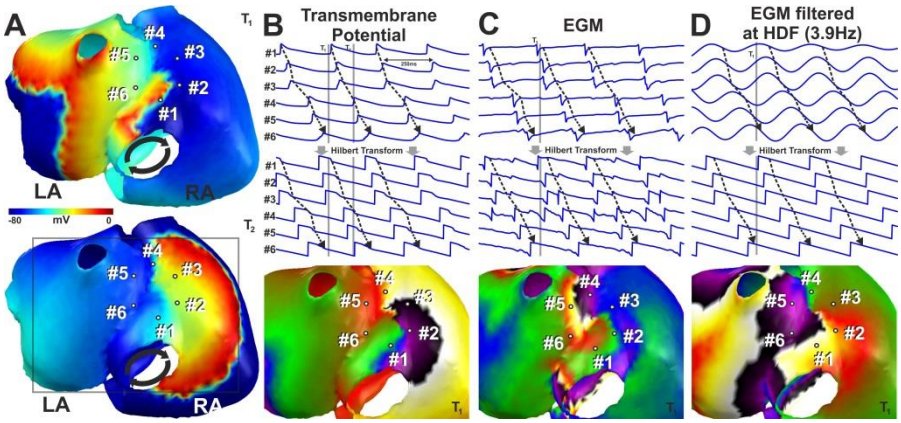

Figure 6.5 – Stable reentries in atrial flutter.
(A) Transmembrane potential map for an Inferior Cava Vein Atrial Flutter. (B) Transmembrane potential at 6 positions marked in (A) (up), its phase transforms (middle) and the correspondent phase map (down). (C) EGMs at 6 positions (up), its phase transform (middle) and the correspondent phase map (down). (D) EGMs filtered at the Highest Dominant Frequency (up), its phase transforms (middle) and the correspondent phase map (down).

6.3.2. Reentrant activity in BSPM and icEGM

We have previously proposed to apply HDF filtering to body surface recordings (BSPM) in order to detect rotors during AF and reported a significant increase in the sensitivity of this detection ***[Rodrigo 2014]*** but were unable to quantify the specificity of the method and whether it could be applied for computation of the inverse problem of electrocardiography.

In Figure 6.6, the surface BSPMs for different mathematical models with and without HDF filtering are shown. As it can be observed, stable rotors can be observed after HDF filtering but not the raw signals. However, HDF filtering also stabilized the patterns generated by random EGMs.

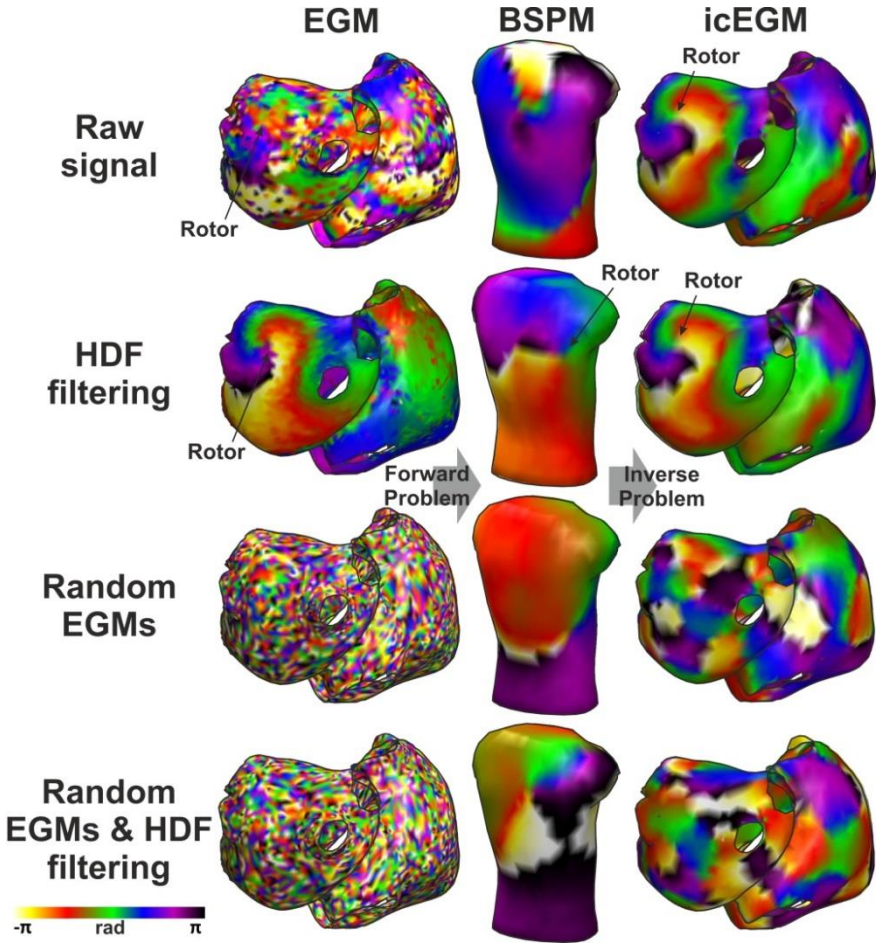

Figure 6.6 – Example of noninvasive phase mapping and HDF filtering. *Computed phase maps for an AF model maintained by a stable rotor in the PWLA and random EGMs, together with their projection onto the torso and their backpropagation to the atrial surface.*

Overall, HDF filtering allowed an increased detection of rotors in AF patterns, from 10.8±18.2% to 92.9±11.9%, see Figure 6.7. However, it also resulted in false detections in AFL, from 10.8±18.2% to 92.9±11.9%, complex AT patterns, from 0% to 15.9±31.8% and even in random AF patterns, from 0% to 32.4±28.4%.

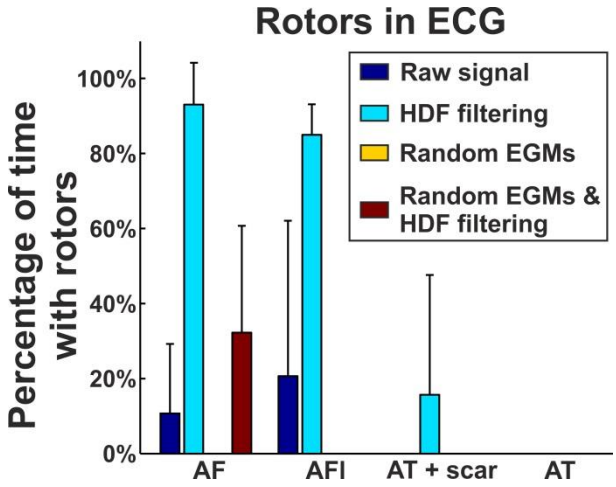

Figure 6.7 – Rotor presence in BSPM.
Percentage of time with rotors lasting at least 2 turns.

When solving the inverse problem of electrocardiography for AF patterns, rotors can be accurately detected even without applying HDF filtering, as it is depicted in Figure 6.6. Overall, true rotors during AF could be detected during 72.5±42.0% of time in AF patterns, with only 4.7±10.7% of time with false detections for AF, 13.2±18.0% for random EGMs and 25.0±50.0% for AFL and no other false detections in the other situations (Figure 6.8). HDF filtering applied after inverse problem resolution, did increase the detection of true rotors during AF up to 80.0±44.7%, but also increased the amount of false detections in all models: i.e. 99.2±1.8% for random AF EGMs, 85.7±5.2% or random AFL EGMs or 81.9±3.1% for complex ATs.

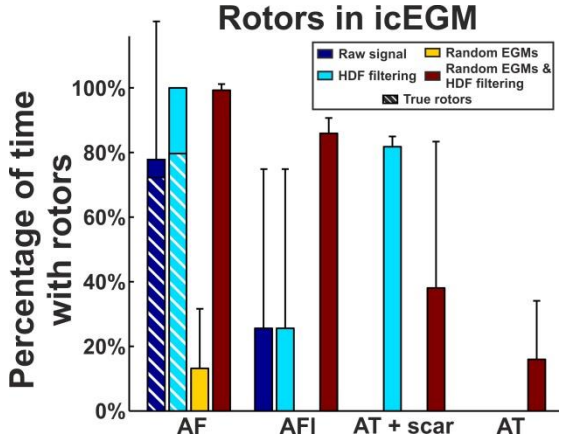

Figure 6.8 – Rotor presence in inverse-computed EGM mapping.
Percentage of time with rotors lasting at least 2 turns.

6.4. Discussion

In this work we have shown that rotor identification based on phase singularities detection is accurate and sensitive and does not require additional signal processing in smooth signals such as unipolar EGMs, either measured or computed non-invasively. Bipolar EGMs and surface ECGs do require HDF filtering in order to detect rotors as phase singularities at the expense of a decreased specificity. HDF filtering should not be applied in the resolution of the inverse problem of electrocardiography because of an increased susceptibility to detect artefactual phase singularities (see Table 6.1).

Table 6.1– Sensitivity and specificity measurements for the EGM, BSPM and ECGI signals.

		Sensitivity	Specificity
Monopolar EGMs	RAW	59.97%	97.94%
	HDF	68.22%	93.39%
Bipolar EGMs	RAW	0%	100%
	HDF	61.95%	93.35%
BSPM	RAW	15.21%	100%
	HDF	89.31%	90.97%
ECGI	RAW	72.50%	94.27%
	HDF	80.00%	49.01%

6.4.1. Rotors and phase singularities

The phase transform has been widely used for the identification of electrical patterns in transmembrane potentials ***[Zlochiver 2008, Berenfeld 2011]***. However, the sole detection of a phase singularity does not imply the presence of an underlying rotor, since singularities may arise from wavebreaks or fibrillatory conduction. However, SPs arising from wavebreaks are more unstable and do not consistently present monotonical increases in phase. In this context, other authors have already proposed to search for phase singularities in two concentric rings around the SP ***[Kuklik 2016]*** and impose a restriction of a temporal span of at least 1 turn in order to increase specificity. In the same direction, we have shown that application of time and space restrictions to detected SPs allows increasing the specificity in the detection. In particular, we propose to require a good fit to a monotonical increase of phase in at least 2 out of 3 concentric rings. The use of 3 rings increases sensitivity as compared to a single ring, since rotors occupying a small region are detected by the inner circles while rotors with a large precession are detected by the outer rings. At the same time, the use of three rings reduces the chance for randomly distributed phases to be considered as SPs.

6.4.2. Phase transformation and signal morphology

We have shown that the equivalence between propagation patterns and phase maps depends on signal morphology. While the Hilbert transform results in an unambiguous phase assignation for signals with simple morphologies, for complex morphologies there is no relationship between the assigned phase values and the phase in the action potential of the tissue. Hilbert Transform is mathematically defined for properly identifying the instantaneous phase value of a sinusoidal wave, assigning the whole range values from $-\pi$ to π to the interval between signal peaks. However, the Hilbert Transformation of complex signals with several deflections the whole range of phase values from $-\pi$ to π is also assigned between two consecutive deflections and thus this assignment does not convey any useful information for pattern identification. We have shown that phase singularities can be detected after the phase transformation of unipolar, noise-free EGMs. However, raw EGMs with multiple deflections, such as bipolar EGMs, are not suitable for PS detection and require for a pre-processing step before applying Hilbert's transform.

6.4.3. HDF filtering and BSPM phase mapping

We have previously proposed the use of a narrow bandpass filter prior to the computation of the phase transformation in order to stabilize phase singularities in BSPM recordings ***[Rodrigo 2014]***. We showed that HDF filtering allows selecting the contribution of areas that activate at the HDF while reduces the contribution on the body surface from regions that activate at a slower rate and are not harbouring rotors ***[Rodrigo 2014]***. In the present work we investigate the effect of HDF filtering on propagation patterns not maintained by rotors in order to quantify the proportion of artefactual detections introduced by our signal processing. According to our results, the narrow bandpass filtering does induce false detections that can be as high as 30% in randomly distributed EGMs from AF models. For this reason, isolated SPs on BSPM maps obtained after HDF filtering, even if they last for longer than 2 turns should be interpreted with care since they are not an unequivocal prove of the presence of a rotational activity. However, we have shown that a high incidence of long-lasting SPs is indicative for rotational activity, since rotors were more than two-fold detected for underlying rotational patters than for non-rotational ones.

HDF filtering results in a particularly high incidence of detected rotational patterns in AFL models. This was to be expected because raw BSPM data already shows rotational patterns that get stabilized by the HDF filtering. This resemblance between AF and AFL patters can be explained by the fact that non-contact potentials do contain far-field components and, as such, the electrical sources on the vicinity of the anatomical obstacle do generate rotational electrical fields without an actual silent central region. For this reason, very stable rotational

patterns on the BSPM phase maps should be considered as indicative of either AFL or AF and activation frequency should allow discriminating between these two mechanisms.

6.4.4. HDF filtering and EGM phase mapping

A quite aggressive band-pass filtering strategy has been proposed for detecting rotational patterns in multipolar catheter baskets ***[Narayan 2013]***, similar to our HDF filtering. In the same direction we have shown here that HDF filtering applied to EGMs increases the detection rate of rotors during AF at the expense of very few false detections (see Table 6.1). In addition, the smoothing effect of the HDF filtering appears to be necessary when the EGMs present multiple deflections so that the phase assignment by the Hilbert Transform is related to a phase in the action potential.

However, HDF filtering of EGMs does result on some artefactual detections that should be taken into consideration. In particular, when the underlying pattern does present a coincidental rotation and not a mother rotor, there is an increased chance of detecting a rotor due to the smothering effect of the HDF filtering. These coincidental rotational patterns were especially relevant in our AFL model population in which either the activation tail or anatomical obstacles do result on non AF-leading rotations. While these coincidental rotational patterns may not fulfill the eligibility criteria for rotors because there is no single rotational center where all phases between $-\pi$ and π converge, phase homogenization that results after HDF filtering may qualify these patterns for rotor detection.

6.4.4. HDF filtering and ECGI phase mapping

Some narrow band-pass filtering has also been employed after inverse problem resolution to detect rotors during AF ***[Haissaguerre 2014]***. However, we demonstrate in this study that a too aggressive filtering strategy shouldn't be applied to the inverse computed electrograms because many artefactual rotors arise. Notice that after resolution of the inverse problem, local EGMs are obtained at each location of the atria, whose activation frequency may differ from one atrial region to another. When applying a narrow band-pass filter to EGMs with an activation frequency different than the passing band, then just a residual component with no physiological meaning is preserved and thus rotor analysis based on this oversmoothed, meaningless information does not convey relevant information.

6.4.5. Limitations

In our work we have made use of mathematical models instead of patient data because current technology does not allow determining whether detected rotors are

artefactual or they are in fact AF drivers. Mathematical models, instead, allow defining specific activation patters in which the presence of mother rotors is known a priori and thus where more suitable for our study. However, our mathematical AF models may be too simplistic and may not fully represent the whole spectra of AF patients.

During the development of this work different thresholds for detection of reentrant activity had to be established, such as phase linearity or the radii of the circles for the phase assessing. The threshold election allows increasing the specificity at the expense of the decrease the specificity of the reentrant activity detection, and vice versa. These thresholds were chosen to achieve a balance between specificity and sensitivity according to our database. It should be further explored whether the proposed thresholds should be adapted to other scenarios.

6.4.6. Conclusions

Phase transformation and singularity point identification is a robust method to identify reentrant activity in the atrial electrical activity. Temporal filtering of electrophysiological signals with complex morphology is necessary for the correct phase transformation, and narrow band-pass filtering at the HDF allows increasing the rotor detection ratio by simplifying the phase maps. HDF filtering is recommended for rotor detection in EGMs with multiple deflections and for BSPM signals. However, a too narrow band-pass filtering should not be employed after resolution of the inverse problem of electrocardiography.

Chapter 7

Highest dominant frequency and rotor positions are stable markers for atrial driver location in non-invasive mapping of atrial fibrillation

7.1. Introduction

Noninvasive identification of rotors by solving the inverse problem of electrocardiography has been recently reported ***[Haissaguerre 2014]***. However, the propagation patterns that result from the inverse problem resolution during atrial fibrillation used for rotor identification appear to be paradoxically simple ***[Cuculich 2010, Haissaguerre 2014]*** as compared to those obtained with contact electrodes and optical mapping ***[Berenfeld 2000, Allessie 2010, Mansour 2001, Sahadevan 2004]***. Although the inverse problem in AF has only been validated indirectly based on the freedom from AF after an ablation procedure ***[Haissaguerre 2014]***, the clinical usefulness and validity of such approach is still a matter of debate.

In this study we utilized mathematical simulations of AF in order to evaluate the stability of non-invasive identification of AF drivers based on rotors or highest DF (HDF) regions detection in the presence of uncertainties in the inverse problem resolution.

7.2. Methods

7.2.1. Mathematical models

A realistic 3D model of the atrial anatomy was used to simulate the atrial electrical activity (see chapter 3.1). An ensemble of 30 different AF episodes was simulated, composed of 14 AF patterns driven by a single rotor at varying locations of the LA (PVs, PLAW and LAA) and 16 AF patterns driven by a single rotor at varying locations of the RA (free RA wall and RAA).

For each simulation, a uniform mesh of 2048 unipolar EGMs was calculated surrounding the epicardial surface and the ECG potentials on the torso model were calculated in a mesh formed by 771 nodes (see chapter 3.3). The electrical conductivities used were 3S/m for blood and 2S/m for the rest of the tissue ***[Pedrón-Torrecilla 2016]***. Baseline of ECGs signals was estimated by decimation to 12.5 Hz and filtering with a Butterworth 10th-order low-pass filter with a cut-off frequency of 2 Hz. This signal was interpolated to 500 Hz and subtracted from the original signal. ECG signals were then low-pass filtered with a 10th-order Butterworth filter with a cut-off frequency of 30 Hz ***[Guillem 2013]***. Then, the inverse-computed EGMs (icEGMs) were calculated in the 2048 points of the atrial mesh by solving the inverse problem (see chapter 3.3).

7.2.2. Addition of model and signal uncertainties for the inverse problem resolution

In order to evaluate the robustness of the inverse solutions against model uncertainties, we evaluated the accuracy of the solution under noise, errors in the location or orientation of the atria inside the torso volume and errors in the conductivity. In particular, white Gaussian noise was added to the synthetic ECG signals with a signal-to-noise ratio (SNR) between 60dBs and 0dBs. Alternatively, the inverse problem was solved for displacements in the atrial position from 0 cm to 5 cm in the lateral axis (X axis in Fig 7.1A), under rotations from 0º to 45º also in the lateral axis and variations in the blood conductivity from 0.5 S/m to 9 S/m (as opposed to the 3 S/m used for the forward problem).

7.2.3. Rotor and dominant frequency identification

Rotor location was carried out by identification of singularity points (SP) in the phase signal map obtained with the Hilbert Transform (see chapter 3.4). Phase values were obtained along 3 different circles surrounding each evaluated point with radii of 0.5 cm, 1 cm and 2 cm. Six points per circle were used for the phase analysis in which the icEGM signal was interpolated by a weighted average of the icEGM signal from neighboring nodes, with d^{-2} the weight for each node and d the

distance between nodes. An evaluated point was defined as a SP only when the phases of at least two of these three circles was monotonically increasing or decreasing for a total of 2π.

A rotor was defined as the connection between SPs across time. The distance between SPs at consecutive time instants should be less than 1 cm to be related and maintain a continuity of rotation. Finally, only long lasting rotors, defined as those that complete at least one rotation were considered as rotors and other SPs were discarded. In order to locate the position of the rotor by inverse solution, histograms of atrial rotor presence were obtained by counting the number of rotors in each atrial node, and the node with highest reentrant presence was considered as the rotor location. The distance between the inverse-computed and original rotor position was assessed.

For the Dominant Frequency (DF) analysis, icEGMs were baseline-removed as described above, and icEGM signals were then low-pass filtered with a 10th-order Butterworth filter with a cut-off frequency of 10 Hz ***[Guillem 2013]***. Power spectral density of all signals was computed using Welch periodogram (65536 point Fast Fourier transform, 1.5 seconds-length Hamming window and 80% overlap) to determine the local DFs with a spectral resolution of 0.01Hz ***[Guillem 2013]***. Highest Dominant Frequency (HDF) regions were defined as those atrial regions whose DF values presented a difference with the rotor DF lower than 0.5 Hz. Inverse-computed DF maps were compared with the departing DF maps by obtaining the concordance of the HDF region as the union area of departing and inverse-computed HDF regions divided by the departing HDF area.

7.3. Results

7.3.1. Illustrating example

Voltage, phase and DF maps of inverse computed potentials always differ from those computed from the departing EGMs. Figure 7.1A illustrates a schematic view of the 3D torso model used for the inverse solution and the atrial surface at its original position and after a displacement of 2 cm. Panels C, D and E compare the inverse-computed maps with the original maps depicted in panel B. In particular, the voltage map (left), the phase map (centre) and the DF map (right) are depicted for an AF pattern driven by a stable rotor in the posterior wall of the LA with an activation rate of 5.5 Hz in the rotor region and 3 Hz for the rest of the fibrotic atria. Panel C shows the inverse-computed maps after the inverse solution under the best conditions, that is, with no added electrical noise to the ECGs and with the atria at their original position. As it can be observed, the inverse-computed voltage map is smoother than the departing EGMs, due to the inability of the inverse problem to reconstruct the wavefront irregularity produced by the fibrosic tissue. However, the activating wavefront (transition from blue to red colors) is at

the same place, which is evidenced in the phase map, in which the location of the singularity point is preserved. Finally, the inverse-computed DF map seems more robust to the inverse computation since the Highest Dominant Frequency (HDF) region has roughly the same distribution than the departing HDF region.

Figure 7.1D and 7.1E depict the inverse-computed maps after the inverse solution with noise added to the ECG (10 dBs SNR) and after a 2 cm displacement in the location of the atria for solving the inverse problem. As expected, the inverse-computed voltage maps differed from the departing map to a greater extent than those computed with the addition of uncertainties, but the phase maps still retained some similarity with the original phase map. In the case of Figure 7.1D the rotor is still accurately identified. The DF maps were in this example also stable against noise and uncertainties in the transfer matrix, since inverse-computed maps present almost the same DF distribution and the same HDF region.

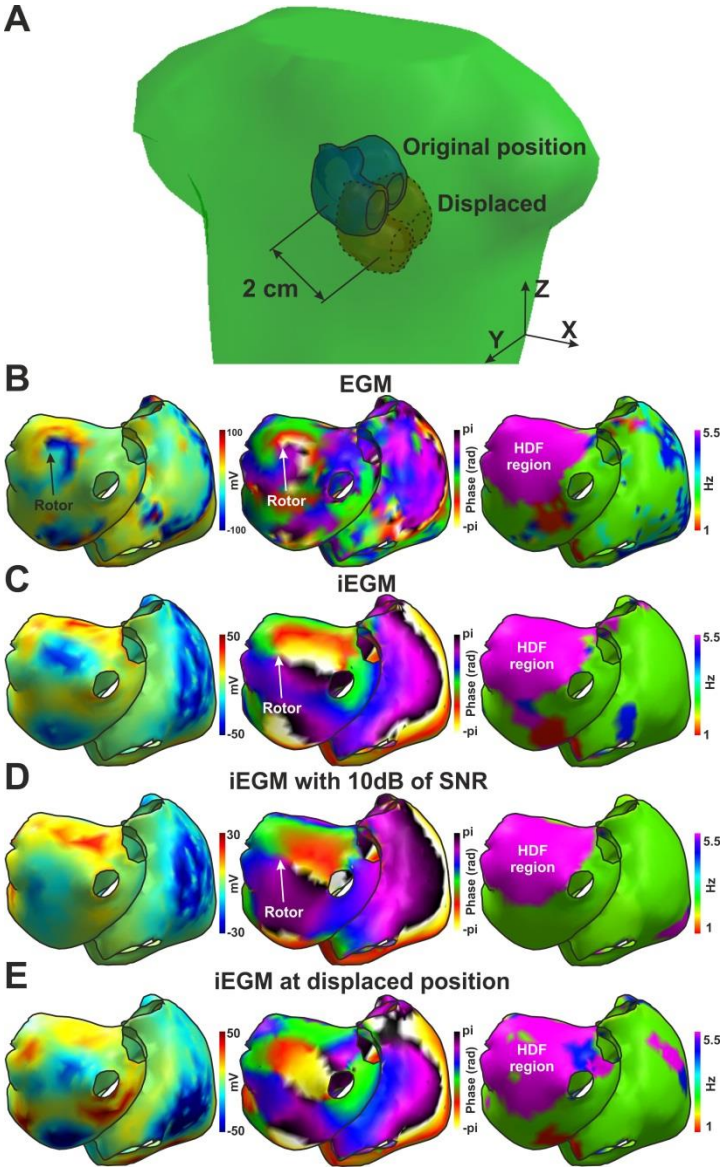

Figure 7.1 – Illustration of the experimental set-up and inverse-computed examples.

(A) Schematic view of the torso surface (green), atrial surface at the original position (blue) and atrial model at displaced position (red). (B) Original maps for an AF episode maintained by a rotor in the RA. (C) Inverse-computed maps for the simulation in B solved at the original position. (D) Inverse-computed maps for the simulation in B solved with 10dB of Noise-to-Signal Ratio. (E) Inverse-computed maps for the simulation in B solved at displaced (2 cm) position. Voltage map (left), phase map (center) and Dominant Frequency map (right).

7.3.2. Signal correlation

Similarity of the icEGMs with the departing EGMs after imposition of signal or model uncertainities was systematically evaluated in our AF model database. A summary of the measured correlation coefficients is presented in Figure 7.2 showing that the correlation coefficient for EGM signals was quite poor (0.45±0.12) even in the absence of noise or model uncertainties. Addition of white noise to the surface ECGs before computing the inverse solution decreased this correlation coefficient down to 0.18±0.1 for a 0 dB SNR. Uncertainties in the model conductivities had no effect on the accuracy of the resolution, as it can be observed in Figure 7.2B. Uncertainties in the location or orientation of the atria inside the torso volume, however, had a large impact on the correlation coefficients, as depicted in Figure 7.2C-D. Correlation coefficients decreased from 0.41±0.13 for 0 cm down to 0.01±0.02 for a 3 cm of displacement or down to 0.03±0.05 for a 27º of rotation.

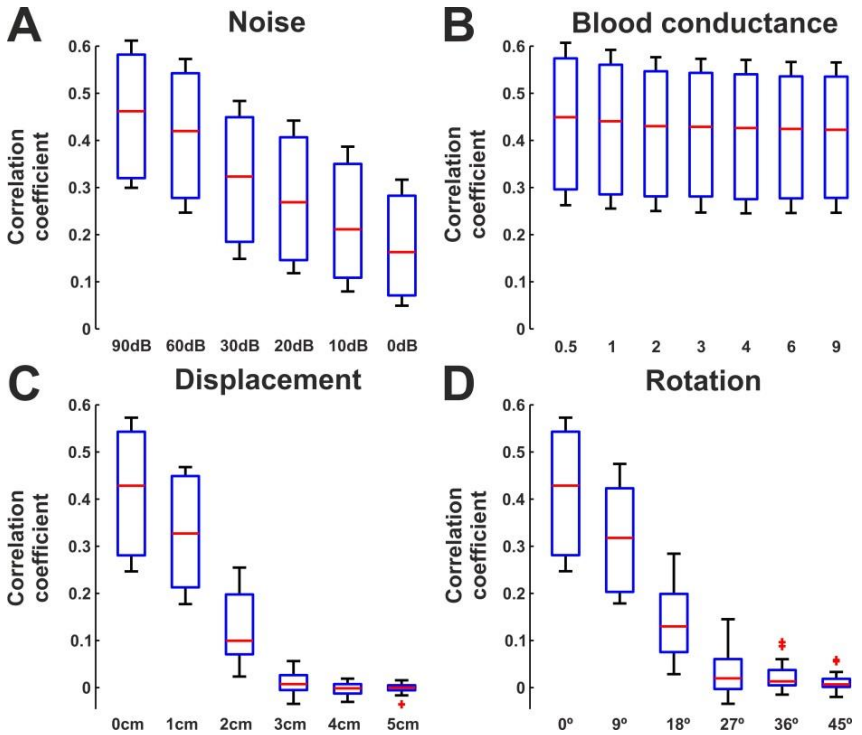

Figure 7.2 – Correlation of inverse-computed EGMs with original EGMs.
Variations in: (A) ECG noise; (B) Blood conductance; (C) Displacement; (D) Rotation.

Notabily, the correlation coefficient between icEGMs and departing EGMs showed significantly higher values in the HDF regions than in the rest of the atrial tissue (see Figure 7.3). This trend was observed for all those scenarios in which the main correlation coefficient was significantly different to 0: for 60dB, 30dB, 20dB and 10dB of white noise in the ECG; for all the blood conductance values; for 1cm, 2 cm and 3 cm of displacement and for rotations of 0º, 9º and 18º. These values could be explained by the more stable propagation patterns in the surroundings of the rotor, detected by the DF analysis, respect to the passive tissue.

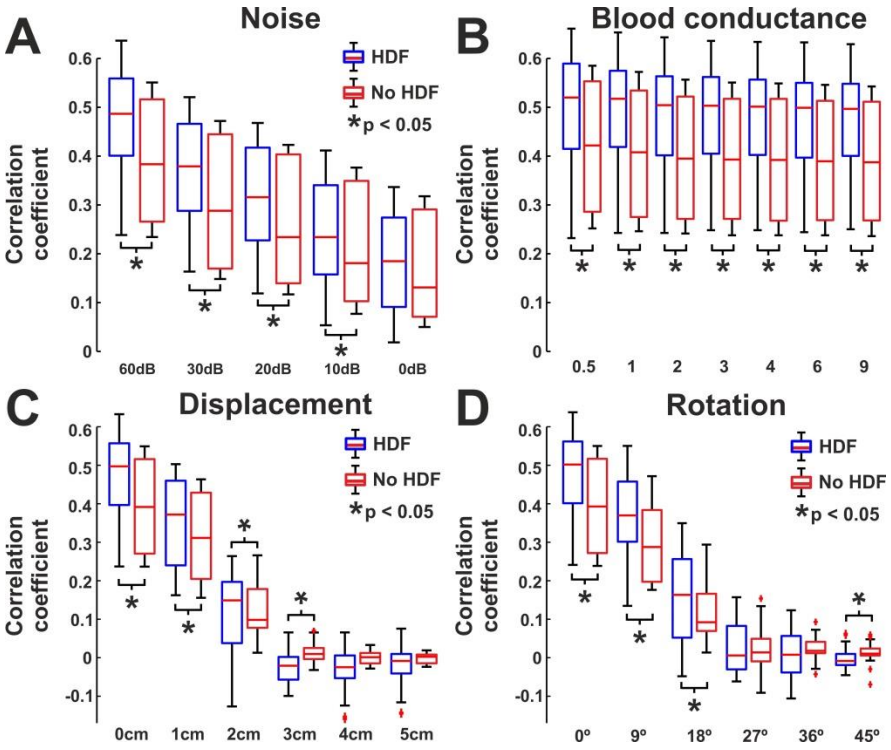

Figure 7.3 – Correlation of inverse-computed EGMs with original EGMs of HDF (blue) and no-HDF regions (red).
Variations in: (A) ECG noise; (B) Blood conductance; (C) Displacement; (D) Rotation.

7.3.3. Highest dominant frequency regions

Although the morphology of icEGMs and their departing EGMs have been shown to be poorly related, they do allow for a robust estimation of the local activation rate (or DF) against signal or model uncertainties (Figure 7.4). Identification of the highest DF region was accomplished with a concordance above 75% for SNRs as low as 10 dB and went down to 56.5±32.3% for 0dB. Again, changes in the blood conductance did not result in perceptible changes in the HDF region concordance rate and remained stable around 85±10%, as previously reported for the correlation coefficients. Quite notably, identification of the HDF region was very stable against uncertainties in the atrial location, with mean concordance values above 75.9±11.9%, corresponding to a 3 cm displacement. Inverse-computed DF maps were more sensitive to angular deviations, since the concordance of the HDF progressively decreased from 84.5±10.6% for 0º down to 56.2±23.0% for 45º.

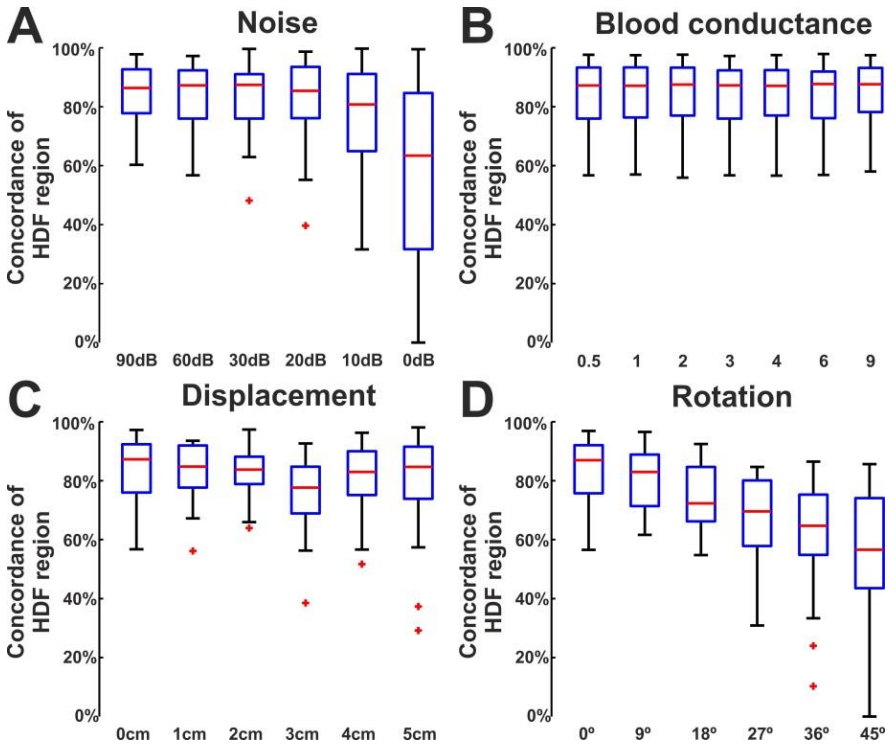

Figure 7.4 – Concordance of inverse-computed HDF region with original HDF region.
Variations in: (A) ECG noise; (B) Blood conductance; (C) Displacement; (D) Rotation.

The rationale behind the ability of the inverse problem resolution in identifying the HDF regions can be further understood from our data in Figure 7.5. As it can be observed, the HDF region is generally expanded in the inverse-computed data as compared to the true HDF region. The addition of noise increased the size of the HDF region by 22.5±27.5% for 90dB or up to 36.7±35.1% for 20dB, although then decreased down to -4.8±53.0% for 0dB SNR. Blood conductance again did not affect in the magnification of the HDF area. Displacement in the atrial position resulted in a considerably higher increase in the HDF region, up to 202.1±169.9% for 5 cm, than the angular deviation which provoked a maximum increase of 59.0±78.6% for 45º.

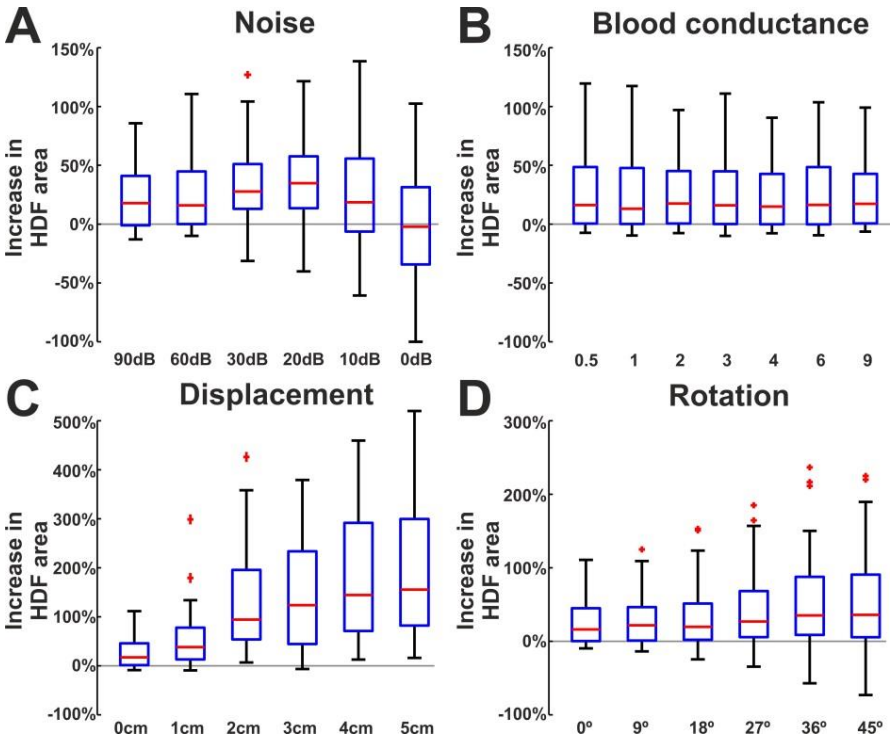

Figure 7.5 – Increase of inverse-computed HDF area compared with original HDF area.

Variations in: (A) ECG noise; (B) Blood conductance; (C) Displacement; (D) Rotation.

Complementary to the data presented in Figure 7.4, the center of the original HDF maps and their inverse-computed counterparts were compared. As it can be observed in Figure 7.6, this deviation presented values lower than 4 cm for every level of electrical noise added to the ECG (Panel 7.6A), being the average value 1.36±0.78 cm for 0db of SNR. Again, changes in the blood conductance had no effect and the difference remained around 0.8 cm. When atrial displacements were present in the inverse calculation, the distance between HDF region centers increased gradually with the displacement, up to 3.12±1.11cm for 5 cm (Panel 7.6C). Finally, the angular deviations also showed a constant increment in the error of HDF center region location, that reached 3.15±1.05 cm for 45º.

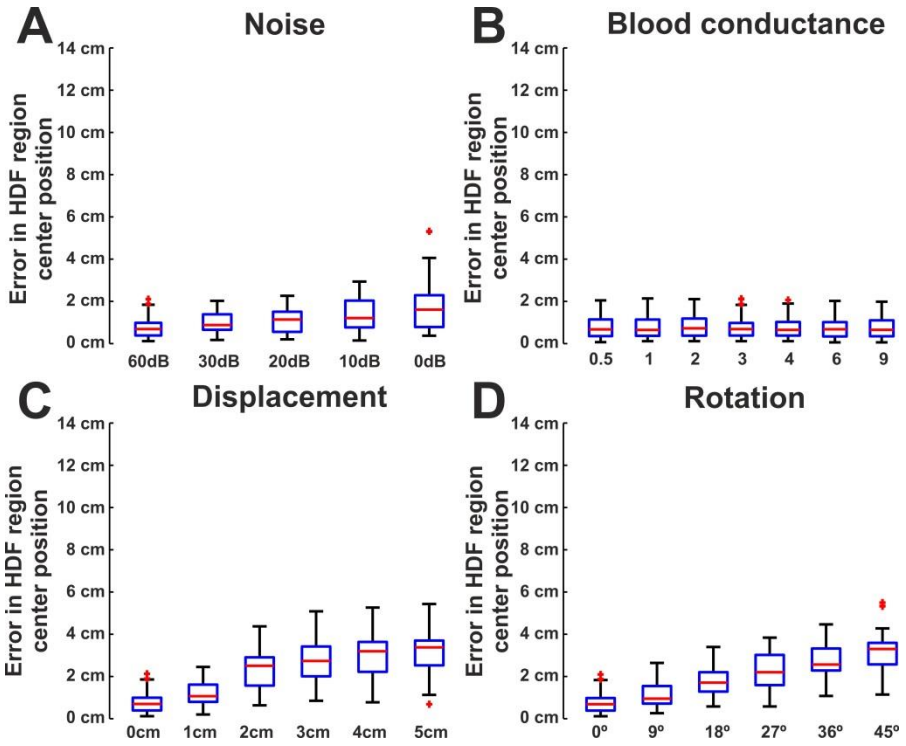

Figure 7.6 – Error in non-invasive HDF center identification.
Variations in: (A) ECG noise; (B) Blood conductance; (C) Displacement; (D) Rotation.

7.3.4. Incidence of SP detections

The resolution of the inverse problem did not allow to truly estimate the complexity of the electrical patterns during our simulated AF. The departing EGM maps presented more simultaneous short-lasting rotors (8.5±5.3) than their inverse-computed counterparts, even for high SNRs (i.e. 4.4±2.5 for 60dB SNR), and this number gradually decreased down to 1.4±0.3 for 0dB SNR (see Figure 7.7). Uncertainties in the atria location or orientation, however, had the opposite effect in the detected number of rotors, with up to 5.6±2.6 for 1 cm or 14.6±1.1 for 5 cm displacements and 4.6±2.4 for 9º or 12.3±4.7 for 45º rotations.

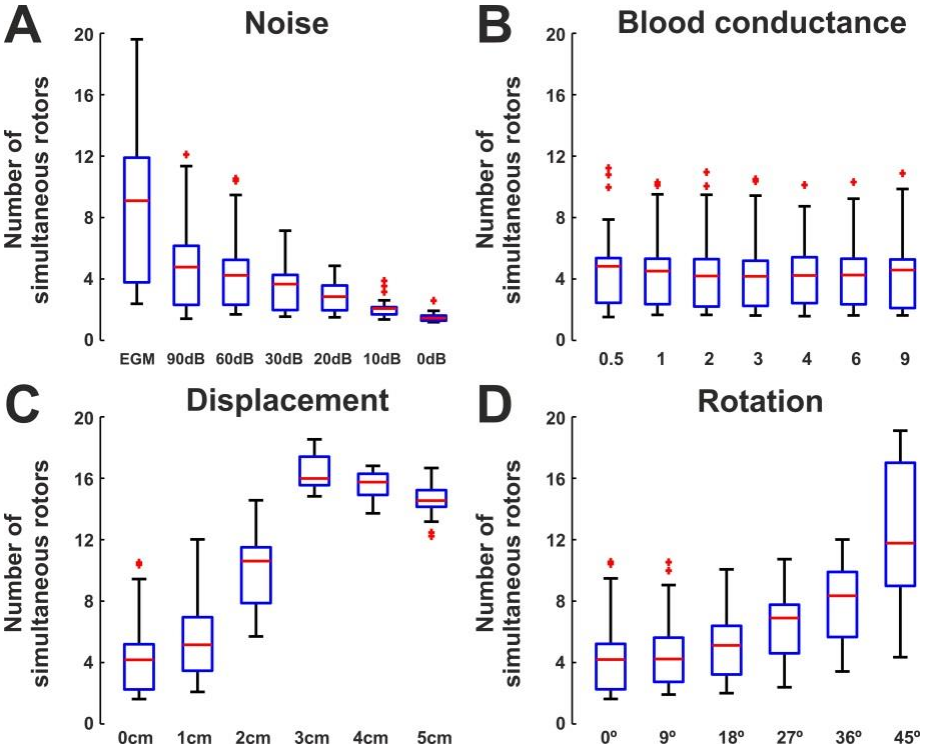

Figure 7.7 – Number of simultaneous rotors.
Variations in: (A) ECG noise; (B) Blood conductance; (C) Displacement; (D) Rotation.

However, despite the sensitivity of rotor detection to signal or model uncertainties, mother rotor identification, defined as the most stable rotor, was quite robust. Figure 7.8 shows rotor location maps in relation to noise and position uncertainties in a sample case. The inverse problem tended to locate rotors into more stable sites, and this effect was more evident in the presence of noise (Figure 7.8C).

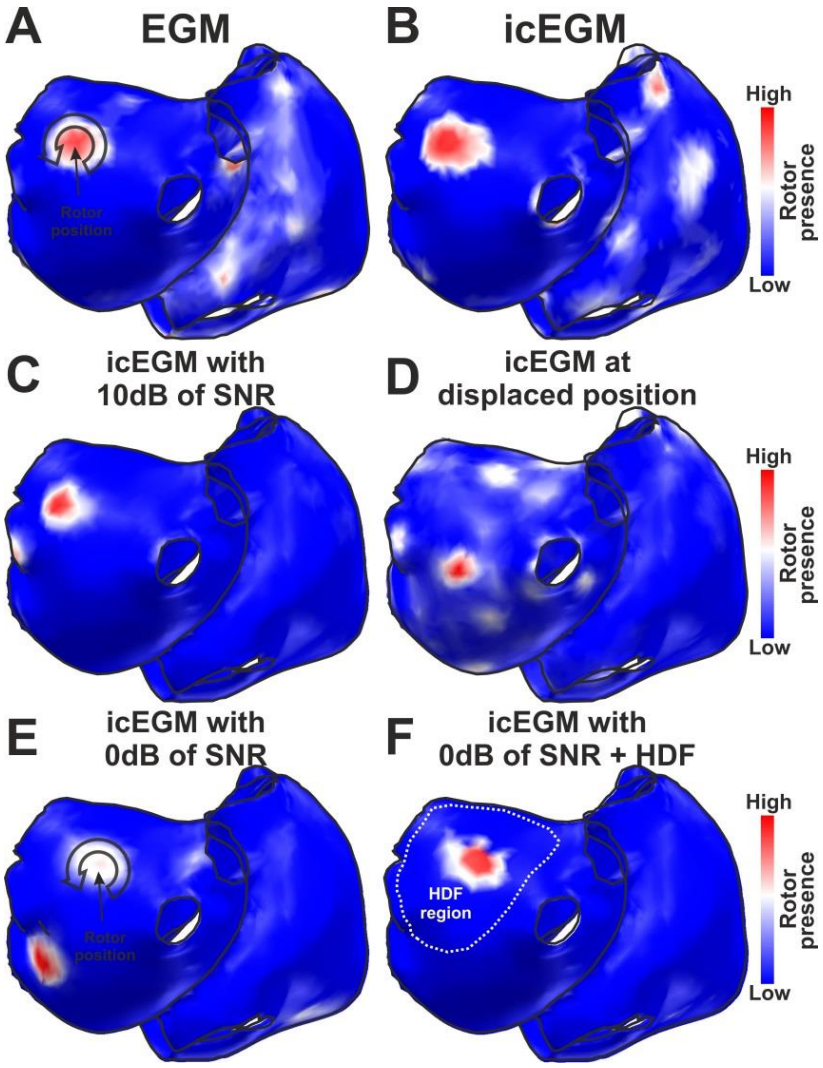

Figure 7.8 – Atrial rotor histograms for inverse-computed activity.
(A) Departed EGM; (B) icEGM with 60dBs SNR; (C) icEGM with 10dBs SNR; (D) icEGM with a displacement of 4 cm; (E) icEGM with 0dBs SNR and (F) icEGM with 0dBs SNR with rotors from the HDF region.

In Figure 7.9, the accuracy of this estimation is presented for the entire database. Panel 7.9A shows this error both for the original phase maps (0.7±0.7 cm) and for the inverse-computed maps under the effect of electrical noise. These average errors remained stable around 1 to 1.5 cm from 90dB to 20dB. For 10dB and 0dB the average value of the error in rotor location raised up to 2.4±3.6 cm and 4.5±4.5 cm respectively, but in both cases 50% of rotors were identified with a deviation below 2 cm. Variations in blood conductance (Figure 7.9B) did not result in significant variations respect to the original location. Displacements in the atrial position provoked a comparable error in the inverse-computed rotor position: from 0.9±1.3 cm for a displacement of 1 cm to 4.7±3.3 cm for a displacement of 5 cm, together with a more scattered rotor map (Figure 7.8D). Rotations of the atria inside the thorax also resulted in incremental errors in the inverse-computed rotor position: from 1.2±1.3 cm for 9º to 4.9±2.6 cm for 45º.

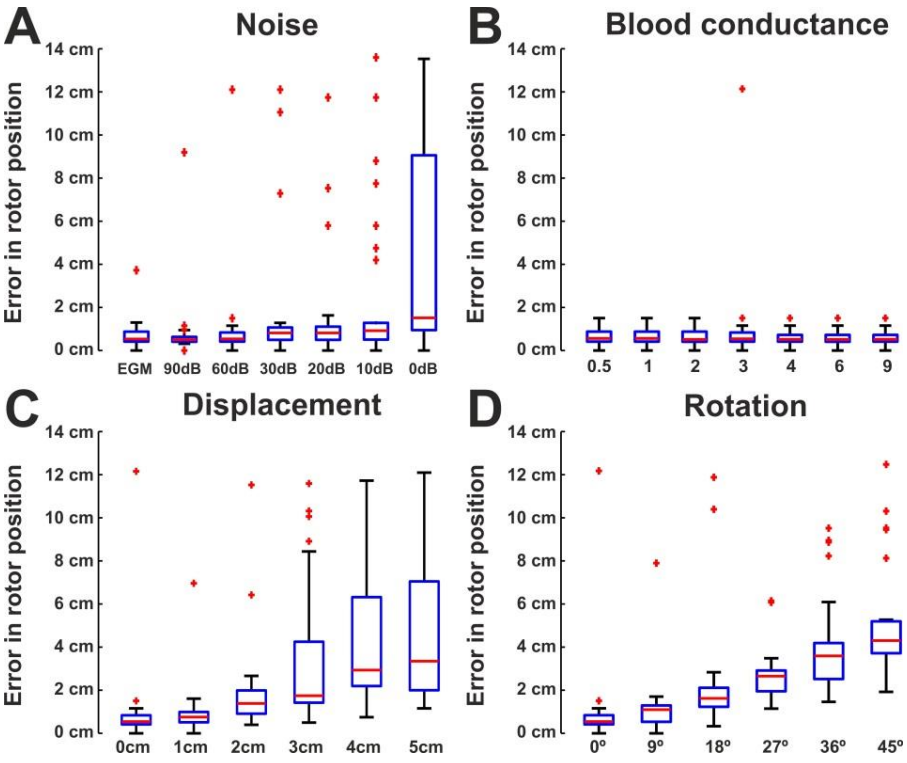

Figure 7.9 – Error in non-invasive rotor position identification.
Variations in: (A) ECG noise; (B) Blood conductance; (C) Displacement; (D) Rotation.

7.3.5. Inverse identification of the driving atrium

Next, the overall ability of the inverse solution in identifying the dominant atrium responsible for AF maintenance was also evaluated both by SP and HDF analysis. The atrial surface was divided into 2 anatomical regions (LA and RA) and the match between the departing and inverse-estimated atrium was quantified. As shown in Figure 7.10A, there was a good match in the SP detection and rotor site (>90%) for all SNRs except for the noisiest case where the match ratio decreased with down to 73% for 0dB. Blood conductance again had little effect on rotor region identification. Rotor region identification was also accurate (>80%) for deviations lower than 4cm or 36º.

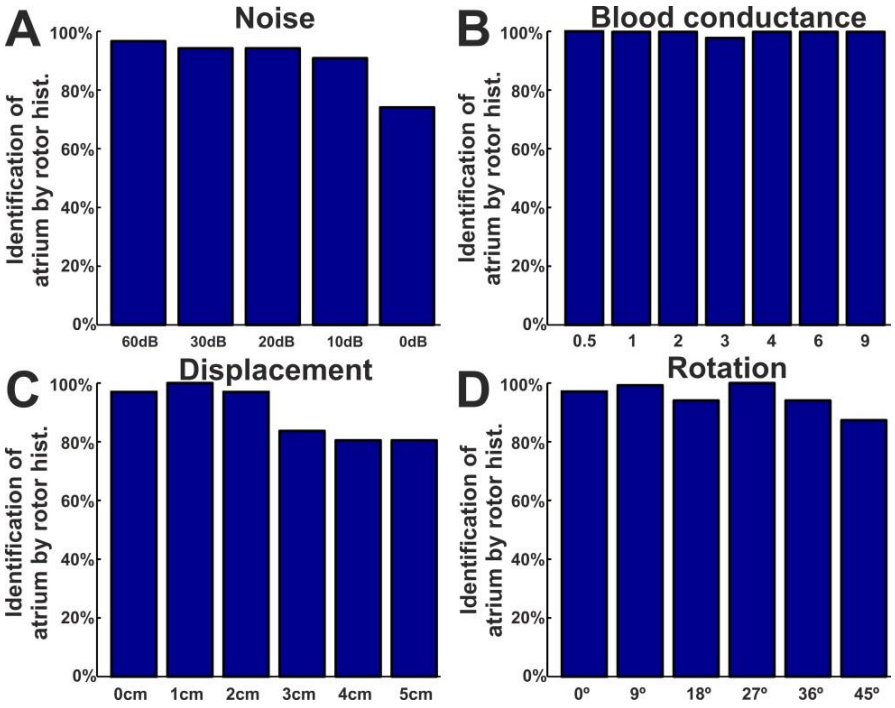

Figure 7.10 – Non-invasive identification of the dominant atrium by rotor histogram.
Variations in: (A) ECG noise; (B) Blood conductance; (C) Displacement; (D) Rotation.

Then the ability to identify the dominant atrium by measuring the extension of the HDF region in each of them was evaluated in Figure 7.11. Here can be observed as there was a good match (>90%) for all SNRs except for the most noisy case where the match ratio decreased with down to 87% for 0dB, results that outperform SP identification. The analysis of the inverse-computed HDF region was able to properly identify the dominant atrium for more than 90% of cases when changes were present in the blood conductance or in the atrial location. However, changes in the atrial orientation decreased this match ratio down to 80% for angular deviations higher than 27º.

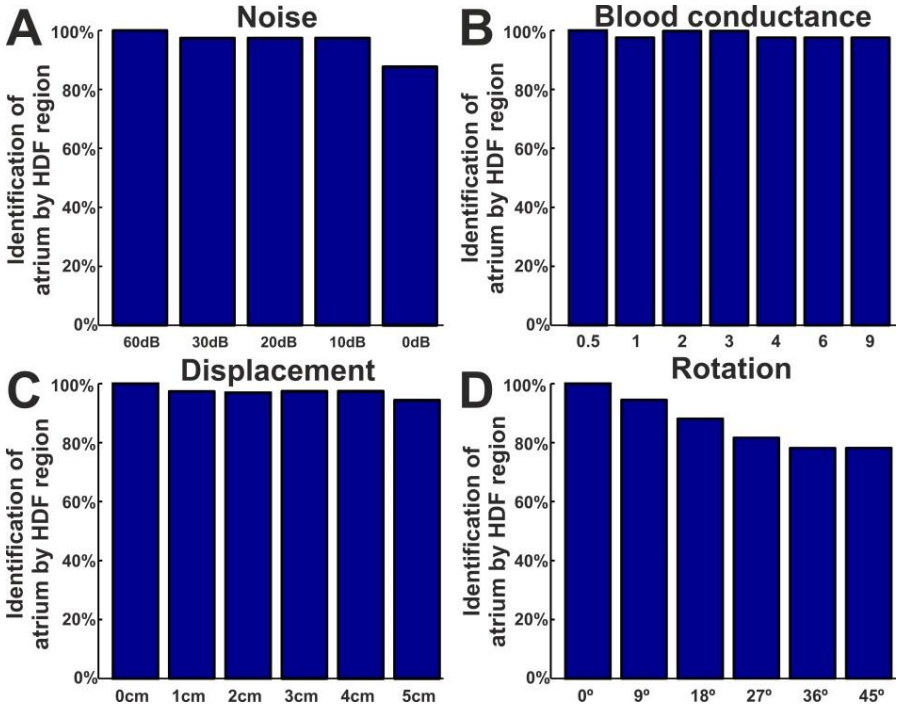

Figure 7.11 – Non-invasive identification of the dominant atrium by HDF region analysis.

Variations in: (A) ECG noise; (B) Blood conductance; (C) Displacement; (D) Rotation.

7.3.6. Combined SP and HDF approach for driver identification

Since driving rotors activate at the fastest rates in the atria and both DF and rotor measurements were robust against inverse problem uncertainties, these two parameters were combined in order to improve driver location. Figure 7.12 depicts the error in the atrial rotor location considering only those inverse-computed rotors present in the HDF region, compared with the error when all inverse-computed rotors were considered. As shown, the combination of information from both measurements can reduce the average error in the driver location. However, this reduction in the inverse-computed rotor location is significant just for the extreme cases, as in the sample case shown in Figure 7.8E-F.

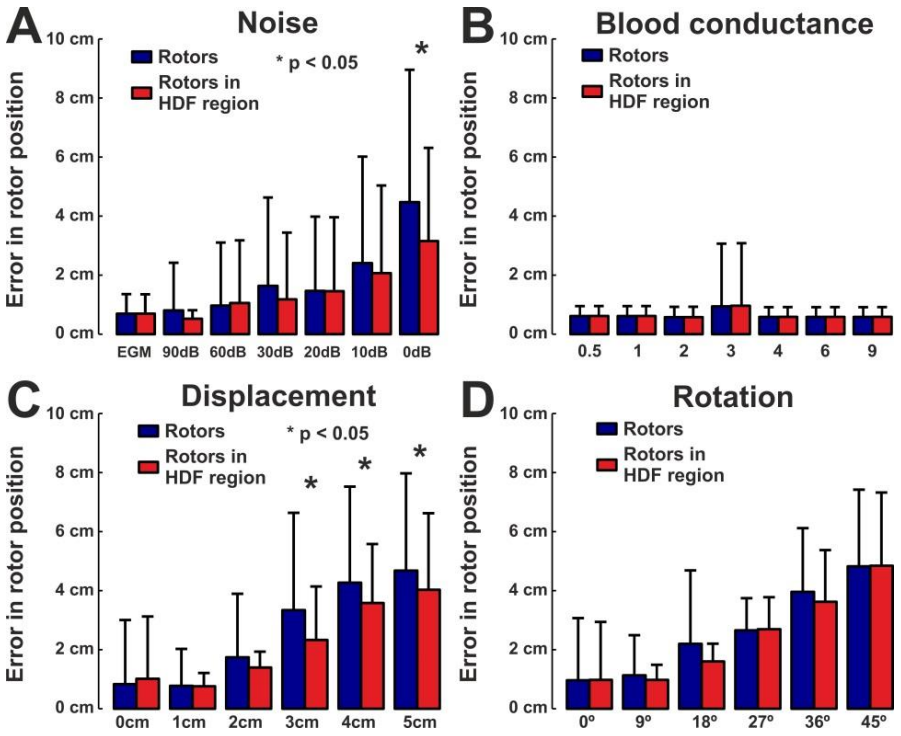

Figure 7.12 – Error in non-invasive rotor position identification by rotational activity (blue) and by rotational activity plus dominant frequency (red)
Variations in: (A) ECG noise; (B) Blood conductance; (C) Displacement; (D) Rotation.

7.4. Discussion

This chapter demonstrates that inverse-computed maps allow for an accurate identification of atrial drivers even in the presence of noise or model uncertainties by making use of mathematical models of human AF and torso propagation. In spite of the limited accuracy of the morphology of inverse-computed epicardial potentials, atrial drivers can be identified because the predominant activation patterns and activation frequencies are preserved. Overall, the identification of atrial drivers restricted to highest DF regions outperforms driver identification based on rotor detection only.

7.4.1. Accuracy of the inverse problem resolution in AF

We have recently shown that inverse-computed EGMs are poorly related to contact electrograms (either experimentally measured or simulated), with large relative errors in the instantaneous phase ***[Pedrón-Torrecilla 2016]***. In this work, we have demonstrated that reconstruction errors can be mostly attributed to a loss of complexity, quantified in terms of the number of simultaneous phase singularities. This loss of complexity is consistent with a mutual cancellation of propagation wavefronts with opposed directions ***[Rodrigo 2014]*** that may not be retrievable by solving the inverse problem.

Despite this loss of information at the body surface level, surface potentials have shown to keep some relevant attributes of AF drivers both in terms of their activation frequency ***[Guillem 2013]*** and rotor location ***[Rodrigo 2014]***. However, other uncertainties may add computational errors to the inverse problem resolution which may restrict the validity of such approach in the context of atrial fibrillation. These uncertainties include, among others, the presence of electrical noise or the inaccuracies in the geometrical model used ***[Cheng 2003]*** due to either an inaccurate volume segmentation or the use of a static torso model that does not account for the dynamic position of the atria inside the thorax during heart contraction and respiration ***[Jiang 2009]***. Although previous works ***[Cheng 2003, Jiang 2009]*** concluded that these uncertainties have a limited impact in inverse problem resolutions in the context of non-fibrillating ventricular activity, they did not account for the more complex scenario of AF, with multiple simultaneous activation wavefronts and lower signal-to-noise ratios. Moreover, the impact of the anticipated atrial surface acquisition could also have a significant impact on position of the atria inside the thorax ***[Haisaguerre 2014]***.

We found that addition of electrical noise to the surface recordings results in an additional smoothening of the surface potentials, already smoothened by the inverse problem resolution without noise, which results in a decrease in the amount of simultaneous phase singularities. This smoothening effect can be attributed to the selection of higher regularization parameters in the presence of noise which, in

turn, results in a spatial smoothing of the potentials. Uncertainties in the geometrical model, however, had the opposite effect by increasing the complexity and simultaneous phase singularities.

However, despite the non-negligible effect of signal or noise inaccuracies on the reconstructed propagation patterns, we found that activation-based parameters, such as the activation frequency computed by spectral analysis or rotor location computed by applying phase transform, are robust against both signal and model uncertainties. This good performance of activation-based parameters suggests that the underlying propagation patterns do reach the torso surface and can be inverse-reconstructed whereas the fibrillatory conduction that surrounds the main rotational activity cancels out and reaches the surface at a lower extent, as we have described elsewhere ***[Rodrigo 2014]***. According to our results, the simple activations patterns computed after inverse problem resolution do not account for the complexity of true activation patterns during AF, but maintain key features that allow the identification of atrial drivers.

7.4.2. Inverse problem and AF mechanisms

There is still no current agreement on which are the mechanisms responsible for AF maintenance since there is both experimental and clinical evidence of the existence of atrial drivers or rotors responsible for AF maintenance ***[Berenfeld 2001, Jalife 2002, Narayan 2013]***. However, recent reports on the success of rotor-guided ablation strategies ***[Narayan 2014]*** have demonstrated the prevailing role of rotors in AF maintenance.

Recently, Haissaguerre et al. ***[Haissaguerre 2014]*** have reported on the identification of rotors noninvasively, by solving the inverse problem of electrocardiography. However, these results were questioned due to the fact that activation maps were too simple as compared to contact mapping activation maps and the lack of validation with simultaneous intracardiac mapping data. According to our results, although the reported epicardial potentials using the inverse problem resolution are highly different to the reported by intracardiac recordings, the non-invasive activation maps may be proving the presence of rotors in human AF.

7.4.3. Study limitations

Here we used mathematical models in order to validate the noninvasive estimation of atrial drivers during atrial fibrillation because current technology does not allow validating such approach in a real scenario. An accurate validation would require precise measurements of the transmembrane voltage in the entire atrial tissue and in the torso, including the endocardium, epicardium and surface ECG at multiple sites. However, the mathematical models used may not represent the whole spectrum of possible atrial substrates during AF and, therefore, our

results cannot be extrapolated to a more general AF population. In addition, all simulations were performed using a simplistic model composed only by the torso and the atrial surface with no structural heterogeneities. Although volume heterogeneities such as the bones or lungs do influence the surface signals, they mainly affect the signal amplitudes but not the activation patterns ***[Ramanathan 2001, Cheng 2003]***, and therefore, may have little impact in our results.

7.4.4. Conclusions

AF driver identification based on the inverse problem resolution is accurate despite the overall simplification of epicardial potentials. In this context, combination of frequency and phase-derived measurements outperforms the sole identification of drivers based on rotor location, especially under noise conditions.

Chapter 8

Solving inaccuracies in anatomical models for electrocardiographic inverse problem resolution by using electrical information

8.1. Introduction

Noninvasive identification of cardiac electrical activity or electrocardiographic imaging (ECGI) has become a technique increasingly used in clinical practice. This technique allows to obtain the electrical activity in the whole heart with much higher spatial resolution than invasive techniques nowadays used, and the potential to simultaneously record the electrical signal everywhere in the myocardium has been exploited in the study of both ventricular ***[Cuculich 2011, Revishvili 2015]*** and atrial arrhythmias ***[Haissaguerre 2011, Cuculich 2010, Wang 2007]***.

Electrocardiographic imaging is based on the resolution of the inverse problem of cardiology, making use of the signals recorded by Body Surface Potential Mapping (BSPM) and the 3D anatomy of the torso and heart of the patients. All this information allows reversing the electrical transfer between myocardial tissue and the patient torso ***[Horácek 1997]***. However, some inaccuracies in these data may appear when the CAT/MRI images and the BSPM recordings are not obtained immediately one after another and have to be taken on different days. This delay can result in a mismatch in the heart location that is

traduced in a loss in accuracy in the inverse-computed signals. Moreover, the heart position is subjected to other sources of movement artifacts, like respiration or ventricular contraction..

One of the parameters used to solve the inverse problem is the L-curve, which allows the system to find a balance between the errors committed in the non-invasive signal estimation and the intrinsic numerical error of the inverse solution ***[Horacek 1997]***. It has been observed that the worsening of the system conditions, such as the displacement of the heart within the torso, affects to the L-curve shape. This paper evaluates whether the measure of the L-curve worsening by its curvature allows minimizing the uncertainties on the system conditions, namely the inaccuracies in the atrial position in a population of patients of atrial fibrillation (AF). An automatic method to remove inaccuracies in atrial position would not only allow to obtain better outcomes with non-invasive techniques, but also to make it feasible to use the ECGI in paroxysmal AF patients.

8.2. Methods

8.2.1. Patient recording

Four patients admitted for ablation of drug-refractory paroxysmal AF (females, 57.2±17.4 years old) were included in the study. The protocol was approved by the Institutional Ethics Committee of our institution and all patients gave informed consent.

Multichannel electrocardiograms (ECGs) were recorded with 57 chest ECG leads by using the Body Surface Potential (BSPM) technique ***[Guillem 2013]***. The signals were recorded using a commercial system (Clearsign^{TM} Amplifier, Boston Scientific, Natick, MA) and the 57 electrodes were distributed as follows: 24 electrodes on the anterior, 24 on the posterior, 3 on each lateral side of the torso and 3 extra leads in order to obtain a Wilson Central Terminal. Pictures from multiple points of view were obtained for each patient wearing the recording electrodes.

The electrophysiological study was performed under general anesthesia and periodic heparin bolus administration. Intracardiac electrograms and atrial anatomy were obtained from both atria during the procedure by using an ablation catheter (Navistar cooled-tip catheter, Biosense Webster, Inc, Diamond Bar, CA) introduced via the right femoral vein and guided by a electroanatomical navigation system (Boston Scientific, Natick, MA). Two patients arrived in sinus rhythm and AF was induced using electrical burst pacing ***[Atienza 2011]***. Then, a central venous bolus of adenosine (12-18 mg) was administered in order to produce a significant atrio-ventricular block and to remove the ventricular activation ***[Atienza 2006]***. At peak adenosine effect, ECGs segments surrounding the longest RR interval were used for the analysis. Nineteen AF signal segments from the 4

patients (4.7±3.1 segments per patient) with duration of 5.6±2.1 seconds were used for the analysis.

MRI images with a spatial resolution of 0.7x0.7x1.5 mm were acquired 2-3 days prior to the ablation procedure. Atria and torso anatomy were obtained by segmentation of MRI images by using by using ITK-SNAP ***[Yushkevich 2006]***. Additionally, the atrial anatomy was retrieved from the electroanatomical navigator and the torso anatomy, together with electrodes location was obtained by processing the conventional images acquired ***[Remondino 2004]***. Anatomical models obtained with the different technologies were co-registered by using an algorithm based on rigid transformations ***[Eggert 1997]*** guided by 8 points manually marked in both atrial models (4 PVs, LAA, RAA and SVC, IVC) or torso models.

8.2.2. Mathematical models

A realistic 3D model of the atrial anatomy was used to simulate the atrial electrical activity (see chapter 3.1). An ensemble of 31 different AF episodes was simulated, composed of 14 AF patterns driven by a single rotor at varying locations of the LA (PVs, PLAW and LAA) and 17 AF patterns driven by a single rotor at varying locations of the RA (free RA wall and RAA).

For each simulation, a uniform mesh of 2048 unipolar EGMs was calculated surrounding the epicardial surface and the ECG potentials on the torso model were calculated in a mesh formed by 771 nodes (see chapter 3.3).

8.2.3. Inverse solution and L-curve

We estimated the inverse-computed EGM (icEGM) from both patient recordings and mathematical models by Tikhonov's regularization method (see chapter 3.3). The optimal regularization parameter was chosen according to the L-curve method, which calculates the maximum curvature of the graph provided by the error norm in the abscissa axis and the solution norm in the ordinate axis for the different regularization parameters (see Figure 8.1). The optimal regularization parameter was chosen at the first local maximum value of the curvature, and the curvature value at this point was used for the location of the atrial surface. Please note that the changes in the atrial position only affected the transfer matrix *M*, and the ECG potentials were not affected by translations or rotations of the atrial surface.

8.2.4. Estimation of the location of the atria based on L curve shape

In order to explore the potential use of the L curve shape to estimate the location of the atria inside the thorax we varied the location and orientation of the atria both in our mathematical models and in our patient data and computed the maximum L-curve curvature under all tested model alterations.

In Figure 8.1, a sample case of the resolution of the inverse problem of electrocardiography with a modification in the model geometry is represented. The forward problem was solved with the atria at the "original location" and then the inverse problem was solved both for the atria at the original and "displaced" location (5 cm distance). With the departing EGMs (Figure 8.1A), a rotor can be identified in the right atrial wall. Inverse-computed phase maps calculated with the same geometries for the forward and inverse calculations do allow to identify the rotor at the same location, despite the differences that can be observed both in potential and phase maps, as it can be observed in Figure 8.1C. However, inverse-computed maps obtained with a displacement in the atrial location (Panel D), no longer allow the identification of the atrial rotor.

The basis of the atrial location identification based on the L-curve shape is shown in Figure 8.1E. It can be observed that the L-curve calculated for the right location shows a sharp corner whereas the L curve computed for an incorrect location of the atria is smoother and, therefore, the curvature is higher for the correct location than for the wrong location (4.53 vs 0.43).

In order to assess the ability of the L-curve curvature for solving the spatial inaccuracies in the atrial surface location, several test were carried out. First, single deviations in every axis (displacements or rotations) were evaluated in a subset of 10 mathematical models and in the whole patient population by measuring the L-curve curvature in presence of gradual deviations. Then, the whole dataset was evaluated in presence of two superimposed rotations: a fixed random deviation in one axis (X) and a gradual deviation in a perpendicular axis (Y) in which the L-curve curvature was measured. Posteriorly, the same experiment was carried out in presence of three superimposed rotations: two fixed random deviations in two axes (X and Y) and a gradual deviation in a perpendicular axis (Z) in which the L-curve curvature was measured. Finally, the whole dataset was evaluated in presence of inaccuracies in every axes: the atrial surface had a random angular deviation in the three axes (X, Y and Z), and the L-curve curvature was evaluated for several distances from the original position to a random displacement in the three axes.

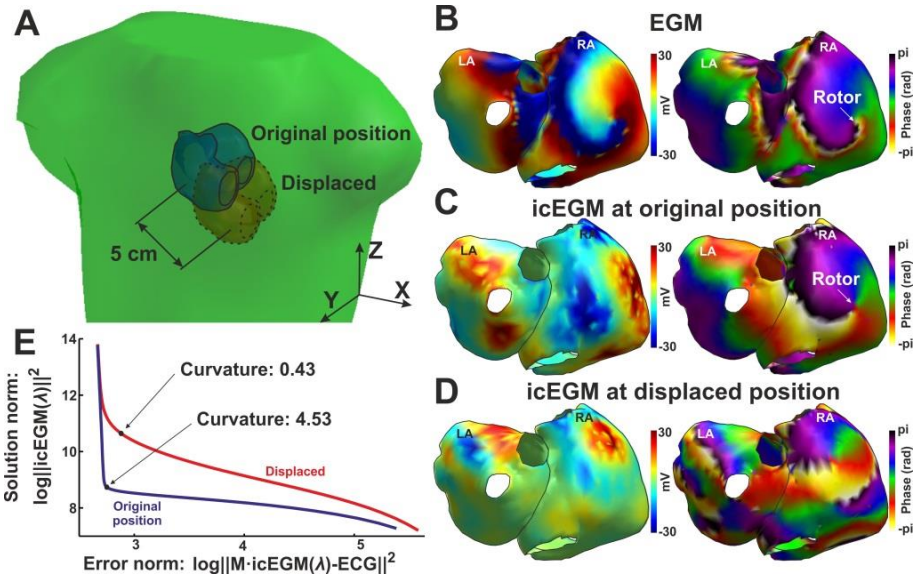

Figure 8.1 – Illustration of the experimental set-up and inverse-computed examples

(A) Schematic view of the torso surface (green), atrial surface at the original position (blue) and atrial model at displaced position (red). (B) EGM (left) and phase map (right) for an AF episode maintained by a rotor in the RA. (C) Inverse-computed EGM (left) and phase map (right) for the simulation in B solved at the original position. (D) Inverse-computed EGM (left) and phase map (right) for the simulation in B solved at displaced (5 cm) position. (E) L-curves of the inverse solution for the original position (blue) and displaced positon (red).

8.3. Results

8.3.1. Single axis displacement vs. curvature

We first evaluated the curvature of the L-curve for displacements in one of each of the x, y, z axis in the location of the atria inside the thorax for the resolution of the inverse problem. For displacements in the X axis (Figure 8.2A), the maximum curvature was found on average for the correct location of the atria. Indeed, 8 simulations showed their maximal curvature for 0 mm of displacement, and 2 simulations for -5 mm. Therefore, if there was an uncertainty in the actual location of the atria inside the thorax in the X axis it could be estimated with a mean error of 1.0±2.1 mm. Similar observations can be made for displacements in the Y and Z axis, with errors in the location of the atria of 3.0±2.6 mm and 1.0±2.1 mm for the displacement in the Y and Z axis, respectively (Figure 8.2C-D). Overall, the mean error was 1.7±2.4 mm.

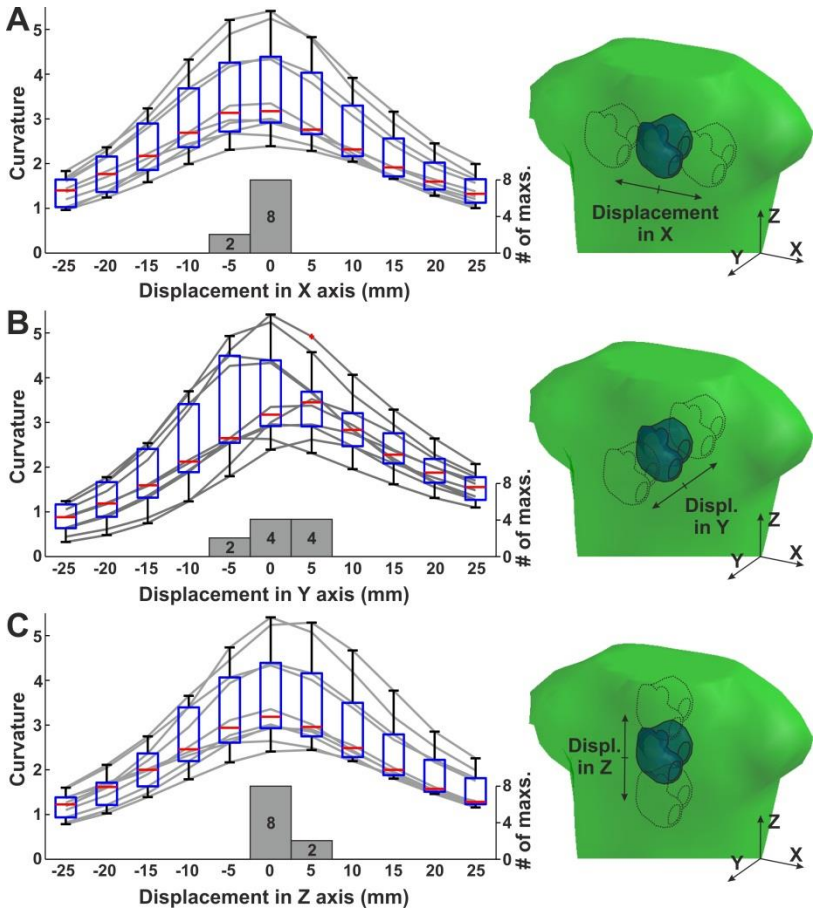

Figure 8.2 – Estimation of atrial position in mathematical models
L-curve curvature for each simulation (gray lines), boxplot of the curvature values for each displacement and number of maximal curvature in each displacement (gray bars). (A) Displacement in X axis; (B) Displacement in Y axis; (C) Displacement in Z axis.

The same experiments were conducted with the patient data, in which the location of the atria, obtained my MRI, was altered in each of the X, Y, Z axis (Figure 8.3). Again, the maximum curvatures were obtained at the actual location of the atria inside the thorax. If the location of the atria is defined as that with the largest L-curve corner curvature, then the observed errors were 5.8±5.1 mm, 7.2±8.9 mm and 14.2±16.1 mm for the X, Y and Z axis, respectively (9.1±11.5 mm on average). By looking at the individual tracings for all the curvature measurements, largest curvatures do cluster around the maximum value. This holds even for the patients in which the location of the atria by the L-curve curvature and MRI did not match, which may be the consequence of an inaccurate registration of the MRI and the electrodes location by conventional images.

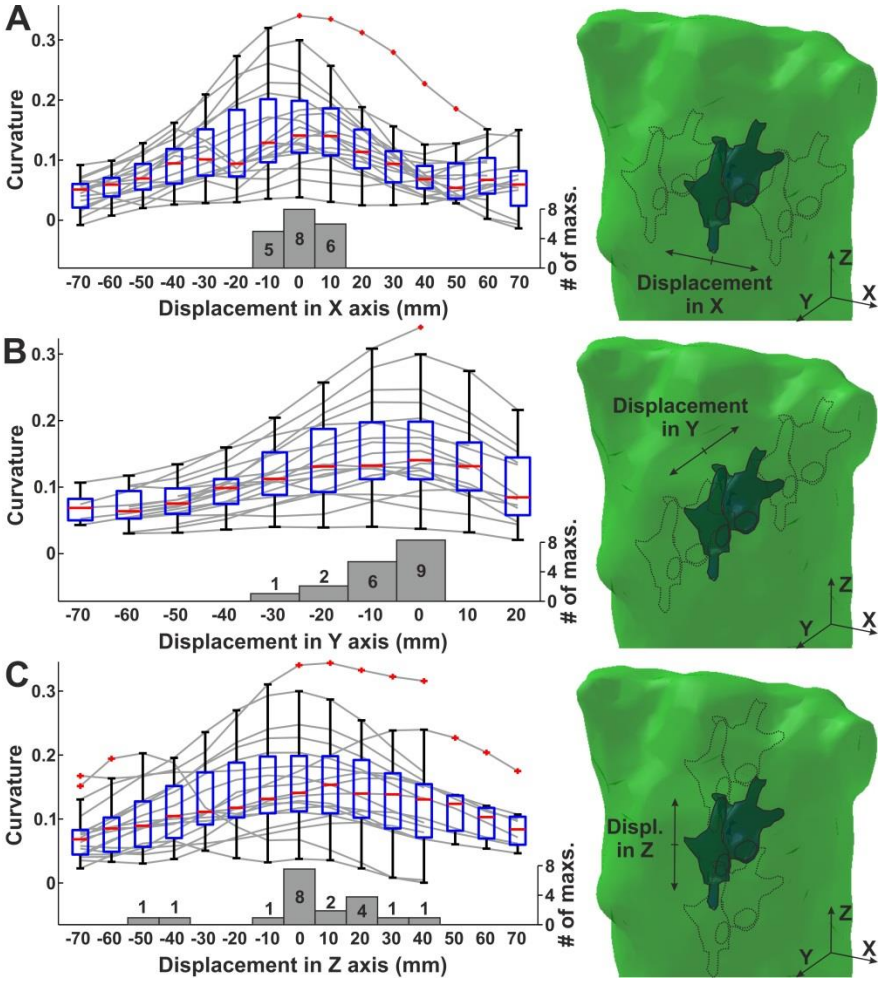

Figure 8.3 – Estimation of atrial position in patients
L-curve curvature for each AF episode (gray lines), boxplot of the curvature values for each displacement and number of maximal curvature in each displacement (gray bars). (A) Displacement in X axis; (B) Displacement in Y axis; (C) Displacement in Z axis.

8.3.2. Single axis rotation vs. curvature

The second stage of the L-curve accuracy assessing was to evaluate its capability to properly detect a rotation in the atria inside the thorax. In Figure 8.4, results of the inverse problem resolution after rotations between -30º and 30º around each of the three axes are presented. In Figure 8.1A the curvatures obtained for each simulation affected by rotations in X axis are depicted, and it can be observed that all of them showed their maximal curvature of the L-curve in the

actual location of the atria and thus the error in rotation identification was 0.0±0.0º. Rotations in Y axis, however, resulted in no clear trends that may allow the identification of the actual location (Figure 8.4B), with maximum values distributed from -18º to 24º and a location error of 13.8±6.4º. Finally, the angular deviation in the Z axis produced an error in the angular location of 3.6±3.1º. The overall mean error was 5.8±7.1º.

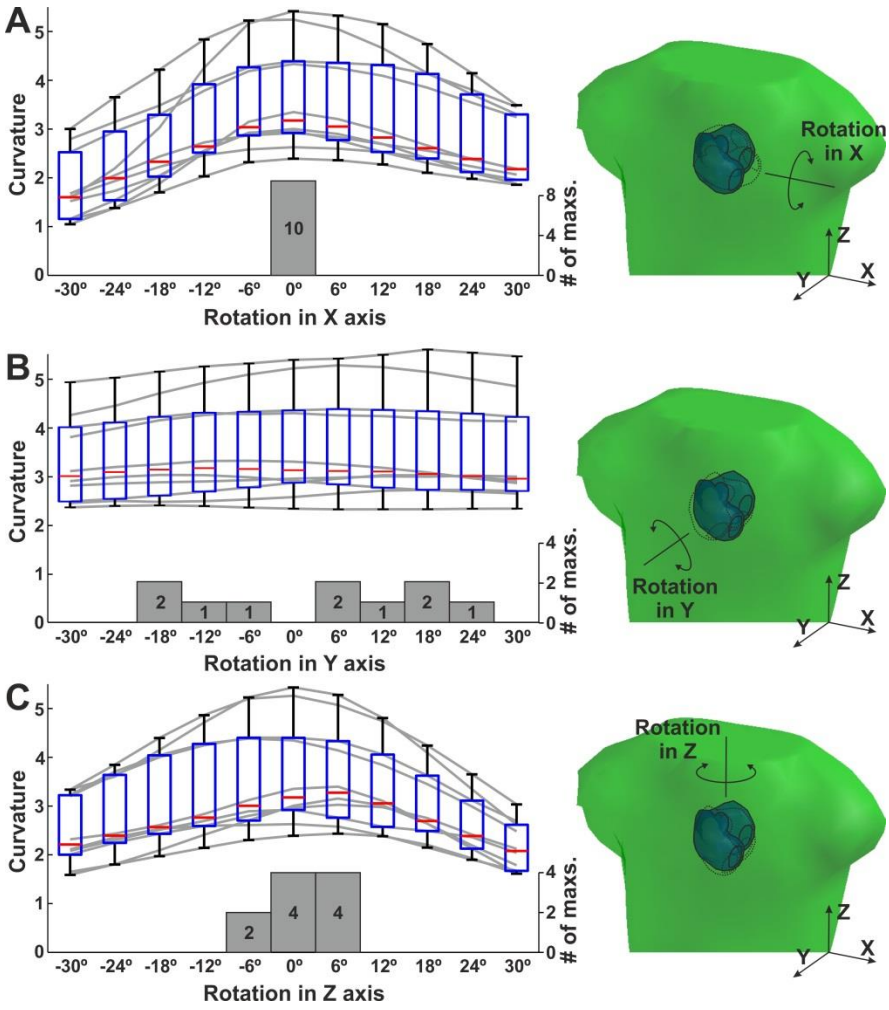

Figure 8.4 – Estimation of atrial rotation in mathematical models
L-curve curvature for each simulation (gray lines), boxplot of the curvature values for each angle and number of maximal curvature in each angle (gray bars). (A) Rotation in X axis; (B) Rotation in Y axis; (C) Rotation in Z axis.

In Figure 8.5 the results from rotations of the atria inside the thorax of AF patients are depicted. Figure 8.5A shows the curvatures obtained after rotations around the X axis, which resulted in an error in the estimation of the angular position of the atria of 4.1±5.1º. As in the mathematical models, the angular deviation in the Y axis produced a more widespread distribution, as it can be observed in Figure 8.5B, with an error in the angle detection of 18.3±15.0º. Finally, the angular deviation in the Z axis provoked an error of 12.6±11.9º (Figure 8.5C) and thus the mean error was 12.4±13.2º.

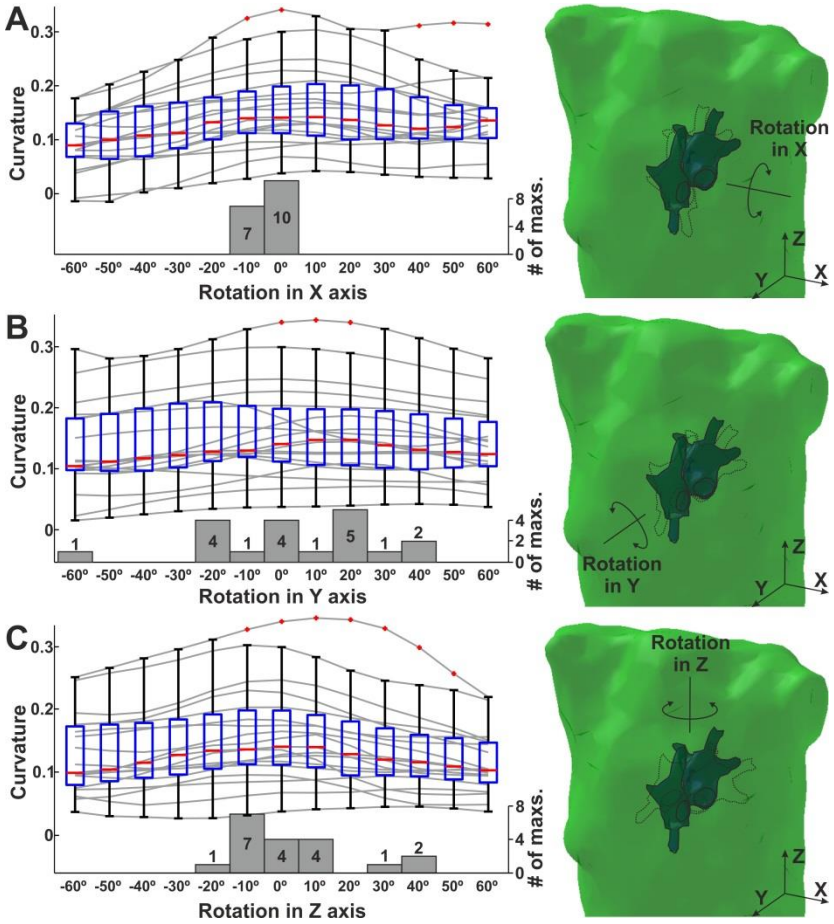

Figure 8.5 – Estimation of atrial rotation in patients

L-curve curvature for each AF episode (gray lines), boxplot of the curvature values for each angle and number of maximal curvature in each angle (gray bars). (A) Rotation in X axis; (B) Rotation in Y axis; (C) Rotation in Z axis.

8.3.3. Combined rotations and displacements vs. curvature

Since errors in location and orientation of the atria inside the thorax can appear in combination, we then evaluated the potential use of the L-curve curvature for identifying these errors in a step-wise manner. In order to answer this question, for each of the mathematical models a random rotation in the X axis was applied and then we evaluated the curvature of the L-curve under known rotations around the Y axis. Again, rotation around the Y axis showed a widespread distribution of curvatures but even in this scenario the error in the angular deviation identification was 8.9±7.6º. In Figure 8.6B, the curvature as a function of a rotation in the Z axis was evaluated after a random angular deviation (-30º to 30º) around both the X and Y axis. This case showed an error of 6.4±7.1º in the angular deviation identification. Finally, we evaluated the curvature as a function of the distance from the actual location of the atria inside the thorax (random distances from 0 to 45 mm) after random rotations (-30º to 30º) around any axis. It can be observed as the curvature showed its maximum values in the vicinities of the actual location, resulting in an error in the position estimation of 2.3±3.2 mm.

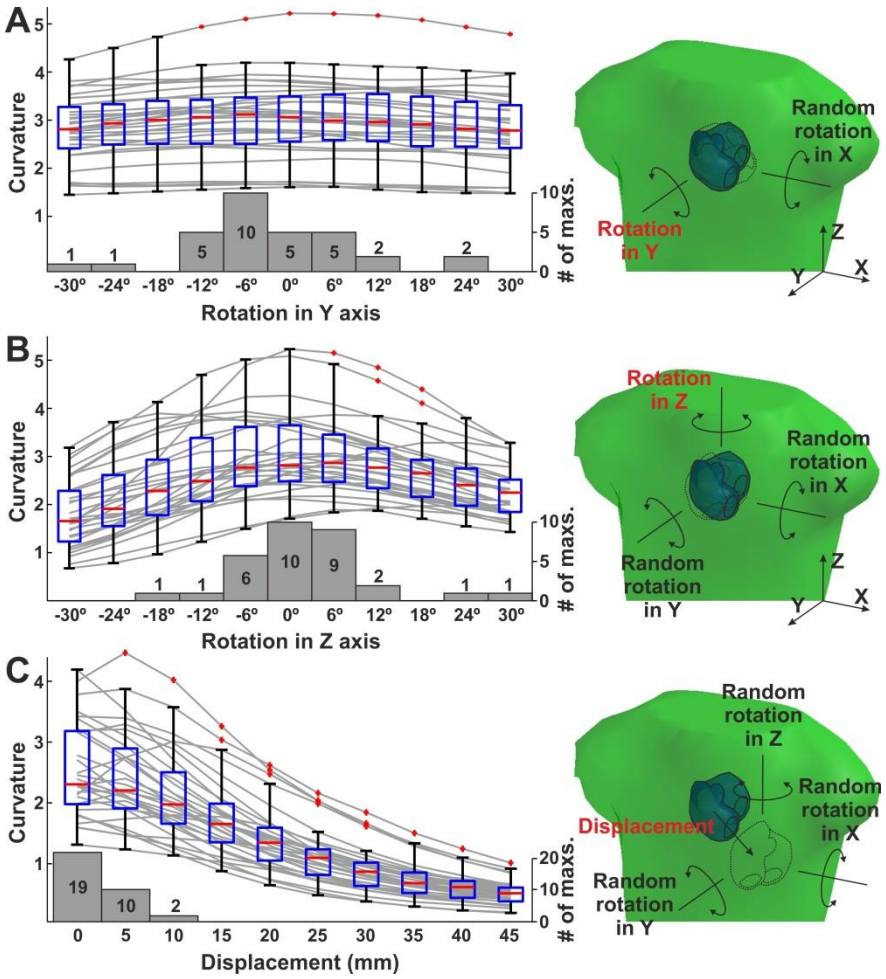

Figure 8.6 – Estimation of accumulated artifacts in mathematical models
L-curve curvature for each simulation (gray lines), boxplot of the curvature values for each angle/displacement and number of maximal curvature in each angle/displacement (gray bars). (A) Rotation in Y axis with a random rotation in X axis; (B) Rotation in Z axis with a random rotation in X axis and Y axis; (C) Displacement with a random rotation in X, Y and Z axis.

Figure 8.7 shows the experiments described before with AF patient data. Here, the error in solving the rotation around the Y axis after a random angular deviation (-30º to 30º) in the X axis was 18.4±14.6º (Figure 8.7A). Errors in identifying rotations in the Z axis in the presence of random rotations (-30º to 30º) in the X and Y axis, resulted in errors of 10.0±12.8º (Figure 8.7B). Finally, errors in the estimation of displacements in the location of the atria inside the thorax under random rotations (-30º to 30º) in the 3 axis were 7.9±10.7 mm.

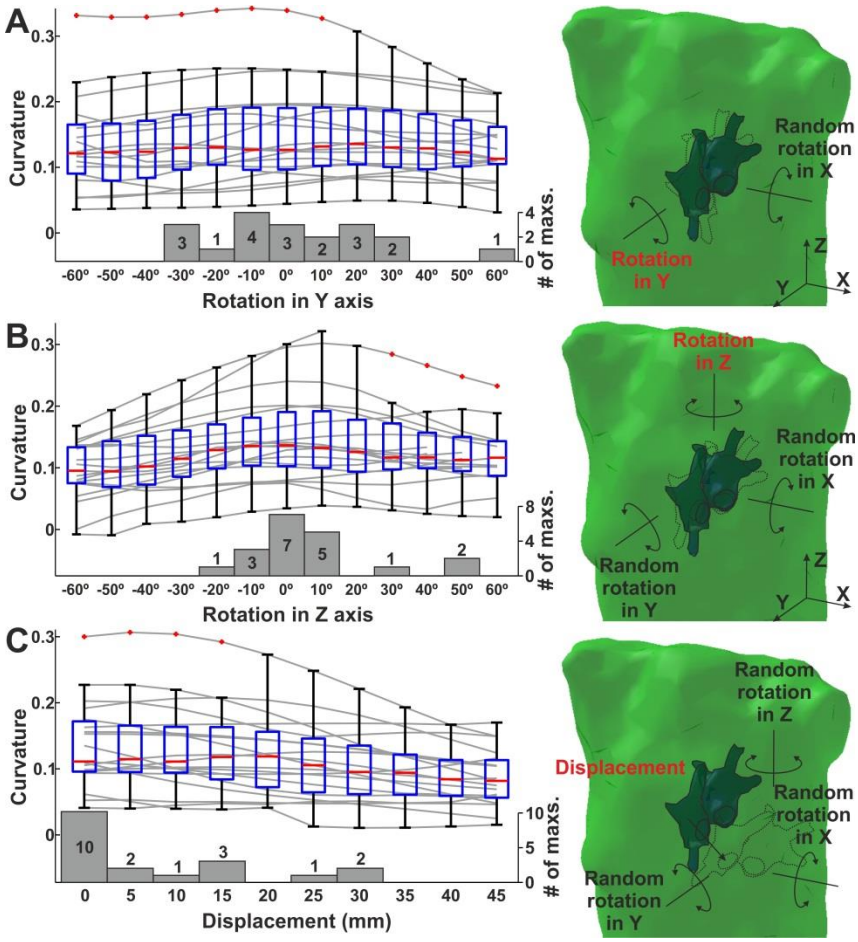

Figure 8.7 – Estimation of accumulated artifacts in patients
L-curve curvature for AF episode (gray lines), boxplot of the curvature values for each angle/displacement and number of maximal curvature in each angle/displacement (gray bars). (A) Rotation in Y axis with a random rotation in X axis; (B) Rotation in Z axis with a random rotation in X axis and Y axis; (C) Displacement with a random rotation in X, Y and Z axis.

8.4. Discussion

This study presents a new approach for refining the location of the atria inside the thorax for solving the inverse problem of electrocardiography based on electrical information, whose validity has been tested both in mathematical models and in patients. The ability of the L-curve curvature for the location and orientation of the atria has been tested under single and multiple combined displacements and rotations with errors in location below 1 cm, and thus could be used in a realistic scenario.

8.4.1. Anatomical models and inverse problem resolution

Solution of the inverse problem of electrocardiography generally involves the recording of MRI or CAT images for obtaining accurate anatomical models of the patients. These MRI or CAT images are obtained with the BSPM electrodes in place so that the geometric parameters are preserved ***[Ramanathan 2001]***. Although previous works have reported that the inverse problem can overcome to spatial uncertainties up to 1cm with similar results ***[Messinger-Raport 1990]***, the proper spatial localization and construction of accurate anatomical models offer better outcomes of the inverse solutions ***[Messinger-Raport 1986]***.

However, it is not always feasible to obtain the MRI together with useful BSPM recordings. This is the case for paroxysmal AF patients that may arrive in sinus rhythm and induction of AF should only be performed in the electrophysiological laboratory. In addition, in order to validate the inverse problem resolution during AF, both BSPM recordings and invasive data should be obtained simultaneously ***[Guillem 2016]*** and cannot be done inside the MRI or CAT scanner. In order to overcome the limitations of the inverse problem resolution in AF, we propose to refine the geometry obtained from a prior scan with electrical information, and thus may allow the use of the inverse problem resolution for paroxysmal AF patients and not only persistent patients.

8.4.2. The L-curve regularization and anatomical model

The L-curve regularization method has been profusely used in the literature to solve ill-posed systems, as the case of the Inverse Problem of Electrocardiology ***[Messinger-Raport 1989, Messinger-Raport 1990, Horacek 1997]***. Previous works has reported changes inverse solutions provoked by the worsening of the problem conditions, like uncertainties on the signals or on the transfer matrix ***[Messinger-Raport 1990, Messinger-Raport 1986, Ramanathan 2001, Ramanathan 2001]***. Our work makes use of the change in the L-curve curvature that occurs when there are inaccuracies in the transfer matrix, in our case caused by uncertainties in the atrial location, which provoke that the possible solutions for all the regularization parameters contains significant errors. In this case, the division between the numerical error and the error on the solution (the two “arms” of the L-curve) is not so abrupt, thus it produces a smothered curvature in the “corner” of the L-curve. However, this is the first work that proposes to take advantage of this property of the L curve in order to refine the geometry of the model.

We have shown that the curvature at the corner of the L curve is maximized for matching forward and inverse problem anatomies. However, this approach seems to be more sensitive for displacements than for rotations, less sensitive for rotations around a main axis of the geometrical model itself (i.e. rotations around the Y axis). Notice that rotations around a main axis of the model do not result in

major changes in location since the atria is inscribed roughly in the same volume while rotations around any other axis do result in a change in the occupied volume. This would explain why both in patients and mathematical models the error in atrial rotation having 3-axis angular deviations is lower than the error having just 2-axis angular deviations, since the 2-axis case was measured in the Y axis and the 3-axis case in the Z-axis. We have also shown that is possible to identify the closest location in each axis in a stepwise manner because the curvature is also maximized even if there are unresolved location errors in other axis.

In our study we have made use both of human data and mathematical models because the gold standard anatomy has to be estimated from CAT images and thus there is some uncertainty about the actual anatomy and the location of electrodes. As expected, results in atrial location and orientation provided better outcomes in mathematical models than in patients, in which there are electrical noise, more complex electrical patterns and more model inaccuracies. In particular, we found larger errors for locating the atria in the Z axis than for the other axis and this was not reproduced in the mathematical models. We attribute this differential effect to model inaccuracies, since the CAT image and the conventional image were obtained with the patients at different postures (laying vs. sitting), which may affect the Z axis to a greater extent than the other axis. We believe that validation with a more accurate geometrical model can only be more favorable and thus we are underestimating its accuracy.

8.4.3. Limitations and future work

For both patients and mathematical models a simplistic torso conductor volume was considered for the inverse solution, without the inclusion of lungs, blood vessels or bones. This decision is supported by the literature, since the inverse-computed signals has been reported to be slightly affected by the inhomogeneities of the torso volume ***[Messinger 1986, Ramanathan 2001, Cheng 2003]*** in comparison with the effect of changes in the heart position. Although previous studies were carried out on ventricular signals, the study of the Forward Problem on atrial signals also reported the relative invariance against the torso inhomogeneities ***[Ferrer 2015, Bear 2015]***.

This study used the curvature of the L-curve only for the atrial location and orientation. However, other parameters related to the L-curve shape may also help in determining the best match for geometrical models. Although we found the curvature of the corner of the L-curve to be the most robust indicator, we did not test any combination of L-curve descriptors which may allow an improved performance.

We have shown that the location of the atria can be resolved in a stepwise manner. An exhaustive search in the entire volume may be too computationally intense. However, the accuracy in the location of the atria may be increased if the

algorithm was run more than once and thus the location was iteratively refined, since the errors in location or angular deviation are lower when no other inaccuracies are involved.

Finally, the validity of the method has been proven just for AF signals, and its extension to other atrial arrhythmias remains unproven. However, AF presents the most complicated electrical pattern that can be present in atrial electrophysiology, and thus more subjected to the low-pass filtering effect of the torso conductor ***[Rodrigo 2014]***. We believe that the method can be extended to other less complicated rhythms but its reliability for conditions should be tested.

8.4.4. Conclusion

This work presents a novel technique based on the curvature of the L-curve for placing the atria inside the chest when solving the inverse problem of electrocardiography. The presented technique has been tested for both mathematical models and patients, and under single or multiple uncertainties on the atrial location. It has been shown that this geometrical identification can be achieved with errors of about 1 cm and 15º. This technique could be useful for avoiding the spatial artifacts present in the inverse problem but also to extend the use of this technique by making it possible to use previously obtained CAT/MRI images of the patient.

Chapter 9

Discussion and conclusion

This chapter contains a global discussion of the results presented in the main chapters of this thesis. First, the main findings are discussed and compared with previous works, and the limitations of this work are commented. Secondly, the main conclusions of this thesis are listed by assessing the resolution of the objectives proposed in the first chapter. Finally, the chapter is closed with guidelines for future work, highlighting aspects of this thesis that can be further explored.

9.1. Main findings

Although the most common treatment for AF patients is the pharmacological therapy, surgical ablation has acquired more relevance due to its ability to eradicate the arrhythmia in many patients, especially when the ablation is conducted at its earliest stage ***[Chao 2012]***. In addition, it has been reported that ablative therapies present higher rates of efficacy when a patient-tailored approach based on the characterization of the fibrillatory process in each patient is used. Therefore, different methods to locate the atrial drivers maintaining the arrhythmia have been used in the clinical practice, mainly based on the analysis of the intracavitary signal recorded with catheters ***[Sanders 2005, Atienza 2009, Narayan 2012]***. However, these characterization methods are only available for patients already in the catheterization laboratory and thus this analysis does not allow to select patients nor to plan the ablation procedure. In order to solve such problem, non-invasive methods for atrial driver identification have been developed, such as BSPM or ECGI. Nevertheless, the novelty of these systems together with the controversy regarding the underlying mechanisms in which they rely are delaying their introduction into the clinical practice. This thesis broadens the scientific and

technical knowledge about the noninvasive identification and localization of atrial drivers.

First, in this thesis it has been shown that in the same way that BSPM systems can non-invasively estimate atrial dominant frequencies ***[Guillem 2013]***, BSPM systems can also detect surface reentrant patterns provoked by atrial rotors. In particular, it has been shown that the position of these surface rotors is dependent on the rotor placement in either the left or the right atrium and thus left or right atrial rotors can be distinguished. However, the electrical activity of these atrial rotors is projected on the torso surface toghether with the electrical activity from other atrial regions. In this thesis it has been shown that a narrow band-pass filtering at the rotor band allows identifying surface rotational activity at the highest DF. This narrow band-pass filtering removes the surface electrical activity caused by atrial regions others than the rotor region and thus only the reentrant electrical activity at the HDF is kept in the surface maps.

The use of mathematical models allowed to investigate such hypothesys, since a clinical scenario does not allow for acquiring electrophysiological signals with a sufficient spatial resolution. The spherical mathematical models provided evidences that the surface ECG contains spectral components from the whole activity in the atria that could affect the way in which atrial rotors are projected onto the torso surface. When the rotor occupies a wide region on the atria, the electrical activity from the non-reetrant region causes a precession on the surface rotor position that can be removed by the narrow band-pass filtering at the rotor band. In addition, when the rotor area is small (<20%) the non-reentrant atrial activity masks the reentrant activity on the surface, and thus rotors cannot be detected on the surface. In these cases, HDF filtering allowed to isolate the spectral components from the atrial rotor and highlights them on the surface. Furthermore, the use of mathematical models has also enabled to study the effect of the spatial smoothing filter provoked by the torso volume conductor on the electrical activity during AF, whose spatial complexity is reduced with increasing distance from the myocardium. This spatial smoothing filter removes the small details and leaves on the surface only the predominant electrical patterns from the myocardium, resulting in a "simplification" of the surface patterns.

According to this simplification of the surface patterns, identification of atrial sources on the surface ECG requires for just a few leads to be recorded. On the one hand, the number of leads needed to noninvasively identifiy the highest DF sites can be accomplished by 12 uniformly distributed leads. Identification of surface rotors after HDF filtering would require far more leads -32- because rotors are detected from spatial maps involving several leads. This little amount of leads may appear to be unrelated to the electrical complexity of atrial fibrillation but is closely related to the effect of spatial filtering by the torso explained above, since the simplification of the surface activity results in a homogeneization of the surface potentials and thus just a few leads account for most of the relevant information.

The effect of the narrow band-pass filtering for the atrial driver localization has been further explored in this thesis, since it has captured some attention in the field and has raised some criticisms. We found that the narrow band-pass filtering, applied after the spatial filtering caused by the torso volume causes some artefactual rotors to appear. However, these rotors have been found to be less stable than the true rotors and thus they are suggestive of rotor presence but not a definite proof. The effect of the HDF filtering in EGM signals, however, has been found that convert the intracavitary signal into a sinusoidal component, which allows retrieving activation times by using the Hilbert transform. Finally, application of a narrow band pass filter to ECGI signals, has been shown to result in too many artefactual rotors and thus it shouldn't be applied.

Raw ECGI signals -without HDF filtering- do allow for accurate rotor identification. We have reported that both rotors and highest DF sites are more stable than signal morphology against uncertainties such as electrical or geometrical noise. It has been shown that the correlation between the original and inverse-computed EGM signals is considerably low and is very sensitive to artifacts. However, both DF analysis and singularity points detection on ECGI signals allows identifying the driver region in up to 80% of our simulations. Furthermore, it has also been found that the combination of these two features (DF and SPs) increases the accuracy in locating dominant atrial regions by ECGI.

Resolution of the inverse problem, however, requires from the segmentation of medical images that may be obtained prior the ECG acquisition and not simultaneously, which may result in geometrical errors. In order to solve this unaccuracies, a new method for refining the location of the atria inside the torso volume has been proposed. The basis of this novel methodolgy is based on the observation that unaccuracies in the atrial location or orientation affect the L-curve shape. In particular, unaccuracies result in a smoothing of the L-curve corner and, therefore, the sharpest L-curve among those obtained for different geometries allow to properly locate the atria inside the torso. This novel technique raises the possibility of developing ECGI systems not dependent on medical imaging techniques as CAT or MRI for obtaining the electrical activity on the myocardium surface, which would represent a breakthrough in the usability of the ECGI in clinical practice.

9.2. Comparison with previous studies

Analysis of electrocardiographic signals for helping in the diagnosis of cardiac arrhythmias has been one of the most relevant fields of our research group. Our group has been one of the pioneers on the use of BSPM for the diagnosis of AF, as they reported that such system could non-invasively reproduce fibrillatory electrical patterns ***[Guillem 2009]***. Latter, they reported that surface electrocardiographic signals could be used to identify the atrial activation

frequencies, by the measurement of the surface DFs ***[Guillem 2013]***. In addition, it was found that the distribution of these surface DFs is subject to the atrial DF distribution and, therefore, the BSPM could be used for discrimination between LA or RA fastest patients. The work described in Chapter 4 is therefore an extension of this study, where the ability of the BSPM to identify atrial reentrant patterns sustaining AF has been demostrated ***[Rodrigo 2014]***. Furthermore, it should be also emphasized that results of Chapter 4 regarding reentrant activity coincide with similar results reported by other studies. Dr. Narayan et al. reported the presence of reentrant activity in 70% of the fibrillatory sources invasively detected, while in our case the percentage of rotor presence is about 70% after HDF filtering ***[Narayan 2012]***. The non-invasively reentrant activity reported by Haissaguerre also coincided in the mean number of rotations per rotor ***[Haissaguerre 2014]***.

The technical functioning of BSPM systems for cardiac arrhythmias has also been extensively studied in the literature. It has been reported that although only about 10 statistically independent components can be identified in the electrocardiographic signal in sinus rhythm ***[Hoekema 1999]***, around 30 leads are needed to reconstruct the surface signal correctly ***[Lux 1978]***. This number has been reported similar for ventricular signals ***[Finlay 2008, Guillem 2009]***. In the case of atrial arrhythmias, our group reported that about 34 leads were sufficient to reconstruct the surface electric activity ***[Guillem 2009].*** These numbers agree with the number of leads for detecting surface rotors proposed by this thesis in Chapter 5, due to the need of reconstructing the whole surface map for the rotor detection. However, since the DF measurement can be carried out in a single lead, the number of uniformly distributed leads for distinguishing between LA and RA fastest patients from DF measurements in BSPM is much lower: 12 leads. This latter correlates well with the study presented by Ferrer et al. in which it was demonstrated with mathematical models that the surface potential distribution provoked by the the atrial electrical activity can be mainly described by the contribution of nine significant regions ***[Ferrer 2015]***.

This low number of leads needed to identify atrial drivers with BSPM systems is related to the smoothing effect of the torso conductor volume studied in Chapter 4 of this thesis. This effect, whose implication on the surface signals is the reduction of the spatial complexity of the signal, has been also reproduced by Ramanathan et al. who reported the major smoothing of the torso potential distribution compared with its corresponding ventricular pattern ***[Ramanathan 2001]***. Ramanathan's work also reported that torso inhomogeneities had a minor effect on the BSPM patterns, fact that has been reported in another study in which the relative error after adding torso inhomogeneities was lower than 15% ***[Klepfer 1997]***. These results seem to validate the smoothing effect of the torso: it is plausible that torso inhomogeneities do not produce large changes in surface potential distribution since they are already smoothened. Moreover, the detailed anatomical torso model plays a minor role in the projection of the atrial electrical

activity on the torso surface and, therefore, it may not be necessary to include torso inhomogeneities or anisotropies to obtain clinically useful results ***[Ramanathan 2001]***. In line with these studies, it has also been reported that the torso inhomogeneities and anisotropies have no significant effect in solving the inverse problem of electrocardiography ***[Ramanathan 2001]***. The results presented in Chapter 6 agree with that report, as we have confirmed that changes in the blood conductance did not affect the inverse-computed EGM shape nor the DF or rotor distribution.

Otherwise, the smoothing effect of the torso volume also affects the resolution of the inverse problem because it limits the spatial information that can be inversely reconstructed to the spatial information contained in the torso potential distribution. Thus, the inverse problem provides inverse-computed EGMs whose correlation with the original EGMs is quite limited even in the best conditions, as we have depicted in Chapter 6. This low correlation between both original and inverse-reconstructed EGMs was reported also for AF patients in previous works from our group ***[Pedrón-Torrecilla 2016]***, and can be also observed in the reported figures by other studies solving the inverse problem for AF patients, whose potential distribution in the atrial surface seems unphysiologically simple ***[Cuculich 2010, Haissaguerre 2014]***. However, although these potential distributions are unrealistic due to the smoothing effect of the torso volume, inverse-computed EGMs contain relevant information regarding the mechanisms that maintain AF. Pedrón-Torrecilla et al. compared invasive with inverse-computed EGMs and reported that, altough the shape and phase of individual signals presented a high relative error, the relative error in the frequency domain remained under the 20% and the DF distributions were consistent between invasive and inverse-computed maps ***[Pedrón-Torrecilla 2016]***. Furthermore, Haisaguerre et al. have conducted a clinical trial in which the inverse-computed rotor identification was used to guide the ablation procedure and in which the radiofrequency delivery was reduced (28±17 vs. 65±33 min) for a similar AF free ratio afer 12 months (85%) than at the control population ***[Haissaguerre 2014]***. Although, unlike the DFs case, these noninvasively located rotors have not been validated by invasive techniques, the ablation outcomes are very encouraging.

One of the most important aspects that this thesis shows is that the signal processing applied to the electrocardiographic recordings alters in great manner the mechanisms of AF maintenance that can be derived from the potential maps ***[Berenfeld 2012]***. Nowadays, whether the maintenance of AF is caused by rotors is still controversial ***[Narayan 2014, Allessie 2014]***. Some authors defend that this mechanism is the responsible of the arrhythmia maintenance ***[Jalife 2002, Berenfeld 2014]***, whereas other schools maintain that rotors do not play a rol in the perpetuation of AF, being other mechanisms the responsible of AF maintenance ***[de Groot 2010, Allessie 2014]***. One of the issues to be considered in this controversia is the importance of the technique used to identify rotors, since

different methodologies can make the difference between rotor under or over-identification ***[Berenfeld 2012, Kuklik 2016]***. Here the importance of the signal processing applied to the electrocardiographic records when looking for rotors, which has been studied in this thesis. Results from Chapter 6 have illustrated that in cases in which the rotors are not detected with the raw signal, the HDF filtering allows their detection: in the case of the BSPM recordings the time with rotors increased from 10% to 90% after the HDF filtering. This fact may be closely related to the differences between detection rates of AF mechanisms (rotor, multiple wavelets, focal) on different studies published both with ECGI ***[Haissaguerre 2014, Cuculich 2010]*** and invasive recordings ***[Narayan 2014, Allessie 2010]***, since all af them used different processing techniques.

Finally, this thesis has addressed one of the most important technical problems of ECGI. Today, segmentation of MRI or CAT images is required in order to obtain the anatomy of the heart surface and the surface of the torso ***[Messinger-Raport 1990, Ramanathan 2004, Wang 2011]*** and this is hampering the access to this technology. The methodology presented in Chapter 8 could solve this limitation and hence allow more patients to benefit by the use of this technique.

9.3. Limitations

As usually occurs in most scientific studies, one of the limitations of this thesis is the number of patients in which the hypotheses have been validated. However, the patient database used in chapters 4 and 5 to study the BSPM has been sufficient to reveal significative results and enabled to show a first approach which may be validated in a larger population. In chapter 8 the database consisted in 4 patients, although each for each patient multiple recordings could be obtained and thus the amount of recordings was 19. This database also allowed to present significant results on the location of the atrial surface from the L-curve curvature.

This thesis has been especially supported by mathematical models that have helped to strengthen the results obtained in chapters 4 and 8. Chapters 6 and 7 have been based solely on mathematical models, but their results were enough to investigate the hypotheses proposed. Nonetheless, results from these chapters must be validated in patient data.

Regarding the patient data used in this thesis, all the database was collected under the effect of adenosine. This was done to prevent alteration of the ECG signal for the ventricular electrical activity, since adenosine causes an atrioventricular block that provides a temporal window of 5 to 8 seconds with no ventricular activity. Although it has been reported that adenosine affects the atrial electrical activity ***[Atienza 2006],*** its effect is usually an increase in the activation rate of the fibrillatory pattern, allowing the stabilization of atrial rotors but preserving the DF gradients. Therefore, the adenosine effect should not be

detrimental to the points raised in this thesis, since it has allowed us to determine that BSPM systems allow to non-invasively detect the reentrant atrial activity, but we did not especulte on the nature of these rotors. Thus, the rotor stabilization provided by the adenosine effect may have resulted in an overestimation of the atrial rotor detection by the BSPM systems, but the hypothesys that atrial rotors can be recorded on the surface remains valid and even more enhanced by the forced appearance of rotors. The acceleration of the atrial activation rate by adenosine infusion also increases the dominant frequency measurement in about 2 or 3 Hz ***[Atienza 2006]*** but this increment is constant in the whole atrium, so the frequency gradients should be conserved and the HDF region should still mark the atrial driver position. Nevertheless, it will be necessary to check the validity of the BSPM under ventricular activity suppression by mathematical algorithms, with the aim of assessing the independence of its diagnostic value with the adenosine effect.

Finally, the anatomical models used in this thesis for the forward and inverse solution were relatively simple, without the inclusion of tissue heterogeneity and anisotropy from lungs, blood vessels or bones. Although the inclusion of such inhomogeneities could increase the accuracy with the cost of an increased computation charge, it has been reported that torso heterogeneities have a relatively little effect in both the calculation of the forward ***[Ferrer 2015, Bear 2015]*** and inverse problem ***[Messigner 1986, Ramanathan 2001, Cheng 2003]***, which has been confirmed at Chapters 7 and 8.

9.4. Conclusion

The main objective of this thesis was to increase the knowledge regarding the non-invasive technologies for atrial driver location in AF. In particlar, whether the non-invasively information obtained about high frequency rotors is univocal and has clinical usefulness. Along the different chapters of this thesis this objective has been achieved through the study of diverse approaches in non-invasive electrocardiography. This objective was broken down into the following points:

- *To study the ability of the BSPM systems to identify surface reentrant fibrillatory patterns in patients with AF, and whether this identification and location is useful for AF diagnosis*. In Chapter 4, we have shown that BSPM maps allow identifying atrial rotors by the analysis of the surface potential distribution. We have shown that HDF filtering allows isolating the surface activity provided by the atrial rotor, and that the rotor distribution on the torso surface can allow to distinguish between left and right dominant atrium.
- *To evaluate the effect of the electrocardiographic projection of the atrial signal on the patient's torso and the consequences of this electrical projection on BSPM and ECGI maps, specifically for AF electrical*

patterns. The effect of the torso conductor volume in the projection of the atrial fibrillatory activity on the torso surface has been studied in Chapter 4, showing that this volume is acting like a smoothing spatial filter which removes the little spatial details. Moreover, the effect of this spatial filtering plus the aggressive HDF filtering has been studied in Chapter 6, demonstrating the spatial filtering provoked by the electrical propagation through the torso conductor volume can affect the suitability of the aggressive temporal filtering when detecting reentrant electrical activity.

- *To assess the spatial resolution of BSPM systems, both regarding the number of electrodes and their distribution, so that the non-invasive identification and location of AF drivers be clinically useful in simplified BSPM systems*. Results from Chapter 5 have shown that 12 uniformly distributed leads are enough for identification of left or right dominant atrium by DF analysis, whereas at least 32 uniformly distributed leads are necessary whether the dominance of right or left atrium by atrial rotor identification wants to be carried out.

- *To evaluate the effect of the signal processing involved in the noninvasive detection of atrial drivers both by BSPM and ECGI, namely the phase transform and the narrow-band filtering, and how this processing affects the atrial driver detection*. Analysis of BSPM recordings during AF revealed that by applying HDF filtering to the surface potential signal and obtaining its phase transform, atrial rotors in form of surface reentries could be located, since this signal processing enhances the reentrant pattern by removing other spectral contributions (Chapter 4). Moreover, results from Chapter 6 have shown that narrow band-pass filtering allows increasing the rotor detection ratio in EGM recording by avoiding the multiple deflections of the EGM signal and fitting the phase signal to the tissue activation sequence. Furthermore, it has been shown that narrow band-pass filtering should be avoided in ECGI recordings, since it may produce an unaffordable amount of false rotor detections, due to the over-smothing of the regularization process added to the aggressive temporal filtering.

- *To assess the reliability of ECGI systems in non-invasively detecting AF drivers against uncertainties in the system conditions, such as electrical noise or spatial errors*. In Chapter 7 the stability of DF and rotor markers were evaluated for ECGI systems under the effect of uncertainties such as electrical noise in the ECG, spatial inaccuracies in form of displacements or rotations of the atrial surface and incoherences in the electrical conductance values. As opposed to the icEGM signal whose morphology rapidly worsened with the uncertainties, DF and rotor markers were robust

against these inconsistencies, demonstrating the suitability of both mapping techniques to locate atrial drivers.

- *To propose new methods to reduce the spatial uncertainties in ECGI systems and increase their diagnostic power*. This thesis has proposed in Chapter 8 a new method for solving unaccuracies in the atrial location and orientation based on the L-curve curvature. This novel methodology allows reducing the spatial uncertainties involved in the inverse solution even in presence of superimposed unaccuracies in several axes of rotation and displacement.

Everything above discussed has facilitated a better understanding of the physical and technical mechanisms involved in the non-invasive mapping of atrial fibrillation. The better understading of these mechanisms encourage to design more efficient non-invasive systems for atrial driver location, in which their diagnostic capacity can be increased at the same time that are optimized for their broader use in clinical practice. BSPM and ECGI systems can be of great clinical utility for selecting and planning ablation procedures, which can result in a benefit for both patients and health systems. Thus, non-invasive systems are a great bet for the future in the treatment of AF whose use should be extended in the coming years.

9.5. Guidelines for future works

The methodologies presented in this thesis have allowed studying the validity of the non-invasive systems for fibrillatory source localization in AF. However, in some cases these results were obtained from databases with a reduced number of patients or formed by mathematical simulations, so they should be studied in depth and on a broad data from AF patients. Currently, our research group is collaborating with the Hospital General Universitario Gregorio Marañón, in order to perform simultaneous surface and intracavitary records to validate the results obtained in this thesis. This database should be useful for the invasive identification of atrial rotors through multipolar catheters ***[Narayan 2013]***, and to assess the surface representation of these atrial rotors. Results from that database analysis could further validate the results from Chapter 4, at the same time that could increase the detection specificity of surface rotors, allowing not only to distinguish between right or left rotors but even their specific location within atrial regions. In addition, this database will be used to validate the inverse problem resolution, since rotor location and DF maps provided by ECGI will be compared with invasively obtained maps in order to validate the ECGI ability to locate atrial drivers described in Chapters 6 and 7.

In order to popularize non-invasive methods in cardiological practice, it is also necessary to validate the proposed methodology under affectation of

ventricular electrical activity. To this end, either ventricular activity suppression by software ***[Castells 2005]*** or the use of temporal segments between QRST intervals without ventricular activity ***[Haissaguerre 2013]*** could be used. The validity of the presented methodologies in the presence of ventricular activity would allow these methods to be used in any clinical circumstances and therefore encourage their implementation in medical practice.

Results shown in Chapter 8 may be the beggining for a new type of ECGI systems not based on medical imaging techniques like MRI or CAT. These medical image techniques are one of the major impediments to the use of ECGI in clinical practice duo to their restrictive acces in most health systems. Therefore, a system able to non-invasively provide the cardiac electric activity without the dependence from these medical imaging techniques would suppose a great advance in cardiac diagnosis. Since it has been observed that the spatial inhomogeneities of the torso do not play a crucial role in solving the inverse problem ***[Messigner 1986, Ramanathan 2001, Cheng 2003]***, ECGI systems could be viable with only the reconstruction of the torso and atrial geometry. On the one hand, torso geometry can be reconstructed by using softare techniques based on photographic image analysis ***[Remondino 2004]***. On the other hand, atrial geometry can be reconstructed by more accessible medical image techniques, such as echocardiography or X-rays. Finally, the placement of the atrium within the torso can be carried out using the methodology explained in Chapter 8. This approach could offer the benefits of the ECGI systems without the impediments that nowadays represent the medical imaging techniques as MRI or CAT, so its implementation will be explored in next studies.

Chapter 10

Contributions

10.1. Main contributions of this thesis

10.1.1. Journal papers

- **Rodrigo M,** Guillem MS, Climent AM, Pedrón-Torrecilla J, Liberos A, Millet J, Fernández-Avilés F, Atienza F, Berenfeld O. Body surface localization of left and right atrial high-frequency rotors in atrial fibrillation patients: A clinical-computational study. Heart Rhythm 2014; 11:1584-1591.
- **Rodrigo M**, Climent AM, Liberos A, Fernández-Aviles F, Guillem MS, Atienza F, Berenfeld O. Minimal configuration of body surface potential mapping for discrimination of left and right atrial drivers during atrial fibrillation. (Submitted)
- **Rodrigo M**, Climent AM, Liberos A, Fernández-Aviles F, Berenfeld O, Atienza F, Guillem MS. Understanding phase mapping and temporal filtering for reentrant activity identification in atrial arrhythmias: electrograms, electrocardiograms and inverse-computed electrograms. (In preparation)
- **Rodrigo M,** Climent AM, Liberos A, Fernández-Aviles F, Berenfeld O, Atienza F, Guillem MS. Highest dominant frequency and rotor positions are stable markers for atrial driver location in non-invasive mapping of atrial fibrillation: a computational study. (Submitted)
- **Rodrigo M,** Climent AM, Liberos A, Fernández-Aviles F, Berenfeld O, Atienza F, Guillem MS. Solving inaccuracies in anatomical models for electrocardiographic inverse problem resolution by using electrical information. (In preparation)

10.1.2. International conferences

- Atienza F, **Rodrigo M**, Climent AM, Liberos A, Fernández-Avilés F, Berenfeld O, Guillem MS. Highest dominant frequency and rotor positions are stable markers for atrial driver location in non-invasive mapping of atrial fibrillation: a computational study. Heart Rhythm 2016, San Francisco, USA.
- Atienza F, **Rodrigo M**, Climent AM, Fernández-Avilés F, Guillem MS and Berenfeld O. Reduced body surface potential mapping system allows discrimination of left and right atrial drivers during atrial fibrillation. Heart Rhythm 2015, Boston, EEUU.
- Guillem MS, Climent AM, **Rodrigo M**, Liberos A, Fernández-Avilés F, Atienza F, Berenfeld O. Non-invasive identification of atrial activation patterns during atrial fibrillation. Atrial signals 2015, Karlsruhe, Germany.
- **Rodrigo M**, Guillem MS, Climent AM, Liberos A, Pedrón–Torrecilla J, Fernández-Avilés F, Atienza F and Berenfeld O. Body surface detection of reentrant activity during atrial fibrillation. Cardiostim 2014, Niza, France.
- **Rodrigo M**, Climent AM, Liberos A, Pedrón–Torrecilla J, Millet J, Fernández-Avilés F, Atienza F, Berenfeld O and Guillem MS. Non-invasive detection of reentrant drivers during atrial fibrillation: a clinical-computational study. Computing in Cardiology 2014, Cambridge, USA.
- **Rodrigo M**, Climent AM, Liberos A, Pedrón–Torrecilla J, Millet J, Fernández-Avilés F, Atienza F, Berenfeld O and Guillem MS. Noninvasive location of re-entrant propagation patterns during atrial fibrillation. ITACA-WIICT 2014, Valencia, Spain.
- **Rodrigo M**, Climent AM, Liberos A, Pedrón–Torrecilla J, Millet J, Fernández-Avilés F, Atienza F, Berenfeld O, Guillem MS. Non-invasive location of re-entrant propagation patterns during atrial fibrillation. Computing in Cardiology 2013, Zaragoza, Spain.
- Berenfeld O**, Rodrigo M**, Climent AM, Liberos A, Pedrón–Torrecilla J, Millet J, Arenal A, Fernández-Avilés F, Atienza F and Guillem MS. Noninvasive identification of reentrant drivers of atrial fibrillation using multi-channel surface recordings. Heart Rhythm 2013, Denver, USA.

10.1.3. National conferences

- **Rodrigo M**, Guillem MS, Climent AM, Berenfeld O, Atienza F, Fernández-Avilés F. Caracterización no invasiva de la fibrilación auricular mediante cartografía eléctrica de superficie de baja resolución. SEC 2015, Bilbao, Spain.
- **Rodrigo M**, Guillem MS, Climent AM, Liberos A, Fernández-Avilés F, Atienza F, Berenfeld O. Localización de fuentes fibrilatorias mediante

sistemas reducidos de cartografía eléctrica de superficie durante fibrilación auricular. CASEIB 2015, Madrid, Spain.

- **Rodrigo M**, Guillem MS, Climent AM, Liberos A, Pedrón–Torrecilla J, Millet J, Berenfeld O, Atienza F. Identificación no invasiva de patrones fibrilatorios mediante registro electrocardiográfico de superficie. SEC 2013, Valencia, Spain.

10.2. Contributions related to this thesis

10.2.1. Journal papers

- **Rodrigo M**, Climent AM, Liberos A, Calvo D, Fernández-Avilés F, Berenfeld O, Atienza F, Guillem MS. Identification of dominant excitation patterns and sources of atrial fibrillation by causality analysis. Annals of Biomedical Enginnering 2016. DOI: 10.1007/s10439-015-1534-x.
- Pedrón–Torrecilla J, **Rodrigo M**, Climent AM, Liberos A, Pérez-David E, Bermejo J, Arenal A, Millet J, Fernández-Avilés F, Berenfeld O, Atienza F, Guillem MS. Noninvasive estimation of epicardial dominant high-frequency regions during atrial fibrillation. Journal of Cardiovascular Electrophysiology 2016;4:435-442.
- Guillem MS, Climent AM, **Rodrigo M,** Fernández-Avilés F, Atienza F, Berenfeld O. Presence and stability of rotors in atrial fibrillation: evidence and therapeutic implications. Cardiovascular Research 2016;109:480-492.
- Liberos A, Bueno–Orovio A, **Rodrigo M**, Ravens U, Guillem MS, Rodriguez B, Climent AM. Balance between sodium and calcium currents underlying chronic atrial fibrillation termination: an in silico inter–subject variability study. Heart Rhythm 2016. DOI: 10.1016/j.hrthm.2016.08.028
- Liberos A, Climent AM, **Rodrigo M**, Pedrón–Torrecilla J, Millet J, Atienza F, Berenfeld O, Quesada A, Guillem MS. Non–invasive characterization of atrial macroreentries during typical and atypical atrial flutter. (In preparation)

10.2.2. Book chapter

- **Rodrigo M**, Pedrón–Torrecilla J, Hernández I, Liberos **A**, Climent AM, Guillem MS. Data analysis in cardiac arrhythmias. Eds: Fernández–Llatas C, García–Gómez JM. Data mining in clinical medicine. Methods in Molecular Biology 2014. 1246:217–236.

10.2.3. International conferences

- **Rodrigo M**, Climent AM, Liberos A, Fernández-Avilés F, Berenfeld O, Atienza F and Guillem MS. Atrial sources identification by causality analysis during atrial fibrillation. EMBC 2015, Milan, Italy.
- **Rodrigo M**, Climent AM, Liberos A, Calvo D, Fernández-Avilés F, Berenfeld O, Atienza F, Guillem MS. Identification of dominant excitation patterns and sources of atrial fibrillation by causality analysis. Atrial signals 2015, Karlsruhe, Germany.
- **Rodrigo M**, Climent AM, Liberos A, Fernández-Avilés F, Berenfeld O, Atienza F and Guillem MS. Identification of atrial sources by causality analysis during atrial fibrillation: a computational study. ITACA-WIICT 2015, Valencia, Spain.
- **Rodrigo M**, Climent AM, Liberos A, Fernández-Avilés F, Atienza F, Berenfeld O and Guillem MS. Causality method detects source of activity during atrial fibrillation. Cardiostim 2014, Niza, France.
- Atienza F, **Rodrigo M**, Climent AM, Liberos A, Fernández-Avilés F, Berenfeld O and Guillem MS. Electroanatomical identification of dominant propagation patterns during atrial fibrillation by causality analysis. Heart Rhythm 2014, San Francisco, USA.
- Pedrón–Torrecilla J, Liberos A, **Rodrigo M**, Millet J, Atienza F, Berenfeld O, Climent AM and Guillem MS. Non-invasive imaging of the atrial arrhythmia sources: patient study during atrial tachyarrhythmia and atrial fibrillation. ITACA-WIICT 2014, Valencia, Spain.
- Pedrón–Torrecilla J, Climent AM, Liberos A, **Rodrigo M**, Pérez-David E, Millet J, Fernández-Avilés F, Berenfeld O, Atienza F and Guillem MS. Accuracy of inverse solution computation of dominant frequencies and phases during atrial fibrillation. Computing in Cardiology 2014, Cambridge, USA.
- Liberos A, Climent AM, **Rodrigo M**, Pedrón–Torrecilla J, Millet J, Quesada-Dorador A and Guillem MS. Non-invasive phase analysis in atrial flutter electrographic maps. Cardiostim 2014, Niza, France.
- **Rodrigo M**, Liberos A, Climent AM, Guillem MS. Identification of ablation sites in atrial flutter by causal method. Computing in cardiology 2013, Zaragoza, Spain.
- Liberos A, Pedrón–Torrecilla J, **Rodrigo M**, Millet J, Climent AM, Guillem MS. Body surface potential propagation maps during macroreentrant atrial arrhythmias. A simulation study. Computing in cardiology 2013, Zaragoza, Spain.

- **Rodrigo M**, Liberos A, Guillem MS, Millet J, Climent AM. Identification of fibrillatory sources by measuring causal relationships. Computing in cardiology 2012, Krakow, Poland.
- **Rodrigo M**, Guillem MS, Liberos A, Millet J, Berenfeld O, Climent AM. Causality relation map: a novel methodology for the identification of hierarchical fibrillatory processes. Computing in cardiology 2011, Hangzhou, China.

10.2.4. National conferences

- Liberos **A**, Climent AM, **Rodrigo M**, Pedrón–Torrecilla J, Berenfeld O, Atienza F, Guillem MS, Fernandez–Avilés F. Análisis de fase en la cartografía eléctrica de superficie en episodios de flutter auricular. Estudio de simulación. SEC 2015, Bilbao, Spain.
- Albert-Martínez R, Climent AM, **Rodrigo M**, Guillem MS. Desarrollo y validación de un sistema de caracterización electrofisiológica cardiaca mediante mapeo óptico en un modelo de corazón aislado porcino. CASEIB 2015, Madrid, Spain.
- Atienza F, Climent AM, Sanz-Ruiz R, Vicent-Alaminos ML, Hernández-Romero I, **Rodrigo M**, Guillem MS, Fernández-Avilés F. Abordaje electroanatómico combinado en pacientes con estenosis mitral grave candidatos a valvuloplastia mitral. Eficacia y seguridad a corto plazo. SEC 2015, Bilbao, Spain.
- Pedrón–Torrecilla J, Guillem MS, Climent AM, Liberos A, **Rodrigo M**, Berenfeld O, Atienza F and Fernández-Avilés F. Reconstrucción no invasiva de los mapas electroanatómicos de frecuencia dominante durante fibrilación auricular. SEC 2014, San Sebastián, Spain.
- Pedrón–Torrecilla J, Guillem MS, Climent AM, Liberos A, **Rodrigo M**, Berenfeld O, Atienza F, Fernández-Avilés F. Reconstrucción no invasiva de los mapas electroanatómicos de frecuencia dominante durante fibrilación auricular. SEC 2014, San Sebastián, Spain.
- **Rodrigo M**, Climent AM, Liberos A, Pedrón–Torrecilla J, Fernández-Avilés F, Berenfeld O, Atienza F, Guillem MS. El análisis causal de la actividad eléctrica durante fibrilación auricular permite identificar los patrones de propagación dominantes. SEC 2013, Valencia, Spain.
- **Rodrigo M**, Guillem MS, Liberos A, Millet J, Berenfeld O, Atienza F, Climent AM. Identificación de fuentes fibrilatorias mediante la medida de relaciones causales. CASEIB 2012, San Sebastián, Spain.
- **Rodrigo M**, Liberos A, Guillem MS, Millet J, Climent AM. Mapa de relación causal: una nueva metodología para la identificación de patrones fibrilatorios jerárquicos. CASEIB 2011, Caceres, Spain.

10.2.5. Patents

- **Rodrigo M**, Climent AM, Guillem MS, Atienza F, Berenfeld O. *Catéter y método para la detección de actividad eléctrica en un órgano*. 2 529 702 B1.
  In proof of concept phase and pending for preclinical studies supported by Microport EP MedTech Co.

10.2.6. Awards

- Finalist in the Young Investigator Awards of the Computing in Cardiology conference in 2014: "Non-invasive detection of reentrant drivers during atrial fibrillation: a clinical-computational study", Boston MA, USA.
- Second award in Healthstart 2015, by the foundation for the knowledge *MadrI+D* to the project "ARRITMIAS (CORIFY)"
- First award to the paper with with highest impact factor in 2015 by the ITACA Institute: "Rodrigo M, Guillem MS, Climent AM, Pedrón-Torrecilla J, Liberos A, Millet J, Fernández-Avilés F, Atienza F, Berenfeld O. Body surface localization of left and right atrial high-frequency rotors in atrial fibrillation patients: A clinical-computational study. Heart Rhythm 2014; 11:1584-1591"
- Finalist in the Young Investigator Awards of the Computing in Cardiology conference in 2016: "Highest dominant frequency and rotor sites are robust markers for atrial driver location in non-invasive mapping of atrial fibrillation", Vancouver, CAN.

10.3. Research stay

During the development of this thesis the author has completed a research stay at University of Michigan, Ann Arbor, MI, USA, in the "Center for Arrhythmia Research" under the guidance of Dr. Omer Berenfeld.

Dates: From 1st September until 30th December 2014.

During this stay a joint work presented in Chapter 5 was developed.

10.4. Research projects

This work has been developed within the framework of several research projects. The interest and relevance of the research activity carried out by our group has been acknowledged by public administrations by means of the following research projects in which the author has participated:

- Instituto de salud Carlos III

Estudio preclínico de la implantación de parches de tejido cardiaco bioartificial electromecánicamente entrenados en un modelo de infarto de miocardio porcino. Desarrollo de biorreactores con estimulación electromecánica.

From Jan 1st, 2014 until Jan 1st, 2017.

Main researcher: Guillem Sánchez, María de la Salud

- Ministerio de economía y competitividad

Desarrollo de computadores biológicos basados en comunicación iónica entre células cardiacas excitables y no excitables.

From Sep 1st, 2014 until Aug 1st, 2015.

Main researcher: Fernandez Avilés, Francisco

- Generalitat Valenciana

PROMAPCOR: Desarrollo de técnicas avanzadas de análisis y caracterización de mapas de propagación para la ayuda al diagnóstico electrocardiográfico. (ACOMP/2010/176).

From Apr 15th, 2010 until Oct 14th, 2010.

Main researcher: Millet Roig, José

- Sociedad Española de Cardiología

Caracterización no invasiva de los mecanismos jerárquicos de mantenimiento de la fibrilación auricular (SEC 2015).

From Jan 1th, 2015 until Jan 1th, 2017.

Main researcher: Atienza, Felipe

- Instituto ITACA, UPV

Solución computacional del modelo multinivel in vivo de la dinámica de la angiogénesis para la detección temprana de respuesta a tratamiento en glioblastomas primarios. EMBLEMA CURIAMG-FDFT

From Jun 1th, 2015 until Jun 1th, 2017.

Main researcher: García Gómez, Juan M.

- Instituto ITACA, UPV

Plataforma Open Source de interconexión de dispositivos de datos biomédicos y servicios para recogida, procesado y automatización de los cuidados transparente y no intrusiva. EMBLEMA: SABIEN

From Jun 1th, 2015 until Jun 1th, 2017.

Main researcher: Fernández Latas, Carlos

10.5. Author contribution

The hyphothesis consideration of this thesis and their development were carried out by the author under the guidance of Dr. Maria S. Guillem and Dr. Andreu Climent and in collaboration with Dr. Felipe Atienza and Dr. Omer Berenfeld. The author implemented all simulations from the mathematical models dataset, and accomplished the data analysis from both models and patient datasets. During the research stay in the "Center for Arrhythmia Research", the author developed the content of Chapter 5 under the guidance of Dr. Omer Berenfeld. Main publications of this thesis were written by the author and revised by Dr. María S. Guillem, Dr. Andreu M. Climent, Dr. Felipe Atienza and Dr. Omer Berenfeld.

Dr. Alejandro Liberos implemented the mathematical environment for the atrial simulations and Dr. Jorge Pedrón-Torrecilla wrote the mathematical formulation for the forward and inverse problem for both realistic and spherical geometries. Dr. Felipe Atienza, Dr. Francisco Fernández-Avilés, Dr. Andreu M. Climent and Mr. Ismael Hernández-Romero carried out the patient recordings used in this thesis.

References

[Abboud 1994] Abboud S, Eshel Y, Levy S, Rosenfeld M. Numerical calculation of the potential distribution due to dipole sources in a spherical model of the head. Comput Biomed Res 1994. 27:441-455.

[Ackerman 1991] Ackerman MJ. The Visible Human Project. The Journal of Biocommunication 1991; 18:14

[Akar 2000] Akar FG, Laurita KR, Rosenbaum DS. Cellular basis for dispersion of repolarization underlying reentrant arrhythmias. J Electrocardiol 2000; 33:23-31.

[Alcaraz 2011] Alcaraz R, Hornero F, Rieta JJ. Surface ECG organization time course analysis along onward episodes of paroxysmal atrial fibrillation. Med Eng Phys 2011; 33:597-603.

[Allessie 1995] Allessie MA, Konings JK, Wijffels M. Electrophysiological mechanisms of atrial fibrillation. Atrial arrhythmias: State of the art. JP DiMarco and EN Prytowsky Futura Publishing Co 1995; 155-161.

[Allessie 1996] Allessie MA, Konings K, Kirchhof CJ, Wijffels M. Electrophysiologic mechanisms of perpetuation of atrial fibrillation. Am J Cardiol 1996; 77:10A-23A.

[Allessie 2002] Allessie M, Ausma J, Schotten U. Electrical, contractile and structural remodeling during atrial fibrillation. Cardiovasc Res 2002; 54:230-246.

[Allessie 2010] Allessie M, de Groot MS, Houben RPM, Schotten U, Boersma E, Smeets JL, Crijns HJ. Electropathological substrate of long-standing persistent atrial fibrillation in patients with structural heart disease: longitudinal dissociation. Circ Arrhythmia and Electrophysiol 2010; 3:606-615

[Allessie 2014] Allessie M, de Groot N. CrossTalk opposing view: Rotors have not been demonstrated to be the drivers of atrial fibrillation. J Physiol 2014; 592:3167-170.

[Ashihara 2012] Ashihara T, Haraguchi R, Nakazawa K, Namba T, Ikeda T, Nakazawa Y, Ozawa T, Ito M, Horie M, Trayanova NA. The role of fibroblasts in

complex fractionated electrograms during persistent/permanent atrial fibrillation: implications for electrogram-based catheter ablation. Circ Res 2012; 110:275-284.

[Aslanidi 2011] Aslanidi OV, Colman MA, Stott J, Dobrzynski H, Boyett MR, Holden AV, Zhang H. 3D virtual human atria: A computational platform for studying clinical atrial fibrillation. Prog Biophys Mol Biol 2011; 107:156-216.

[Atienza 2006] Atienza F, Almendral J, Moreno J, Vaidyanathan R, Talkachou A, Kalifa J, Arenal A, Villacastín JP, Torrecilla EG, Sánchez A, Ploutz-Snyder R, Jalife J, Berenfeld O. Activation of inward rectifier potassium channels accelerates atrial fibrillation in humans-Evidence for a reentrant mechanism. Circulation 2006; 114:2434-2442.

[Atienza 2009] Atienza F, Almendral J, Jalife J, Zlochiver S, Ploutz-Snyder R, Torrecilla EG, Arenal A, Kalifa J, Fernández-Avilés F, Berenfeld O. Real-time dominant frequency mapping and ablation of dominant frequency sites in atrial fibrillation with left-to-right frequency gradients predicts long-term maintenance of sinus rhythm. Heart Rhythm 2009; 6:33-40.

[Atienza 2011] Atienza F, Calvo D, Almendral J, Zlochiver S, Grzeda KR, Martínez-Alzamora N, González-Torrecilla E, Arenal A, Fernández-Avilés F, Berenfeld O. Mechanisms of fractionated electrograms formation in the posterior left atrium during paroxysmal atrial fibrillation in humans. J Am Coll Cardiol 2011; 57:1081-1092.

[Atienza 2014] Atienza F, Almendral J, Ormaetxe JM, Moya A, Martínez-Alday JD, Hernández-Madrid A, Castellanos E, Arribas F, Arias MÁ, Tercedor L, Peinado R, Arcocha MF, Ortiz M, Martínez-Alzamora N, Arenal A, Fernández-Avilés F, Jalife J; RADAR-AF Investigators. Comparison of radiofrequency catheter ablation of drivers and circumferential pulmonary vein isolation in atrial fibrillation: a noninferiority randomized multicenter RADAR-AF trial. J Am Coll Cardiol 2014; 64:2455-2467.

[Bear 2015] Bear LR, Cheng LK, LeGrice IJ, Sands GB, Lever NA, Paterson DJ, Smaill BH. Forward problem of electrocardiography: is it solved? Circ Arrhythm Electrophysiol 2015; 8:677-684.

[Beeler 1977] Beeler GW and Reuter H. Reconstruction of action potential of ventricular myocardial fibers. Journal of Physiology-London 1977; 268:177-210.

[Benharash 2015] Benharash P, Buch E, Frank P, Share M, Tung R, Shivkumar K, Mandapati R. Quantitative analysis of localized sources identified by focal impulse and rotor modulation mapping in atrial fibrillation. Circ Arrhythm Electrophysiol 2015; 8:554-561.

[Berenfeld 2000] Berenfeld O, Mandapati R, Dixit S, Skanes AC, Chen J, Mansour M, Jalife J. Spatially distributed dominant excitation frequencies reveal hidden organization in atrial fibrillation in the Langendorff-perfused sheep heart. J Cardiovasc Electrophysiol 2000; 11:869-879.

[Berenfeld 2001] Berenfeld O, Wellner M, Jalife J, Pertsov AM. Shaping of a scroll wave filament by cardiac fibers. Phys Rev E Stat Nonlin Soft Matter Phys 2001; 63:061901.

[Berenfeld 2011] Berenfeld O, Ennis S, Hwang E, Hooven B, Grzeda K, Mironov S, Yamazaki M, Kalifa J, Jalife J. Time- and frequency-domain analyses of atrial fibrillation activation rate: the optical mapping reference. Heart Rhythm 2011; 8:1758-1765.

[Berenfeld 2012] Berenfeld O, Oral H. The quest for rotors in atrial fibrillation: different nets catch different fishes. Heart Rhythm 2012; 9:1440-1441

[Berenfeld 2014] Mechanisms of atrial fibrillation: rotors, ionic determinants, and excitation frequency. Cardiol Clin 2014; 32:495-506.

[Berger 2011] Berger T, Pfeifer B, Hanser FF, Hintringer F, Fischer G, Netzer M, Trieb T, Stuehlinger M, Dichtl W, Baumgartner C, Pachinger O, Seger M. Single-beat noninvasive imaging of ventricular endocardial and epicardial activation in patients undergoing CRT. PLoS ONE 2011; 6:e16255.

[Blanc 2001] Blanc O, Virag N, Vesin JM and Kappenberger L. A computer model of human atria with reasonable computation load and realistic anatomical properties. IEEE Trans Biomed Eng 2001; 48:1229-1237.

[Bollmann 2008] Bollmann A, Tveit A, Husser D, Stridh M, Sörnmo L, Smith P, Olsson SB. Fibrillatory rate response to candesartan in persistent atrial fibrillation. Europace 2008; 10:1138–1144.

[Brundel 2001] Brundel BJ, Van Gelder IC, Henning RH, Tuinenburg AE, Wietses M, Grandjean JG, Wilde AA, Van Gilst WH, Crijns HJ. Alterations in potassium channel gene expression in atria of patients with persistent and paroxysmal atrial fibrillation: Differential regulation of protein and mRNA levels for K+ channels. J Am Coll Cardiol 2001; 37:926-932.

[Bruns 2002] Bruns HJ, Eckardt L, Vahlhaus C, Schulze-Bahr E, Haverkamp W, Borggrefe M, Breithardt G, Wichter T. Body surface potential mapping in patients with brugada syndrome: Right precordial ST segment variations and reverse changes in left precordial leads. Cardiovasc Res 2002; 54:58-66.

[Burdumy 2012] Burdumy M, Luik A, Neher P, Hanna R, Krueger MW, Schilling C, Barschdorf H, Lorenz C, Seemann G, Schmitt C, Doessel O, Weber FM. Comparing measured and simulated wave directions in the left atrium - a workflow

for model personalization and validation. Biomedical Engineering-Biomedizinische Technik 2012; 57:79-87.

[Calkins 2007] Calkins H, Brugada J, Packer DL, Cappato R, Chen SA, Crijns HJ, Damiano RJ Jr, Davies DW, Haines DE, Haissaguerre M, Iesaka Y, Jackman W, Jais P, Kottkamp H, Kuck KH, Lindsay BD, Marchlinski FE, McCarthy PM, Mont JL, Morady F, Nademanee K, Natale A, Pappone C, Prystowsky E, Raviele A, Ruskin JN, Shemin RJ; Heart Rhythm Society; European Heart Rhythm Association; European Cardiac Arrhythmia Society; American College of Cardiology; American Heart Association; Society of Thoracic Surgeons. HRS/EHRA/ECAS expert consensus statement on catheter and surgical ablation of atrial fibrillation: recommendations for personnel, policy, procedures and follow-up. A report of the Heart Rhythm Society (HRS) Task Force on Catheter and Surgical Ablation of Atrial Fibrillation developed in partnership with the European Heart Rhythm Association (EHRA) and the European Cardiac Arrhythmia Society (ECAS); in collaboration with the American College of Cardiology (ACC), American Heart Association (AHA), and the Society of Thoracic Surgeons (STS). Endorsed and approved by the governing bodies of the American College of Cardiology, the American Heart Association, the European Cardiac Arrhythmia Society, the European Heart Rhythm Association, the Society of Thoracic Surgeons, and the Heart Rhythm Society. Europace 2007; 9:335-379.

[Calvo 2014] Calvo CJ, Deo M, Zlochiver S, Millet J, Berenfeld O. Attraction of rotors to the pulmonary veins in paroxysmal atrial fibrillation: A modeling study. Biophys J 2014; 106:1811-1821.

[Campbell 2012] Campbell KF, Calvo CJ, Mironov S, Herron T, Berenfeld O, Jalife J. Spatial gradients in action potential duration created by regional magnetofection of hERG are a substrate for wavebreak and turbulent propagation in cardiomyocyte monolayers. J Physiol 2012; 590:6363–6379.

[Carley 2003] Carley SD. Beyond the 12 lead: Review of the use of additional leads for the early electrocardiographic diagnosis of acute myocardial infarction. Emergency medicine 2003; 15:143-154.

[Castells 2005] Castells F, Mora C, Rieta JJ, Moratal-Pérez D, Millet J. Estimation of atrial fibrillatory wave from single-lead atrial fibrillation electrocardiograms using principal component analysis concepts. Med Biol Eng Comput 2005; 43:557–560.

[Chao 2012] Chao TF, Tsao HM, Lin YJ, Tsai CF, Lin WS, Chang SL, Lo LW, Hu YF, Tuan TC, Suenari K, Li CH, Hartono B, Chang HY, Ambrose K, Wu TJ, Chen SA. Clinical outcome of catheter ablation in patients with nonparoxysmal atrial fibrillation: results of 3-year follow-up. Circ Arrhythm Electrophysiol 2012; 5:514-520.

[Chen 1999] Chen SA, Hsieh MH, Tai CT, Tsai CF, Prakash VS, Yu WC, Hsu TL, Ding YA, Chang MS. Initiation of atrial fibrillation by ectopic beats originating from the pulmonary veins: electrophysiological characteristics, pharmacological responses, and effects of radiofrequency ablation. Circulation 1999; 100:1879-1886.

[Cheng 2003] Cheng LK, Bodley JM, Pullan AJ. Effects of experimental and modeling errors on electrocardiographic inverse formulations. IEEE Trans Biomed Eng 2003; 50:23-32.

[Cheng 2013] Cheng Z, Deng H, Cheng K, Chen T, Gao P, Yu M, Fang Q. The amplitude of fibrillatory waves on leads aVF and V1 predicting the recurrence of persistent atrial fibrillation patients who underwent catheter ablation. Ann Noninvasive Electrocardiol 2013; 18:352–358.

[Clayton 2006] Clayton RH, Zhuchkova EA, Panfilov AV. Phase singularities and filaments: simplifying complexity in computational models of ventricular fibrillation. Prog Biophys Mol Biol 2006; 90:378-398.

[Clayton 2008] Clayton RH and Panfilov AV. A guide to modelling cardiac electrical activity in anatomically detailed ventricles. Prog Biophys Mol Biol 2008; 96:19-43.

[Colli-Franzone 1985] Colli Franzone P, Gnerri L, Tentonia S, Viganotti C, Baruffi S. A mathematical procedure for solving the inverse potential problem of electrocardiography. Analysis of the timespace accuracy from in vitro experimental data. Math Biosci 1985; 77:353-396.

[Colman 2013] Colman MA, Aslanidi OV, Kharche S, Boyett MR, Garratt C, Hancox JC, Zhang H. Pro-arrhythmogenic effects of atrial fibrillation-induced electrical remodelling: insights from the three-dimensional virtual human atria. J Physiol 2013; 591:4249-4272.

[Corradi 2012] Corradi D, Callegari S, Maestri R, Ferrara D, Mangieri D, Alinovi R, Mozzoni P, Pinelli S, Goldoni M, Privitera YA, Bartoli V, Astorri E, Macchi E, Vaglio A, Benussi S, Alfieri O. Differential structural remodeling of the left-atrial posterior wall in patients affected by mitral regurgitation with or without persistent atrial fibrillation: A morphological and molecular study. J Cardiovasc Electrophysiol 2012; 23:271-279.

[Courtemanche 1998] Courtemanche M, Ramirez RJ, Nattel S. Ionic mechanisms underlying human atrial action potential properties: insights from a mathematical model. Am J Physiol 1998; 275:301-321.

[Cuppen 1984] Cuppen JJM, van Oosterom A. Model studies with the inversely calculated isochrones of ventricular depolarization. IEEE Trans Biomed Eng 1984; 31:652-659.

[Cuculich 2010] Cuculich PS, Wang Y, Lindsay BD, Faddis MN, Schuessler RB, Damiano RJ Jr, Li L, Rudy Y. Noninvasive characterization of epicardial activation in humans with diverse atrial fibrillation patterns. Circulation 2010; 122:1364–1372.

[Cuculich 2011] Cuculich PS, Zhang J, Wang Y, Desouza KA, Vijayakumar R, Woodard PK, Rudy Y. The electrophysiological cardiac ventricular substrate in patients after myocardial infarction: noninvasive characterization with electrocardiographic imaging. J Am Coll Cardiol 2011; 58:1893-1902.

[Dang 2005] Dang L, Virag N, Ihara Z, Jacquemet V, Vesin JM, Schlaepfer J, Ruchat P, Kappenberger L. Evaluation of ablation patterns using a biophysical model of atrial fibrillation. Ann Biomed Eng 2005; 33:465-474.

[de Groot 2010] de Groot NM, Houben RP, Smeets JL, Boersma E, Schotten U, Schalij MJ, Crijns H, Allessie MA. Electropathological substrate of longstanding persistent atrial fibrillation in patients with structural heart disease: epicardial breakthrough. Circulation 2010; 122:1674-1682.

[De Simone 1999] De Simone A, Stabile G, Vitale DF, Turco P, Di Stasio M, Petrazzuoli F, Gasparini M, De Matteis C, Rotunno R, Di Napoli T. Pretreatment with verapamil in patients with persistent or chronic atrial fibrillation who underwent electrical cardioversion. J Am Coll Cardiol 1999; 34:810-814.

[Dewire 2010] Dewire J, Calkins H. State-of-the-art and emerging technologies for atrial fibrillation ablation. Nat Rev Cardiol 2010; 7:129-138.

[Dibs 2008] Dibs SR, Ng J, Arora R, Passman RS, Kadish AH, Goldberger JJ. Spatiotemporal characterization of atrial activation in persistent human atrial fibrillation: multisite electrogram analysis and surface electrocardiographic correlations–a pilot study. Heart Rhythm 2008; 5:686-693.

[Difrancesco 1985] Difrancesco D and Noble D. A model of cardiac electrical-activity incorporating ionic pumps and concentration changes. Philos Trans R Soc Lond B Biol Sci 1985; 307:353-398.

[Dimaano 2010] Dimaano VLJ, Abraham TP. The role of echocardiography and tissue doppler imaging in optimal cardiac resynchronization therapy. Circulation 2010; 59–75.

[Dössel 2012] Dössel O, Krueger MW, Weber FM, Wilhelms M, Seemann G. Computational modeling of the human atrial anatomy and electrophysiology. Med Biol Eng Comput 2012; 50:773-799.

[Dubuc 1993] Dubuc M, Nadeau R, Tremblay G, Kus T, Molin F, Savard P. Pace mapping using body-surface potential maps to guide catheter ablation of accessory pathways in patients with wolff-parkinson-white syndrome. Circulation 1993; 87:135-143.

[Eckardt 2002] Eckardt L, Bruns HJ, Paul M, Kirchhof P, Schulze-Bahr E, Wichter T, Breithardt G, Borggrefe M, Haverkamp W. Body surface area of ST elevation and the presence of late potentials correlate to the inducibility of ventricular tachyarrhythmias in brugada syndrome. J Cardiovasc Electrophysiol 2002; 13:742-749.

[Eckstein 2013] Eckstein J, Zeemering S, Linz D, Maesen D, Verheule S, van Hunnik A, Crijns H, Allessie MA, Schotten U. Transmural conduction is the predominant mechanism of breakthrough during atrial fibrillation: evidence from simultaneous endo-epicardial high density activation mapping. Circ Arrhythmia Electrophysiol 2013; 6:1–42.

[Eggert 1997] Eggert DW, Lorusso A, Fish RB. Estimating 3-D rigid body transformations: a comparison of four major algorithms. Machine Vision and Applications 1997; 9:272–290.

[Einthoven 1906] Einthoven W. Le telecardiogramme. Arch Internat Physiol 1906; 4:132-164.

[Ferrer 2015] Ferrer A, Sebastián R, Sánchez-Quintana D, Rodríguez JF, Godoy EJ, Martínez L, Saiz J. Detailed anatomical and electrophysiological models of human atria and torso for the simulation of atrial activation. PLoS One 2015; 10:e0141573.

[Finlay 2005] Finlay DD, Nugent CD, McCullagh PJ and Black ND. Mining for diagnostic information in body surface potential maps: A comparison of feature selection techniques. Biomedical engineering online 2005; 4:51-51.

[Finlay 2008] Finlay DD, Nugent CD, Donnelly MP, Black ND. Selection of optimal recording sites for limited lead body surface potential mapping in myocardial infarction and left ventricular hypertrophy. J Electrocardiol 2008; 41: 264-271.

[Fischer 2000] Fischer G, Tilg B, Modre R, Huiskamp GJ, Fetzer J, Rucker W, Wach P. A bidomain model based BEM-FEM coupling formulation for anisotropic cardiac tissue. Ann Biomed Eng 2000; 28:1229-1243.

[Frank 1954] Frank E. An equivalent circuit for the human heart-body electrical system. Am Heart J 1954; 48:738-745.

[Fuster 2006] Fuster V, Rydén LE, Cannom DS, Crijns HJ, Curtis AB, Ellenbogen KA, Halperin JL, Le Heuzey JY, Kay GN, Lowe JE, Olsson SB, Prystowsky EN,

Tamargo JL, Wann S, Smith SC Jr, Jacobs AK, Adams CD, Anderson JL, Antman EM, Hunt SA, Nishimura R, Ornato JP, Page RL, Riegel B, Priori SG, Blanc JJ, Budaj A, Camm AJ, Dean V, Deckers JW, Despres C, Dickstein K, Lekakis J, McGregor K, Metra M, Morais J, Osterspey A, Zamorano JL. ACC/AHA/ESC 2006 guidelines for the management of patients with atrial fibrillation - executive summary. J Am Coll Cardiol 2006; 48:854-906.

[García 2013] Garcia-Molla VM, Liberos A, Vidal A, Guillem MS, Millet J, Gonzalez A, Martinez-Zaldivar FJ, Climent AM. Adaptive step ODE algorithms for the 3D simulation of electric heart activity with graphics processing units. Comput Biol Med 2014; 44:15-26.

[García-Cosio 2012] Garcia-Cosio F, Pastor Fuentes A, Nunez Angulo A. Clinical approach to atrial tachycardia and atrial flutter from an understanding of the mechanisms. electrophysiology based on anatomy. Rev Esp Cardiol 2012; 65:363-375.

[Ghanem 2005] Ghanem RN, Jia P, Ramanathan C, Ryu K, Markowitz A, Rudy Y. Noninvasive electrocardiographic imaging (ECGI): comparison to intraoperative mapping in patients. Heart Rhythm 2005; 2:339–354.

[Ghosh 2011] Ghosh S, Silva JN, Canham RM, Bowman TM, Zhang J, Rhee EK, Woodard PK, Rudy Y. Electrophysiologic substrate and intraventricular left ventricular dyssynchrony in nonischemic heart failure patients undergoing cardiac resynchronization therapy. Heart Rhythm 2011; 8:692-699.

[Gerstenfeld 2000] Gerstenfeld EP, SippensGroenewegen A, Lux RL, Lesh MD. Derivation of an optimal lead set for measuring ectopic atrial activation from the pulmonary veins by using body surface mapping. J Electrocardiol 2000; 33:179-185.

[Golub 1979] Golub GH, Heath M, Wahba G. Generalized cross-validation as a method for choosing a good ridge parameter. Technometrics 1979; 21:215-223.

[Grandi 2011] Grandi E, Pandit SV, Voigt N, Workman AJ, Dobrev D, Jalife J, Bers DM. Human atrial action potential and Ca2+ model sinus rhythm and chronic atrial fibrillation. Circ Res 2011; 109:1055-1066.

[Gray 1998] Gray RA, Pertsov AM, Jalife J. Spatial and temporal organization during cardiac fibrillation. Nature 1998; 392:75-78.

[Guillem 2008] Guillem MS. Activation patterns in atrial fibrillation: contributions of body surface potential mapping. PhD thesis.

[Guillem 2008] Guillem MS, Castells F, Climent AM, Bodí V, Chorro FJ, Millet J. Evaluation of lead selection methods for optimal reconstruction of body surface potentials. J Electrocardiol 2008; 41:26-34.

[Guillem 2009] Guillem MS, Climent AM, Castells F, Husser D, Millet J, Arya A, Piorkowski C, Bollmann A. Noninvasive mapping of human atrial fibrillation. J Cardiovasc Electrophysiol 2009; 20:507-513.

[Guillem 2013] Guillem MS, Climent AM, Millet J, Arenal A, Fernández-Avilés F, Jalife J, Atienza F, Berenfeld O. Noninvasive localization of maximal frequency sites of atrial fibrillation by body surface potential mapping. Circ Arrhythm Electrophysiol 2013; 6:294-301.

[Guillem 2016] Guillem MS, Climent AM, Rodrigo M, Fernández-Avilés F, Atienza F, Berenfeld O. Presence and stability of rotors in atrial fibrillation: evidence and therapeutic implications. Cardiovasc Res 2016; 109:480-492.

[Haïssaguerre 1998] Haïssaguerre M, Jaïs P, Shah DC, Takahashi A, Hocini M, Quiniou G, Garrigue S, Le Mouroux A, Le Métayer P, Clémenty J. Spontaneous initiation of atrial fibrillation by ectopic beats originating in the pulmonary veins. N Engl J Med 1998; 339:659-566.

[Haïssaguerre 2013] Haissaguerre M, Hocini M, Shah AJ, Derval N, Sacher F, Jais P, Dubois R. Noninvasive panoramic mapping of human atrial fibrillation mechanisms: a feasibility report. J Cardiovasc Electrophysiol 2013; 24:711-717.

[Haïssaguerre 2014] Haissaguerre M, Hocini M, Denis A, Shah AJ, Komatsu Y, Yamashita S, Daly M, Amraoui S, Zellerhoff S, Picat MQ, Quotb A, Jesel L, Lim H, Ploux S, Bordachar P, Attuel G, Meillet V, Ritter P, Derval N, Sacher F, Bernus O, Cochet H, Jais P, Dubois R. Driver domains in persistent atrial fibrillation. Circulation 2014; 130:530-538.

[Hansen 1990] Hansen C. Truncated singular value decomposition solutions to discrete ill-posed problems with ill-determined numerical rank. SIAM J Sci Stat Comput 1990; 11:503-518.

[Hansen 1993] Hansen PC, O'Leary DP: The use of the L-curve in the regularization of discrete ill-posed problems. SIAM J Sci Stat Comput 1993; 14:1487-1503.

[Hansen 2015] Hansen BJ, Zhao J, Csepe TA, Moore BT, Li N, Jayne LA, Kalyanasundaram A, Lim P, Bratasz A, Powell KA, Simonetti OP, Higgins RS, Kilic A, Mohler PJ, Janssen PM, Weiss R, Hummel JD, Fedorov VV. Atrial fibrillation driven by micro-anatomic intramural re-entry revealed by simultaneous sub-epicardial and sub-endocardial optical mapping in explanted human hearts. Eur Heart J 2015; 36:2390-2401.

[He 2003] He B, Li G, Zhang X. Noninvasive imaging of cardiac transmembrane potentials within three-dimensional myocardium by means of a realistic geometry aniostropic heart model. IEEE Trans Biomed Eng 2003; 50:1190–1202.

[Hocini 2015] Hocini M, Shah AJ, Neumann T, Kuniss M, Erkapic D, Chaumeil A, Copley SJ, Lim PB, Kanagaratnam P, Denis A, Derval N, Dubois R, Cochet H, Jais P, Haissaguerre M. Focal arrhythmia ablation determined by high-resolution noninvasive maps: multicenter feasibility study. J Cardiovasc Electrophysiol 2015; 26:754-760.

[Hodgkin and Huxley 1952] Hodgkin AL and Huxley AF. A quantitative description of membrane current and its application to conduction and excitation in nerve. J Physiol 1952; 117:500-544.

[Hoekema 1999] Hoekema R, Uijen G, van Oosterom A. The number of independent signals in body surface maps. Methods Inf Med 1999; 38:119-124.

[Holm 1998] Holm M, Pehrson S, Ingemansson M, Sörnmo L, Johansson R, Sandhall L, Sunemark M, Smideberg B, Olsson C, Olsson SB. Non-invasive assessment of the atrial cycle length during atrial fibrillation in man: introducing, validating and illustrating a new ECG method. Cardiovasc Res 1998; 38:69–81.

[Horácek 1997] Horácek BM, Clements JC. The inverse problem of electrocardiography: a solution in terms of single- and double-layer sources of the epicardial surface. Math Biosci 1997; 144:119-154.

[Hsu 2004] Hsu LF, Jaïs P, Keane D, Wharton JM, Deisenhofer I, Hocini M, Shah DC, Sanders P, Scavée C, Weerasooriya R, Clémenty J, Haïssaguerre M. Atrial fibrillation originating from persistent left superior vena cava. Circulation 2004; 109:828-832.

[Huiskamp 1997] Huiskamp G, Greensite F. A new method for myocardial activation imaging. IEEE Trans Biomed Eng 1997; 44:433-446.

[Hwang 2016] Hwang M, Song JS, Lee YS, Li C, Shim EB, Pak HN. Electrophysiological rotor ablation in in-silico modeling of atrial fibrillation: comparisons with dominant frequency, Shannon entropy, and phase singularity. PLoS One 2016; 24:11:e0149695.

[Ihara 2007] Ihara Z, van Oosterom A, Jacquemet V, Hoekema R. Adaptation of the standard 12-lead electrocardiogram system dedicated to the analysis of atrial fibrillation. J Electrocardiol 2007; 40: 68.e1-e8.

[Iyer 2001] Iyer A, Gray R. An Experimentalist's Approach to Accurate Localization of Phase Singularities during Reentry. Ann Biomed Eng 2001; 29:47-59.

[Iyer 2004] Iyer V, Mazhari R and Winslow RL. A computational model of the human left-ventricular epicardial myocyte. Biophys J 2004; 87: 1507-1525.

[Jacquemet 2006] Jacquemet V, van Oosterom A, Vesin J and Kappenberger L. Analysis of electrocardiograms during atrial fibrillation - A biophysical model approach. IEEE Eng Med Biol Mag 2006; 25:79-88.

[Jalife 1998] Jalife J, Berenfeld O, Skanes A, Mandapati R. Mechanisms of atrial fibrillation: mother rotors or multiple daughter wavelets, or both? J Cardiovasc Electrophysiol 1998; 9:S2–S12.

[Jalife 2002] Jalife J, Berenfeld O, Mansour M. Mother rotors and fibrillatory conduction: a mechanism of atrial fibrillation. Cardiovasc Res 2002; 54:204-216.

[Jalife 2004] Jalife J, Berenfeld O. Molecular mechanisms and global dynamics of fibrillation: an integrative approach to the underlying basis of vortex-like reentry. J Theor Biol 2004; 230:475-487.

[Jalife 2009] Jose Jalife, Mario Delmar, Justus Anumonwo, Omer Berenfeld, Jerome Kalifa. Basic cardiac electrophysiology for the clinician, 2nd Edition. 2009.

[Jalife 2011] Jalife J. Déjà vu in the theories of atrial fibrillation dynamics. Cardiovasc Res 2011; 89:766-775.

[Jalife 2015] Jalife J, Filgueiras Rama D, Berenfeld O. Letter by Jalife et al Regarding Article, "Quantitative analysis of localized sources identified by focal impulse and rotor modulation mapping in atrial fibrillation". Circ Arrhythm Electrophysiol 2015; 8:1296-1298.

[Jarman 2012] Jarman JW, Wong T, Kojodjojo P, Spohr H, Davies JE, Roughton M, Francis DP, Kanagaratnam P, Markides V, Davies DW, Peters NS. Spatiotemporal behavior of high dominant frequency during paroxysmal and persistent atrial fibrillation in the human left atrium. Circ Arrhythm Electrophysiol 2012; 5:650-658.

[Jia 2006] Jia P, Ramanathan C, Ghanem RN, Ryu K, Varma N, Rudy Y. Electrocardiographic imaging of cardiac resynchronization therapy in heart failure: observation of variable electrophysiologic responses. Heart Rhythm 2006; 3:296–310.

[Jiang 2009] Jiang M, Xia L, Shou G, Wei Q, Liu F, Crozier S. Effect of cardiac motion on solution of the electrocardiography inverse problem. IEEE Trans Biomed Eng 2009; 56:923-31.

[Johnston 1997] Johnston PR, Gulrajani RM. A new method for regularization parameter determination in the inverse problem of electrocardiography. IEEE Trans Biomed Eng 1997; 44:19-39.

[Kalifa 2006] Kalifa J, Tanaka K, Zaitsev AV, Warren M, Vaidyanathan R, Auerbach D, Pandit S, Vikstrom KL, Ploutz-Snyder R, Talkachou A, Atienza F,

Guiraudon G, Jalife J, Berenfeld O. Mechanisms of wave fractionation at boundaries of high-frequency excitation in the posterior left atrium of the isolated sheep heart during atrial fibrillation. Circulation 2006; 113:626-633.

[Kharche 2008] Kharche S, Zhang H. Simulating the effects of atrial fibrillation induced electrical remodeling: a comprehensive simulation study. Conf Proc IEEE Eng Med Biol Soc 2008; 2008:593-596.

[Klepfer 1997] Klepfer RN, CR Johnson, RS Macleod. Zhang H. The effects of inhomogeneities and anisotropies on electrocardiographic fields: a 3-D finite-element study. IEEE Trans Biomed Eng 1997; 44:706-719.

[Kneller 2002] Kneller J, Zou R, Vigmond EJ, Wang Z, Leon LJ, Nattel S. Cholinergic atrial fibrillation in a computer model of a two-dimensional sheet of canine atrial cells with realistic ionic properties. Circ Res 2002; 90:73-87.

[Koivumaki 2011] Koivumaki JT, Korhonen T and Tavi P. Impact of sarcoplasmic reticulum calcium release on calcium dynamics and action potential morphology in human atrial myocytes: A computational study. PLoS Comput Biol 2011; 7: e1001067.

[Koivumaki 2014] Koivumaki JT, Seemann G, Maleckar MM and Tavi P. In silico screening of the key cellular remodeling targets in chronic atrial fibrillation. PLoS Comput Biol 2014; 10:e1003620.

[Krahn 1995] Krahn AD, Manfreda J, Tate RB, Mathewson FA, Cuddy TE. The natural history of atrial fibrillation: incidence, risk factors, and prognosis in the Manitoba Follow-Up Study. Am J Med 1995; 98:476-484.

[Krueger 2011] Krueger MW, Schmidt V, Tobon C, Weber FM, Lorenz C, Keller DUJ, Barschdorf H, Burdumy M, Neher P, Plank G, Rhode K, Seeman G, Sanchez-Quintana D, Saiz J, Razavi R, Dössel O. Modeling atrial fiber orientation in patient-specific geometries: A semi-automatic rule-based approach. Functional Imaging and Modeling of the Heart 2011; 6666:223-232.

[Krueger 2013] Krueger MW, Seemann G, Rhode K, Keller DU, Schilling C, Arujuna A, Gill J, O'Neill MD, Razavi R, Dössel O. Personalization of atrial anatomy and electrophysiology as a basis for clinical modeling of radio-frequency ablation of atrial fibrillation. IEEE Trans Med Imaging 2013; 32:73-84.

[Krueger 2013] Krueger MW, Dorn A, Keller DU, Holmqvist F, Carlson J, Platonov PG, Rhode KS, Razavi R, Seemann G, Dössel O. In-silico modeling of atrial repolarization in normal and atrial fibrillation remodeled state. Med Biol Eng Comput 2013; 51:1105-19.

[Kuklik 2016] Kuklik P, Zeemering S, van Hunnik A, Maesen B, Pison L, Lau D, Maessen J, Podziemski P, Meyer C, Schaffer B, Crijns H, Willems S, Schotten U.

Identification of rotors during human atrial fibrillation using contact mapping and phase singularity detection: technical considerations. IEEE Trans Biomed Eng 2016. Ahead of print.

[Lankveld 2014] Lankveld TA, Zeemering S, Crijns HJ, Schotten U. The ECG as a tool to determine atrial fibrillation complexity. Heart 2014; 100:1077-1084.

[Lawson 1984] Lawson CL. C1 surface interpolation for scattered data on a sphere. Journal of Mathematics 1984; 14:177-202.

[Lee 2009] Lee R, Kruse J, McCarthy PM. Surgery for atrial fibrillation. Nat Rev Cardiol 2009; 6:505-513.

[Lee 2013] Lee S, Sahadevan J, Khrestian CM, Durand DM, Waldo AL. High density mapping of atrial fibrillation during vagal nerve stimulation in the canine heart: restudying the Moe hypothesis. J Cardiovasc Electrophysiol 2013; 24:328-335.

[Lee 2015] Lee AM. Maze permutations during minimally invasive mitral valve surgery. Ann Cardiothorac Surg 2015; 4:463-468.

[Lewis 1921] Lewis T: Oliver-Sharpey Lectures. On the nature of flutter and fibrillation of the auricle. Br Med J 1921; 1:590–593.

[Lian 2002] Lian J, Li G, Cheng J, Avitall B, He B. Body surface Laplacian mapping of atrial depolarization in healthy human subjects. Med Biol Eng Comput 2002; 40:650-659.

[Lim 2015] Lim HS, Zellerhoff S, Derval N, Denis A, Yamashita S, Berte B, Mahida S, Hooks D, Aljefairi N, Shah AJ, Sacher F, Hocini M, Jais P, Haissaguerre M. Noninvasive mapping to guide atrial fibrillation ablation. Card Electrophysiol Clin 2015; 7:89-98.

[Lin 2003] Lin WS, Tai CT, Hsieh MH, Tsai CF, Lin YK, Tsao HM, Huang JL, Yu WC, Yang SP, Ding YA, Chang MS, Chen SA. Catheter ablation of paroxysmal atrial fibrillation initiated by non-pulmonary vein ectopy. Circulation 2003; 107:3176-3183.

[Liu 2006] Liu Z, Liu C, He B. Noninvasive reconstruction of three-dimensional ventricular activation sequence from the inverse solution of distributed equivalent current density. IEEE Trans Biomed Eng 2006; 25:1307-1318.

[Luo and Rudy 1991] Luo CH and Rudy Y. A model of the ventricular cardiac action-potential - depolarization, repolarization, and their interaction. Circ Res 1991; 68: 1501-1526.

[Lux 1978] Lux RL, Smith CR, Wyatt RF, Abildskov JA. Limited lead selection for estimation of body surface potential maps in electrocardiography. IEEE Trans Biomed Eng 1978; 25: 270-276.

[MacLeod 1991] MacLeod RS, Johnson CR, Ershler PR. Construction of an inhomogeneous model of the human torso for use in computational electrocardiography. IEEE Eng Med and Biol Soc 1991:688-689.

[MacLeod 1995] MacLeod RS, Gardner M, Miller RM, Horácek BM. Application of an electrocardiographic inverse solution to localize ischemia during coronary angioplasty. J Cardiovasc Electrophysiol 1995; 6:2-18

[Maleckar 2008] Maleckar MM, Greenstein JL, Trayanova NA and Giles WR. Mathematical simulations of ligand-gated and cell-type specific effects on the action potential of human atrium. Prog Biophys Mol Biol 2008; 98:161-170;

[Maleckar 2009] Maleckar MM, Greenstein JL, Giles WR, Trayanova NA. Electrotonic coupling between human atrial myocytes and fibroblasts alters myocyte excitability and repolarization. Biophys J 2009; 97:2179-2190.

[Mandapati 2000] Mandapati R, Skanes A, Chen J, Berenfeld O, Jalife J. Stable microreentrant sources as a mechanism of atrial fibrillation in the isolated sheep heart. Circulation 2000; 101:194-199.

[Mansour 2001] Mansour M, Mandapati R, Berenfeld O, Chen J, Samie FH, Jalife J. Left-to-right gradient of atrial frequencies during acute atrial fibrillation in the isolated sheep heart. Circulation 2001; 103:2631-2636.

[Messinger-Raport 1986] Messinger-Rapport BJ, Rudy Y. The inverse problem in electrocardiography: a model study of the effects of geometry and conductivity parameters on the reconstruction of epicardial potentials. IEEE Trans Biomed Eng 1986; 33:667-676.

[Messinger-Raport 1989] Messinger-Rapport BJ, Rudy Y. Computational issues of importance to the inverse recovery of epicardial potentials in a realistic heart-torso geometry. Math Biosci 1989; 97:85-120.

[Messinger-Raport 1990] Messinger-Rapport BJ, Rudy Y. Noninvasive recovery of epicardial potentials in a realistic heart-torso geometry. Normal sinus rhythm. Circ Res 1990; 66:1023-1039.

[Mines 1913] Mines GR. On dynamic equilibrium in the heart. J Physiol 1913; 46:349-383.

[Miller 1970] Miller K. Least squares methods for ill-posed problems with a prescribed bound. SIAM J Math Anal 1970; 1:52-74.

[Moe 1959] Moe GK, Abildskov JA. Atrial fibrillation as a self-sustaining arrhythmia independent of focal discharge. Am Heart J 1959; 58:59-70.

[Moe 1964] Moe GK, Rheinboldt WC, Abildskov JA. A computer model of atrial fibrillation. Am Heart J 1964; 67:200-220.

[McAllister 1975] McAllister RE, Noble D and Tsien RW. Reconstruction of electrical-activity of cardiac purkinje-fibers. J Physiol -London 1975; 251:1-59.

[McDowell 2012] McDowell KS, Vadakkumpadan F, Blake R, Blauer J, Plank G, MacLeod RS, Trayanova NA. Methodology for patient-specific modeling of atrial fibrosis as a substrate for atrial fibrillation. J Electrocardiol 2012; 45:640-645.

[Morozov 1984] Morozov VA. Methods for solving incorrectly posed problems. Springer-Verlag 1984; 44-47.

[Nademanee 2004] Nademanee K, McKenzie J, Kosar E, Schwab M, Sunsaneewitayakul B, Vasavakul T, Khunnawat C, Ngarmukos T. A new approach for catheter ablation of atrial fibrillation: Mapping of the electrophysiologic substrate. J Am Coll Cardiol 2004; 43:2044-2053.

[Nattel 1998] Nattel S. Experimental evidence for proarrhythmic mechanisms of antiarrhythmic drugs. Cardiovasc Res 1998; 37:567-577.

[Nattel 2002] Nattel S. New ideas about atrial fibrillation 50 years on. Nature 2002; 415:219-226.

[Narayan 2012] Narayan SM, Krummen DE, Shivkumar K, Clopton P, Rappel WJ, Miller JM. Treatment of atrial fibrillation by the ablation of localized sources: CONFIRM (Conventional Ablation for Atrial Fibrillation With or Without Focal Impulse and Rotor Modulation) trial. J Am Coll Cardiol 2012; 60:628-636.

[Narayan 2013] Narayan SM, Krummen DE, Clopton P, Shivkumar K, Miller JM. Direct or coincidental elimination of stable rotors or focal sources may explain successful atrial fibrillation ablation: On-treatment analysis of the confirm trial (conventional ablation for af with or without focal impulse and rotor modulation). J Am Coll Cardiol 2013; 62:138-147.

[Narayan 2014] Narayan SM, Baykaner T, Clopton P, Schricker A, Lalani GG, Krummen DE, Shivkumar K, Miller JM. Ablation of rotor and focal sources reduces late recurrence of atrial fibrillation compared with trigger ablation alone: extended follow-up of the CONFIRM trial (Conventional Ablation for Atrial Fibrillation With or Without Focal Impulse and Rotor Modulation). J Am Coll Cardiol 2014; 63:1761-1768.

[Narayan 2014] Narayan SM, Jalife J. CrossTalk proposal: Rotors have been demonstrated to drive human atrial fibrillation. J Physiol 2014; 592:3163-3166.

[Noble 1962] Noble D. A modification of the Hodgkin–Huxley equations applicable to purkinje fibre action and pacemaker potentials. J Physiol 1962; 160:317-352.

[Nygren 1998] Nygren A, Fiset C, Firek L, Clark JW, Lindblad DS, Clark RB, Giles WR. Mathematical model of an adult human atrial cell - the role of K+ currents in repolarization. Circ Res 1998; 82:63-81.

[Oster 1992] Oster H, Rudy Y. The use of temporal information in the regularization of the inverse problem of electrocardiography. IEEE Trans Biomed Eng 1992; 39:65-75.

[Oster 1997] Oster HS, Taccardi B, Lux RL, Ershler PR, Rudy Y. Noninvasive electrocardiographic imaging: reconstruction of epicardial potentials, electrograms, and isochrones and localization of single and multiple electrocardiac events. Circulation 1997; 96:1012–1024.

[Pedrón-Torrecilla 2016] Pedrón-Torrecilla J, Rodrigo M, Climent AM, Liberos A, Pérez-David E, Bermejo J, Arenal Á, Millet J, Berenfeld O, Fernández-Avilés F, Atienza F, Guillem MS. Noninvasive estimation of epicardial dominant high-frequency regions during atrial fibrillation. J Cardiovasc Electrophysiol 2016; 27:435-442.

[Petrutiu 2009] Petrutiu S, Sahakian AV, Fisher W, Swiryn S. Manifestation of left atrial events and interatrial frequency gradients in the surface electrocardiogram during atrial fibrillation: contributions from posterior leads. J Cardiovasc Electrophysiol 2009; 20:1231–1236.

[Providência 2015] Providência R, Lambiase PD, Srinivasan N, Ganesh Babu G, Bronis K, Ahsan S, Khan FZ, Chow AW, Rowland E, Lowe M, Segal OR. Is there still a role for complex fractionated atrial electrogram ablation in addition to pulmonary vein isolation in patients with paroxysmal and persistent atrial fibrillation? Meta-analysis of 1415 patients. Circ Arrhythm Electrophysiol 2015; 8:1017-1029.

[Rahimi 2016] Rahimi A, Sapp J, Xu J, Bajorski P, Horacek M, Wang L. Examining the impact of prior models in transmural electrophysiological imaging: a hierarchical multiple-model bayesian approach. IEEE Trans Med Imaging 2016; 35:229-243.

[Ramanathan 2001] Ramanathan C, Rudy Y. Electrocardiographic imaging: I. Effect of torso inhomogeneities on body surface electrocardiographic potentials. J Cardiovasc Electrophysiol. 2001; 12:229-140.

[Ramanathan 2001] Ramanathan C, Rudy Y. Electrocardiographic imaging: II. Effect of torso inhomogeneities on noninvasive reconstruction of epicardial

potentials, electrograms, and isochrones. J Cardiovasc Electrophysiol 2001; 12:241-252.

[Ramanathan 2004] Ramanathan C, Ghanem RN, Jia P, Ryu K, Rudy Y. Noninvasive electrocardiographic imaging for cardiac electrophysiology and arrhythmia. Nat Med 2004; 10:422-428.

[Rappel 2013] Rappel WJ, Narayan SM. Theoretical considerations for mapping activation in human cardiac fibrillation. Chaos 2013; 23:023113.

[Rappel 2015] Rappel WJ, Zaman JA, Narayan SM. Mechanisms for the termination of atrial fibrillation by localized ablation: computational and clinical studies. Circ Arrhythm Electrophysiol 2015; 8:1325-1333.

[Remondino 2004] Remondino R. 3-D reconstruction of static human body shape from image sequence. Computer Vision and Image Understanding 2004; 93;65-85.

[Reumann 2008] Reumann M, Bohnert J, Seemann G, Osswald B, Dössel O. Preventive ablation strategies in a biophysical model of atrial fibrillation based on realistic anatomical data. IEEE Trans Biomed Eng 2008; 55:399-406.

[Revishvili 2015] Revishvili AS, Wissner E, Lebedev DS, Lemes C, Deiss S, Metzner A, Kalinin VV, Sopov OV, Labartkava EZ, Kalinin AV, Chmelevsky M, Zubarev SV, Chaykovskaya MK, Tsiklauri MG, Kuck KH. Validation of the mapping accuracy of a novel non-invasive epicardial and endocardial electrophysiology system. Europace 2015; 17:1282-1288.

[Rodrigo 2014] Rodrigo M, Guillem MS, Climent AM, Pedron-Torrecilla J, Liberos A, Millet J, Fernandez-Aviles F, Atienza F, Berenfeld O. Body surface localization of left and right atrial high-frequency rotors in atrial fibrillation patients: A clinical-computational study. Heart rhythm 2014; 11:1584-1591.

[Rodrigo 2014] Rodrigo M, Pedrón–Torrecilla J, Hernández I, Liberos A, Climent AM, Guillem MS. Data Analysis in cardiac arrhythmias. Data Mining in Clinical Medicine. Methods in Molecular Biology 2014; 1246:217–236.

[Rosenblueth 1947] Rosenblueth A, Garcia Ramos J. Studies on flutter and fibrillation; the influence of artificial obstacles on experimental auricular flutter. Am Heart J 1947; 33:677-684.

[Roten 2012] Roten L, Pedersen M, Pasacale P, Shah A, Eliautou S, Scherr D, Sacher F, Haïssaguerre M. Noninvasive electrocardiographic mapping for prediction of tachycardia mechanism and origin of atrial tachycardia following bilateral pulmonary transplantation. J Cardiovasc Electrophysiol 2012; 23:553-555.

[Sanders 2005] Sanders P, Berenfeld O, Hocini M, Jais P, Vaidyanathan R, Hsu LF, Garrigue S, Takahashi Y, Rotter M, Sacher F, Scavee C, Ploutz-Snyder R, Jalife J, Haissaguerre M. Spectral analysis identifies sites of high-frequency activity maintaining atrial fibrillation in humans. Circulation 2005; 112:789-797.

[Sahadevan 2004] Sahadevan J, Ryu K, Peltz L, Khrestian CM, Stewart RW, Markowitz AH, Waldo AL. Epicardial mapping of chronic atrial fibrillation in patients: preliminary observations. Circulation 2004; 110:3293-3299.

[Seger 2005] Seger M, Fischer G, Modre R, Messnarz B, Hanser F, Tilg B. Lead field computation for the electrocardiographic inverse problem: finite elements versus boundary elements. Comput Methods Programs Biomed 2005; 77:241-252.

[Shah 2013] Shah AJ, Hocini M, Xhaet O, Pascale P, Roten L, Wilton SB, Linton N, Scherr D, Miyazaki S, Jadidi AS, Liu X, Forclaz A, Nault I, Rivard L, Pedersen ME, Derval N, Sacher F, Knecht S, Jais P, Dubois R, Eliautou S, Bokan R, Strom M, Ramanathan C, Cakulev I, Sahadevan J, Lindsay B, Waldo AL, Haissaguerre M. Validation of novel 3-dimensional electrocardiographic mapping of atrial tachycardias by invasive mapping and ablation: a multicenter study. J Am Coll Cardiol 2013; 62:889-897.

[Silva 2009] Silva JN, Ghosh S, Bowman TM, Rhee EK, Woodard PK, Rudy Y. Cardiac resynchronization therapy in pediatric congenital heart disease: insights from noninvasive electrocardiographic imaging. Heart Rhythm 2009; 6:1178–1185.

[SippensGroenewegen 1998] SippensGroenewegen A, Peeters HA, Jessurun ER, Linnenbank AC, Robles de Medina EO, Lesh MD, van Hemel NM. Body surface mapping during pacing at multiple sites in the human atrium - P-wave morphology of ectopic right atrial activation. Circulation 1998; 97:369-380.

[SippensGroenewegen 2000] SippensGroenewegen A, Lesh MD, Roithinger FX, Ellis WS, Steiner PR, Saxon LA, Lee RJ, Scheinman MM. Body surface mapping of counterclockwise and clockwise typical atrial flutter: A comparative analysis with endocardial activation sequence mapping. J Am Coll Cardiol 2000; 35:1276-1287.

[Scherf 1958] Scherf D, Romano FJ, Terranova R. Experimental studies on auricular flutter and auricular fibrillation. Am Heart J 1958; 36:241-255.

[Schotten 2001] Schotten U, Ausma J, Stellbrink C, Sabatschus I, Vogel M, Frechen D, Schoendube F, Hanrath P, Allessie MA. Cellular mechanisms of depressed atrial contractility in patients with chronic atrial fibrillation. Circulation 2001; 103:691-698.

[Schotten 2002] Schotten U, Greiser M, Benke D, Buerkel K, Ehrenteidt B, Stellbrink C, Vazquez-Jimenez JF, Schoendube F, Hanrath P, Allessie M. Atrial fibrillation-induced atrial contractile dysfunction: A tachycardiomyopathy of a different sort. Cardiovasc Res 2002; 53: 192-201.

[Shou 2008] Shou G, Xia L, Jiang M, Wei Q, Liu F, Crozier S. Truncated total least squares: a new regularization method for the solution of ECG inverse problems. IEEE Trans Biomed Eng 2008; 55:1327-1335.

[Skasa 2001] Skasa M, Jüngling E, Picht E, Schöndube F, Lückhoff A. L-type calcium currents in atrial myocytes from patients with persistent and non-persistent atrial fibrillation. Basic Res Cardiol 2001; 96:151-159.

[Slocum 1992] Slocum J, Sahakian A, Swiryn S. Diagnosis of atrial fibrillation from surface electrocardiograms based on computer-detected atrial activity. J Electrocardiol 1992; 25:1-8.

[Su 2013] Su L, Borov S, Zrenner B. 12-lead Holter electrocardiography. Review of the literature and clinical application update. Herzschrittmacherther Elektrophysiol 2013; 24:92-96.

[Taccardi 1963] Taccardi B. Distribution of heart potentials on thoracic surface of normal human subjects. Circ Res 1963; 12: 341-352.

[Taccardi 1998] Taccardi B, Punske BB, Lux RL, MacLeod RS, Ershler PR, Dustman TJ, Vyhmeister Y. Useful lessons from body surface mapping. J Cardiovasc Electrophysiol 1998; 9:773-786.

[ten Tusscher 2004] ten Tusscher KHWJ, Noble D, Noble PJ and Panfilov AV. A model for human ventricular tissue. Am J Physiol Heart Circ Physio 2004; 286:H1573-H1589.

[Throne 1994] Throne RD, Olson LG. A generalized eigensystem approach to the inverse problem of electrocardiography. IEEE Trans Biomed Eng 1994; 41:592-600.

[Tikhonov 1963] Tikhonov AN. On the solution of incorrectly posed problems and the method of regularization. Sov Math Dokl 1963; 4:1035-1038.

[Tobon 2010] Tobon C, Ruiz C, Rodriguez JF, Hornero F, Ferrero JM (Jr.), Saiz J. A biophysical model of atrial fibrillation to simulate the maze III ablation pattern. Computing in Cardiology 2010; 37:621-624.

[Tobon 2013] Tobón C, Ruiz-Villa CA, Heidenreich E, Romero L, Hornero F, Saiz J. A three-dimensional human atrial model with fiber orientation. electrograms and arrhythmic activation patterns relationship. Plos One 2013; 8:e50883.

[Trayanova 2006] Trayanova N. Defibrillation of the heart: Insights into mechanisms from modelling studies. Exp Physiol 2006; 91:323-337.

[Tsai 2000] Tsai CF, Tai CT, Hsieh MH, Lin WS, Yu WC, Ueng KC, Ding YA, Chang MS, Chen SA. Initiation of atrial fibrillation by ectopic beats originating from the superior vena cava: electrophysiological characteristics and results of radiofrequency ablation. Circulation 2000; 102:67-74.

[Twomey 1963] Twomey S. On the numerical solution of Fredholm integral equations of the first kind by the inversion of the linear system produced by quadrature. JACM 1963; 10:97-101.

[van Dam 2003] van Dam PM and van Oosterom A. Atrial excitation assuming uniform propagation. J Cardiovasc Electrophysiol 2003; 14:S166-S171.

[Vazouras 2004] Vazouras CN. EEG source distribution localization using minimum-product and CRESO criteria for Tikhonov regularization. Conf Proc IEEE Eng Med Biol Soc 2004; 6:4457-4460.

[Virag 2002] Virag N, Jacquemet V, Henriquez CS, Zozor S, Blanc O, Vesin JM, Pruvot E, Kappenberger L. Study of atrial arrhythmias in a computer model based on magnetic resonance images of human atria. Chaos 2002; 12:754-763.

[Wahha 1977] Wahha G. Practical approximate solutions to linear operator equations when the data are noisy. SIAM J NumAnal 1977; 14:651-661.

[Walker 1987] Walker S, Kilpatrick D. Forward and inverse electrocardiographic calculations using resistor network models of the human torso. Circ Res 1987; 61:504-513.

[Wang 2007] Wang Y, Schuessler RB, Damiano RJ, Woodard PK, Rudy Y. Noninvasive electrocardiographic imaging (ECGI) of scar-related atypical atrial flutter. Heart Rhythm 2007; 4:1565-1567.

[Wang 2010] Wang D, Kirby RM, Johnson CR. Resolution strategies for the finite-element-based solution of the ECG inverse problem. IEEE Trans Biomed Eng 2010; 57:220-237.

[Wang 2011] Wang Y, Cuculich PS, Zhang J, Desouza KA, Vijayakumar R, Chen J, Faddis MN, Lindsay BD, Smith TW, Rudy Y. Noninvasive electroanatomic mapping of human ventricular arrhythmias with electrocardiographic imaging. Sci Transl Med 2011; 3:98-84.

[Wellner 2002] Wellner M, Berenfeld O, Jalife J, Pertsov AM. Minimal principle for rotor filaments. Proc Natl Acad Sci USA 2002; 99:8015-8018.

[Winterberg 1907] Winterberg H. Studien über herzflimmern. I. Über die wirkung des N. vagus und accelerans auf das Flimmern des Herzens. Pflügers Arch Physiol 1907; 117:223-256.

[Workman 2001] Workman AJ, Kane AK and Rankin AC. The contribution of ionic currents to changes in refractoriness of human atrial myocytes associated with chronic atrial fibrillation. Cardiovasc Res 2001; 52:226-235.

[Wyse 2004] Wyse DG, Gersh BJ. Atrial fibrillation: a perspective: thinking inside and outside the box. Circulation 2004; 109:3089-3095.

[Yamazaki 2009] Yamazaki M, Vaquero LM, Hou L, Campbell K, Zlochiver S, Klos M, Mironov S, Berenfeld O, Honjo H, Kodama I, Jalife J, Kalifa J. Mechanisms of stretch-induced atrial fibrillation in the presence and the absence of adrenocholinergic stimulation: interplay between rotors and focal discharges. Heart Rhythm 2009; 6:1009-1017.

[Yushkevich 2006] Yushkevich PA, Piven J, Hazlett HC, Smith RG, Ho S, Gee JC, Gerig G. User-guided 3D active contour segmentation of anatomical structures: significantly improved efficiency and reliability. Neuroimage 2006; 31:1116-1128.

[Zlochiver 2008] Zlochiver S, Yamazaki M, Kalifa J, Berenfeld O. Rotor meandering contributes to irregularity in electrograms during atrial fibrillation. Heart Rhythm 2008; 5:846-854.